CONSIDERING STRAIN COMPATIBILITY IN LIMIT EQUILIBRIUM ANALYSIS FOR THREE TAILINGS MATERIALS

YASHAY NARAINSAMY

A project report submitted in partial fulfilment of the requirements for the degree of
MASTERS IN ENGINEERING (CIVIL ENGINEERING)
In the
FACULTY OF ENGINEERING
UNIVERSITY OF PRETORIA

June 2021

PROJECT REPORT SUMMARY

CONSIDERING STRAIN COMPATIBILITY IN LIMIT EQUILIBRIUM ANALYSIS FOR THREE TAILINGS MATERIALS

YASHAY NARAINSAMY

Supervisor: Professor S. W. Jacobsz
Department: Civil Engineering
University: University of Pretoria
Degree: Masters in Engineering (Civil engineering)

Recent tailings dam failures around the world have highlighted the real risk posed by undrained slope failures. Undrained failures are fundamentally different to drained failures in the sense that different mechanisms are involved (i.e. a slope may be stable against drained failure but unstable against undrained failure). Popular methods to assess the stability of slopes against undrained failure involve the use of limit equilibrium analyses with both drained and undrained strengths assigned in the same analysis. A potential shortcoming of these methods is that no consideration is given to strain compatibility. This is important as soil loaded under drained and undrained conditions do no develop peak strength at the same strain level.

In this study, a limit equilibrium based method where strain compatibility is maintained on the failure surface was developed. The method, referred to as the strain mobilisation method, considers a Mohr circle of stress at failure to determine the shear strength mobilised on the failure plane for use in the stability analysis as a function of the deviator stress imposed on the triaxial test result. The mobilisation of stress on a failure plane with strain was determined based on the stress-strain relationships observed during triaxial tests.

A Factor of Safety (FoS) was used to express the stability of the slope as a function of the mobilised strain and the calculated FoS results obtained using the proposed method were compared to calculated FoS results using traditional methods. This was done for three tailings materials (gold, iron and platinum) for three specific hypothetical slopes. As an additional check, the proposed method was tested on Nerlerk sand, a well-known sand showing strain-softening behaviour during undrained shearing.

It was found that, in general, as mobilised strain is increased, the FoS calculated using the proposed method converges to that of traditional methods so that there was no significant difference in calculated FoS between the current methods and the proposed method that does consider strain compatibility. This indicates that the proposed method provides FoS values comparable to those calculated using currently accepted methods where the failure surface passes predominantly through a single material type. For such a case, there does not appear to be a need to consider limit equilibrium methods where strain compatibility is maintained.

It should be noted that the good correlation may be somewhat specific to the slip surface and cross section geometry analysed and may not be applicable to all cross sections. For example, the cross section where the failure surface passes through more than one material type did not show a correlation between the two methods, illustrating that interslice forces probably need more careful consideration than in the current implementation.

The proposed method provides an indication of the amount of strain that may be expected to mobilise to provide the FoS. Given that this amount of strain is not excessive, the current methods which do not consider strain compatibility perform satisfactorily and can continue to be used.

TABLE OF CONTENTS

LIST OF FIGURES

LIST OF TABLES

LIST OF ACRONYMS

AP	Air pluviated
CD	Consolidated drained
CSL	Critical state locus
CSSM	Critical state soil mechanics
CPTu	Cone penetration test with pore pressure measurements
CU	Consolidated undrained
DSS	Direct simple shear
ESA	Effective stress analysis
FE	Finite element
FoS	Factor of safety (dimensionless)
GLE	General limit equilibrium
ICL	Isotropic compression line
MT	Moist tamped
NCL	Normal consolidation line
RDWPSS	Remoulded discontinuously wet pluvial soil sample
sCPTu	Seismic cone penetration test with pore pressure measurements
SD	Slurry deposition
SF	Safety factor
S.F.	Stability factor
SHANSEP	Stress history and normalised soil engineering properties
SRF	Strength reduction factor
SRS	Strength reduction stability
TXC	Triaxial compression
TXE	Triaxial extension
USA	Undrained stress analysis
UU	Unconsolidated undrained
VBA	Visual basic for applications
VST	Vane shear test
WP	Water pluviated
YSR	Yield stress ratio (unitless)

LIST OF SYMBOLS

a	Perpendicular distance from the resultant water force to the centre of rotation (m)
A	Resultant water forces (kN)
α	Slice base angle (°)
c'	Cohesion (kPa)
c'_f	Cohesion at failure (kPa)
c_v	Coefficient of consolidation (mm^2/s)
c_u	Undrained shear strength, also referred to as s_u (kPa)
d	Perpendicular distance from the line load to the centre of rotation (m)
D	Cone diameter (mm)
E	Interslice normal force (kN)
E	Young's modulus (kPa)
e	Vertical distance from the centroid of each slice to the centre of rotation (m)
ε_a	Axial strain (%)
ε_s	Shear strain (%)
ε_v	Volumetric strain (%)
f	Perpendicular offset of the normal force from the centre of rotation (m)
F_f	FoS with respect to force equilibrium (dimensionless)
F_m	FoS with respect to moment equilibrium (dimensionless)
$F_{destabilising}$	Destabilising force causing failure (kN)
$F_{stabilising}$	Stabilising force resisting failure (kN)
G	Shear modulus (kPa)
I_B	Undrained brittleness index (dimensionless)
k	Seismic coefficient (dimensionless)
K	Bulk modulus (kPa)
l	Slice base length (m)
L	Line load (kN/m)
L	Subscript designating left side
N_{kt}	Cone factor (typically 14)
P	Normal force on the base of the slice over a length l (kN)
p'	Mean effective stress (kPa)
p'_0	Initial confining stress (kPa)
p'_f	Mean effective stress at failure (kPa)

ψ	Dilation angle (°)
q	Deviatoric stress (kPa)
q_c	Measured cone resistance (MPa)
q_{c1}	Normalised cone resistance (MPa), also noted as Q_t
q_t	Corrected cone resistance (kPa)
q_y	Yield deviator stress at collapse point (kPa)
$\left(\frac{q}{p'_f}\right)_i$	Shear stress ratio, based on the shear strain i mobilised (dimensionless)
Q_t	Normalised cone resistance (kPa), also noted as q_{c1}
R	Radius or the movement arm associated with the mobilised shear force S_m (m)
R	Subscript designating right side
S_r	Total available shear resistance (kN)
S_m	Total mobilised shear along the length of the slip surface (kN)
$s_u(yield)$	Peak (yield) undrained shear strength, also referred to as c_u and s_u (kPa)
$\frac{s_{u(yield)}}{\sigma'_{v0}}$	Yield undrained strength ratio (dimensionless)
$s_u(critical)$	Steady state (critical) undrained shear strength (kPa)
t_{50}	Time for 50% consolidation (s)
S_m	Shear force mobilised on the base of the slice (kN)
τ_n	Shear stress mobilised at the slice base (kPa)
u_2	Pore pressure measures at position 2 (kPa)
V	Penetration rate (dimensionless)
W	Weight of the slice of width b and height h (kN)
v	Penetration rate (mm/s)
X	Interslice shear force (kN)
$\sigma_h.$	Horizontal stress (kPa)
$\sigma'_n.$	Normal effective stress (kPa)
$\sigma'_v.$	Vertical effective stress (kPa)
σ_{v0}	Total vertical stress at one atmosphere (kPa)
$\sigma'_{v0}.$	Vertical effective stress at one atmosphere (kPa)
φ'	Mohr-Coulomb friction angle (°)
φ'_f	Mohr-Coulomb friction angle at failure (°)
ω	Angle of the line load from the horizontal (°)

1 INTRODUCTION

1.1 BACKGROUND

South Africa has a rich mining heritage and as such, is home to a vast number of tailings dams. These dams are required to safely contain the large volume of waste produced as part of the mining process. Typically, ore is extracted from the ground and then sent through a break down process to facilitate extraction of the desired minerals. The waste from this refining process is directed to the tailings dams for storage. These structures are generally very large and therefore have a large consequence of failure even if the probability of failure may be low. Unlike water storage dams, the development of upstream tailings dams is continuous and therefore needs careful monitoring over its operational life.

In general, there are three basic causes of tailings dam incidents: engineering, operations and regulators (e.g. Morgenstern, 2018). Engineering related refers to matters relating to design, construction, quality control and quality assurance. Operations related refers to operational deviations from the approved Operations, Maintenance and Surveillance (OMS) Manual. Regulatory related refers to decisions made, or decisions not made in some cases, by a regulatory authority in relation to tailings dams design, construction, operation and closure. In terms of engineering related causes, which is the focus of this study, there are two main aspects to consider when reviewing the safety of tailings dams: preventing overtopping and preventing slope failure. If these two aspects are considered, the risk of catastrophic failure can be managed effectively in most cases.

To address the overtopping concern, a freeboard target is typically prescribed and routinely checked to confirm adherence. The intent with the freeboard target, which is simply the elevation difference between the current pond elevation and lowest point on the outer wall, is to ensure there is sufficient capacity within the tailings dam to safely contain or convey design storm events as well as associated secondary effects such as wind set-up and wave run-up. There are several statutory freeboard requirements, and the South African National Committee on Large Dams (SANCOLD) has published detailed guidelines on the calculation of freeboard requirements (Bosman et al., 2011).

There are several methods available to assess the slope stability of tailings facilities. The conventional method is to conduct a limit equilibrium analysis using the method of slices (Vick et al., 1983; Blight, 2009). The stability of tailings dams is the focus of this research.

Historically, in South Africa, tailings dams have only been assessed for slope stability in terms of effective, drained strength parameters as these are the only strengths specified in the local standard, SANS 10286, to which compliance is required by legislation (SABS, 1998). However, several recent tailings dam failures around the world have highlighted the devastating effect a tailings dam can have on the surrounding communities and the environment. The cause of these failures have been attributed to undrained shearing (Fourie et al., 2001; Morgenstern et al., 2016; Robertson et al., 2019). By not considering undrained shear strengths, which are typically only half of the peak drained strengths for the same effective stress (Olson & Stark, 2003b), the true stability of the slope under undrained conditions cannot be adequately assessed.

A criticism of using conventional limit equilibrium methods, where both drained and undrained strengths are mobilised in the same slope is that compatibility of strains is not considered. It is clear that the mobilisation of shear strength with respect to shear strain is different depending on the drainage boundary condition being considered. Therefore, it follows that, if strain compatibility must be maintained, it is possible that the mobilisation of strength will be different depending on whether drained or undrained shearing is considered. This study attempts to address this by incrementally mobilising shear strength in limit equilibrium slope stability analyses based on an assumed mobilised strain value which is then incrementally increased. A Factor of Safety (FoS) is then calculated which is directly related to the mobilised strain value and therefore an indication of the amount of strain required to mobilise the FoS is obtained.

While there is extensive literature on the field of drained failures and undrained failures respectively (e.g. Ladd, 1991; Duncan et al., 2014), there is little work in the field of failures where both drained and undrained strengths are mobilised. This is important as many failures do not necessarily involve purely drained or purely undrained shearing. Instead, there is a combination of drainage conditions during shearing in a soil mass (Eckersley, 1990). This can be seen when a slip surface develops between partially saturated and saturated zones in a soil mass. This study will attempt to advance the state of knowledge in this area.

1.2 OBJECTIVES OF THE STUDY

This study has the following objectives:

The primary objective was to determine the effect of different amounts of strain mobilisation, based on triaxial compression test data, on the calculated Factor of Safety (FoS) against failure obtained using limit equilibrium methods for slope stability analysis for three tailings materials: gold, iron and platinum.

A second objective was to investigate the effect of the sample preparation method on the stress-strain behaviour of reconstituted samples during undrained shearing in triaxial compression and to compare this to the stress-strain behaviour of undisturbed samples during triaxial compression.

A third objective was to compare the stress-strain behaviour noted during consolidated undrained triaxial compression testing to the expected theoretical behaviour in loose tailings.

A fourth objective was to compare the mobilised undrained shear strengths measured during triaxial compression to the range of theoretical strengths based on the method proposed by Sadrekarimi (2014). This method provides a means to estimate the undrained shear strength of a soil based on Cone Penetration with pore pressure measurement Testing (CPTu) data. The method is routinely used in industry and is based on a database of laboratory test data, verified using back analysis of field case histories where flow liquefaction occurred and undrained shear strengths were mobilised.

1.3 SCOPE OF THE STUDY

To achieve the objectives of the study, limit equilibrium slope stability analyses were conducted using the proposed FoS formulation where strain compatibility is maintained. The mobilised strengths were varied based on increasing amounts of strain mobilised at the base of each slice to determine the evolution of the calculated FoS values. Three geometrically simple hypothetical slopes were chosen, and the stability of each slope was assessed using conventional methods to assess slope stability and the results were compared to the new FoS implementation where strain compatibility was maintained. For the conventional methods, limit equilibrium and finite element analysis methods were used. In particular, the method described by Spencer (1967) was used for the limit equilibrium analysis and the Strength Reduction Stability method was used for the finite element analysis.

Initial stability analysis was conducted using the SLOPE/W and SIGMA/W components of the GeoStudio 2020 software package and subsequent analysis were conducted using spreadsheet-based strain mobilisation methods. Within SLOPE/W, only circular failure

surfaces were considered as these can easily be verified using spreadsheet-based methods. Optimised slip surfaces were not considered. The Mohr-Coulomb strength model was used as the constitutive model for the finite element analyses. For the spreadsheet-based methods, a new formulation was proposed to determine a mobilised FoS against failure using limit equilibrium methods where strain compatibility is maintained. The method, referred to as the strain mobilisation method, considers a Mohr circle of stress at failure to determine the shear strength mobilised on the failure plane for use in the stability analysis as a function of the deviator stress imposed on the triaxial test result. The normal practice of ensuring an equal FoS for all slices equal to the global FoS in not enforced. Further, the method assumes that the relationship between the mobilised shear stress on the failure plane and the imposed deviator stress at failure is also applicable during the strain mobilisation.

Data were obtained from a series of consolidated drained and consolidated undrained triaxial compression tests were conducted on three tailings materials: gold, iron and platinum tailings. Test were conducted at the University of Pretoria and were conducted at effective confining pressures of 75 kPa and 200 kPa. Reconstituted samples were used, and the samples were prepared using the Slurry Deposition sample preparation method in an attempt to replicate the placement method of tailings on an actual tailings dam. In addition, the performance of the proposed method on data from triaxial testing on Nerlerk sand done by others (Jefferies & Been, 2015) was also assessed. These tests were conducted at confining pressures of 200 kPa and 500 kPa and the samples were prepared using the Moist Tamping sample preparation method. Soil properties were determined from the triaxial test results and were used in subsequent analysis.

A limitation of this study was that only triaxial compression stress paths were considered. Such stress paths may deviate from that imposed during strain mobilisation in an actual tailings dam. In addition, only two very specific drainage conditions were considered: completely drained and completely undrained. It is known that stress paths in real soil structures are not limited to these extreme conditions and any degree of partial drainage can exist. However, these conditions represent the bounds of the drainage conditions possible. The influence of other drainage conditions and stress paths is outside the scope of this work.

1.4 METHODOLOGY

A literature review was performed to determine the current state of knowledge in the field of soil mechanics and geotechnical engineering with a particular emphasis on the definition of soil strength, types of soil strength with regard to drainage conditions, methods to determine

these strengths and a comparison between these methods. The assessment of slope stability using these strengths was then reviewed, the various methods available were assessed and the advantages and limitations of each method discussed. Tailings dams and tailings materials were reviewed, with particular focus on the characteristics of these materials. Current practice to assess slope stability considering drained and undrained strengths implemented in limit equilibrium slope stability analyses was also reviewed.

To achieve the desired objectives, results from a series of Consolidated Drained (CD) and Consolidated Undrained (CU) triaxial compression tests were used to derived strain dependent strength characteristics of three tailings materials: gold, iron and platinum. These strength characteristics were then used in a limit equilibrium analysis and a Factor of Safety (FoS) against failure was obtained for three hypothetical slopes. Particular emphasis was placed on the mobilisation of strength with strain when comparing drained and undrained stress paths. To enable the focus on mobilisation of stress, a spreadsheet-based strain mobilisation limit equilibrium slope stability analysis method to determine the FoS against failure was developed. The accuracy of this method was confirmed by comparing the FoS values obtained from the strain mobilisation method to the FoS values obtained from the commercial SLOPE/W software package. This was done for various slopes types, pore pressure conditions, material zones and material strengths for the Bishop, Janbu and Spencer methods.

Once the accuracy of the slope analysis tool was verified, the resulting FoS values were compared for the various scenarios considered, and conclusions were drawn. Uniform shear strains along the slip surface were mobilised in fixed increments and calculated FoS values were obtained based on the strength inferred from the triaxial test results for the applicable strain value. The strength assigned at the base of each slice was varied, depending on the scenario, and ranged from the use of CD strengths only, the use of CU strengths only and a combination of CD and CU strengths. As an additional comparison, finite element strength reduction analyses were also used to determine a Safety Factor (SF). In total, six scenarios in terms of assumptions regarding drained and undrained behaviour and the method of stability analysis used, were assessed. These six scenarios were assessed for each of the three cross sections defined and this was done for each tailings material. As an additional check, the proposed method was tested using test data on Nerlerk sand, a well know sand showing strain-softening during undrained shearing. Conclusions were then drawn based on the results of these analyses.

1.5 ORGANISATION OF THE REPORT

The report consists of the following chapters and appendices:

- Chapter 1 serves as introduction to the report. It contains the introduction, objectives, scope and methodology followed during the study.
- Chapter 2 contains a literature study on the topic of this report. It provides a background to the study as well as the current state of knowledge of the topic. Details include the definition of soil strength, methods to determine the strength of a soil both in the field and in the laboratory, a comparison of these methods, general details of tailings dams and tailings material, methods to assess the stability of slopes, as well as general comments on the current practice for slope stability analysis.
- Chapter 3 describes the methodology followed during this study. Results from the series of triaxial tests, the development and use of a spreadsheet-based strain mobilisation method to calculate a FoS and the variation of strength based on strain compatibility are discussed.
- Chapter 4 contains the results from the analysis as well as a review and discussion of these results.
- Chapter 5 contains the conclusions and recommendations of the study.
- A list of references used in the report is provided.
- Appendix A contains detailed results from the triaxial tests reviewed.
- Appendix B contains the assumptions made when interpreting axial and shear strains from the triaxial test results.
- Appendix C presents the verification of the spreadsheet used to implement the proposed limit equilibrium method.
- Appendix D contains detailed results of the GeoStudio analyses.
- Appendix E contains detailed FoS results and a comparison of the calculated FoS values for the various scenarios.

2 LITERATURE REVIEW

2.1 INTRODUCTION

The previous chapter provides an introduction to the report. The background, objectives and scope of the study were presented as well as a methodology detailing how the objectives would be achieved. This chapter provides an overview of the current state of knowledge in the areas relevant to this study by means of a literature review. These areas include tailings materials and tailings dams, soil strength, the determination of soil strength using field and laboratory test methods and its use in slope stability analysis.

In particular, methods to estimate drained and undrained soil strength from laboratory and field test were reviewed. As the basis for this study was the use of triaxial test data, the various types of triaxial tests are discussed and methods to assess the raw data and estimate soil parameters from triaxial compression tests were reviewed. Tailings dams and tailings materials were also investigated, with particular focus on the characteristics of tailings materials. The assessment of slope stability using drained and undrained strengths was then reviewed, the various methods available were assessed and the advantages and limitations of each method discussed. Current practice to assess slope stability considering drained and undrained strengths implemented in limit equilibrium slope stability analyses was also investigated.

2.2 TAILINGS DAMS

2.2.1 Tailings dam fundamentals

The term tailings (or slimes) is used to refer to the crushed rock particles produced as a by-product of the mining process (Vick, 1983). To enable the optimum resource extraction, the ore is typically ground to silt size particles, pumped in slurry form, and hydraulically deposited onto large stockpiles called tailings dams**.** In general, there are three types of construction methods for tailings dams and these are shown in Figure 2.1. Upstream construction (Figure 2.1a) is the oldest and most common method used in South Africa. Although it can be the most cost-effective option, it is the most susceptible to liquefactions and post-earthquake deformations.

Downstream construction (Figure 2.1b) is a more stable option compared to upstream constructed dams as there is no possibility of a slip surface developing through previously deposited tailings material. However significantly more coarse material is required to construct the outer wall. As shown in Figure 2.1b, for the same dam height, this volume of embankment fill material required

can be in the order of three times as much as that required for the upstream constructed method. Downstream methods also require careful advance planning as the footprint of the dam increases with each successive lift.

The centreline method shares advantages from both the upstream and downstream methods (see Figure 2.1c). For example, less embankment fill material is required that the downstream method and there is an improvement in seismic resistance compared to the upstream method. The type of construction method used is usually based on a range of site-specific factors including tailings type, deposition method, deposition rate, water requirements, seismic activity in the area, available area, local geology, local communities, etc.

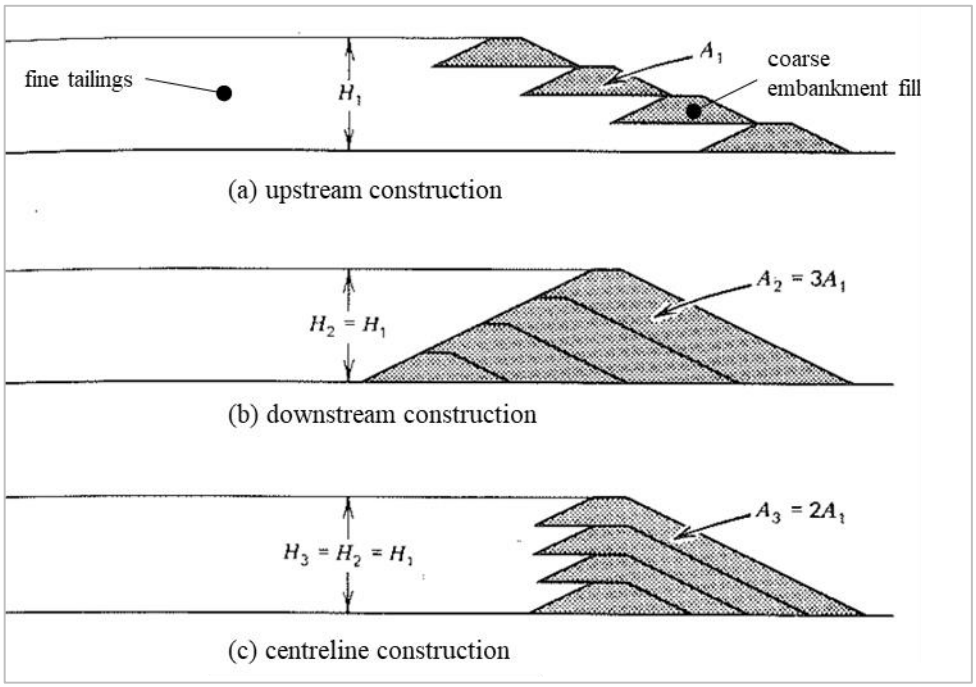

Figure 2.1: Typical tailings dam construction methods, after Vick (1983)

For the majority of tailings dams, tailings is deposited as a slurry. However, with the advent of new technologies, methods to dewater the tailings prior to deposition including thickened, paste and filtered tailings are being explored (e.g. KCB, 2017). Another challenge is that there is no single, centralised global tailings database. To address this, the Investor Mining and Tailings Safety Initiative group issued a tailings information disclosure request to 726 publicly listed mining companies in 2019. Based on the results of this request, several researchers around the world have collaborated and developed an informal database using this publicly available information (e.g. Franks et al., 2021). The aim of this initiative is to provide insights into the global composition of tailings dams and assist in global governance of tailings dam stability risks.

2.2.2 Variation of density within tailings dams

Tailings is not a natural occurring material, rather, it is a product of a carefully controlled ore extraction process. As a result, the natural variance expected in most soils is not expected for tailings. As the tailings is generally deposited as a slurry, the initial void ratio is high. However, once the tailings is deposited onto the tailings dam, the free water naturally flows towards the centre of the dam and the particles begin to settle along the beach (e.g. Vick, 1983). At this point, drying of the tailings by the sun results in desiccation which reduces the void ratio and consolidation begins. Over time this process results in a general decrease in void ratio with depth (e.g. Vermeulen, 2001). However, several researchers have shown that there is not a significant change in density with depth in typical tailings dams where the production and deposition process (and rate) has remained unchanged.

In one particular study (Jamiolkowski & Masella, 2015), a combination of field tests (cross hole tests) and triaxial compression tests using undisturbed samples obtained from gel push samplers gathered over a period of almost two decades from a copper tailings dam in Poland were assessed. Based on the assessment of these test results, the calculated void ratios with depth were estimated as shown in Figure 2.2. Assuming the material was saturated and, using the specific gravity of 2.75 provided, the saturated densities ranged from 1.88 kN/m^3 to 2.09 kN/m^3. This implies that the results showed that there is very little change in density with depth (<12%), even over the 60 m depth of the tailings dam. A similar trend was found by Blight (2009) as shown in Figure 2.3, although it is unclear at which facility these measurements were obtained.

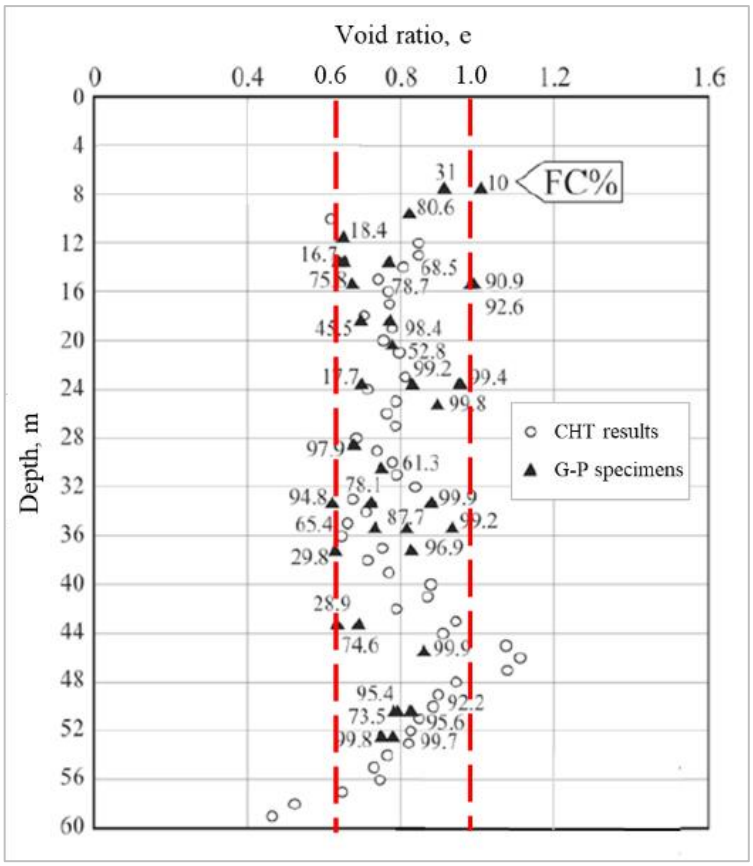

Figure 2.2: Void ratio with depth at Zelazny Most tailings dam, after Jamiolkowski & Masella (2015)

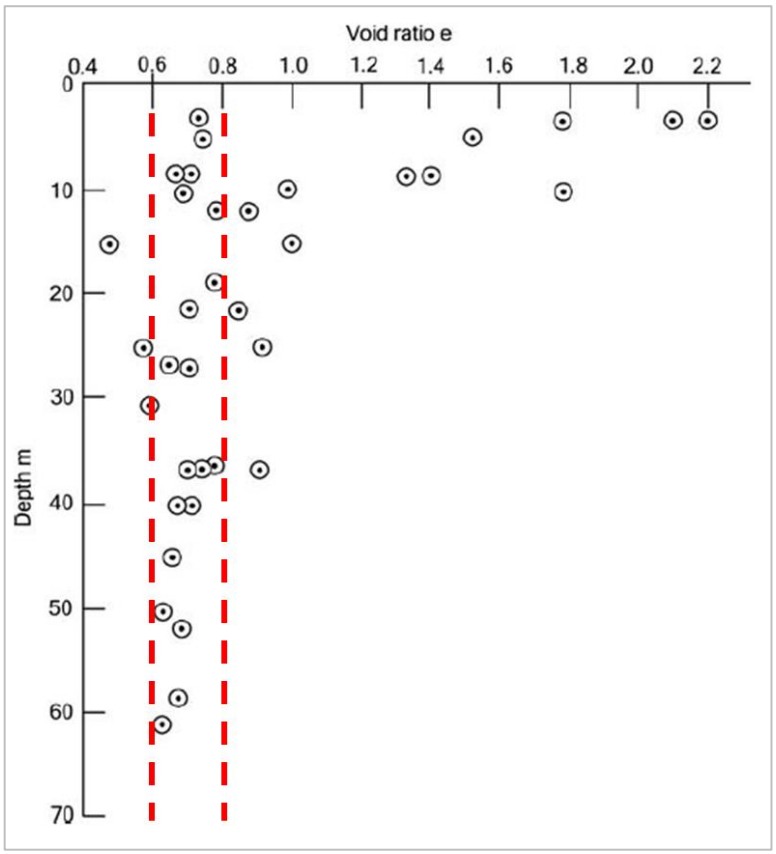

Figure 2.3: Measured void ratio with depth on a copper tailings facility, after Blight (2009)

It is well established that the behaviour of soil is dependent on the state of the soil (i.e. density, fabric and stress state). This is discussed further in Section 2.3.1. However, if it is assumed that the tailings is a homogeneous material, and that there is no significant change in density with depth and no significant fabric effects, then it can be assumed that the behaviour of tailings within the tailings dam is only dependent on the stress state (confining pressure). This assumption can significantly simplify the modelling of soil behaviour.

However, it is important to note that this may only be applicable to the type of tailings being considered. For example, as part of the deposition process, the tailings naturally segregates into a fine and coarse fractions and the density of these two fractions vary significantly (Vermeulen, 2001). Therefore, this assumption of uniform density with depth can only be made within the bounds of these fine and coarse material zones.

2.2.3 Review of recent tailings dam failures

As mentioned in the Introduction, an important motivation for this research was the recent international tailings dam failures reported widely in the media. Three events in particular were mentioned and are discussed further in this chapter.

2.2.3.1 Merriespruit tailings dam, South Africa

The Merriespruit gold tailings dam in Virginia, South Africa, failed in 1994 and resulted in 17 deaths (Fourie et al., 2001). The dam was operated using the upstream daywall paddock construction method which is the most common method of construction of gold tailings dams in South Africa due to the country's favourable climate. The failure occurred after a rainfall event and approximately 0.6 million m^3 of tailings material was released to the downstream village of Merriespruit. It remains one of the worst tailings dam failures in South Africa in terms of environmental and social impact.

Stability analyses were conducted by the tailings dam operator prior to the failure. Bishops' method and effective stress parameters (friction angle of 35° and cohesion of 2 kPa) were used and a FoS against failure of 1.34 was calculated. The analysis was reviewed after the failure by Fourie et al. (2001) with updated material properties (friction angle of 33° and cohesion of 0 kPa, which were believed to be lower bound strength values) and a FoS against failure of 1.24 was calculated.

It was concluded that the FoS was acceptably safe from a slope-stability perspective. Rather, it was theorised that failure occurred due to overtopping of the outer wall and the subsequent progressive failure of the lower benches as shown in Figure 2.4 (Wagener, 1997).

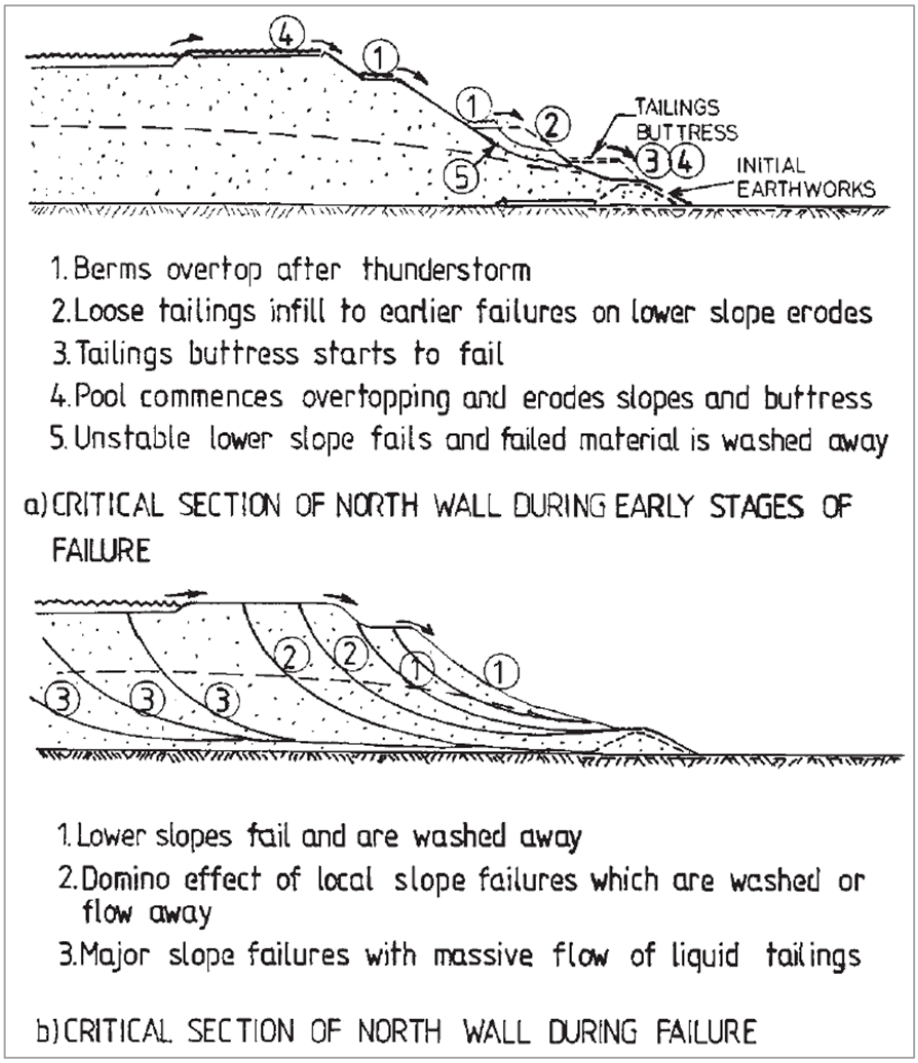

Figure 2.4: Sequence of progressive failures as postulated by (Wagener, 1997)

2.2.3.2 Fundão tailings dam, Brazil

The Fundão iron ore tailings dam in Minas Gerais, Brazil, failed in 2015 and resulted in 19 deaths (do Carmo et al., 2017). As is common for iron ore tailings dams, the dam was constructed in an upstream manner with a wide outer zone consisting of coarse sands (equal portions of sand and silt-sized particles) which retained the slimes (fine grained particles, clayey in nature) (Morgenstern et al., 2016). The failure occurred 90 minutes after a seismic event (although it was later shown that this was not the cause) and approximately 43 Mm^3 of tailings material flowed 660 km to the Atlantic Ocean. As part of the investigation report, two critical cross sections were identified: the left abutment and the right abutment. The location of these abutments is shown in Figure 2.5.

Figure 2.5: Location of the right and left abutments of the Fundão tailings dam, after Morgenstern et al. (2016)

As part of the investigation, stability analyses were conducted by the panel. The method suggested by Brown & Gillani (2016) was used where material exhibiting potentially dilative behaviour under undrained shearing is assigned effective strengths and material exhibiting potentially contractive behaviour under undrained shearing is assigned undrained shear strengths. In this case, a friction angle of 33° and cohesion of 0 kPa were used for the effective strengths and an undrained stress ratio, $\frac{s_u(yield)}{\sigma'_{v0}} = 0.22\ for\ Direct\ Simple\ Shear$ was used for the undrained strengths.

Failure was attributed to liquefaction of the sands as a result of the lateral extrusion of a slimes layer that had encroached onto the sands zone. This extrusion resulted in a significant loss of horizontal confining stress of the sand which resulted in the sand changing to a looser state and essentially collapsing.

It is interesting to note is that the calculated FoS against failure for the left abutment (where failure did occur) was 3.01 considering effective strengths and 1.33 considering undrained strengths while the FoS for the right abutment (where failure did not occur) was 1.91 considering effective strengths and 0.92 considering undrained strengths.

Regarding the left abutment, where failure did occur, it should be noted that the calculated FoS was based on the assumed peak (yield) undrained shear strength. Due to the extrusion of the slimes layer, significant shear strains were induced in the sands resulting in the mobilisation of the residual (steady state) shear strength. As shown in Figure 2.9, for materials in a contractive state

the residual shear strength is significantly lower than the peak shear strength. The calculated FoS associated with the residual shear strength is below 1.0 which explains why failure occurred at the left abutment.

Despite the fact that a FoS less than 1.0 was calculated, failure did not occur at the right abutment. This is due to the fact that the FoS was calculated assuming the conditions were such that undrained shearing occurred. These conditions were not present and therefore the failure mechanism for which the FoS was calculated did not occur. The calculated FoS considering effective strengths was 1.91 which is why failure did not occur at the right abutment.

2.2.3.3 Feijão tailings dam, Brazil

The Feijão iron ore tailings dam in Minas Gerais, Brazil, failed in 2019 and resulted in 250 deaths (Robertson et al., 2019). The dam was constructed using the upstream method and was dormant at the time of failure, with the most recent deposition occurring in 2016. After the failure, approximately 9.7 Mm^3 of tailings material flowed through the downstream town of Brumadinho. This is one of the more interesting failures as, due to the recent Fundão tailings dam failure in 2015, video monitoring was in place for high-risk facilities. As such, there is a video available online showing the moment of failure (https://www.youtube.com/watch?v=sKZUZQytads). The video provides a stark reminder to the sudden and violent failure mechanism of undrained failure.

Due to the high iron content, light chemical bonds formed between the tailings particles. While these bonds remained in place, the material exhibited certain strength characteristic but once the bonds were broken, there was a sudden loss in strength. This is shown in Figure 2.6.

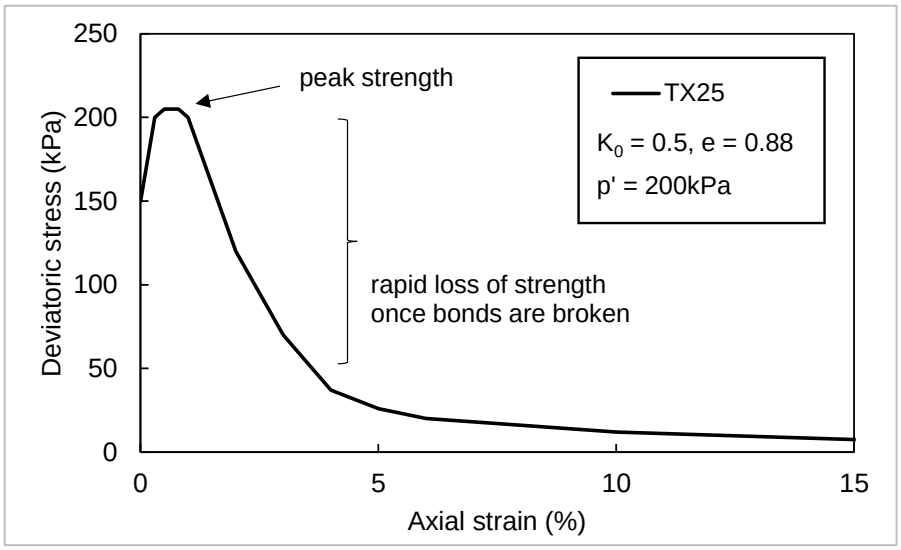

Figure 2.6: Results from a triaxial compression test performed on the Feijão iron tailings

An audit of the facility was conducted in 2018 and Line E-E was identified as the critical cross section as shown in Figure 2.7 (TÜV-SÜD, 2018). Stability analyses were conducted considering effective strengths (friction angle of 35° and cohesion of 0 kPa in this case) and undrained strengths (undrained stress ratio $\frac{s_u(yield)}{\sigma'_{v0}} = 0.26$ in this case). A FoS of 1.60 was determined for effective strengths and a FoS of 1.09 was determined for undrained strengths, respectively.

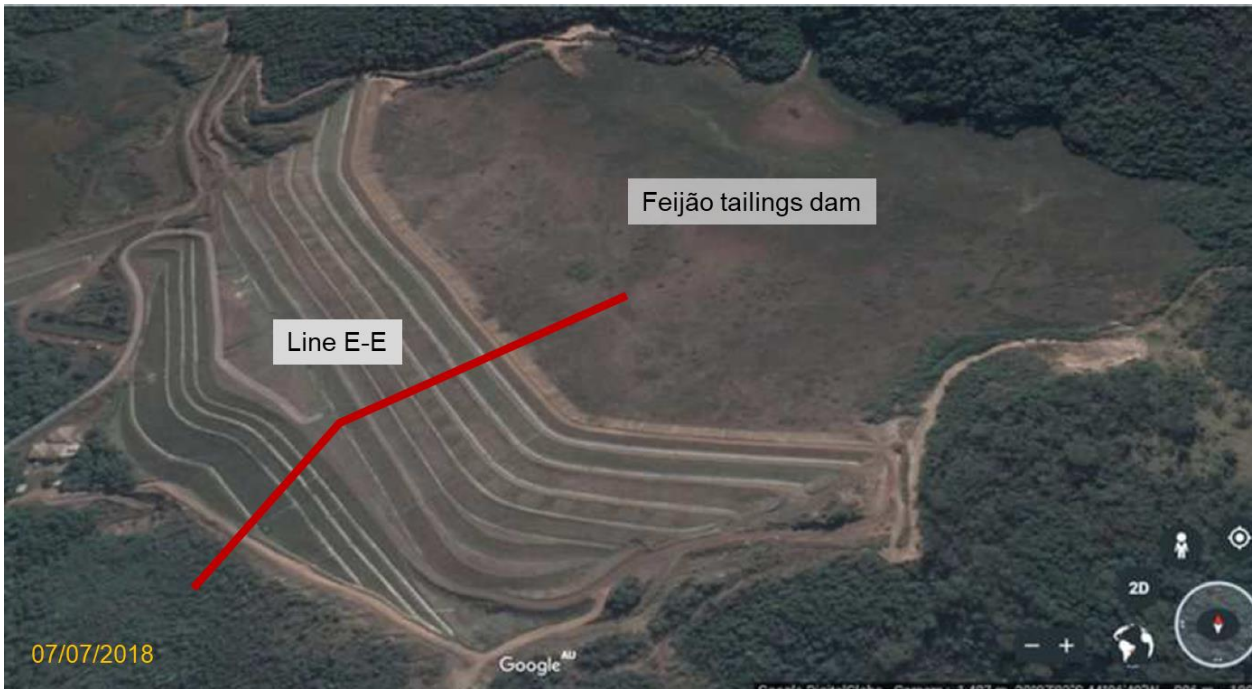

Figure 2.7: Location of Line E-E, after TÜV-SÜD (2018) and Robertson et al. (2019)

Although toe drains and blanket drains were constructed in most of the recent raisings, no internal drainage systems were installed as part of the initial starter wall construction. This resulted in poor drainage and high water levels in the facility. In addition, infiltration during storm events was determined to be 50% of the mean annual precipitation of 1 400 mm. The combination of the infiltration and poor drainage resulted in a loss of suction in the previously unsaturated regions of the slope, thereby reducing the stability of the slope. The effects of both the loss of suction and internal creep resulted in the breaking of the bonds between the tailings particles and failure of the embankment (Robertson et al., 2019).

It is interesting to note that the facility included a robust monitoring system comprising standpipe piezometers, survey markers, inclinometers and flow meters. However, due to the sudden and abrupt nature of the failure, none of the monitoring devices detected precursors to failure. This seems to suggest that alternate methods of monitoring are required when brittle failure

mechanisms are expected.

2.2.3.4 Summary

Three tailings dam failure case histories were briefly presented and key parameters in terms of FoS values, triggers and failures are noted in Table 2.1. Of particular interest is the left abutment at Fundão and Line E-E at Feijão where failure occurred with a USA FoS > 1.0 (trigger present) and the right abutment at Fundão where failure did not occur with a USA FoS < 1.0 (trigger not present). Based on this, it is clear that there are still some shortcomings in the conventional methods of assessing slope stability. It should be noted that all the analyses were conducted using the method proposed by Brown & Gillani (2016) and, in using this method, compatibility of strains is not considered.

Table 2.1: Summary of stability analyses of tailings dam case histories

	FoS (effective stress analysis)	FoS (undrained stress analysis)	Trigger?	Failure?
Merriespruit (North wall)	1.24	-	Yes (overtopping)	Yes
Fundão (left abutment)	3.01	1.33	Yes (lateral extrusion)	Yes
Fundão (right abutment)	1.91	0.92	No	No
Feijão (Line E-E)	1.60	1.09	Yes (internal creep and rainfall infiltration)	Yes

2.3 SOIL STRENGTH

2.3.1 Soil shear strength

Critical State Soil Mechanics (CSSM) provides a framework for the mathematical modelling of soil behaviour. The fundamental principle of CSSM is that the mechanical behaviour of soil depends on the state of the soil. However, it is important to note that the resultant shear strength of a soil is not an intrinsic parameter and varies according to the state of the soil (i.e. void ratio, stress conditions and the arrangement of the particles) (Jefferies & Been, 2015).

2.3.2 Drained and undrained shear strengths

Depending on the state of the soil and the associated shearing conditions, different shear strengths can be mobilised. These range from pure drained strengths to pure undrained strengths and include a combination of the two.

For a given soil at a particular state, the fundamental difference between drained and undrained strengths lies in the shearing conditions. During shear, soil can behave in one of three manners: completely undrained, partially drained or completely drained. For a saturated soil, the mere action of shearing will always induce a change in the pore pressures in the soil. The type of pore pressure change depends on the state of the soil (i.e. a contractive soil will generate positive pore pressures and a dilative soil will generate negative pore pressures) but, at the moment of shearing, there will always be a change in the pore pressure of the soil.

If the shearing is sufficiently fast that there is no drainage of shear induced pore pressure, the undrained strength is mobilised, and undrained strength parameters can be used (i.e. s_u/σ'_{v0}). If, however, the shearing is at a slow enough rate that all the shear induced pore pressures dissipate, the drained shear strength will be mobilised, and effective strength parameters can be used (i.e. ϕ' and c').

If the shearing is neither fast enough for undrained conditions to develop nor slow enough for drained conditions to develop, then partially drained conditions will occur and a strength between the drained and undrained strength will be mobilised. It is important to identify these conditions as there is a significant difference in strength. Under the same effective stress, peak undrained strengths are typically only half of the peak drained strengths (Olson & Stark, 2003a).

2.3.2.1 Undrained strength responses

Castro (1969) performed a series of triaxial compression tests on Ottowa Sand and observed that the soil behaved in one of three manners when subjected to monotonic undrained shear. As shown in Figure 2.8; at low void ratios the soil has a Dilative Response (DR); at intermediate void ratios the soil has a Limited Liquefaction (LL) response and at high void ratios the soil has a Liquefaction Failure (LF) response. The undrained strength of a soil is therefore highly dependent on the void ratio.

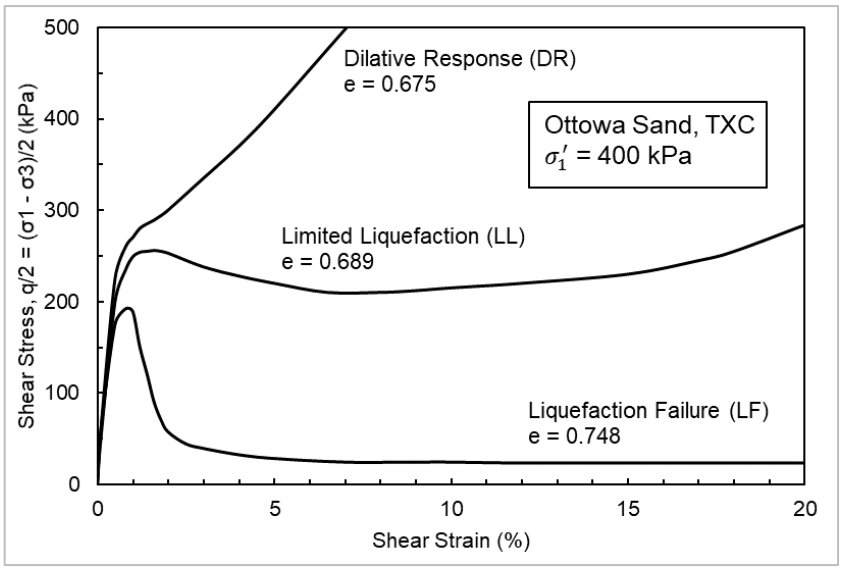

Figure 2.8: Three material responses to monotonic undrained shear, after Castro (1969)

For this assessment, only the peak (yield) undrained strength as defined by Olson & Mattson (2008) is considered (see Figure 2.9). This distinction is not required for drained strengths as all three responses yield the same drained strength properties (friction angle and cohesion intercept) as shown in Figure 2.10.

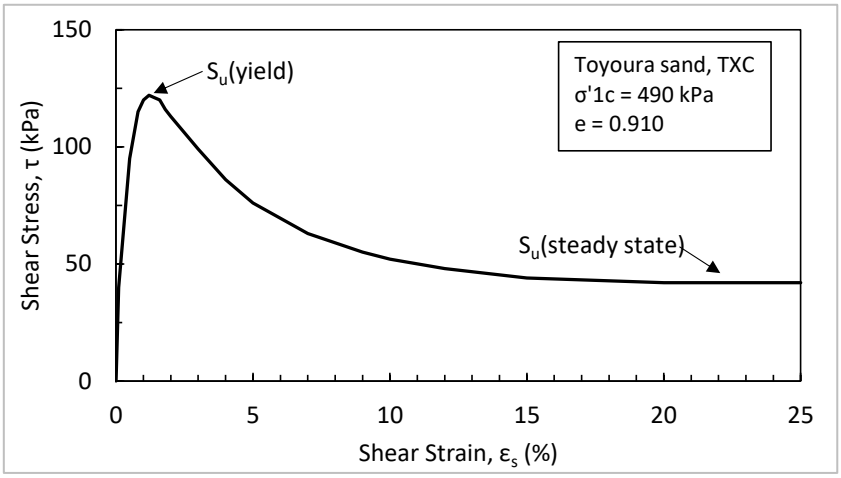

Figure 2.9: Yield and steady state undrained shear strength, after Olson & Mattson (2008)

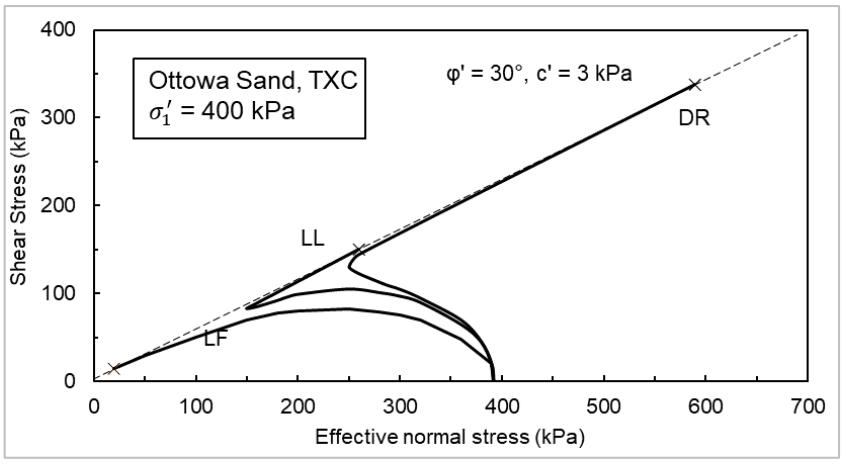

Figure 2.10: Consistent effective stress strength properties for all three responses, after Castro (1969)

2.3.2.2 Yield strength envelope

Several researchers have conducted consolidated undrained triaxial compression tests on loose contractive sands at various densities and effective stress values (e.g. Sladen et al., 1985; Sasitharan et al., 1993). Based on these results, it was found that the yield undrained shear strengths when plotted in deviator stress vs. mean effective stress space approximated a similar envelope to the failure envelope. This was termed the peak strength envelope (sometimes also referred to as the collapse surface) and can be seen in Figure 2.11. In the figure, the peak (yield) undrained shear strengths are denoted with squares and the steady state (residual) undrained shear strengths are denoted with circles. It is clear that there is a significant difference in mobilised shear strength between these two states.

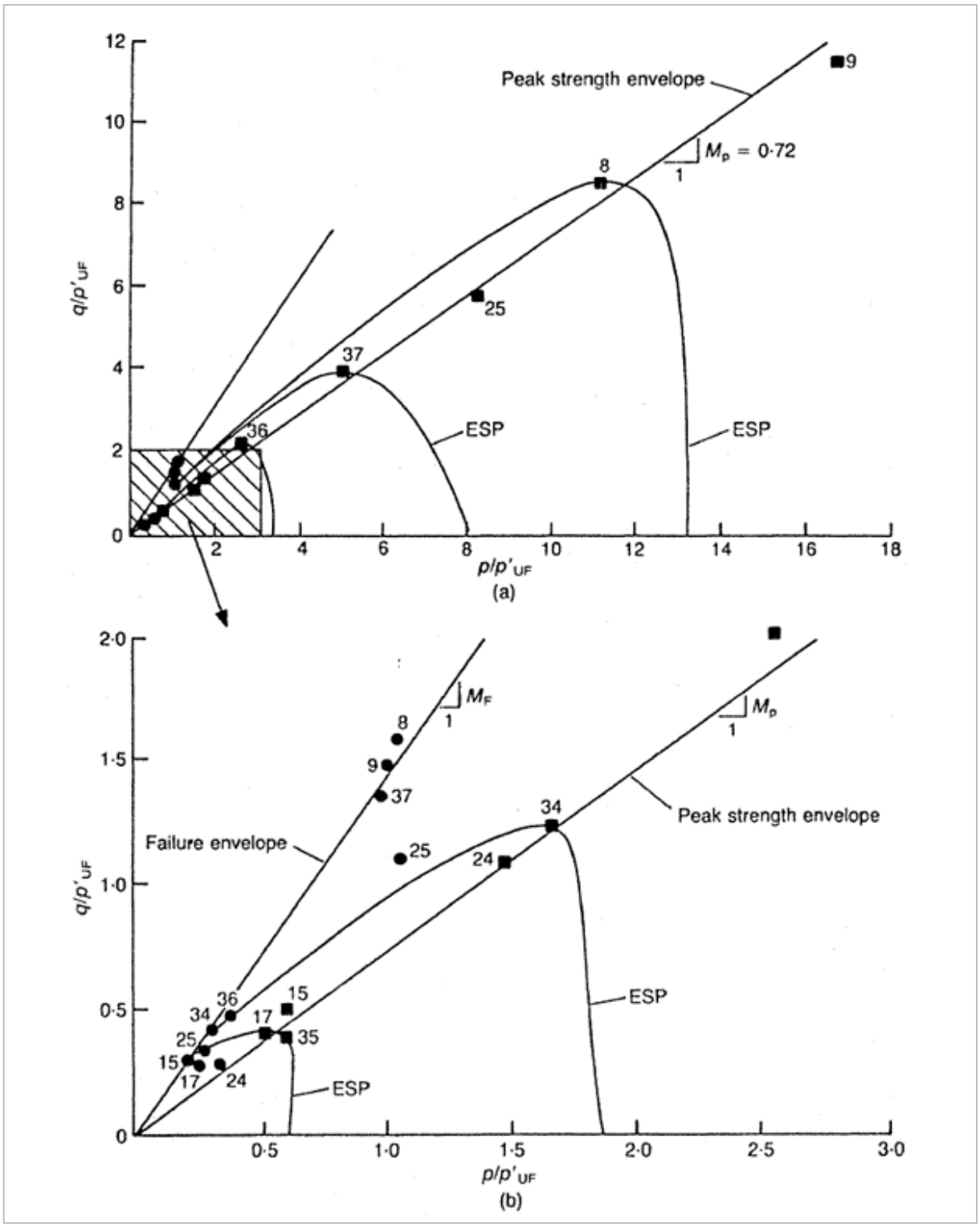

Figure 2.11: Summary of consolidated undrained triaxial compression tests on Hostun RF sand (Konrad, 1993)

The slope of the line that represent the peak strength envelope can be defined as the Yield Strength Ratio (YSR) as shown in Equation (1). Although the expression is in terms of vertical effective stress (as opposed to normal effective stress as in the case of the failure envelope), in most cases

the effect is minimal and these two envelopes can be compared directly (Olson, 2001).

$$YSR = \frac{s_u(yield)}{\sigma'_{v0}} \approx \tan \varphi_y \quad (1)$$

2.3.3 Applicability of undrained shear strengths

Undrained shear strengths can only be mobilised when shearing occurs in such a manner that the shear-induced pore pressures are not able to dissipate and there is a subsequent change in the effective stress of the soil. Since the dissipation is a time-dependent process, it follows that only fine-grained soils which typically exhibit low permeability and slow drainage properties would be susceptible to undrained shearing.

However, several researchers have shown that this is not the case. In one particular study (Eckersley, 1990), a series of scale tests were conducted on coarse-grained coal stockpiles. Failure was induced by slowly raising the phreatic surface in the model, thereby reducing the effective stress. After a careful analysis of the results, and expanding on previous research, it was concluded that flowslides can initiate under static, drained conditions with failure occurring due to shear induced excess pore pressures in thin shear zone along the slip surface. This process of instability under static loading was eloquently described as follows:

“When subjected to very slow, drained increases in shear stress, the soil contracts, and water is expelled from the voids until a point of inherent instability is reached. At this point even the slightest increment of stress or strain results in such rapid generation of excess pore pressures in comparison to the drainage capacity of the soil that shear strength drops rapidly to the steady state value. The applied stresses can then no longer be sustained, and rapid acceleration occurs.”

It should be noted that undrained shear strengths can only be mobilised if the conditions exist that are conducive to undrained shearing. Olson (2001) describes the presence of these conditions and the subsequent mobilisation of undrained shear strengths as a triggering mechanism. Attempts to quantify potential trigger mechanisms have been made, many with regard specifically to upstream tailings dams (e.g. Martin & McRoberts, 1999). In their research, Martin & McRoberts (1999) developed a list of potential triggers for upstream tailings dam, applicable over the entire life cycle. This list is shown in Table 2.2. It was concluded that a prudent approach would be to assume that, if a plausible trigger existed, undrained strengths could be mobilised.

Table 2.2: Triggering mechanisms for undrained failures of upstream tailings dams (Martin & McRoberts, 1999)

Mechanism	Trigger
Oversteepening at the toe due to:	• erosion (for example as a result of storm run-off or pipeline break causing washout); • localised, initially drained sloughing; and/or • construction activities (such as excavations).
Overloading due to:	• rapid rate of impoundment raising; • steepening at the crest; and/or • construction activities at the crest.
Changes in pore pressures due to:	• seepage breakout on the face of the dam; • deterioration in performance of underdrainage measures; • inhibited volumetric creep; • concentrated tailings discharge from one location for an extended period; • leakage/rupture of low level outlet; • accelerated rate of construction; • foundation and/or embankment movement; • intense rainstorms; and/or • increased pond levels.
Triggering collapse surface by reduction in mean effective stress	Consider an element of soil below the collapse surface with a low shear stress and high mean effective stress due to low or absent phreatic surface. Saturating the slope reduces mean effective stress, but leaves shear stress constant. The reducing mean effective stress results in contact with the collapse surface and liquefaction is triggered.
Overtopping due to:	• severe storm run-off; • failure of diversion dams/ditches; • blockage and failure of spillways/decants; and/or • seismic deformation and loss of freeboard.
Acceleration/vibrations due to:	• earthquakes; • construction traffic; and/or • blasting.

Further work has since been carried out by Anglo American Plc as part of their internal standard on the management of tailings storage facilities (AA TS 602). In a supporting guideline document,

the following is noted (Anglo American, 2018):

"Hydraulically-deposited tailings, the void spaces of which are pore-water saturated, shall be assumed susceptible to liquefaction unless demonstrated otherwise by rigorous field and soils laboratory investigations"

As liquefaction is a consequence of failure and is typically a result of undrained shearing, the statement above can be interpreted that any saturated tailings material should be considered as potentially contractive during undrained shearing It should be noted that this document is still in draft form and was developed specifically with upstream constructed tailings dams in mind. Nonetheless, this guidance is still valuable in terms of a first order or screening assessment.

2.3.3.1 SHANSEP soil strength model

Measured undrained shear strengths, whether measured in the laboratory or in the field, are only applicable to a soil for the state at which the strength was measured. If the state of the soil changes, the measured undrained shear strength is no longer applicable. To overcome this, the Stress History and Normalised Soil Engineering Properties (SHANSEP) technique can be used. When using the SHANSEP technique, the undrained shear strength is defined as a ratio to the vertical effective stress on the soil. Using this ratio, the measured strength can be adjusted and used at varying effective stress levels (Ladd, 1991).

The SHANSEP strength model is very similar to a Mohr-Coulomb strength envelope with the difference that the derived shear strength is a function of the vertical effective stresses instead of the normal effective stresses. Since most undrained failures are dominated by Direct Simple Shear (DSS), this does not have a significant difference in the calculated FoS for undrained failures (Olson, 2001).

2.3.4 Effect of mode of shear

It is well established that the strength of a soil is dependent on the orientation of the applied principal stresses (e.g. Soydemir, 1972; Olson & Mattson, 2008; Sadrekarimi, 2014). There are three modes of shear that are applicable to slope stability problems: compression, simple shear and extension. An example of these modes of shear in a typical slipe surface is shown in Figure 2.12. For a slip from left to right, the initial segment will experience compression shear, the middle segment will experience simple shear and the last segment will experience extension shear. Boundaries between these segments have been proposed by Sadrekarimi (2014) and are based

on the counter-clockwise angle (α) of the failure plane to the horizontal. α values greater than or equal to 30° are considered to be in compression shear, α values less than 30° but greater than -15° are considered to be in simple shear and α values less than or equal to -15° are considered to be in extension shear.

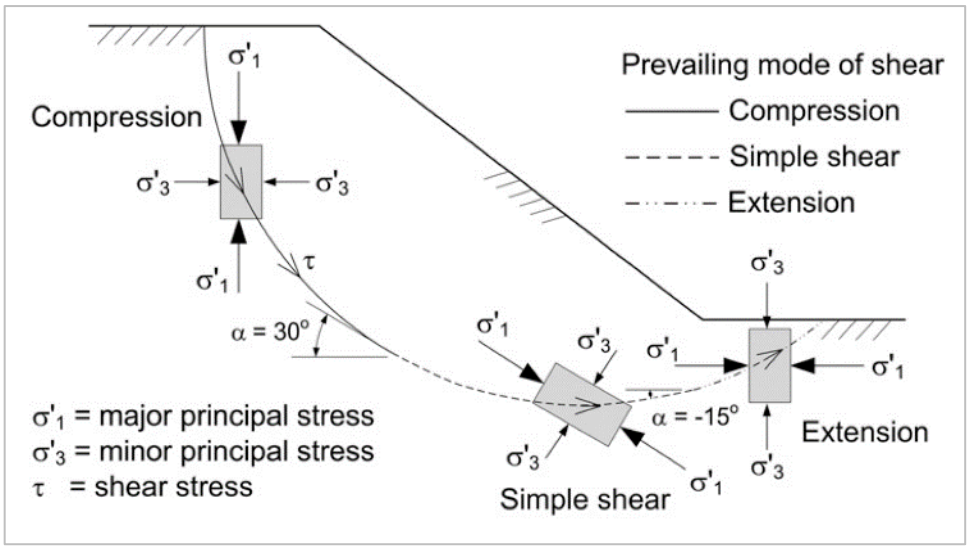

Figure 2.12: Mode of shear (Sadrekarimi, 2014)

As identified by Narainsamy et al. (2019), the inclusion of mode of shear strengths does appear to influence the FoS against slope failure for upstream constructed tailings dams. Although this influence is not significant, it is likely to make a difference in undrained slope stability analysis where FoS values are generally close to unity. It was recommended that the strength parameters based on the correct mode of shear values be included wherever undrained shear is likely to occur.

2.3.4.1 Comparison of strengths based on mode of shear

Several researchers have investigated the magnitude of shear strength mobilised dependent on the mode of shear being applied. In one particular study (Sadrekarimi, 2014), a comprehensive database of triaxial compression (TXC), triaxial extension (TXE) and direct simple shear (DSS) tests was analysed. Using this database, a unique relationship between undrained shear strength and undrained brittleness index (see Equation 21) was derived. In parallel, a database of field test results from liquefaction flow failures was also studied and a unique relationship between normalised cone resistance and undrained brittleness index was derived. By combining these relationships, a method to estimate the undrained shear strength based on normalised cone resistance, depending on the expected mode of shear was proposed. These relationships are presented graphically in Figure 2.13.

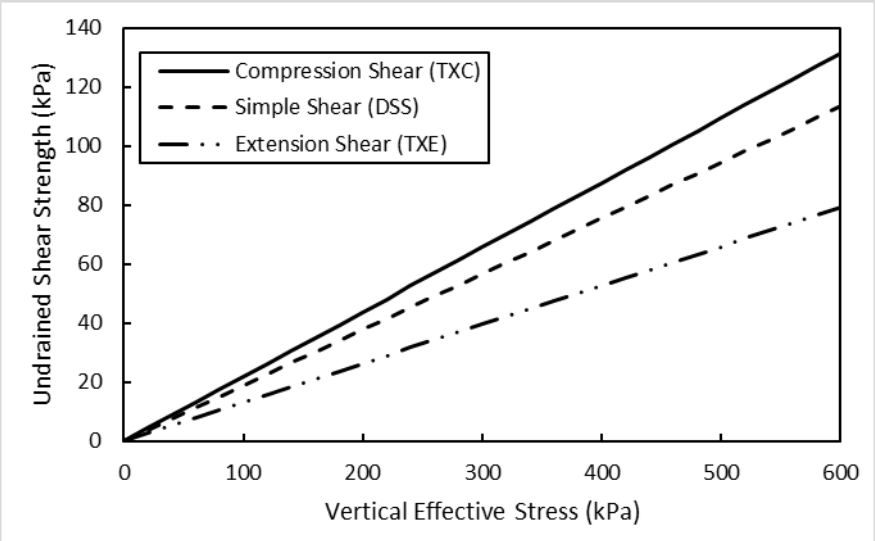

Figure 2.13: Difference in undrained strength between modes of shear, after Sadrekarimi (2014)

There are two key points that are relevant from this work. The first is that TXC strengths, which are typically used in South Africa, tend to overestimate the undrained shear strength of the soil in the DSS and TXE region. The second is that this overestimation is a function of the vertical effective stress the soil is subject to. At low stresses, the difference is minimal but at larger stresses the magnitude of the overestimation of the strength can be substantial. For example, consider a soil element as the base of a 30 m high tailings dam. Depending on the mode of shear, this particle could have an undrained shear strength on 90 kPa in TXC, 75 kPa in DSS and only 50 kPa in TXE.

2.3.4.2 Alternative methods of incorporating mode of shear

Although it is understood that the undrained shear strength of a soil is dependent on the mode of shear, it is not feasible to independently determine all three mode of shear strengths and the split between the zones for all projects. Therefore, several alternative methods have been investigated over the years. Two such alternatives are briefly discussed here.

The first method is based on the observation by Olson (2001), that the majority of the slip surface lies within the DSS region. This observation was made by conducting a comprehensive study of recorded liquefaction flow failure case histories. It was subsequently proposed that for material susceptible to undrained shearing, the use of the DSS strength over the entire slip surface was appropriate as the majority of the slip surface lies within this region. This method therefore only requires the DSS strength to be known.

A second method is that proposed by Koutsoftas & Ladd (1985) where an equal distribution between the three shear modes is assumed. An average stress-strain curve is then developed and

is used as the strength function for the stability assessment. This process is shown graphically in Figure 2.14. Although this method removes the requirement for determining the split between the zones where each mode of shear is applicable, it unfortunately still requires the TXC, TXE and DSS strengths to be known.

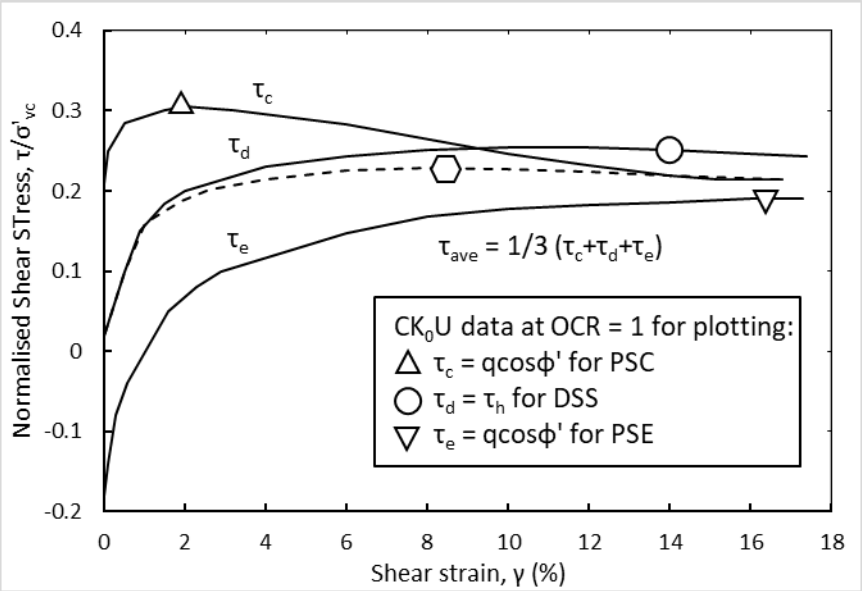

Figure 2.14: Normalised stress-strain data for AGS Marine Clay illustrating the strain compatibility technique, after Koutsoftas & Ladd (1985)

2.4 DETERMINING SOIL SHEAR STRENGTH USING LABORATORY TESTS

2.4.1 Determining shear strength using triaxial tests

2.4.1.1 Triaxial test fundamentals

The triaxial test is almost always chosen for soil studies because of its relative simplicity and versatility (Lade, 2016). The first triaxial compression tests were developed in the early 1910's (e.g. Lade, 2016) and have improved significantly since then. A diagrammatic layout of the basic components of a modern triaxial test is shown in Figure 2.15.

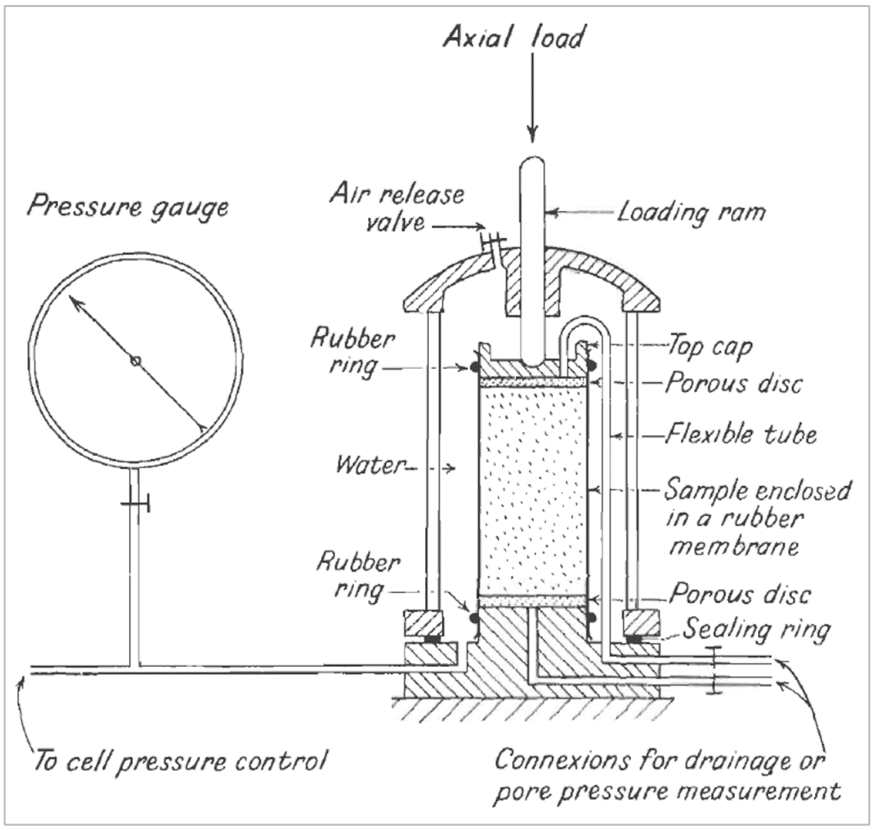

Figure 2.15: Diagrammatic layout of the triaxial test (Bishop & Henkel, 1962)

Triaxial testing is conducted to determine the mechanical properties of soil under loading conditions that are expected in the field. The properties typically sought are stress-strain relationships, volume change or pore pressure response to loading (depending on whether shearing is drained or undrained) and the shear strength of the soil. Depending on the type of test conducted, samples are either prepared at the desired density and moisture content, consolidated to the desired stress, and then sheared; or the samples are taken in situ and simply loaded into the triaxial test and sheared. An advantage of the triaxial test is that the loading conditions can be carefully controlled and pore pressure responses and volume changes can be accurately measured. A disadvantage is that only axis-symmetrical stress conditions can be applied to the specimen whereas field loading may be plane strain or three-dimensional.

Three types of triaxial tests are typically identified, although many other options are possible:

1. Consolidated Drained (CD). For the CD test, a reconstituted sample is typically used that is prepared to the desired density and moisture content. The sample is then consolidated to the desired effective stress and then sheared drained. CD tests take longer for slow draining materials but have the advantage that tests can be conducted at higher effective stresses.
2. Consolidated Undrained (CU). As per the CD test, a reconstituted sample is typically

used. Prepared at the desired density and moisture content, the sample is consolidated to the desired effective stress and then sheared undrained. Arguably the most popular test, CU tests have the advantage that, for slower draining materials, they can be conducted significantly faster than drained tests as the excess pore water pressure need only to stabilise and not return to zero. As these tests are typically conducted in commercial laboratories, a reduction in testing time results in a direct decrease in testing cost. A disadvantage of undrained tests is that the effective stress at which the sample can be tested is limited.

3. Unconsolidated Undrained (UU). Here there is no sample preparation or consolidation stage as the sample is tested in the in situ conditions (i.e. the current moisture content, density and effective stresses are representative of those in the field). The sample is loaded into the triaxial setup and sheared undrained. These tests are typically only possible of fine-grained materials for which obtaining undisturbed samples is possible.

Depending on the applied stress conditions, the above-mentioned tests can either be performed in triaxial compression (TXC) or triaxial extension (TXE). The difference between the two being the orientation of the major principal stresses. For TXC, the major principal stress is in the vertical (axial) direction where as in TXE, the major principal stress is in the horizontal (radial) direction.

2.4.1.2 Effect of sample preparation method

Various researchers have shown that the sample preparation methods used to create reconstituted samples affect the stress path followed in CU triaxial tests (e.g. Zlatovic & Ishihara 1997; Chang et al., 2011; Reid & Fanni, 2020). Two common methods are briefly described here as well as their typical effect on the stress path followed during shearing.

The preferred approach to capture the behaviour of soil under shearing at its in situ state is to perform tests on undisturbed samples. However, obtaining undisturbed silt samples is generally difficult, costly, and not part of routine geotechnical testing. Therefore, disturbed samples are generally collected from site and must be reconstituted before testing. A common method of loose sample preparation is the Moist Tamping (MT) method, where the sample is created by compacting moist material in a split mould to a target density (Ladd, 1978). A more recent method is the Remoulded Discontinuously Wet Pluvial Soil Sample (RDWPSS) method, also referred to as the Slurry Deposition (SD) method, where the sample is created in layers by pouring a predetermined mass of dry material into a split mould that is filled with de-aired water (Baziar & Dobry, 1991).

Chang et al. (2011) conducted a series of CU triaxial test to determine the effect of the two above-mentioned sample preparation methods on the behaviour of gold tailings. Although it was found that neither method was able to capture the behaviour of the undisturbed samples (see Figure 2.16), it was recommended that the SD method be used as a better fit was found than was the case for the MT samples. This is in line with the findings from Corrêa & Filho (2019) where the SD method was noted as the preferred method for sample preparation of tailings material as it results in a closer representation of the conditions under which the tailings is deposited.

This discrepancy between the stress-strain behaviour of tailings samples when comparing undisturbed and reconstituted samples, specifically on loose saturated materials is so fundamental that some researchers have recommended that stress paths obtained from reconstituted samples should neither be used in geotechnical design nor safety evaluation if an attempt has not been made to reproduce the in situ fabric (e.g. Høeg et al., 2000).

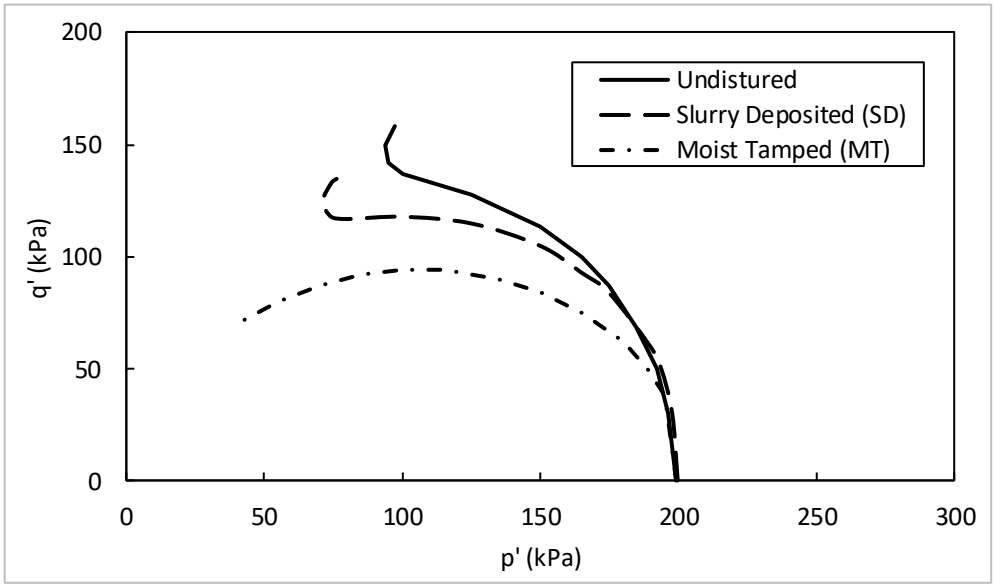

Figure 2.16: Effect of sample preparation method on soil behaviour during shear (Chang et al., 2011)

In general, it was found that for loosely prepared MT samples tended to exhibit a contractive tendency to steady state while SD samples tended to initially exhibit a contractive tendency and then undergo a phase transfer and exhibit a dilative tendency to steady state (Zlatovic & Ishihara, 1997). This is shown in Figure 2.17. Note that the curves have been normalised to the initial confining stress p_0.

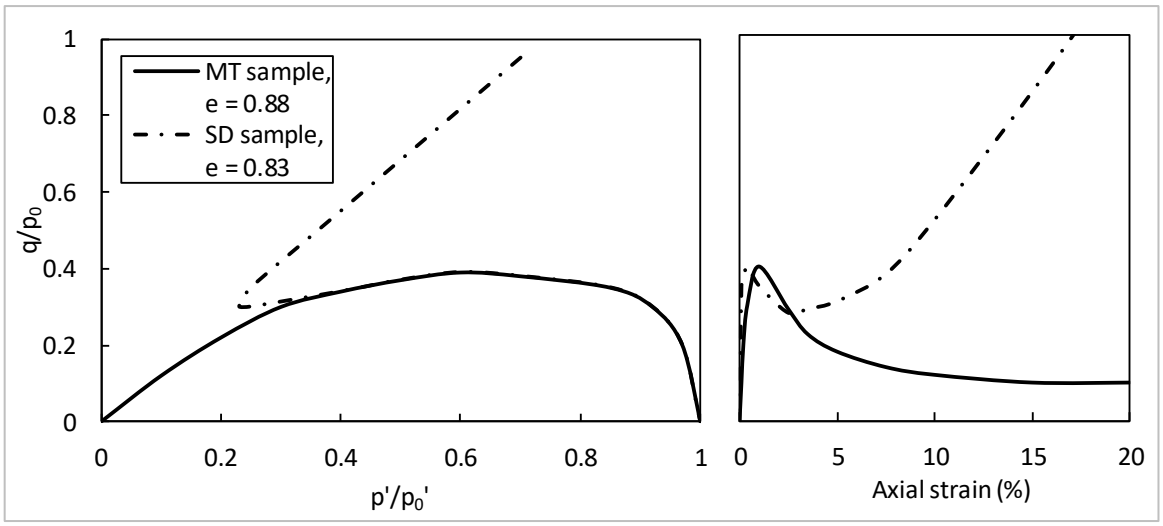

Figure 2.17: Typical stress paths of loose samples based on sample preparation method (after Zlatovic & Ishihara, 1997)

2.4.1.3 Estimating drained shear strength from triaxial tests

The results from triaxial tests are typically plotted using stress invariants as shown in Equations (2), (3) and (4).

$$s = \frac{\sigma_a - \sigma_r}{2} \quad \left(= \frac{\sigma_1 - \sigma_3}{2} \ for\ TXC\right) \tag{2}$$

$$t = \frac{\sigma_a + \sigma_r}{2} \quad \left(= \frac{\sigma_1 + \sigma_3}{2} \ for\ TXC\right) \tag{3}$$

$$s = t\,.\sin\varphi' + c'.\cos\varphi' \tag{4}$$

Where:

σ_a = Axial stress (kPa)

σ_r = Radial stress (kPa)

φ'= Mohr-Coulomb friction angle (°)

c' = Cohesion (kPa)

A diagram showing the derivation of the equations to calculate the Mohr-Coulomb strength parameters from the triaxial test data is shown in Figure 2.18.

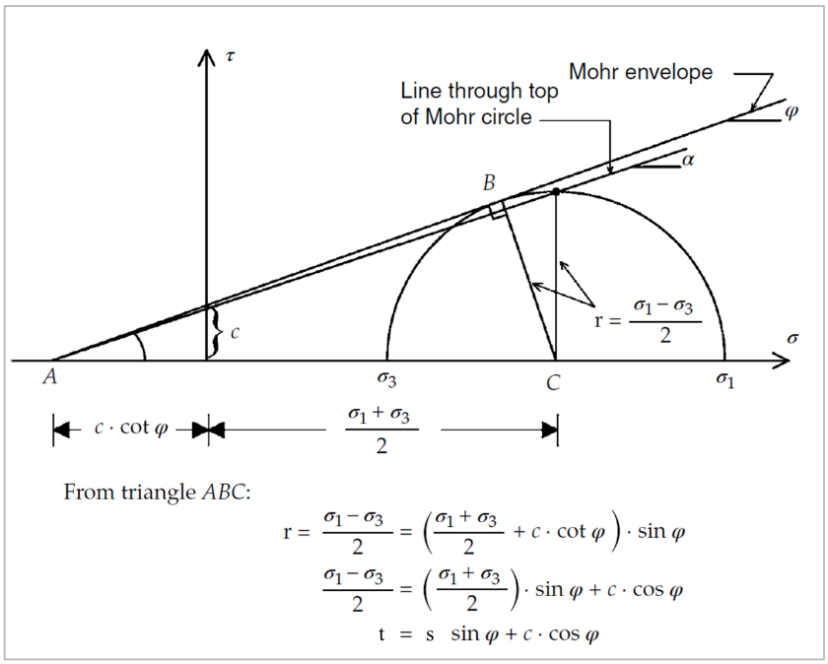

Figure 2.18: Derivation of the Mohr-Coulomb strength parameters, after Lade (2016)

2.4.1.4 Estimating undrained shear strength from triaxial tests

Undrained shear strength can be measured by performing UU triaxial tests. Note that it is only possible to measure a single value for the undrained shear strength of a soil using an UU triaxial test. By design, the UU triaxial test enables the measurement of the undrained shear strength at the assumed in situ conditions. A method of determining the undrained shear strength from the UU triaxial test data is shown in Equation (5). A sketch of the Mohr-circles that can be plotted from these results is shown in Figure 2.19.

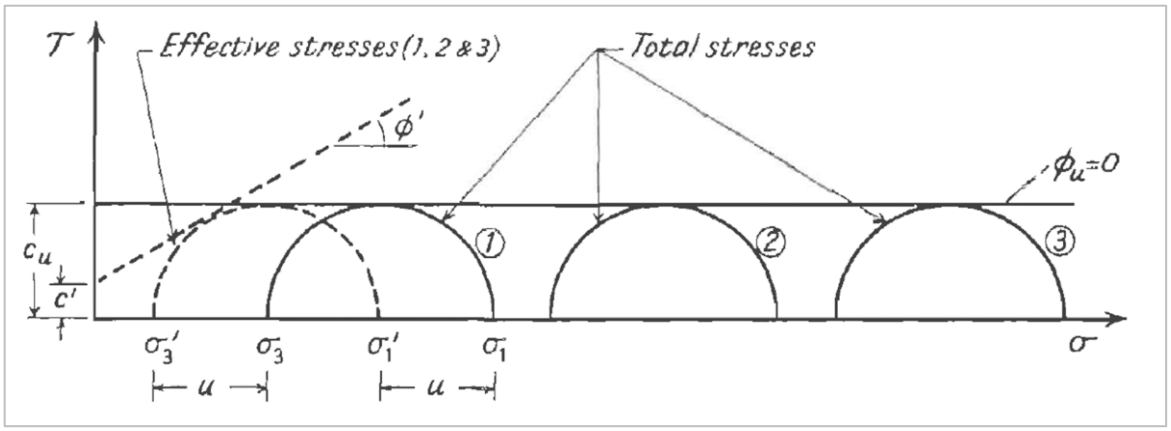

Figure 2.19: Determination of undrained strength from UU triaxial test (Bishop & Henkel, 1962)

$$c_u = \frac{\sigma_a - \sigma_r}{2} \quad \left(= \frac{\sigma_1 - \sigma_3}{2} \; for\; TXC\right) \tag{5}$$

Where:

c_u = Undrained shear strength, also referred to as s_u (kPa)

Alternatively, the yield and steady state undrained shear strength can be determined by interpreting the stress-strain graph from CU tests as shown in Figure 2.20. The distinct peak and then reduction to a steady state value is typical of strain-softening material.

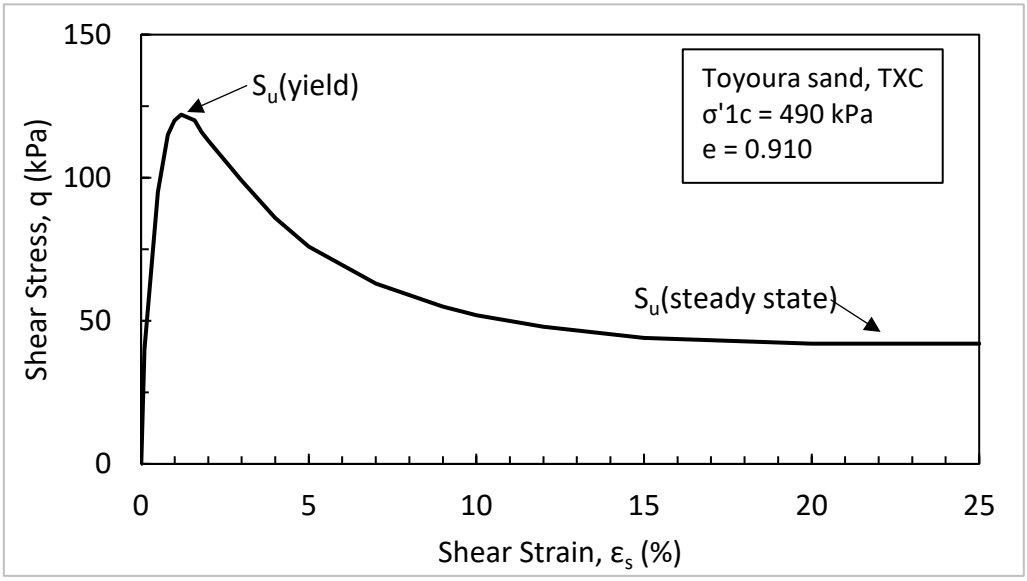

Figure 2.20: Results from TXC tests on Toyoura sand, after Olson & Mattson (2008)

Depending on the state of the soil, the yield undrained strength can either be lower than the drained strength (if the material is normally consolidated or lightly overconsolidated) or greater than the drained strength (if the material is heavily overconsolidated). The terms lightly overconsolidated and heavily overconsolidated are analogous with the terms “on the wet side of the CSL” and “on the dry side of the Critical State Locus (CSL)” respectively. Note that this is general statement and is more applicable to fine grained soils that tend to have a unique Normal Consolidation Line (NCL), also referred to as an Isotropic Compression Line (ICL). The behaviour of coarse-grained soils that tend to have an infinite number of NCL cannot easily be classified in terms of degree of overconsolidation.

2.4.1.5 Interpreting shear stresses from triaxial test data

Due to the nature of the shearing phase of a triaxial test, where the load and the deflection is applied and measured axially, the behaviour of the soil during shear is typically plotted on a shear stress (deviatoric stress) versus axial strain graph. However, during shear failure in the field, it is

useful to relate soil behaviour to shear strains and not axial strains.

As it is simplest, the relationships for CU tests, where there is no change in volume, will be presented first. Equation (6) is based on conservation of mass during the shear phase and Equation (7) shows the relationship between the axial strains (ε_a) and radial strains (ε_r) as a result of the boundary conditions imposed during a CU test.

$$\varepsilon_v = \varepsilon_a + 2\varepsilon_r \ \ (= \varepsilon_1 + 2\varepsilon_3 \ for \ TXC) \tag{6}$$

For CU tests, the volumetric strain (ε_V) is zero which implies that the radial strain is half the axial strain but as a negative value as shown in Equation (7).

$$\varepsilon_a = -0.5\varepsilon_r \ \ (\varepsilon_1 = -0.5\varepsilon_3 \ for \ TXC) \tag{7}$$

Several correlations between the shear strain (ε_s) and axial strain have been proposed and two of these are discussed here. The first if the relationship proposed by Terzaghi et al. (1996) and is shown as Equation (8). Used in conjunction with Equation (7), Equation (9) was derived as the relationship between the axial and radial strains in a CU test (Vardanega et al., 2012).

$$\frac{\varepsilon_s}{2} = \frac{(\varepsilon_a - \varepsilon_r)}{2} \ \left(= \frac{\varepsilon_1 - \varepsilon_3}{2} \ for \ TXC\right) \tag{8}$$

$$\varepsilon_s = 1.5\varepsilon_a \ (= 1.5\varepsilon_1 \ for \ TXC) \tag{9}$$

A similar relationship was proposed by Wroth (1965). This equation, shown in Equation (10), was used for this study. Using Equation (7), Equation (11) was derived as the relationship between the axial and radial strains in a CU test (Lade, 2016). This was used to convert axial strains to shear strain for this study.

$$\frac{\varepsilon_s}{2} = \frac{(\varepsilon_a - \varepsilon_r)}{3} \ \left(= \frac{\varepsilon_1 - \varepsilon_3}{3} \ for \ TXC\right) \tag{10}$$

$$\varepsilon_s = 1.0\varepsilon_a \ (= 1.0\varepsilon_1 \ for \ TXC) \tag{11}$$

Based on the observations by Wroth (1965), that there is a linear relationship between the shear strains developed in CD and CU tests to achieve the same q/p' ratio, it was assumed for the

purposes of this study that the relationship between shear strains and axial strains is the same for CU and CD triaxial tests, i.e. that they are numerically equivalent. By assuming the relationship for CU and CD tests is the same, it means there will be a constant linear error when interpreting the shear strains for CD tests. For this study, it was assumed that this error was sufficiently small so as to not affect the outcome of the analyses conducted. This was also identified by Torres Cruz (2016) and it was suggested that Equation (11) be used for CD triaxial tests. Appendix B provides additional details regarding the relationship between axial and shear strains in triaxial compression tests.

2.4.1.6 Interpreting Mohr-Coulomb soil parameters from triaxial test data

The Mohr-Coulomb strength model is a plastic strength model that is available in the finite element software package SIGMA/W. The parameters show in Table 2.3 are required to fully define the strength model and can be determined from triaxial test data.

Table 2.3: Parameters required for the Mohr-Coulomb strength model as implemented in SIGMA/A

Parameter	Description
E_i	Initial tangent modulus
ψ	Dilation angle
ν	Poisson's ratio
φ'	Friction angle
c'	Cohesion intercept

The friction angle and cohesion intercept can easily be determined from triaxial test results as discussed in Section 2.4.1. The determination of Poisson's ratio (ν) is more difficult to obtain as radial strain measurements during the shear phase of a CD triaxial test are required. Since this is not routinely done and was not done in the testing regime conducted as part of this assessment, this ratio was estimated. In the absence of more accurate information, the use of a Poisson's ratio of 0.3 is deemed an appropriate assumption in this geotechnical engineering application (Griffiths & Lane, 1999).

The initial tangent modulus of a soil is not a unique value and is dependent on drainage condition, stress level and strain level. During drained shearing, distortion and volume change is possible while during undrained shearing only distortion (under constant volume) is possible. Using elastic theory, it can be shown that the Bulk Modulus (K) can be used to describe only the volumetric strain and that Shear Modulus (G) can be used to describe only the shear strain. It is for this reason that a more fundamental approach is to use the Bulk Modulus and Shear Modulus elastic

parameters instead of the Young's Modulus.

However, for the implementation of the Mohr-Coulomb strength model, only a single Young's Modulus value is required. The Shear Modulus can be determined using the initial slope of the deviatoric stress vs. shear strain function, irrespective of drainage condition as shown in Equation (12). The initial tangent modulus (E_i), for a specific drainage condition and stress level can then be determined using Equation (13).

$$3\mathrm{G} = \frac{\Delta q}{\Delta \varepsilon_s} \tag{12}$$

$$G = \frac{E_i}{2(1+v)} \tag{13}$$

As shown in Equation (14), the dilation angle (ψ) is the ratio of the change in volumetric strain to the change in axial strain (Knappett & Craig, 2012).

$$\psi = \frac{\Delta \varepsilon_v}{\Delta \varepsilon_a} \tag{14}$$

2.4.2 Determining shear strength using direct simple shear tests

2.4.2.1 Fundamentals of the direct simple shear test

The Direct Simple Shear (DSS) test was initially developed to overcome the significant stress non-uniformities imposed by the direct shear (also referred to as the direct shear box) test (Dabeet, 2014). The stresses and strain imposed during the DSS test are shown in Figure 2.21a.There are two commonly used types of DSS tests: the Cambridge -type (see Figure 2.21b) and the Norwegian Geotechnical Institute (NGI)-type (see Figure 2.21c). The Cambridge-type tests cubical specimens with rigid side boundaries and was initially developed by Roscoe (1953) while the NGI-type tests cylindrical specimens with a wire-reinforced membrane providing lateral confinement as developed by Bjerrum & Landva (1966).

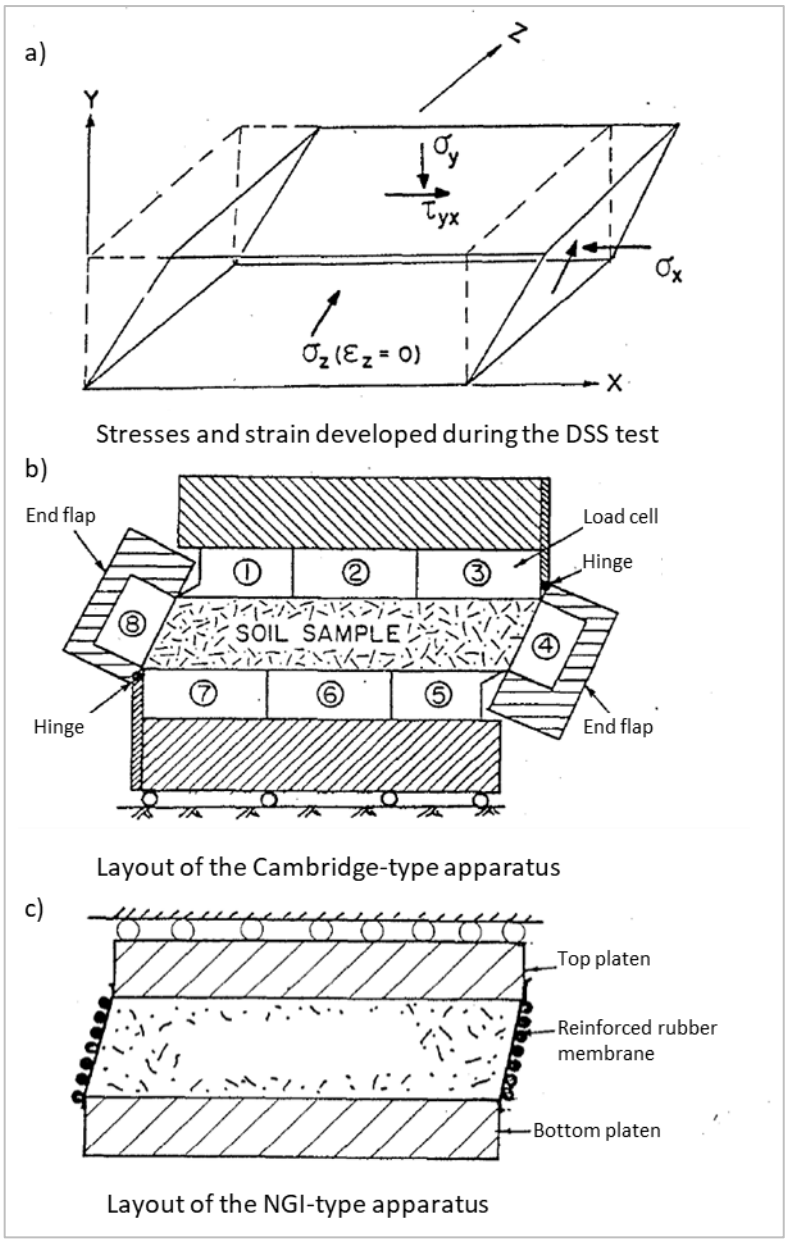

Figure 2.21: Fundamentals of the DSS test, after Budhu & Britto (1987)

2.4.2.2 Determination of drained shear strength

The drained shear strength of a soil can be determined from the results of the DSS test using Equation (15) (Dabeet, 2014). This equation is based on simple geometry based on Mohr-Circle interpretations of the stress state of the material at failure.

$$\varphi' = \sin^{-1}\left(\frac{\sigma_1' - \sigma_3'}{\sigma_1' + \sigma_3'}\right) \tag{15}$$

2.4.2.3 Determination of undrained shear strength

The undrained shear strengths can be determined in a similar manner to the triaxial tests, where the yield undrained shear strength is interpreted from the shear stress-strain graph. An example of this is shown in Figure 2.22, based on DSS tests of loose Fraser River Sand conducted by Wijewickreme et al. (2005).

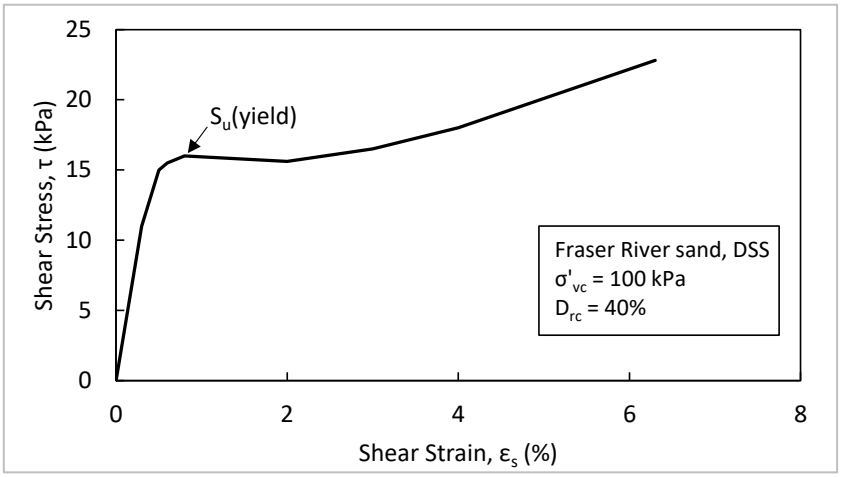

Figure 2.22: Determining undrained shear strength from the DSS test, after Wijewickremeet al (2005)

2.5 DETERMINING SHEAR STRENGTH USING FIELD TESTS

2.5.1 Determining shear strength using the cone penetration test

2.5.1.1 Cone Penetration Testing (CPT) fundamentals

The Cone Penetration Test with pore pressure measurement (CPTu) is a versatile field test commonly used for geotechnical site investigations due to its low cost and proven repeatability. A CPTu (also referred to as a piezocone) is an instrumented rod that is pushed into the ground and is capable of measuring the resistance at the tip (cone resistance), the pressure just behind the tip (pore pressure) and the friction around the cone, just behind the tip (sleeve friction). As the rod is pushed into the ground, the soil is compressed ahead of the probe and then sheared as the probe passes through. The response of the soil to this loading is continuously recorded and by assessing these responses, several key soil properties such as undrained shear strength, permeability and coefficient of vertical consolidation can be estimated (Meigh, 1987).

2.5.1.2 Effects of material properties on drainage conditions

During probing, the soil is sheared as the piezocone is pushed through the soil and shear-induced pore pressures are generated within the soil. The dissipation of these pore pressures is a function

of the rate of penetration of the piezocone and the hydraulic properties of the soil. The standard rate of penetration is 20 ± 5 mm/s and is specified in the ASTM standard D5778 (ASTM, 2012). This is important as certain strength parameters, such as undrained shear strength, can only be accurately assessed from piezocone test results if the tests are performed in an undrained manner.

Kim et al. (2010) studied the effects of penetration rate to determine the boundary between drained and undrained piezocone testing. To determine this boundary, the dimensionless penetration rate V is used as shown in Equation (16).

$$V = \frac{vD}{c_v} \tag{16}$$

Where:

V = Penetration rate (dimensionless)

v = Penetration rate (mm/s)

D = Cone diameter (mm)

c_v = Coefficient of vertical consolidation (mm^2/s)

The study concluded that the transition between fully undrained and partially drained was V = 10, which is in line with previous studies. A series of field CPTu tests and laboratory centrifuge tests were conducted and the value of the dimensionless penetration rate (V) defining the transition between completely drained and completely undrained probing was found to be between 4 and 10 for the CPTu tests (Kim et al., 2008) and between 10 and 30 for the centrifuge tests (Randolph & Hope, 2004). Therefore, the change between undrained and drained penetration can be determined based on the coefficient of vertical consolidation (c_v). To summarise, for a standard cone with a diameter of 35.7 mm, probed at the standard penetration rate of 20 mm/s, material with a c_v value greater than 1x10^{-2} m^2/s will be fully drained and materials with a c_v value less than 7x10^{-4} m^2/s will be undrained. It should be noted that the coefficient of horizontal consolidation (c_h) is generally inferred from the CPTu tests and a conversion from this to the coefficient of vertical consolidation (c_v) is required before direct comparisons can be drawn.

An alternative method to determine whether the shearing induced during probing is being conducted drained or undrained, is based on the time required for 50% consolidation (t_{50}) of the shear induced pore pressures due to the probing. This value can be determined by reviewing the dissipation data obtained when the probing is halted periodically to allow dissipation of these shear induced excess pore pressures. For a standard cone with a diameter of 35.7 mm, it was suggested that t_{50} values greater than 30 seconds indicate that the cone penetration is undrained while t_{50} values less than 30 seconds indicate that the cone penetration is likely partially drained (Robertson,

2010).

In summary, two simple methods are available for determining whether probing is drained or undrained. It is important to adequately identify the type of probing before empirical correlations are used to infer material properties.

2.5.1.3 Estimating drained shear strength from CPTu

As described in Section 2.5.1.2, the physical properties of the material being probed limit the interpretation of the shear strength properties. Drained strength properties (i.e. a Mohr-Coulomb friction angle and cohesion intercept) can therefore only be obtained from coarse-grained materials or materials which are probed drained. Although there are several empirical methods of determining the drained strength of soil (e.g. Robertson & Campanella, 1983; Kulhawy & Mayne, 1990), Robertson (2012) developed a table of perceived applicability of in situ tests and only rated the CPTu as "moderate". It is therefore recommended that the CPTu be used only to infer qualitative drained shear strength parameters. For reference, the proposed equations are detailed below.

Calculation of the Mohr-Coulomb friction angle as proposed by Robertson & Campanella (1983) is shown in Equation (17).

$$\varphi' = \frac{1}{2.68}\left[0.29 + \log\left(\frac{q_c}{\sigma'_{v0}}\right)\right] \quad (17)$$

Where:

φ' = Mohr-Coulomb friction angle (°)

q_c = Measured cone resistance (kN)

σ'_{v0} = Vertical effective stress at one atmosphere (kPa)

Calculation of the Mohr-Coulomb friction angle as proposed by Kulhawy & Mayne (1990) is shown in Equation (18).

$$\varphi' = \tan^{-1}\left[0.1 + 0.38\log\left(\frac{q_c}{\sigma'_{v0}}\right)\right] \quad (18)$$

2.5.1.4 Estimating undrained shear strength from CPTu

In contrast to drained strength, the perceived applicability of the CPTu to measure the undrained strength as "high" (Robertson, 2012). Again, note that undrained strengths can only be obtained

from fine-grained materials or material that are probed undrained. Three methods for determining the undrained shear strength from CPTu data are presented below. As discussed in Section 2.3.2.1, when reference is made to the undrained strength in this assessment, it is the yield undrained strength that is being referred to. Further, note that the strengths referred to are DSS strengths.

The first method is that proposed by Olson & Stark (2003). A study was conducted on 30 recorded cases of liquefaction flow failures where CPT and SPT data were available. By back analysing the failures to determine the shear soil shear strengths, Equation (19) was developed thereby linking the yield undrained shear strength ratio to the normalised cone tip resistance.

$$\frac{S_{u(yield)}}{\sigma'_{v0}} = 0.205 + 0.0143(q_{c1}) \pm 0.04 \; for \; q_{c1} \leq 6.5 \; MPa \tag{19}$$

Where:

$\frac{S_{u(yield)}}{\sigma'_{v0}}$ = Yield undrained strength ratio

q_{c1} = Normalised cone tip resistance (MPa), also noted as Q_t. Note that $q_{c1} = Q_t = \frac{q_t - \sigma_{v0}}{\sigma'_{v0}}$ where $q_t = q_c + u_2(1 - a)$ with q_c = measured tip resistance, u_2 = pore pressure measured at position 2 (see Robertson (2010) for more details), a = net area ratio and σ_{v0} = total vertical stress at one atmosphere.

The second method is that proposed by Robertson (2009). Equation (20) was developed based on critical state soil mechanics framework and the earlier work done by Jamiolkowski et al. (1985).

$$\frac{S_{u(yield)}}{\sigma'_{v0}} = \frac{1}{N_{kt}} \frac{q_t - \sigma_{v0}}{\sigma'_{v0}} \; (= 0.0714 \; q_{c1} \; for \; N_{kt} = 14) \tag{20}$$

Where:

N_{kt} = Cone factor (typically 14)

q_t = Corrected cone resistance (kPa)

The third method is that proposed by Sadrekarimi (2014). A large database of TXC, TXE and DSS tests were studied and, for each type of test, a relationship was defined between the interpreted yield undrained shear strength an “undrained brittleness index”. The undrained brittleness index (I_B), defined in Equation (21), is a representation of the degree of strain-softening a material is expected to undergo during undrained shearing. A material that has a large difference between the yield and critical undrained shear strength will have an undrained brittleness index of close to

1.0 while a material that does not exhibit strain-softening behaviour will have an undrained brittleness index close to 0.

$$I_B = \frac{s_{u(yield)} - s_{u(critical)}}{s_{u(yield)}} \quad (21)$$

Where:

I_B = Undrained brittleness index

$s_{u(critical)}$ = Critical undrained shear strength (kPa), also referred to as residual or liquefied undrained shear strength

A database of field test results from liquefaction flow failures was also studied and a relationship between the normalised cone tip resistance and undrained brittleness index was developed. It should be noted that it appears that this database, with specific reference the triaxial compression tests, appears to be biased towards material that exhibits strain-softening behaviour. As can be seen in Figure 2.23, the majority of the data points indicate large undrained brittleness index values. The suggests that these proposed equations may only be applicable to materials that exhibit relatively large undrained brittleness index values.

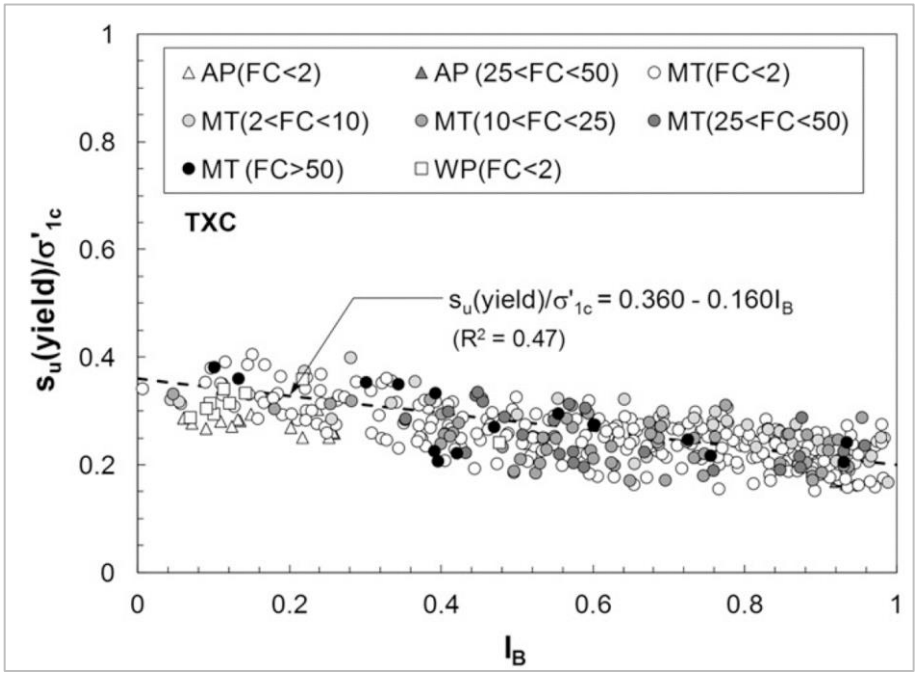

Figure 2.23: Comparison of yield undrained shear strength and undrained brittleness index for several soils, after Sadrekarimi (2014)

By comparing these two relationships, a link between the normalised cone tip resistance and yield undrained shear strength for each type of laboratory test was developed. The proposed

relationship between the normalised cone resistance and the DSS undrained yield strength is shown in Equation (22).

$$\frac{S_{u(yield)}}{\sigma'_{v0}} = 0.189 + 0.008(q_{c1}) \pm 0.025 \; for \; q_{c1} \leq 8 \; MPa \tag{22}$$

2.5.2 Determining shear strength using the vane shear test

An alternative field test to the CPTu is the vane shear test (VST). The VST is used in clays and clayey silts to determine the undrained intact and remoulded shear strength (Gylland et al., 2016). An advantage of the test is that it can be performed quickly and by hand. As with most field tests, it was also capable of measuring local fabric effects in the soil. A disadvantage is that testing depths are limited without some sort of drilling.

2.5.3 Comparison between strengths determined using field and laboratory tests

Several researchers have spent considerable time looking for relationships between field and laboratory testing. As there are a wide range of tests available, the comparison made below is limited to the CPTu probing and vane shear tests for the field tests and TXC, TXE and DSS tests for the laboratory tests.

It is important to remember that the strength of soil depends on the state of the soil as discussed in Section 2.3.1. Laboratory samples are typically reconstituted samples which are then consolidated to the desired state before shearing. A disadvantage of laboratory testing, specifically on fine tailings material, is that undisturbed sampling is very difficult and expensive and therefore most tests are performed on reconstituted samples. During remoulding, the material is reconstituted and loses all of its stress history and fabric. Since tailings is typically a processed material, the history may not be too important. However, the fabric is key (Chang et al., 2011; Li & Coop, 2019). Field tests, on the other hand, are designed to measure the response of the material in situ and the fabric effects are therefore considered. Two examples of comparison of laboratory and field test results are described below.

Sadrekarimi (2014) studied a database of TXC, TXE and DSS tests and, for each type of test, defined a relationship between the interpreted yield undrained shear strength an undrained brittleness index. An example of this is shown in Figure 2.24a. Note the abbreviations used for the sample preparation method:

- Air pluviated (AP)
- Moist tamped (MT)
- Water pluviated (WP), this is similar to the slurry deposition method described in Section 2.4.1

A database of field test results from liquefaction flow failures was also studied and a relationship between the normalised cone resistance and undrained brittleness index was developed, see Figure 2.24b. By comparing these two relationships, a link between the normalised cone resistance and yield undrained shear strength for each type of laboratory test was developed as shown in Figure 2.24c. Here, an empirical method was developed to easily convert from field measured strength values to laboratory values.

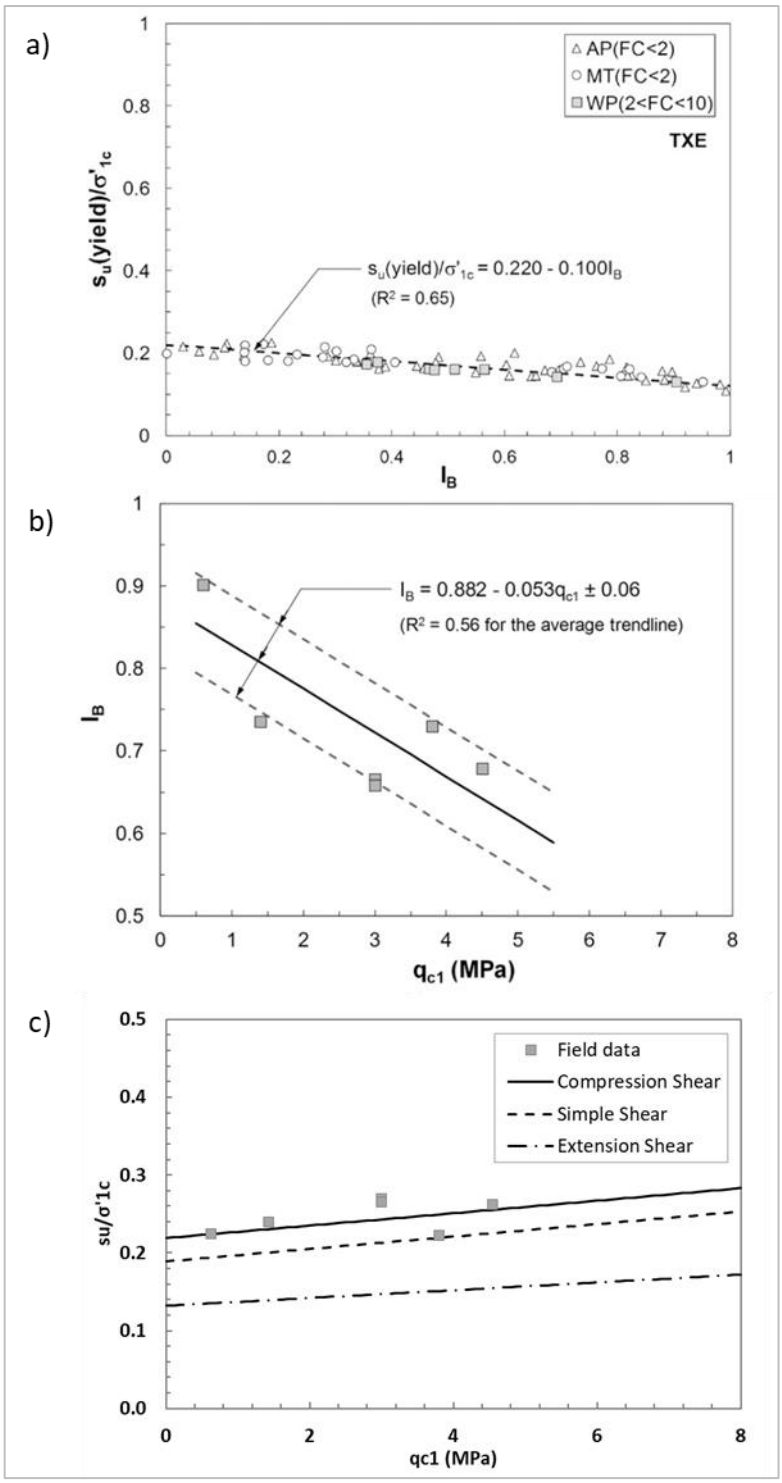

Figure 2.24: Comparison of laboratory and field data, after Sadrekarimi (2014)

Tumay et al. (2017) reviewed a large database of CPTu, VST and TXC tests on clays and found a good correlation between the undrained shear strengths determined by each of these tests. An example of this correlation is shown in Figure 2.25. Here, it was shown that several methods of determining the undrained shear strength of clay can be used, all of which yield comparable results.

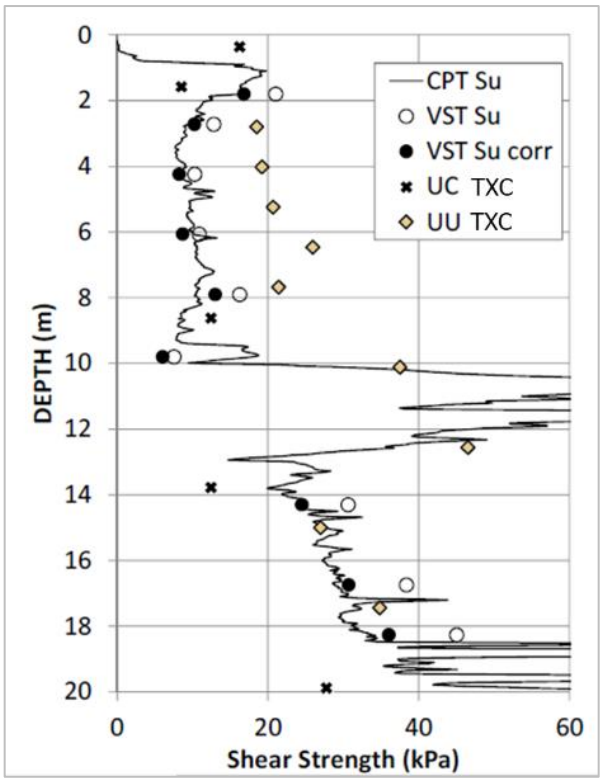

Figure 2.25: Undrained shear strengths derived from laboratory and field tests, after Tumay et al. (2017)

Two examples were presented showing relatively good correlation between laboratory and field measured data. However, the constraint regarding fabric effects which cannot be captured testing reconstituted samples still remains. A good soil testing programme, therefore, usually incorporates both field and laboratory testing. For tailings, which are often of a silty nature, an excellent testing programme is suggested by Been (2016).

As discussed in Section 2.5.1.3, the field tests mentioned in this assessment are not the most effective tools for determining the drained strength of the soil and therefore the comparison is limited to undrained shear strengths. It is assumed that the drained shear strengths measured using the laboratory tests are the representative strengths.

2.6 SLOPE STABILITY

2.6.1 Limit equilibrium method

Limit equilibrium analysis is the oldest form of analysis and was first used in a geotechnical stability context by Coulomb (1773). It is a purely static approach, where a failure surface is assumed and there is no consideration of the relationship between stress and strain (i.e. there is no constitutive relationship). The static admissibility of the stress field is not satisfied, and some arbitrary assumptions are required to remove the statical indeterminacy. Further, only a global equilibrium

condition is satisfied as opposed to equilibrium conditions at every point in the soil (Yu et al, 1998). A key advantage, however, of the limit equilibrium method is that is has been used for many years and the Factor of Safety (FoS) values achieved have been calibrated with experience and observations (Krahn, 2003).

A specific limit equilibrium method is the method of slices. Over time, this method has been improved upon, but the formulation remains the same. It is merely the assumptions regarding the forces considered, the consideration of force and/or moment equilibrium and the slip geometry. A general limit equilibrium (GLE) formulation was developed by Fredlund et al. (1981) which encompasses all the key elements of the method of slices. A sketch showing the key variables in the GLE is shown in Figure 2.26.

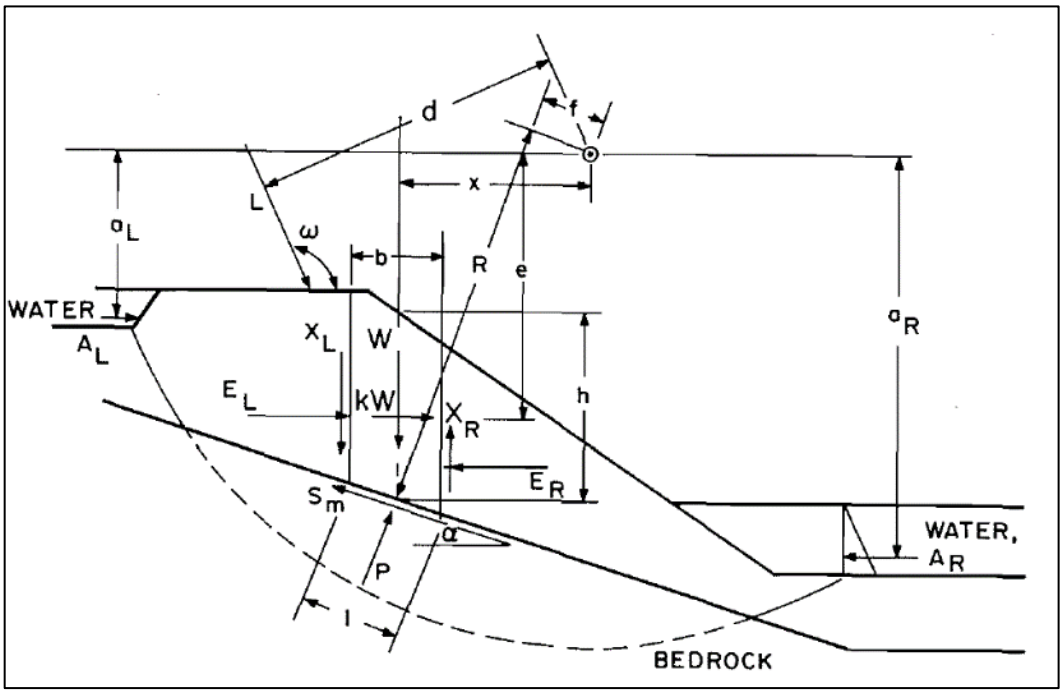

Figure 2.26: Forces acting on a composite slip surface for the method of slices (Fredlund & Krahn, 1977)

Each parameter shown in Figure 2.26 is defined as follows:

W = weight of the slice of width b and height h

P = normal force on the base of the slice over a length l

S_m = shear force mobilised on the base of the slice. It is a percentage of the shear strength as defined by the Mohr-Coulomb equation: $S_m = l\,\{c' + [P/l - u]\tan\varphi'\}/F$ where c' = effective cohesion parameter, φ' = effective angle of internal friction, F = factor of safety, and u = porewater pressure

R = radius or the movement arm associated with the mobilised shear force S_m

f = perpendicular offset of the normal force from the centre of rotation

x = horizontal distance from the slice to the centre of rotation

α = angle between the tangent to the centre of the base of each slice and the horizontal

E = horizontal interslice forces

L = subscript designating left side

R = subscript designating right side

X = vertical interslice forces

k = seismic coefficient to account for dynamic horizontal forces

e = vertical distance from the centroid of each slice to the centre of rotation

L = line load (force per unit width)

ω = angle of the line load from the horizontal

d = perpendicular distance from the line load to the centre of rotation

A = resultant water forces (due to partial submergence of the slope or tension cracks)

a = perpendicular distance from the resultant water force to the centre of rotation

There are three fundamental equations used for the method of slices. Depending on the factor of safety method used, some of these equations fall away. For example, if Janbu's simplified method is used, moment equilibrium is not considered and Equation (23) is not used (Janbu, 1954). Similarly, if Bishop's simplified method is used, force equilibrium is not considered and Equation (24) is not used (Bishop, 1955). The first is the FoS with respect to moment equilibrium (F_m) which can be calculated using Equation (23).

$$F_m = \frac{\sum c'lR + \sum (P - ul)R \tan \varphi'}{\sum Wx - \sum Pf + \sum kWe \ \pm Aa + Ld} \tag{23}$$

The second is the FoS with respect to force equilibrium (F_f) which can be calculated using Equation (24).

$$F_f = \frac{\sum c'l \cos \alpha + \sum (P - ul) \tan \varphi' \cos \alpha}{\sum P \sin \alpha + \sum kW \pm A - L \cos \omega} \tag{24}$$

Finally, the normal force (P) is calculated using Equation (25). From the Equation, it is clear that an iterative approach is required.

$$P = \frac{W - (X_R - X_L) - \frac{c'l \sin a}{F} + \frac{ul \tan \varphi' \sin \alpha}{F}}{\cos \alpha + (\sin \alpha \tan \varphi' / F)} \tag{25}$$

Within the limit equilibrium framework, there exist several factor of safety methods that are widely used and accepted by industry. When selecting a method for use, it is important to confirm whether force equilibrium is considered, whether moment equilibrium is considered and what method is

used to resolve the fundamentally indeterminate FoS equation. Earlier models were limited by slip geometry, but this has since been resolved and a brief description of the most common methods used are described here. For each of the three methods described both force and moment equilibrium are achieved.

2.6.1.1 Spencer's Method

The Spencer method considers both force and moment equilibrium and was developed based on the assumption that the angle of the resultant of the interslice forces (θ) is constant for all the slices (Spencer, 1967). Another assumption of this method is that the normal force acts on the centre of the base of the slice. However, as noted by Duncan et al. (2014), this has a negligible effect on the computed FoS provided there are a sufficient number of slices (i.e. there are a sufficient number of slices to capture the changes in slip geometry and/or material properties along the slip surface). The solution was first presented for circular slip surfaces but can be extended to non-circular slip surfaces. The relationship between the interslice forces is shown in Equation (26).

$$\mathrm{X} = \tan(\theta)\, E \tag{26}$$

Where:
θ = angle of the resultant interslice force from the horizontal (°)

This method remains popular amongst researchers, notably the PhD theses of Stark (1987) and Olson (2001) who are leading researchers in the field of slope stability analysis with an emphasis on undrained slope stability.

2.6.1.2 Morgenstern-Price Method

The Morgenstern-Price method is arguably the most popular method used for limit equilibrium slope stability analysis as it considers both force and moment equilibrium and the assumptions regarding the interslice forces can be changed to suit the site conditions. Its popularity is noted as it was the method used to assess the two most recent catastrophic tailings dams failures: the Mount Polley tailings dam failure in 2014 (Morgenstern et al., 2015) and the Fundão failure in 2015 (Morgenstern et al., 2016).

As described earlier, the fundamental limit equilibrium FoS equations are statically indeterminate and some assumptions need to be made in order to solve the equation. For the Morgenstern-Price method, an assumption is made regarding the interslice forces (Morgenstern & Price, 1965). It is assumed that the direction of the interslice forces is defined by an arbitrary mathematical function

$f(x)$. A constant, λ, is also defined and the relationship between the interslice normal and shear forces is shown in Equation (27).

$$X = \lambda f(x) E \tag{27}$$

Where:

λ = a constant to be evaluated in the solving for the factor of safety

$f(x)$ = functional variation with respect to x

The Newton-Raphson numerical technique is used to solve the force and moment equations for the factor of safety and λ. If the function is constant, then the Morgenstern-Price method is the same as the Spencer method (see Section 2.6.1.1 for more details). Note that this method involves many iterations and typically cannot be solved without the use of a computer.

2.6.1.3 Sarma's Method

A different approach is taken in the Sarma method, where an acceleration is determined and the FoS calculated from this value. The Sarma method is a non-iterative method and was developed with the aim of determining the critical earthquake acceleration (K_c) required to bring a soil mass to a state of equilibrium (Sarma, 1973).

Again, both force and moment equilibrium are considered. Regarding the interslice forces, it is assumed that the shear strength on the interface between the adjacent slices is mobilised to the same degree as at the failure surface. This is shown in Equation (28).

$$X = c'h + \tan(\varphi')\,(E - u) \tag{28}$$

Based on the critical earthquake acceleration calculated, a FoS value is determined. An iterative process involving reducing the strength of the material systematically until a critical acceleration of 0 is achieved is suggested. However, it was concluded that the above-mentioned iteration is unnecessary and that the critical acceleration can be taken as a measure of the static FoS.

The accuracy of the Sarma method against the Morgenstern-Price method was also compared and it was concluded that the accuracy is the same provided the slip surface is valid (i.e. the surface must be kinematically admissible and there should not be tensile forces within the soil mass).

2.6.1.4 Summary of factor of safety methods

Three popular factor of safety methods that consider both force and moment equilibrium were investigated, and it was found that the fundamental difference between the methods is the assumptions regarding the interslice forces. The Morgenstern & Price method assumes the magnitude and orientation of the forces can vary by slice, the Spencer method assumes that the resultant of the shear and normal forces are parallel for all the slices and the Sarma method assumes that the strength mobilised at the interface between the slices is the same as at the base of the slice. Several studies, including those by Zhu et al. (2003) and Sloan (2013), have been conducted to compare the methods and the general consensus is that, for typical slopes, all three methods yield similar answers.

2.6.1.5 Limitations of the limit equilibrium method

There are several limitations to the limit equilibrium method that need to be considered when implementing these approaches (Krahn, 2003). Two examples of these limitations are discussed here.

Firstly, no consideration is given to strain compatibility. For example, it is well known that the density of a soil can significantly affect its behaviour in shear (as is shown in Figure 2.27a). Within the limit equilibrium framework, a single function is assigned to all three stress paths (as shown in Figure 2.27b) and the fundamental difference in behaviour between the three stress paths is lost.

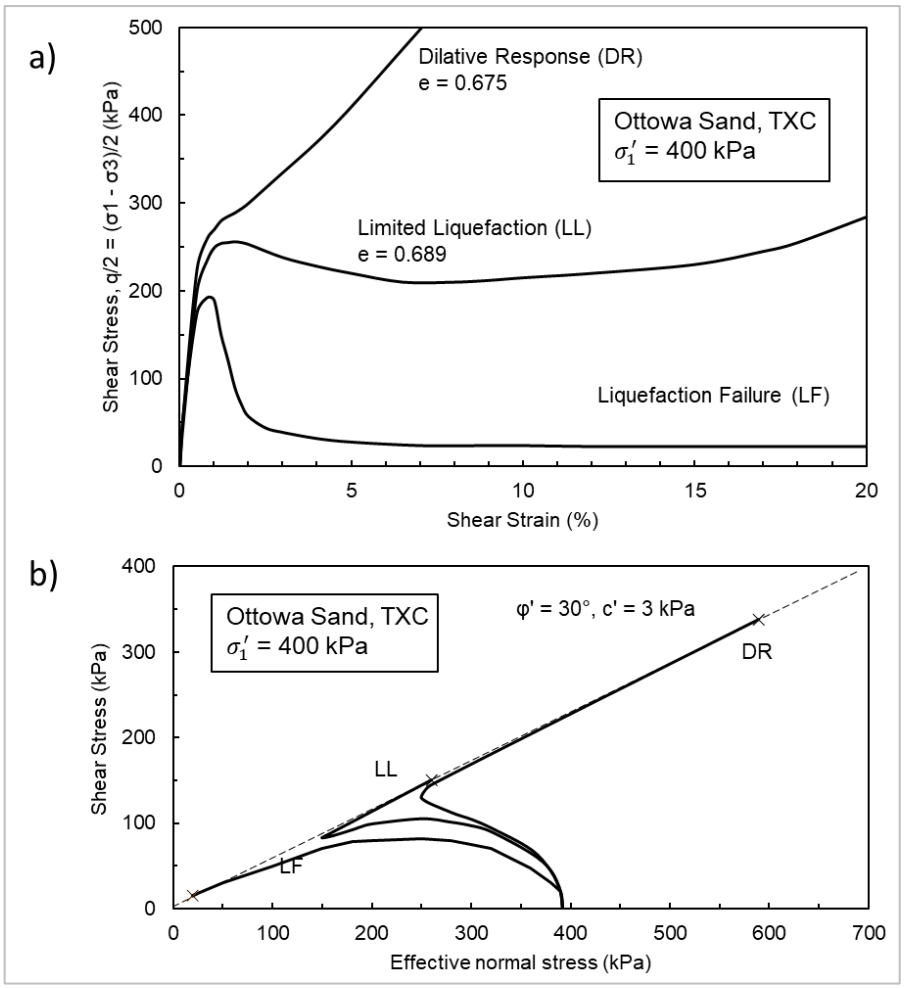

Figure 2.27: Stress paths of Ottawa sand at various densities, after Castro (1969)

Secondly, stress concentrations are not handled well. This is due to the requirement that the local FoS (when considering an individual slice) must be the same as the global FoS (when considering the entire slip surface). Consider a retaining wall with two soil anchors as shown in Figure 2.28a. The anchors pass through slices 8 and 13 and the force polygons for each slice is shown in Figure 2.28b and Figure 2.28c respectively. If a method is selected that requires force equilibrium to be satisfied, then the concentrated load results in tensile interslice forces which is not possible in soil. Further, this tensile force will change the base normal force which will affect the calculated FoS.

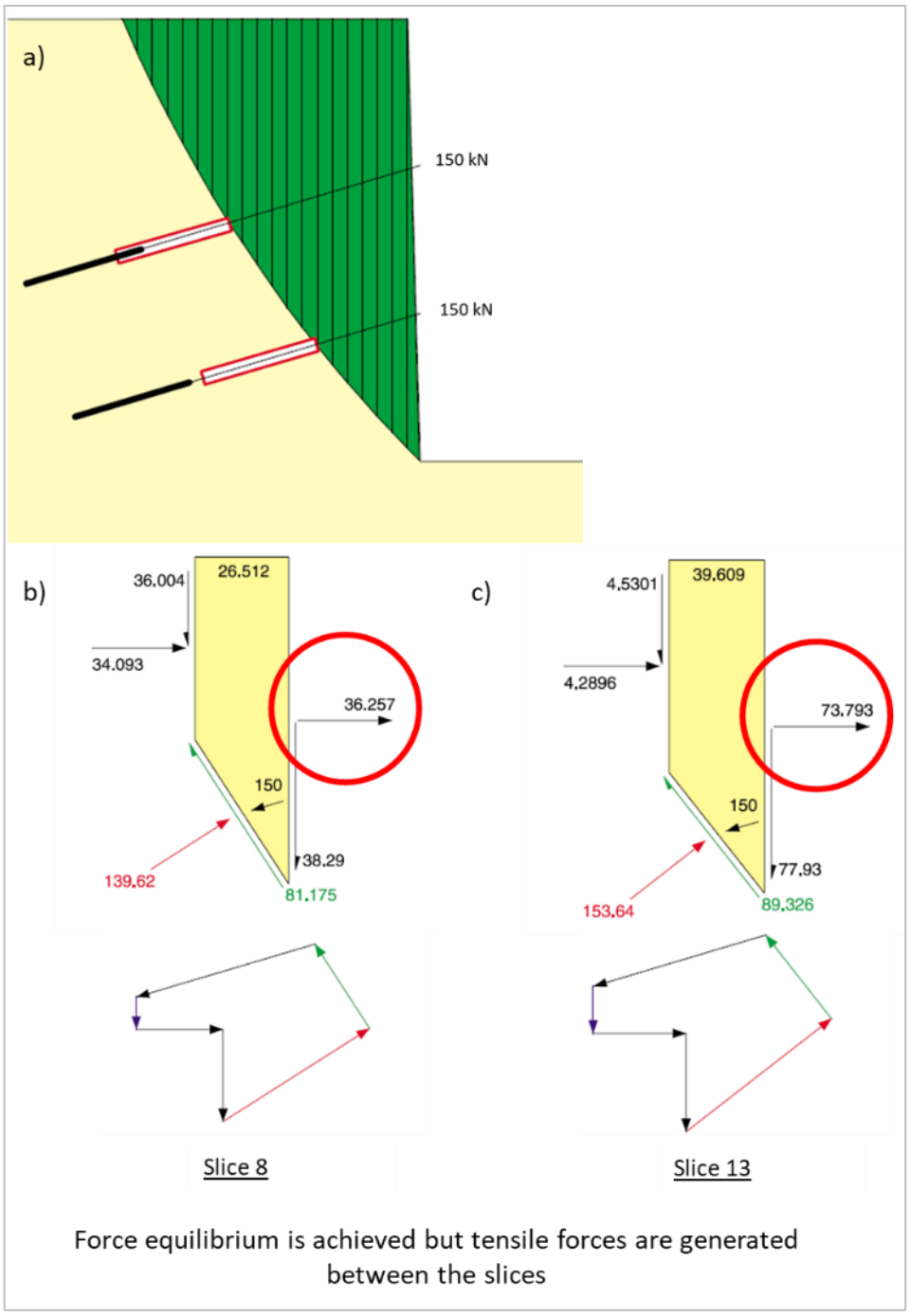

Figure 2.28: Tensile interslice forces induced due to stress concentrations, after Krahn (2003)

These limitations do not mean that limit equilibrium methods should not be used but they must be evaluated on a case-by-case basis to determine if these limitations may significantly affect the results of the analysis. To overcome these limitations, it is suggested that alternative methods such as finite element analyses be pursued. Details of these methods are described further in Section 2.6.2.

2.6.2 Alternatives to the limit equilibrium method

2.6.2.1 Limit analysis method

The limit analysis method models the soil as a perfectly plastic material with an associated flow rule (Yu et al., 1998). Within this model, two plastic bounding theorems (an upper bound and a lower bound) can be proved (e.g. Drucker et al., 1952; Chen, 1975).

For the upper bound theorem, a set of external loads acting on a failure mechanism is considered. If the work done by the external loads in an increment of displacement equals the work done by the internal stresses, then the external loads are not lower that the true collapse loads. By reviewing different failure mechanisms, the critical (lowest) upper bound solution can be found. Note that, for the upper bound solution, the set of external loads considered may not be in equilibrium and the failure mechanism considered may not be the actual failure mechanism.

For the lower bound theorem, an equilibrium distribution of stress covering the whole body is considered. If a distribution can be found that balances a set of external loads on the stress boundary that is nowhere above the failure criterion, then the external loads are not higher that the true collapse loads. By reviewing different admissible states of stress, the critical (highest) lower bound solution can be found. Note that, for the lower bound solution, strain and displacements are not considered and, the state of stress determined is not necessarily the state of stress at collapse.

By employing this method, an upper bound and lower bound of the solution can generally be determined. This method is therefore typically used when an exact solution cannot be determined.

2.6.2.2 Finite Element Analysis and the Strength Reduction Method

An alternative to limit equilibrium slope stability analysis is the use of finite element analysis. The Finite Element (FE) method is fundamentally different to limit equilibrium as equilibrium for the entire model is solved and not just along the slip surface as in the case of limit equilibrium (Griffiths & Lane, 1999).

An advantage of this method is that the slip surface does not need to be assumed as is the case for limit equilibrium analyses. Since there is no concept of slices in this method, there is no need for assumptions regarding the interslice forces. Further, the local FoS does not need to be equal to the global FoS and the FE method is able to simulate progressive failure up to and including overall shear failure.

A disadvantage is that a single FoS value is not achieved, rather a Safety Factor (SF) value is obtained as a result. The SF is typically determined using the Phi-c reduction technique (sometimes referred to as the Strength Reduction Method). Using this technique, the strength of the soil (in terms of the $\tan \varphi'$ and c') are systematically reduced until a factor of safety of unity is achieved. The ratio by which the strength was reduced to obtain the factor of safety of 1.0 is deemed the SF, see equation (29).

$$SF = \frac{\tan \varphi'}{\tan \varphi'_f} = \frac{c'}{c'_f} \tag{29}$$

Where:

φ'_f = Mohr-Coulomb friction angle at failure (°)

c'_f = Cohesion at failure (kPa)

The exact point of failure (or FoS = 1.0) is difficult to determine. However, the approach suggested by Zienkiewicz (1971) where the point of failure is defined when there is non-convergence of the solution is generally accepted and used.

Although the finite element approach has several advantages over conventional limit equilibrium analysis, there is a significant disadvantage that there is no reference point. As discussed in Section 2.6.1, one of the key benefits of using the limit equilibrium method is that it has been used for many years and the FoS values achieved have been calibrated with experience and observations (Krahn, 2003).

2.6.2.3 Finite element computed stresses used in limit equilibrium framework

One of the key parameters in the GLE formulation is the normal force at the base of each slice (Krahn, 2003). In the conventional GLE formulation, the normal base force is calculated considering the interslice forces and force equilibrium. Since the GLE formulation is statically indeterminate, an assumption needs to be made regarding these interslice forces.

However, using a simple stress-strain finite element approach, the stresses in the soil mass can be calculated without any assumptions. If these can then be incorporated into the limit equilibrium model, there will be no need for interslice assumptions as the forces acting on each slice can be calculated using Mohr circle techniques. This solution is called the finite element computed stresses used in a limit equilibrium framework and is readily available in many commercial software packages, including the SLOPE/W package of the GeoStudio Software suite (SLOPE/W, 2001). Once the forces along the slip are determined, the Stability Factor ($S.F.$) can then be calculated

using Equation (30).

$$S.F. = \frac{\sum S_r}{\sum S_m} \tag{30}$$

Where:

S_r = Total available shear resistance (kN)

S_m = Total mobilised shear along the length of the slip surface (kN)

2.6.3 Computer software packages

The limit equilibrium formulation is an iterative process which lends itself well to computer algorithms. There are several commercial software packages available that are capable of performing slope stability analyses and a common program used in engineering practice is the SLOPE/W module of the GeoStudio suite of geotechnical engineering software packages developed by GEOSLOPE. SLOPE/W is capable of performing limit equilibrium slopes stability analyses for complex geometries, loadings and pore pressure conditions (SLOPE/W, 2001).

2.6.4 Optimisation of slip surfaces

A recent development in the analysis of slope stability has been the introduction of optimised slip surfaces. Several commercial software packages already offer some form of slip surface optimisation including: Finesoftware's GEO5, SoilVision's SVSLOPE, GEOSLOPE's SLOPE/W and Rocscience's SLIDE2. A simple explanation of the optimisation procedure used in these packages is given below.

At its simplest, a Monte Carlo method is a structured, random search and optimization technique., Monte Carlo methods can be split into two main classes: random jumping and random walk. In random jumping, with regard to finding slip surfaces with a lower FoS, a large number of random trial surfaces are generated with the key point that each trial solution is generated without consideration of the previous trial. In the random walk methods, each trial is constructively generated such that the i^{th} trial is modified to get the $(i+1)^{\text{th}}$ solution. In this way, a series of improved approximations to the minimum is achieved with fewer iterations (Malkawi et al., 2001). The methods employed in the above-mentioned software are all variations of the random walk method.

In SLOPE/W, after finding the critical slip surface, a segmental technique is applied to optimise the

solution. This technique, as described by Krahn (2018), is detailed below:

1. The slip surface is divided into a specified number of straight-line segments.
2. The end points of these line segments are moved to investigate the possibility of a lower factor of safety. This process starts with the point where the slip enters the ground surface; this point is moved randomly within an elliptical search area and the movement is done using a statistical random walk procedure based on the Monte Carlo method until the lowest FoS is found.
3. Adjustments are then made to the next point along the slip surface. This is repeated for all points along the slip surface.
4. For the next iteration, the longest slip surface line segment is subdivided into two parts and a new point is inserted in the middle. This process is repeated until changes in the calculated FoS are within a specified tolerance or the maximum number of trials has been reached.

The optimization process in an iterative procedure and some limits and controls are required. These include the following:

- FoS tolerance
- Maximum number of optimization trials (iterations); and
- Number of line segments

The optimisation implementation in SLOPE/W is similar to the method employed in the other commercial software packages (noted above) and is based on the work by Malkawi et al. (2001). An illustration of this method is shown in Figure 2.29.

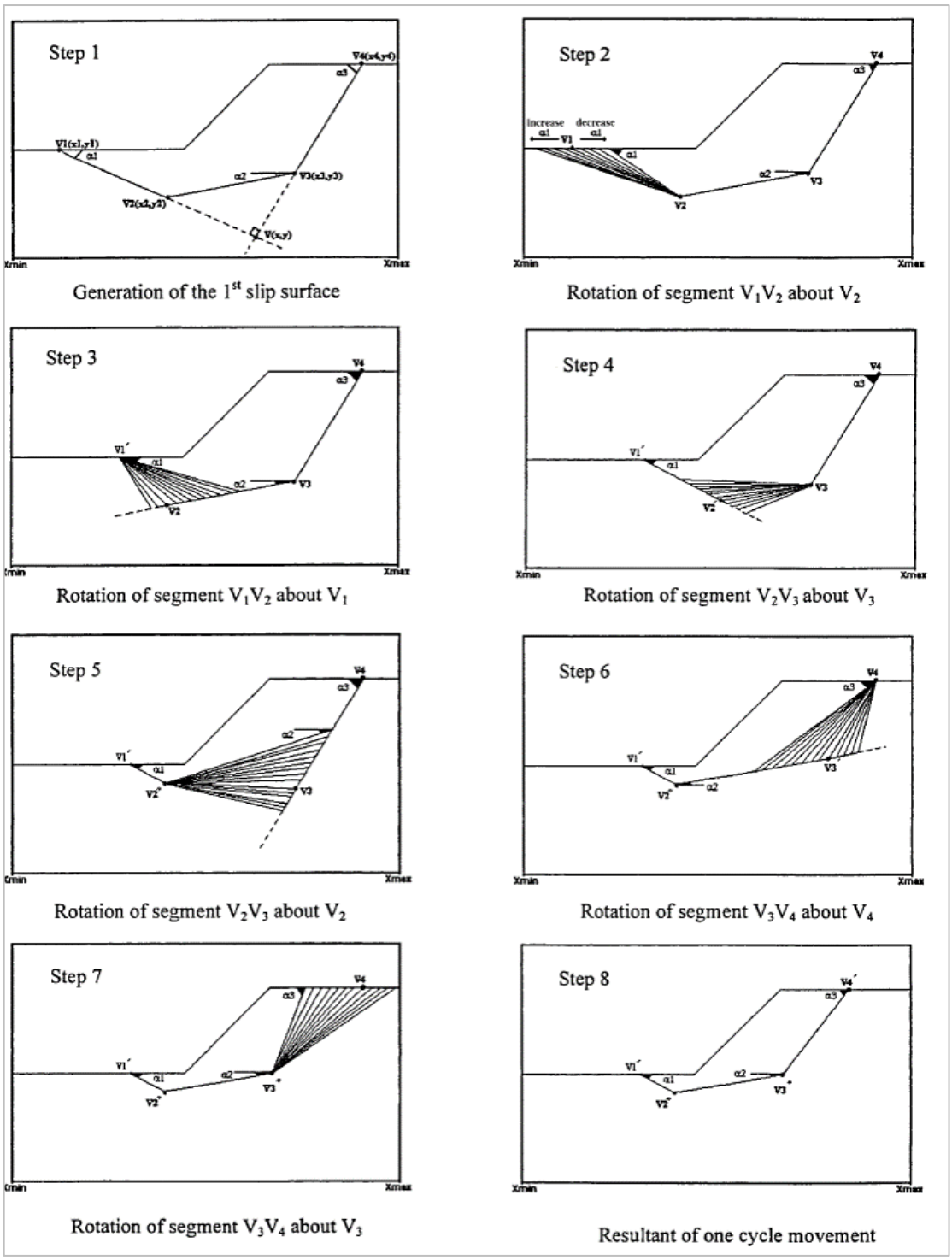

Figure 2.29: Illustration of the random walk optimisation technique (Malkawi et al., 2001)

All optimised slip surfaces should be rigorously inspected before accepted as, based on the optimization process, concave shapes may be achieved which in some instances may not be physically admissible. This is because the optimisation process is a mathematical process. This typically occurs in areas where there are high external loads or large variations in material strength. To limit this, maximum concave angles can be specified for the upstream and downstream sides.

2.6.5 Defining shear strengths on slope stability analysis

There are two general approaches for conducted slope stability analyses. An Effective Stress Analysis (ESA) approach and an Undrained Stress Analysis Approach (USA) (Ladd, 1991). Using the ESA approach, effective stress parameters (i.e. a Mohr-Coulomb friction angle ϕ' and cohesion c') are used while using the USA approach, undrained strength parameters (i.e. undrained stress ratios s_u/σ'_{v0}) are used.

When implementing the ESA approach, the Mohr-Coulomb failure criteria are used and when implementing the USA approach, the SHANSEP failure criteria are used. Note that the USA analyses were conducted in line with the methods suggested by Ladd (1991) and Brown & Gillani (2016), where effective strengths are applied in the zones deemed to be potentially dilative during undrained shearing and undrained strengths are applied in the zones deemed to be potentially contractive during undrained shearing.

2.6.6 Shear strain distribution during slope failure

During slope failure, shear strains are developed along a critical slip surface until the soil mass reaches critical state and fails. The development of these strains have been investigated via physical and numerical modelling (e.g. Zheng et al., 2008; Fern et al., 2017). After reviewing the results from these analyses, it was found that there appears to be a difference in shear strain distribution found between the physical and numerical models. Specifically, at failure, shear strains are observed to be uniform within the shear band in physical models but are discontinuous in numerical models. This difference can be seen in Figure 2.30.

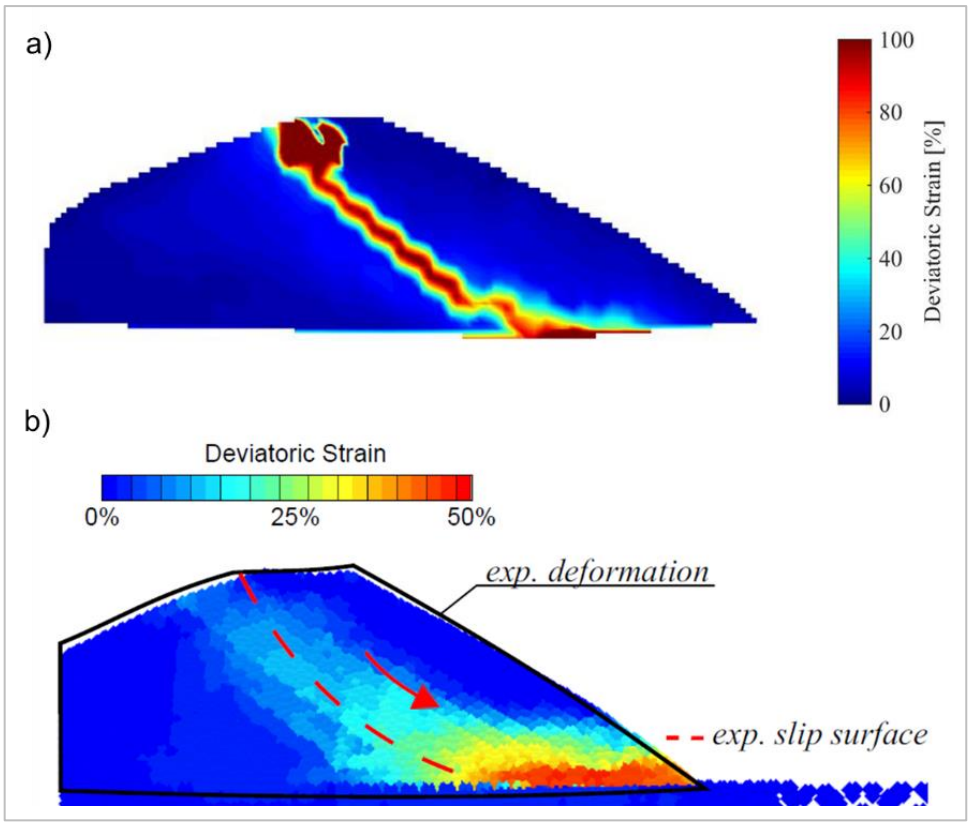

Figure 2.30: Shear strain distributions: a) in a centrifuge model and b) in a numerical model, after Fern et al. (2017)

It was also found that, during numerical modelling when elastic-perfectly plastic strength models are used, the plastic zones are usually overestimated and therefore the shear band is not clearly defined (Zheng et al., 2008). This is shown in Figure 2.31a. However, the overestimated plastic zones usually only undergo limited plastic deformation and by filtering the display of the strain level, a clearer view of the shear band can be obtained as shown in Figure 2.31b. Further, it was observed that the shear strains start developing at the toe of the slope and propagate to the crest.

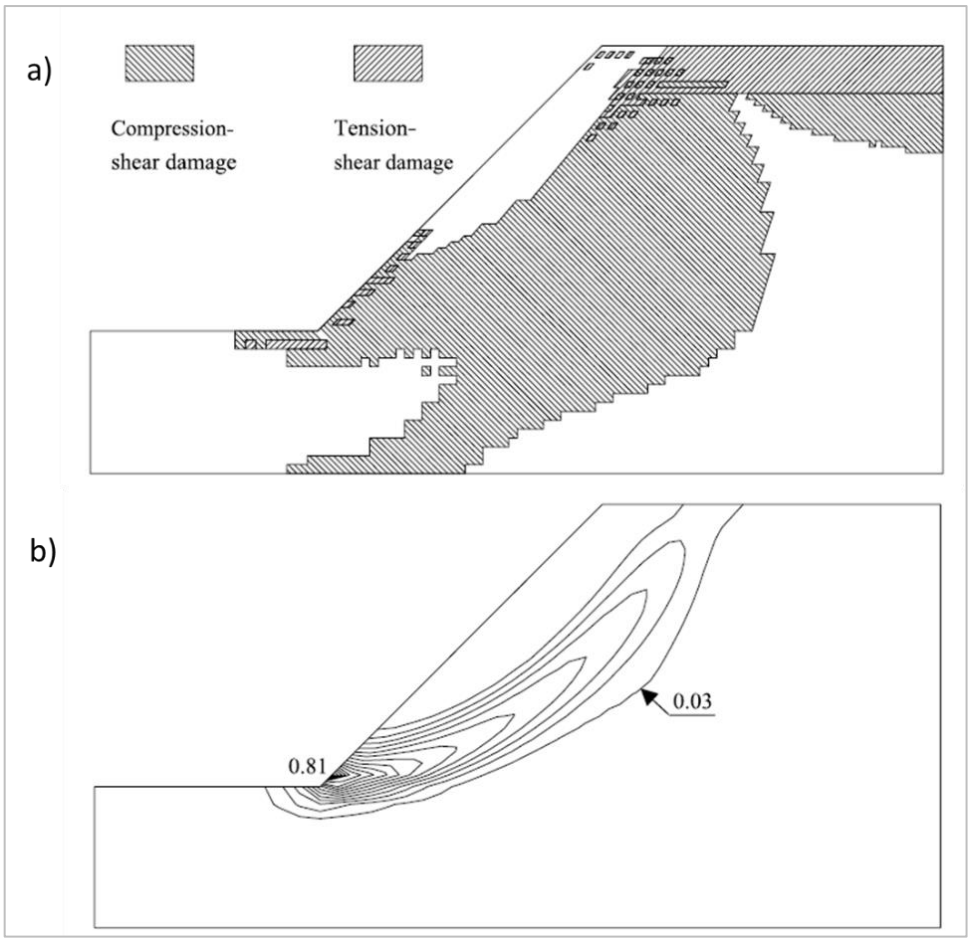

Figure 2.31: Results from a numerical model showing: a) plastic zones and b) contours of strain with overestimated plastic zones filtered out (Zheng et al., 2008)

2.7 SUMMARY

This literature review shows that there has been significant research in the field of drained and undrained strengths of soil and its effect in slope stability analyses, but there has been very little focus on strain compatibility when these strength models are used in the same analysis.

It was found that for homogenous tailings deposits, the density of the material does not vary significantly with depth. If this is assumed, then there is one less variable to influence the state of the material which means a function of the strength of the material can be derived as a function of effective stress only. This will have the limitation that these calculations can only be used for homogenous materials such as tailings dams.

The mode of shear was noted to affect the undrained shear strength of the soil. Triaxial compression tests tend to overestimate the strength of the soil by between 15% and 40% in respect to simple shear and extension, respectively. However, in typical slip surfaces limited portions of

the slip surface cut through zones where direct shear is expected and even less where extension is expected. Therefore, the overestimation of strength, which can be approximated at about 20%, is generally not considered a concern.

Both laboratory and field tests can be used to determine the shear strength of soils. There are several advantages and disadvantages of each approach but it is clear that a combination of both laboratory and field tests are required to gain a thorough understanding of the material being investigated. It was also noted that laboratory and field interpretations on undrained shear strengths seem to correlate well for fine-grained materials. The sample preparation method was noted to affect the stress path followed in CU triaxial compression tests. For loosely reconstituted samples, MT preparation methods were found to produce stress paths exhibiting a contractive tendency while SD preparation methods were found to produce stress paths with an initial contractive tendency and then a dilative tendency. Chang et al. (2011) showed that SD methods appeared to prove better fits to stress paths of CU tests conducted on undisturbed samples. This agrees with the findings of Corrêa & Filho (2019) who found that the SD preparation method was closer to the slurry deposition method employed on actual tailings dams.

Various methods of slope stability analysis were investigated, and it was concluded that the current preferred method of conducting slope stability analysis is the use of limit equilibrium methods as opposed to finite element or limit analysis methods. There are several limitations of limit equilibrium methods (e.g. Krahn, 2003), but the fact that the method is simple to implement, has been calibrated by experience and shows good correlations to back-analysed failure, means it is still widely used today. Alternative methods to overcome the limitations are presented but these are rarely used in industry. Several methods exist for using the limit equilibrium framework to determine a FoS and they vary mostly by means of assumptions regarding the inter-slice forces. A GLE formulation was developed by Fredlund & Krahn (1977) which enable a single algorithm to be run regardless of the method chosen. It was also noted that an optimisation algorithm was developed to find slip surfaces with lower FoS values than circular surfaces typically determined using the conventional methods. It was found that most of the commercial software packages available use the optimisation approach suggested by Malkawi et al. (2001).

Regarding the integration of field and laboratory tests in slope stability assessments, it was found that field tests are effective at inferring the state of the soil in situ and that laboratory tests are effective at determining the theoretical behavioural parameters of the soil (e.g. Robertson, 2012; Jefferies & Been, 2015). This is even more pronounced for silty tailings materials for which undisturbed samples are notoriously difficult to obtain (Chang et al., 2011). Therefore, the recommendation, and the current practice in industry, is to use laboratory tests to define the

appropriate CSSM parameters. Then, with the field tests, infer the state of the material in situ (e) and compare this to the theoretical critical state void ratio (e_c) to determine if the material will potentially dilate ($e < e_c$) or contract ($e > e_c$) to failure. This is easier for fine grained soils which follow a cam clay type behaviour (i.e. a unique NCL) (Atkinson & Bransby, 1978). Behaviour becomes more challenging when dealing with coarse grained material which can have an infinite number of (parallel) NCLs (Jefferies, 1993).

In the next chapter, a limit equilibrium method that considers strain compatibility along the failure surface will be developed.

3 METHODOLOGY

3.1 INTRODUCTION

The previous chapter provides an overview of the current state of knowledge in the areas of tailings material and tailings dams, soil strength, the determination of soil strength using field and laboratory test methods and its use in slope stability analysis. This chapter discusses the methodology used to achieve the objectives of the study.

The intent of the investigation was to compare calculated FoS values from conventional limit equilibrium analysis where drained and undrained material properties were considered against the results of limit equilibrium analysis in which an attempt to satisfy strain compatibility was made. This was done to investigate whether attempting to maintain strain compatibility provides the same or different FoS values to conventional analysis to determine whether this type of analysis should be considered in the future.

A new formulation was proposed to determine a FoS against failure using limit equilibrium methods where strain compatibility is maintained along the failure surface. The method (referred to as the strain mobilisation method) considers a Mohr circle of stress at failure to determine the shear strength mobilised on the failure plane for use in the stability analysis as a function of the deviator stress imposed on the triaxial test results. As part of this method, the strength at the base of each slice was determined using the stress-strain relationships derived from the triaxial test results, based on an assumed increment of mobilised shear strain which was progressively increased.

As the method requires triaxial data for implementation, a review was conducted on a series of consolidated drained and consolidated undrained triaxial compression tests that were performed on reconstituted gold, iron and platinum tailings samples. The review was done to determine the shear strength mobilised on the failure plane for use in the subsequent stability analyses. Some normalisation and adjusting of the measured data were required to enable direct comparison between the different tailings materials, test drainage and effective stress conditions.

Once the soil parameters were established, a spreadsheet capable of solving limit equilibrium slope stability analysis for a given critical slip surface was developed. The spreadsheet was validated by comparing the outputs to the outputs generate by a commercial software package SLOPE/W for a series of test slopes. After the accuracy of the spreadsheet was verified, it was used to assess several scenarios as described below.

For the FoS comparison, three slope cross sections were assessed. For each cross section, up to three material zones were identified. Slope stability analyses were then conducted for the three above-mentioned tailings materials. The properties of Nerlerk sand were also reviewed as an additional material. For each material, six scenarios in terms of assumptions with regard to drained or undrained behaviour and the method of stability analysis used were assessed.

3.2 FOS FORMULATION MAINTAINING STRAIN COMPATIBILITY

The main objective of this study was to investigate a means by which the FoS against slope failure can be assessed by using a limit equilibrium analysis in which strain compatibility is satisfied on the failure surface. The intention was to use triaxial laboratory data to relate the mobilised shear stress to an incrementally increasing shear strain value and then to implement this mobilised stress in an equation to determine the FoS. The development of this formulation is explained in this section. Two key aspects are discussed: the first is the relationship between the shear stress mobilised at the base of each slice in the slope under consideration and the shear stress measured during the triaxial test. The second is a manner to ensure the method can be implemented over a range of effective stress values and is not limited to the discrete values upon which the triaxial tests were conducted.

3.2.1 Shear stress relationship

To ensure strain compatibility was maintained, the Mohr circle of stress at failure in a triaxial compression test was developed (see Figure 3.1). Several key points are highlighted, and these were used to develop the relationships shown below. When considering triaxial compression tests, which provide axis-symmetrical conditions, the principal stresses can be simplified such that the axial stress become the major principal stress (σ'_1) and the radial stress becomes the minor principal stress (σ'_3). The pole of the Mohr circle is therefore located at σ'_3 and the angle of the rupture plane can be determined as shown in Equation (31). The relationship between the deviatoric stress (q) and the major and minor principal stresses is shown in Equation (32). Full derivations of these relationships can be found in many undergraduate textbooks (e.g. Parry, 2004).

$$\hat{E} = 45 + \frac{\varphi'}{2} \tag{31}$$

$$q = \sigma'_1 - \sigma'_3 \tag{32}$$

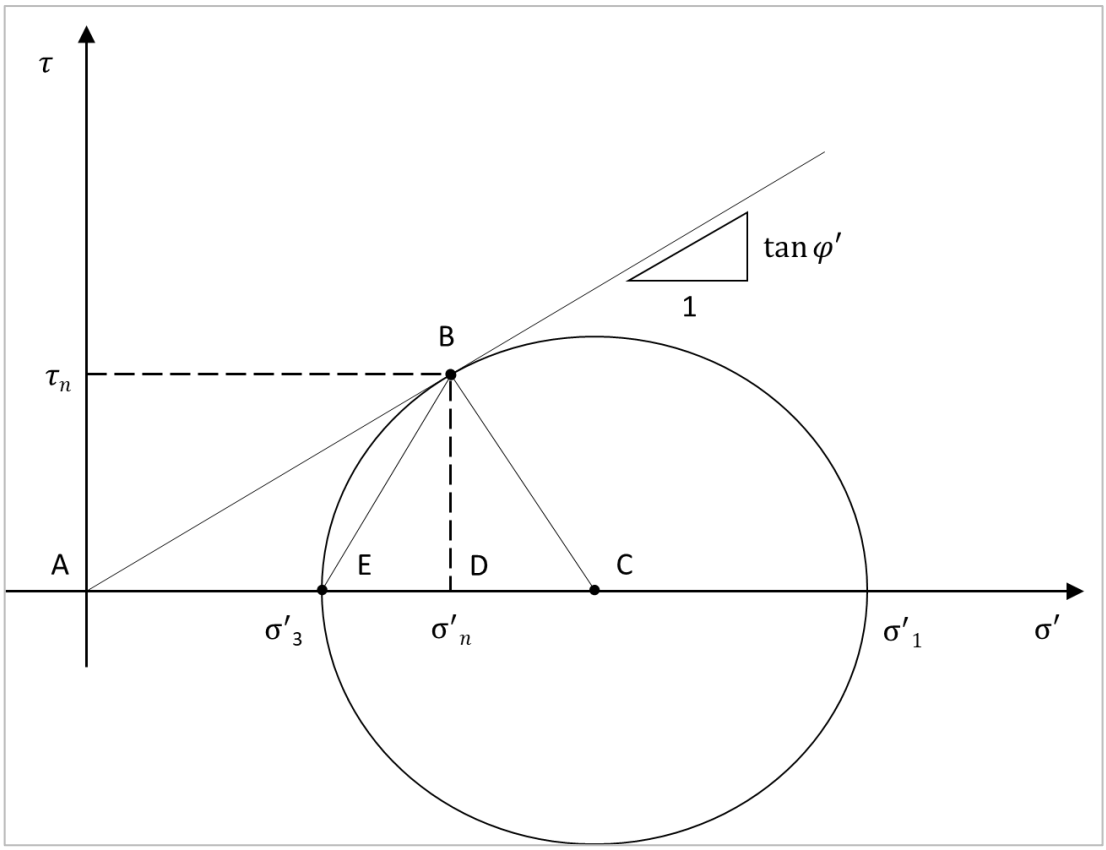

Figure 3.1: Mohr circle at failure, applicable to both CD and CU triaxial tests

By considering additional triangles and defining the appropriate angles and side lengths, it is also possible to develop a relationship between the shear stress mobilised at the base of each slice (τ_n) and the deviatoric stress measured during the triaxial test (q). This relationship, shown in Equation (33), allows the shear stress measured in a triaxial test to be used in a limit equilibrium formulation. For use in the proposed formulation, it was assumed that these relationships remain valid, not only at failure, but also during the mobilisation of strain.

Consider triangle EBC:

$$\hat{E} = \hat{B} = 45 + \frac{\varphi'}{2} \qquad (EC = EB)$$

$$\hat{C} = 90 - \varphi' \qquad (Sum\ angles\ \Delta EBC = 180°)$$

Consider triangle BCD:

$$\sin(90 - \varphi') = \frac{\tau_n}{0.5q} \qquad (BC = 0.5q)$$

$$\tau_n = 0.5 * q * \cos\varphi' \quad (33)$$

3.2.2 Stress level relationship

Since the triaxial tests were conducted at discrete effective stress values and the intent was not to have the method limited to these discrete values, a manner to normalise the measured triaxial data was required. This normalisation would enable the implementation of the method over a wide range of effective stress values in the slip surface under consideration.

The deviator stress versus shear strain functions obtained from the triaxial tests were normalised based on the mean effective stress at failure (p'_f) to provide a stress-strain curve that could be scaled based on the stress level in the slope. This process is explained further in Section 3.3.2. The deviator stress versus shear strain function then became a shear stress ratio versus shear strain function. Note that this was done for both the drained and undrained tests such that drained stress ratios $\left(\frac{q}{p'_f}\right)_{CD,i}$ and undrained stress ratios were determined $\left(\frac{q}{p'_f}\right)_{CU,i}$, dependent on strain increment i. An illustration of these normalised curves is shown in Figure 3.2. To obtain the shear stress applicable at the stress level in the slope, the stress ratio would be multiplied by the normal effective stress at the base of each slice under consideration as shown in Equation (34).

For this study, it was assumed that the normal effective stress (σ'_n) was related to the vertical effective stress (σ'_v) as a function of the slice base angle (α), disregarding the effect of interslice forces, similar to the method by Fellenius (Swedish method).

$$q_i = \sigma'_n * \left(\frac{q}{p'_f}\right)_i \quad (34)$$

Where:

q_i = the deviatoric stress mobilised, based on the shear strain i mobilised (kPa)

$\left(\frac{q}{p'_f}\right)_i$ = the shear stress ratio, based on the amount of shear strain i mobilised.

$\sigma'_n = \sigma'_v * \cos\alpha$ (kPa)

3.2.3 FoS relationship

In its simplest form, the FoS against failure of a slope can be considered in terms of moment equilibrium of forces along the base of each slice along the potential slip surface. Assuming there are no additional forces applied to the soil such as point loads, line loads or accelerations due to earthquake loading, the only forces acting on each slice are the forces due to the mass of the slice and the forces due to pore pressures, as well as interslice forces. Expressions for the two opposing sets of forces can be derived: stabilising forces resisting failure ($F_{stabilising}$) as shown in Equation (35) and destabilising forces causing failure ($F_{stabilising}$) as shown in Equation (36).

$$F_{stabilising} = 0.5 * q * \cos\varphi' * l \tag{35}$$

Where:

$F_{stabilising}$ = Stabilising force resisting failure (kN)

l = Slice base length (m)

$$F_{destabilising} = W * \sin\alpha \tag{36}$$

Where:

$F_{destabilising}$ = Destabilising force causing failure (kN)

Considering all the forces along the base of the slip surface, the FoS against failure for shear strain increment i can be calculated by combining Equations (35) and (36) to form Equation (37). It was assumed that the resultant of the interslice forces is zero, similar to what is assumed as part of the Fellenius method. In addition, the requirement that the local FoS should be equal to the global FoS as in the case of general limit equilibrium formulations is not enforced. Instead, it is assumed that the shear strains at the bases of all slices are identical. The following expression for the FoS as a function of the mobilised deviator stress (q_i) is therefore obtained.

$$FoS_i = \frac{\sum 0.5 * q_i * \cos\varphi' * l * R}{\sum W * \sin\alpha * R} \tag{37}$$

Where:

FoS_i = Calculated FoS, based on the shear strain i mobilised

q_i = Deviatoric stress mobilised, based on the shear strain i mobilised (kPa)

R = Radius of the slip circle (m)

3.2.4 Implementation

Once the required relationships were established, a methodology for the implementation of the strain compatibility method was required. For each scenario assessed, the following workflow was developed:

1. Determine the shear strain increment (ε_i) being considered. For this assessment, the shear strain increment was selected such that there was a minimum of 10 strain increments per stress-strain curve.
2. For the strain increment under consideration read off the applicable stress ratios $\left(\frac{q}{p'_f}\right)_{CD,i}$ and $\left(\frac{q}{p'_f}\right)_{CU,i}$ from the stress normalised triaxial data. This process is illustrated in Figure 3.2.
3. For each slice j, calculate q_i based on the vertical effective stress acting on the base of the slice as shown in Equation (34). This is shown in Figure 3.3.
4. Calculate the strain dependent FoS using Equation (37).
5. Increase the shear strain increment and repeat.

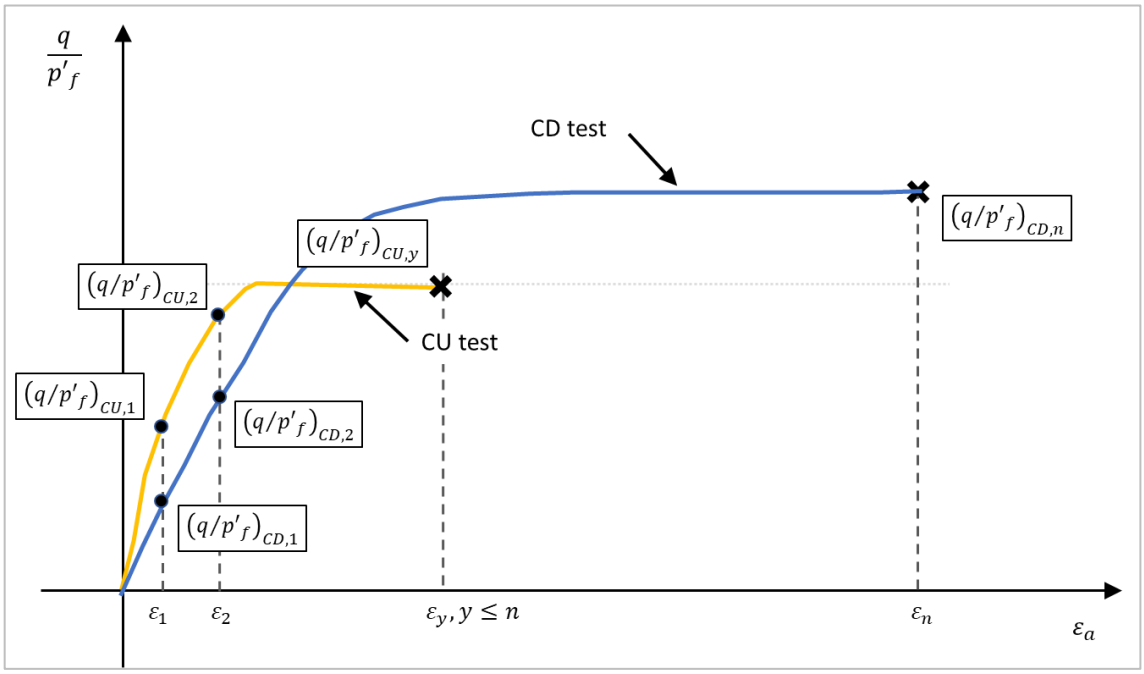

Figure 3.2: Illustration of the determination of the stress ratio based on strain increment

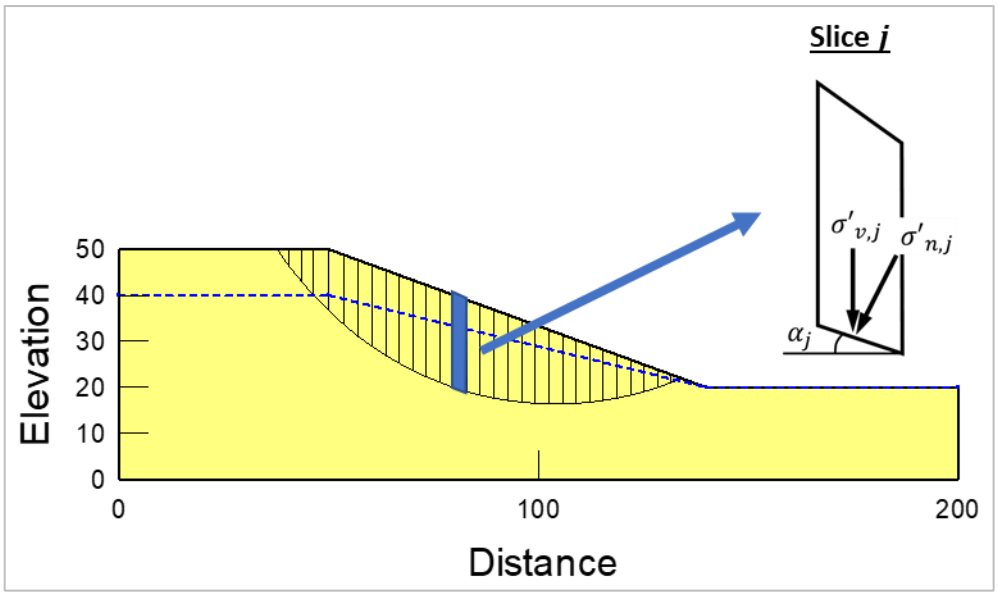

Figure 3.3: Typical slope showing a slip surface and selected parameters for slice *j*

3.3 REVIEW OF TRIAXIAL TEST DATA

The strain compatibility method presented requires triaxial data for implementation. The treatment of the data prior to the implementation of the proposed method is presented here.

A series of drained and undrained triaxial compression tests were conducted by students at the University of Pretoria's geotechnical laboratory in 2018 on three tailings materials. The tests were part of a larger testing regime aimed at identifying the material response for a range of tailings materials under various drainage conditions and effective stresses. In addition, tests conducted on Nerlerk sand, obtained from Jefferies & Been (2015) were also reviewed. The results from these tests were made available for this study and were assessed in detail. Details of this assessment are discussed further in this chapter. A summary of the tests conducted is shown in Table 3.1.

There are concerns regarding the effect of sample preparation method on the stress paths observed during the shear phase. However, it is believed that the Slurry Deposition (SD) method, which was used for the tailings material, does attempt to capture the fabric of the material and is currently the preferred method of sample preparation of loose silty material. This view is supported by other researchers (e.g. Høeg et al., 2000; Corrêa & Oliveira Filho, 2019). The sample preparation method used for the tests conducted at the University of Pretoria was the Slurry Deposition method in an attempt to replicate the field deposition method. The sample preparation method used for the Nerlerk sands was the Moist Tamped method.

Table 3.1: Key parameters of the triaxial tests assessed

Test ID	Material	Triaxial test type	Sample preparation method	Initial confining effective stress (p_0)
GCU_75*	Gold tailings	CU	Slurry Deposition	75 kPa
GCU_200*	Gold tailings	CU	Slurry Deposition	200 kPa
GCD_75*	Gold tailings	CD	Slurry Deposition	75 kPa
GCD_200*	Gold tailings	CD	Slurry Deposition	200 kPa
ICU_75*	Iron tailings	CU	Slurry Deposition	75 kPa
ICU_200*	Iron tailings	CU	Slurry Deposition	200 kPa
ICD_75*	Iron tailings	CD	Slurry Deposition	75 kPa
ICD_200*	Iron tailings	CD	Slurry Deposition	200 kPa
PCU_75*	Platinum tailings	CU	Slurry Deposition	75 kPa
PCU_200*	Platinum tailings	CU	Slurry Deposition	200 kPa
PCD_75*	Platinum tailings	CD	Slurry Deposition	75 kPa
PCD_200*	Platinum tailings	CD	Slurry Deposition	200 kPa
NCU_G101**	Nerlerk sand	CU	Moist Tamped	500 kPa
NCU_G108**	Nerlerk sand	CU	Moist Tamped	500 kPa
NCD_G151**	Nerlerk sand	CD	Moist Tamped	200 kPa
NCD_G155**	Nerlerk sand	CD	Moist Tamped	500 kPa

* tested at the University of Pretoria

** data from Jefferies & Been (2015)

Grading analyses were conducted on the materials and the particle size distribution curves shown in Figure 3.4 were developed. The gold and platinum tailings have a similar distribution and can be classified as a silty sand while the iron tailings is finer and can be classified as a silt. The Nerlerk sand is narrowly graded and can be classified as a sand.

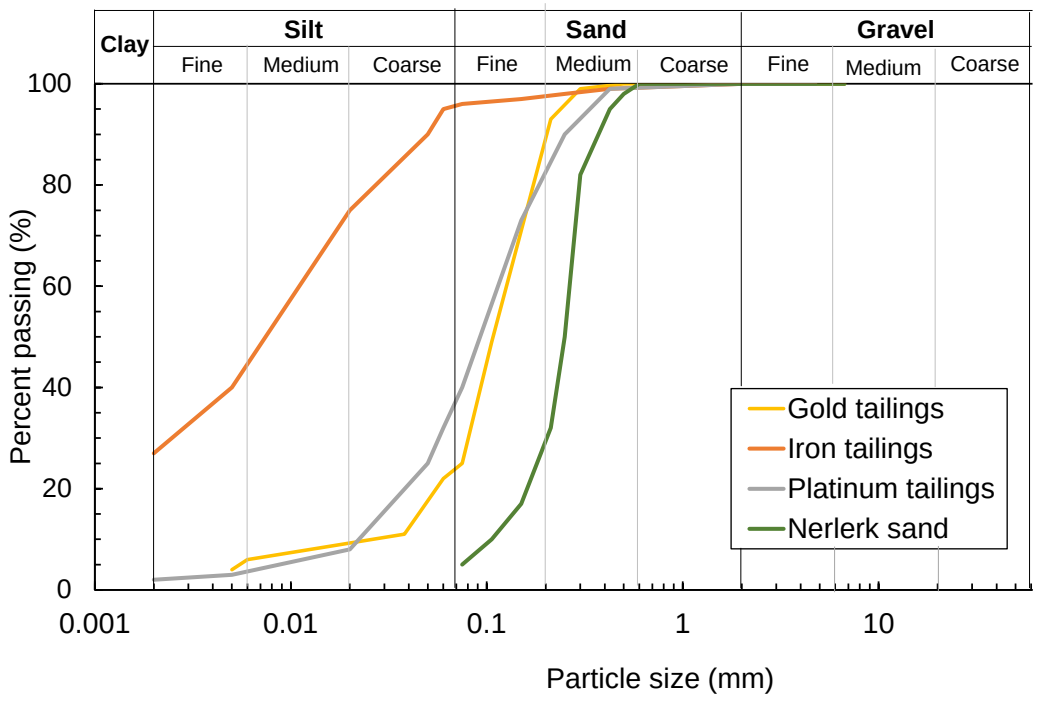

Figure 3.4: Particle size distribution analysis of the three tailings materials

3.3.1 Stress paths

For each tailings type, four triaxial compression tests were conducted, i.e. a Consolidated Drained (CD) test at an initial confining effective stress of 75 kPa, a Consolidated Undrained (CU) test at 75 kPa, a CD test at 200 kPa and a CU test at 200 kPa. Testing using these boundary conditions and effective stresses allowed the material behaviour to be observed at typical loading ranges expected on tailings dams in South Africa.

Friction angles and cohesion intercept values were determined using a line of best fit through the failure points in s-t space, in conjunction with the Mohr circles at failure. Initially, failure was defined as the point in the shear phase of the triaxial test where there was no further change in void ratio for the CD tests and no further change in pore pressure for the CU test. This definition is in line with the classical definition of steady state. However, not all the tests were conducted at strains sufficiently large to reach such a state and, in those cases, failure was defined as the final data point in the shear phase. It is for this reason that the end point shown for each shear phase is referred to as the end of test point and not steady state. As part of the normalisation process, a different failure point was defined for the CU tests and this is described in detail later in the chapter.

In addition to the friction angle and cohesion intercept parameters interpreted from the stress paths,

the initial tangent modulus (E_i) and the dilation angle (ψ) can also be determined from the triaxial test data. These parameters were used in the finite element analyses described in Section 3.5.2. By plotting the deviatoric stress vs. axial strain, the initial tangent modulus can be determined as a function of the slope of the initial, linear section of the function. More details of this can be found in Section 2.4.1.

The dilation angle can be determined as the slope of the function when plotted in volumetric strain vs. shear strain space. As discussed in Section 2.4.1, the measured axial strain in a consolidated undrained triaxial test is equivalent to the shear strain mobilised. For this study, it was assumed that this relationship is applicable to consolidated drained tests as well.

Additional details of the triaxial test results can be found in Appendix A.

3.3.1.1 Gold tailings

The measured responses during the shear phase for the gold tailings are shown in Figure 3.5. Due to the dilative tendency that occurred after the initial contractive tendency, the deviatoric strengths at failure were greater for the CU tests compared to the CD tests as can be seen in Figure 3.5a. It is clear from the excess pore pressure vs axial strain graph (Figure 3.5b) that the pore pressures had not yet reached equilibrium in the CU tests. This is an example of where steady state was not reached and why the end point of the test is rather referred to as the end of test point. Similarly, the GCD_200 test indicated that there was still a noticeable rate of change of volumetric strain at the end point (Figure 3.5c). However, the GCD_75 test did appear to have stabilised in terms of volumetric strain and this could be considered steady state.

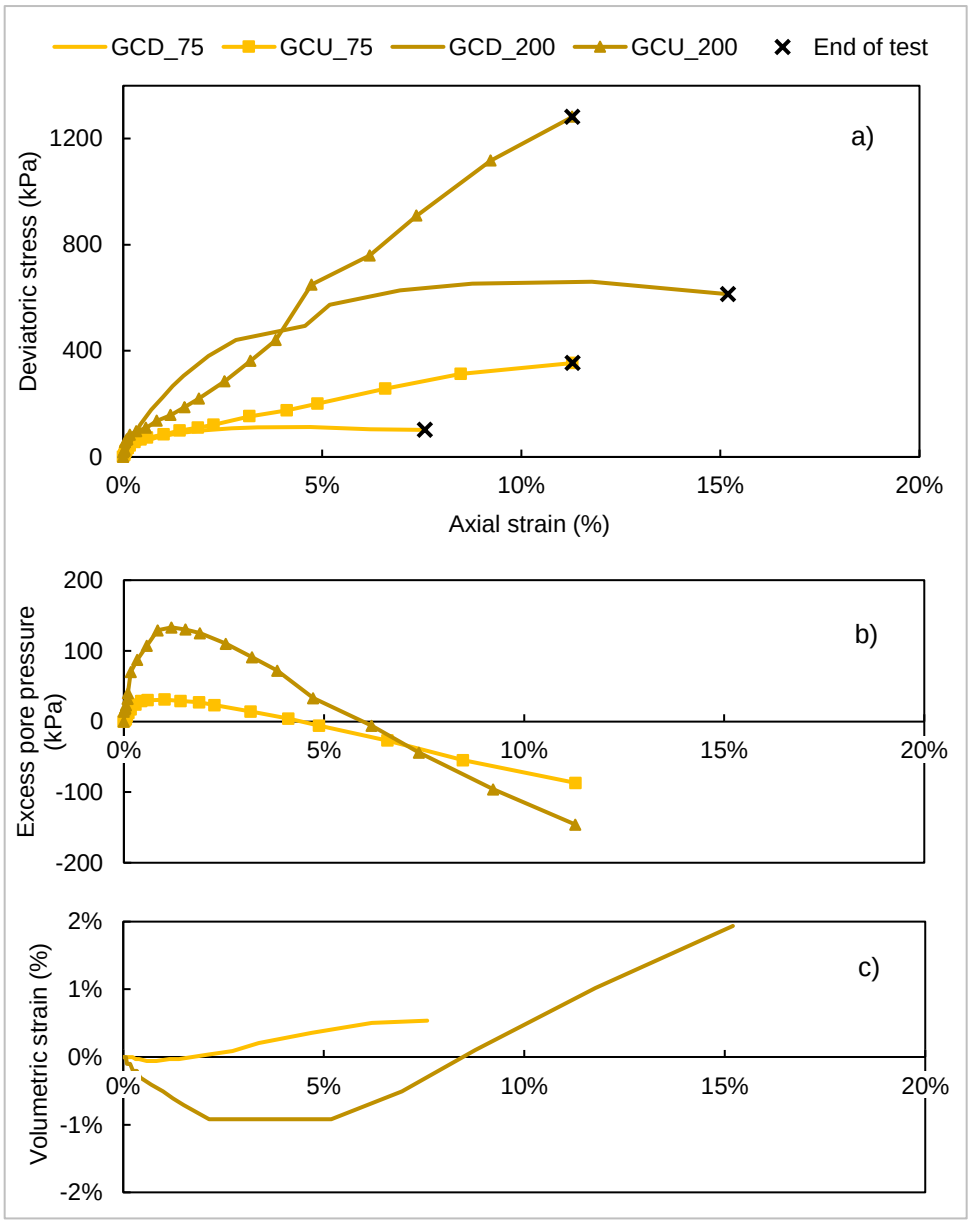

Figure 3.5: Triaxial test results for the gold tailings: a) deviatoric stress, b) excess pore pressure, c) volumetric strain vs. axial strain.

The intent with obtaining the failure point was to determine the effective friction angle of the material. The stress paths observed during the tests, plotted in s-t space, are shown in Figure 3.6. A friction angle of 39° and a cohesion intercept of 0 kPa was found as a best fit to match the data. The undrained tests showed initial contractive tendency and then strong dilative tendency which is in line with the behaviour expected from SD samples as reported in the literature.

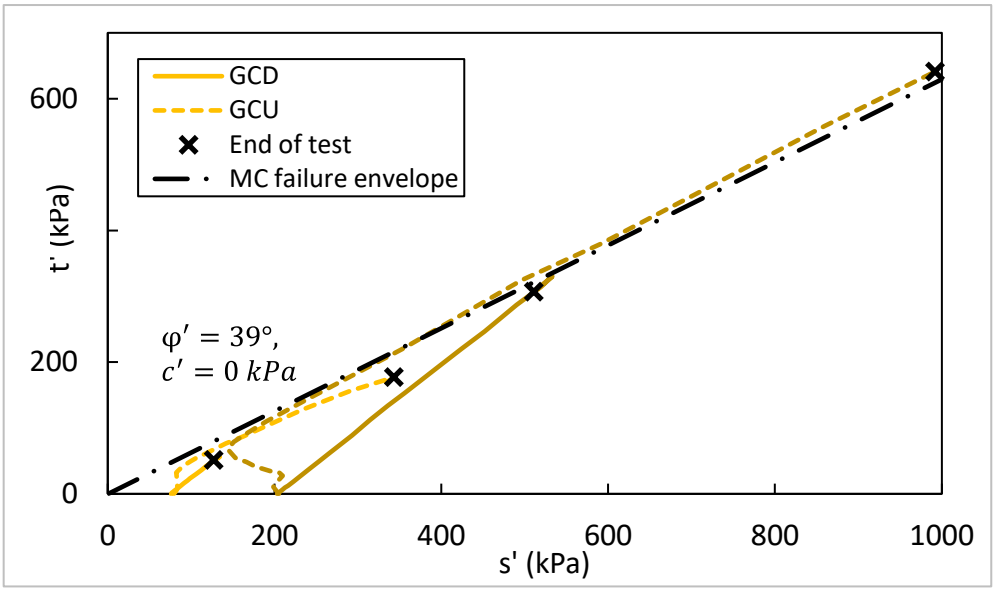

Figure 3.6: Stress paths for the gold tailings

The initial tangent shear modulus was determined as a best fit for the stress-strain curves shown in Figure 3.7a. Although there is no consistent linear slope in the curves, a value of 30 000 kPa was chosen as a representative value for the gold tailings. The GCD_200 test follows this slope through to 0.3% axial strain and the GCU_75 through to 0.1% axial strain. The GCU_200 is steeper than the chosen value while the GCD_75 is flatter.

The volumetric strain is plotted against the axial strain in Figure 3.7b. Knowledge of the dilation angle is required to conduct the numerical analyses presented in Section 3.5.2. Although the dilation angles vary with strain, it was decided that a dilation angle of 0° should be used for the gold tailings as it is believed that it would be more representative of a loose gold tailings sample prone to liquefaction.

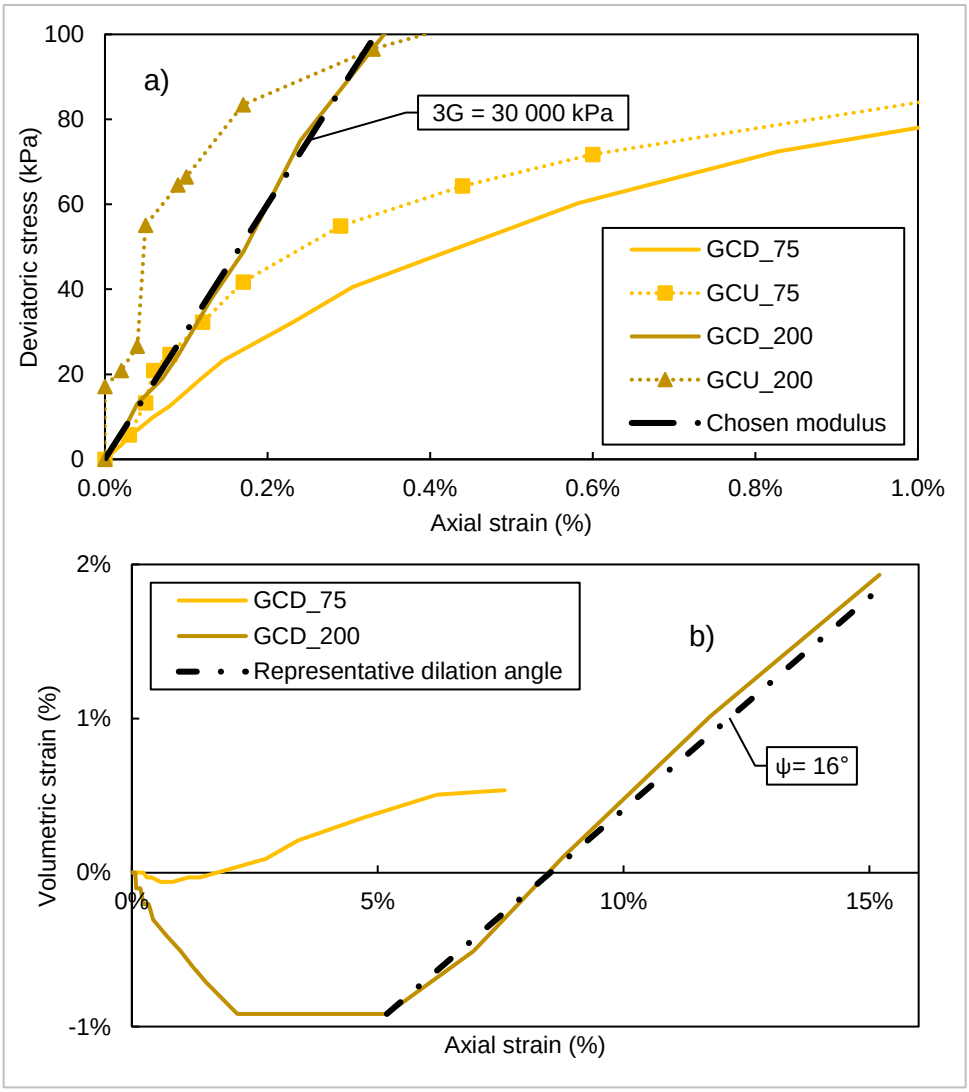

Figure 3.7: Determination of parameters for the gold tailings: (a) shear modulus and (b) dilation angle

3.3.1.2 Iron tailings

The measured responses during the shear phase for the iron tailings are shown in Figure 3.8a. The excess pore pressure vs. axial strain graph, shown in Figure 3.8b, indicates that the pore pressures had stabilised by the end of the test and that the samples were close to steady state. The volumetric strain vs. axial strain graph, shown in Figure 3.8c, also shows this feature. Note that due to the poor data obtained for the ICD_200 test, these results were not plotted.

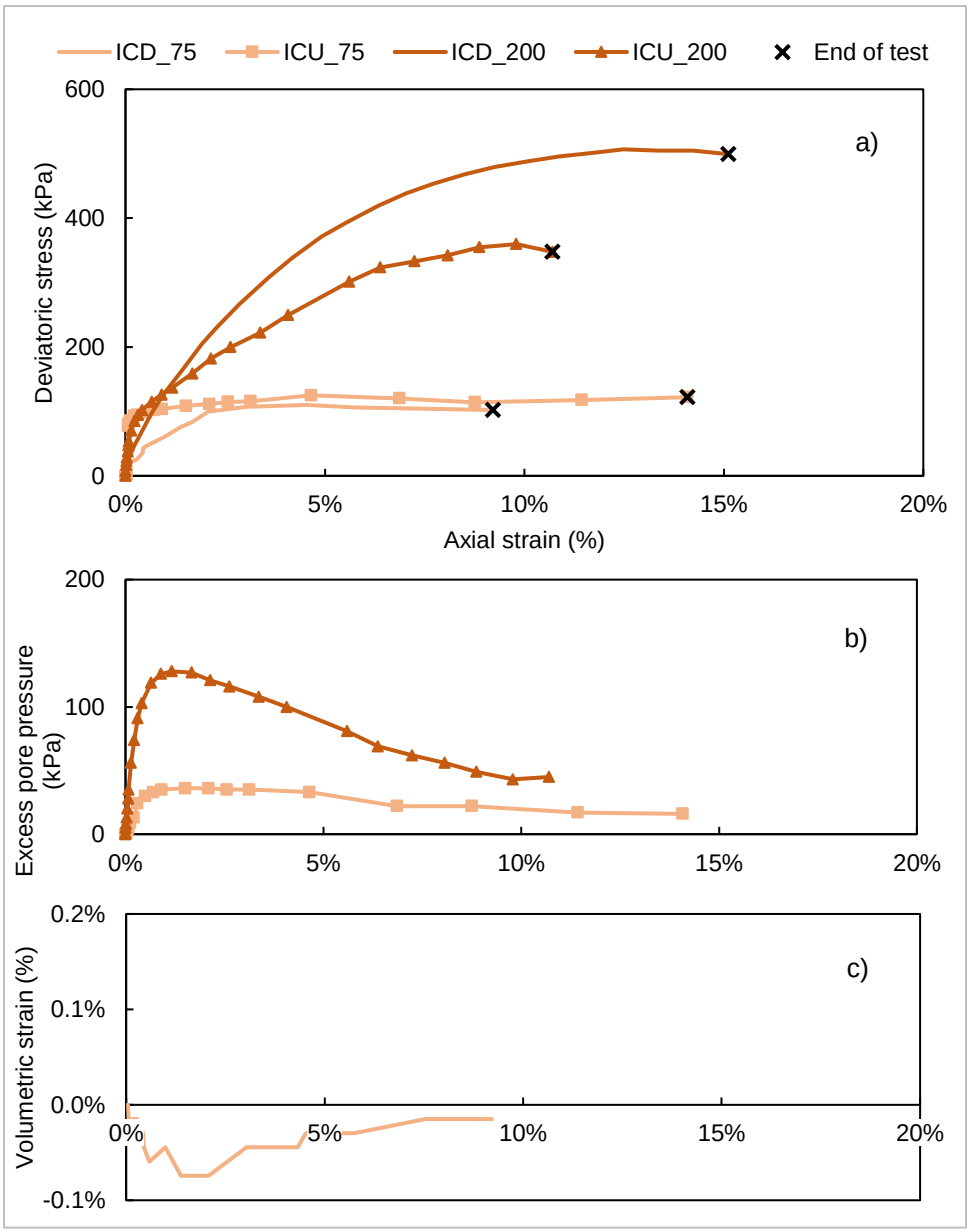

Figure 3.8: Triaxial test results for the iron tailings: a) deviatoric stress, b) excess pore pressure, c) volumetric strain vs. axial strain.

The stress paths observed during the tests, plotted in s-t space, are shown in Figure 3.9. A friction angle of 35° and a cohesion intercept of 0 kPa was found as a best fit to match the data. It is believed that the apparent difference in friction angle between the high and low stresses is due to the ram friction which is likely to be more significant at low stresses. It is for this reason that tests are normally conducted at effective stress values exceeding 100 kPa. Note that the applied load was externally measured.

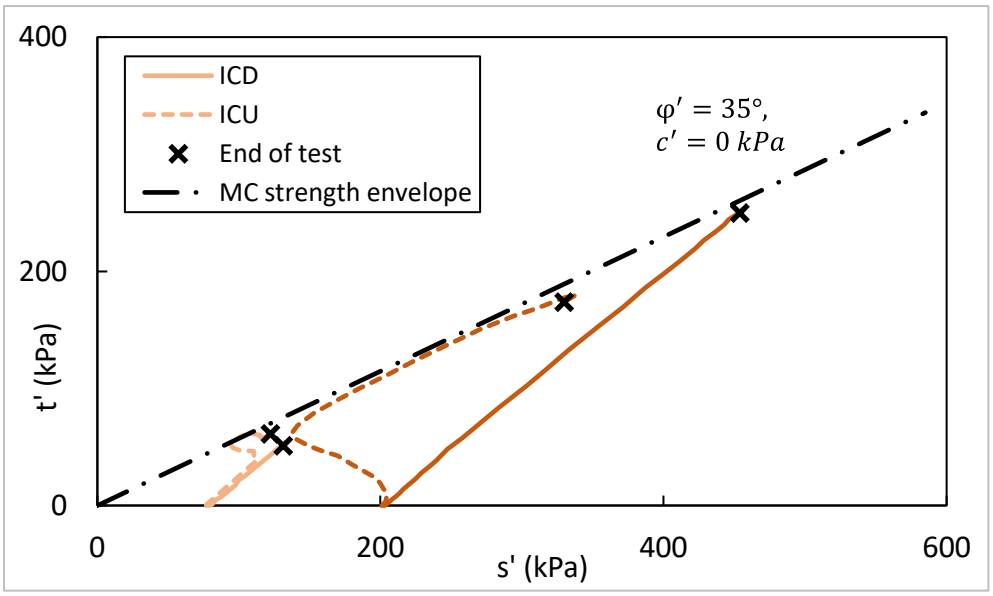

Figure 3.9: Stress paths for the iron tailings

The initial tangent shear modulus for the iron tailings was determined as a best fit for the stress-strain curves shown in Figure 3.10a. Although there is no consistent linear slope in the curves, a value of 40 000 kPa was chosen as a representative value for the iron tailings. The ICU_75 and ICU_200 tests show steeper functions and the ICD_75 and ICD_200 tests show flatter functions than the chosen modulus. The volumetric strain is plotted against the axial strain in Figure 3.10b. Only the results for the ICD_75 test were plotted since the results from the ICD_200 test did not plot adequately. Although a dilation angle of 0.4° can theoretically be derived, it was decided that a dilation angle of 0° should be used as the function did not extend back into the positive volumetric strain space (i.e. the information available was not adequate to make a definite conclusion).

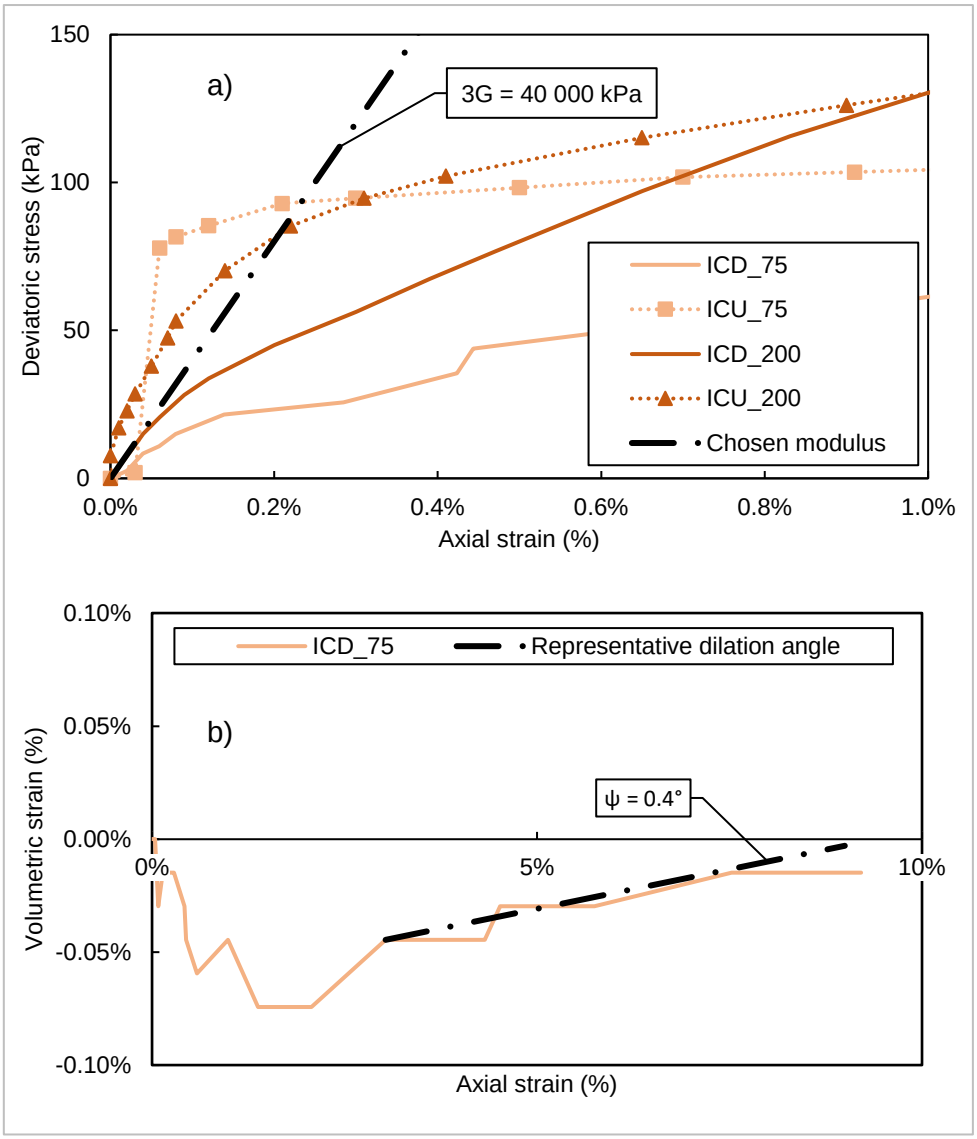

Figure 3.10: Determination of parameters for the iron tailings: a) shear modulus and b) dilation angle

3.3.1.3 Platinum tailings

The measured responses during the shear phase for the platinum tailings are shown in Figure 3.11a. The excess pore pressure vs. axial strain graph is shown in Figure 3.11b and the volumetric strain vs, axial strain graph is shown in Figure 3.11c. Figure 3.11c appears to suggest that steady state was close to being achieved for the CD tests.

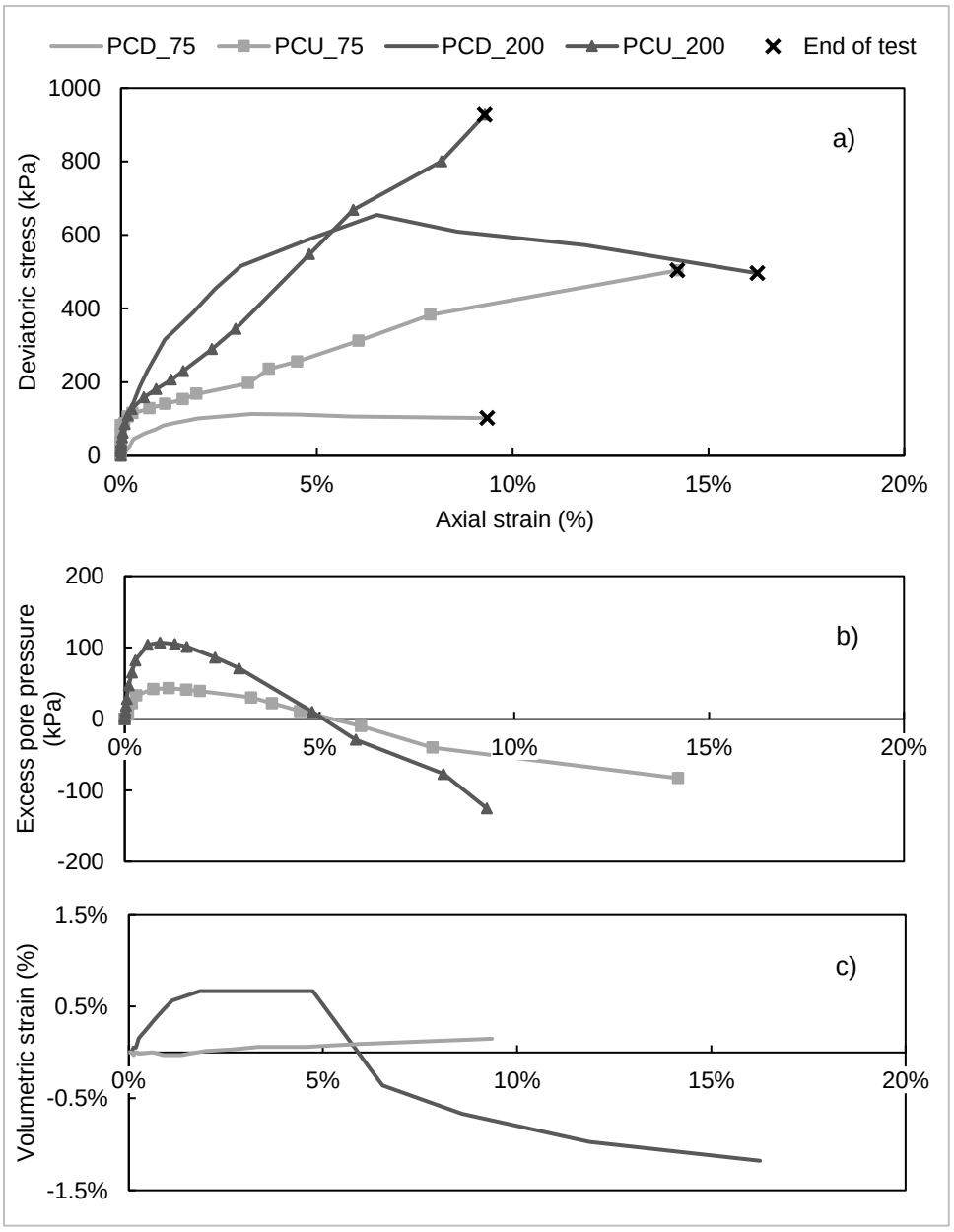

Figure 3.11: Triaxial test results for the platinum tailings: a) deviatoric stress, b) excess pore pressure, c) volumetric strain vs. axial strain.

The stress paths observed during the tests, plotted in s-t space, are shown in Figure 3.12. A friction angle of 38° and a cohesion intercept of 0 kPa was found as a best fit to the data. Although Figure 3.11b indicates that the pore pressures had not yet reached equilibrium by the end of the test, it is believed the stress paths provided sufficient information to determine the friction angle.

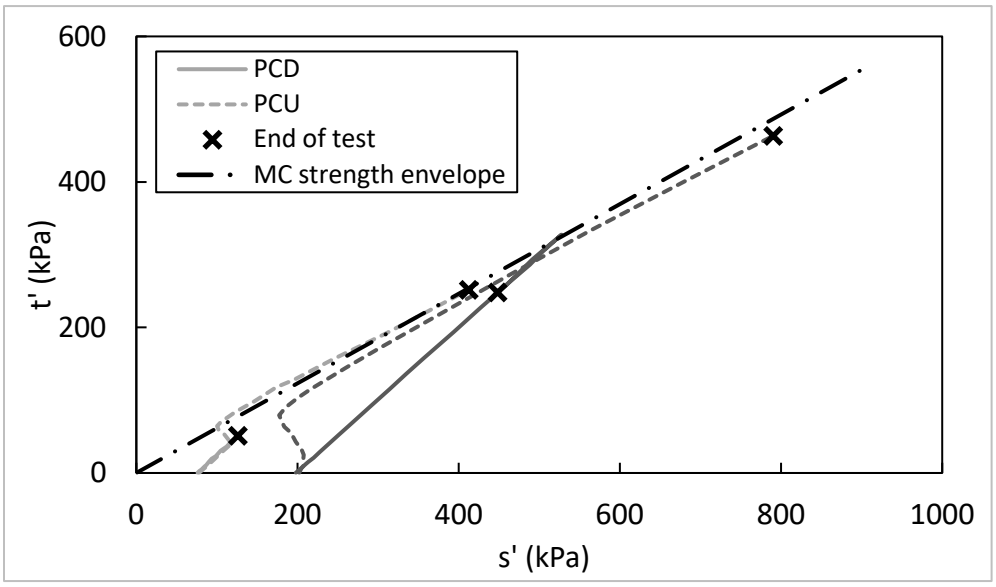

Figure 3.12: Stress paths for the platinum tailings

As with the gold and iron tailings, the initial tangent shear modulus for the platinum tailings was determined as a best fit for the stress-strain curves shown in Figure 3.13a. A value of 75 000 kPa was chosen as a representative value for the platinum tailings as it matched the PCD_200 and PCU_200 test up to 0.1% axial strain. However, the PCD_75 and PCU_75 tests show significantly steeper and flatter functions than the chosen function, respectively. The volumetric strain is plotted against the axial strain in Figure 3.13b. The PCD_75 test showed a dilation angle of 1°. However, since the PCD_200 test showed a negative dilation angle, it was decided that a dilation angle of 0° should be applied to the platinum tailings.

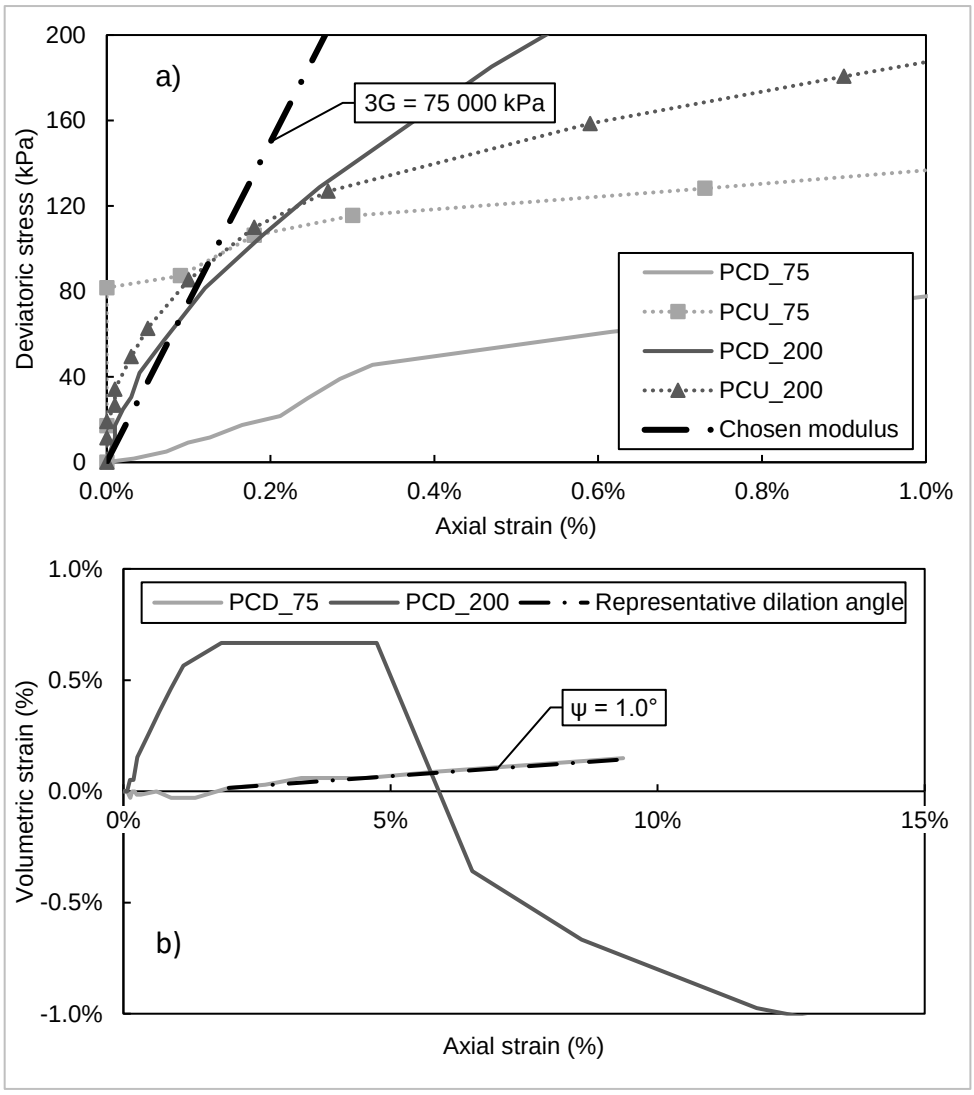

Figure 3.13: Determination of parameters for the platinum tailings: a) shear modulus and b) dilation angle

3.3.1.4 Nerlerk sand

The measured responses during the shear phase for the Nerlerk sand are shown in Figure 3.14a. The excess pore pressure vs. axial strain graph is shown in Figure 3.14b and the volumetric strain vs, axial strain graph is shown in Figure 3.14c. Figure 3.14b appears to suggest that steady state was close to being achieved for the CU tests. The same feature can be seen in Figure 3.14c regarding the NCD_G151 test. However, it does appear that there is a still a rate of change in the NCD_G155 test indicating that steady state had not been reached.

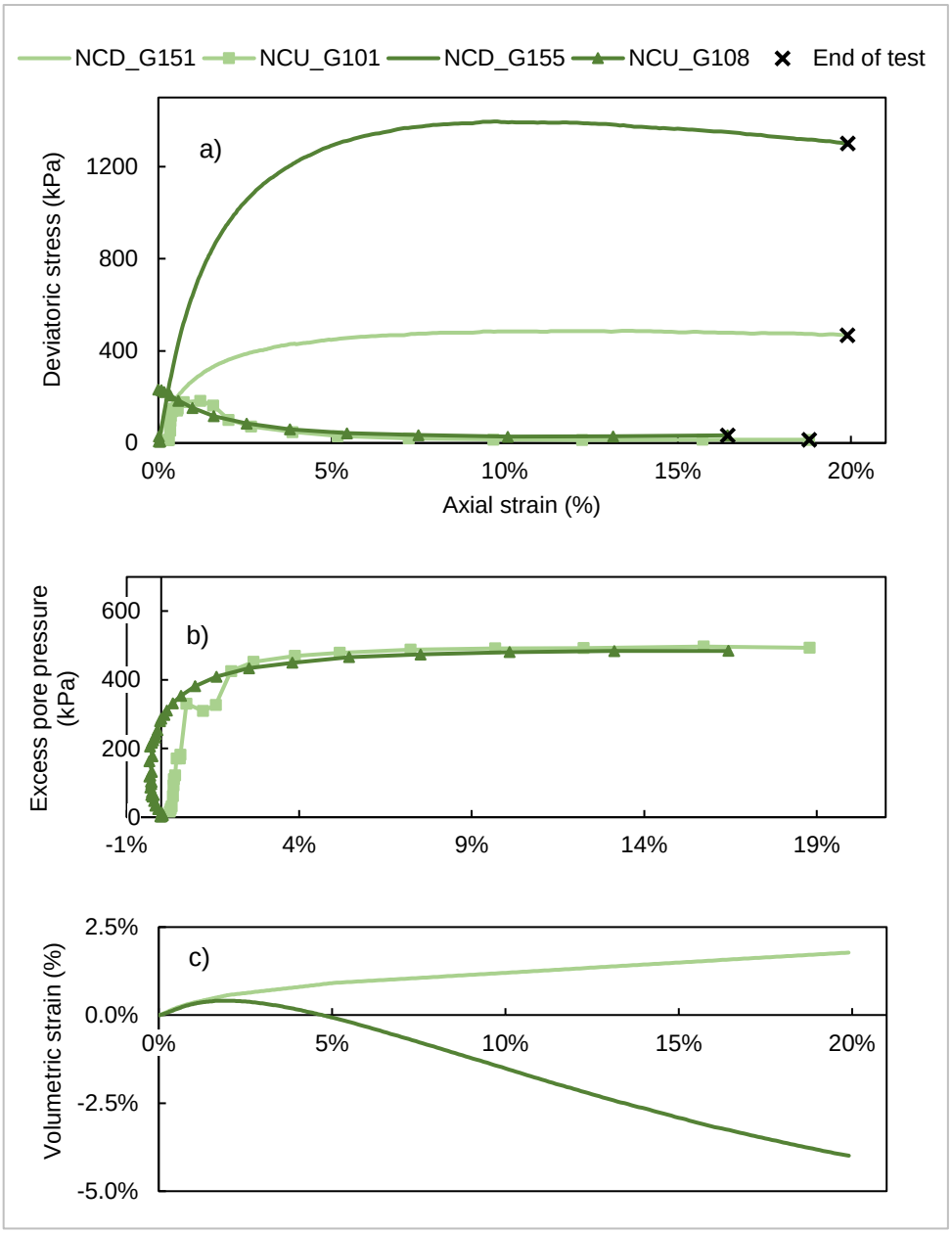

Figure 3.14: Triaxial test results for the Nerlerk sand: a) deviatoric stress, b) excess pore pressure, c) volumetric strain vs. axial strain

The stress paths observed during the tests, plotted in s-t space, are shown in Figure 3.15. A friction angle of 34.4° and a cohesion intercept of 0 kPa was found as a best fit to the data. It can be seen that the CU tests contracted to failure and failed at very low values of shear stress. This is consistent with the results expected from samples prepared using the MT sample preparation method.

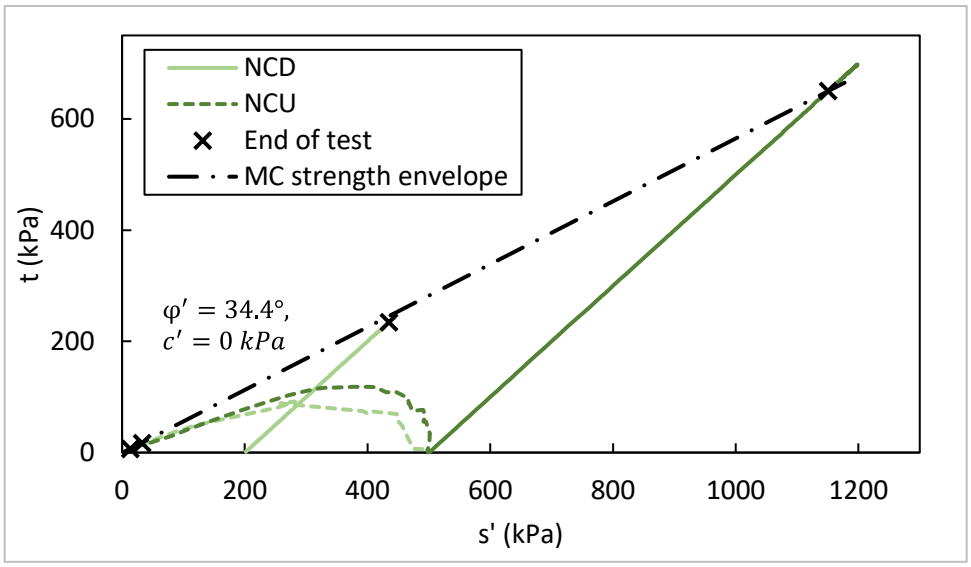

Figure 3.15: Stress paths for the Nerlerk sand

The initial tangent shear modulus for the Nerlerk sand was determined as a best fit for the stress-strain curves shown in Figure 3.16a. Although there is no single slope that represents all the tests, a value of 30 000 kPa was chosen as a representative value for the Nerlerk sand. Conversely to the tailings materials, the CD tests showed steeper functions when compared to the CU tests at the same initial confining stress. The volumetric strain is plotted against the axial strain in Figure 3.16b. As the samples did not dilate during drained shearing, no dilation angle could be assigned.

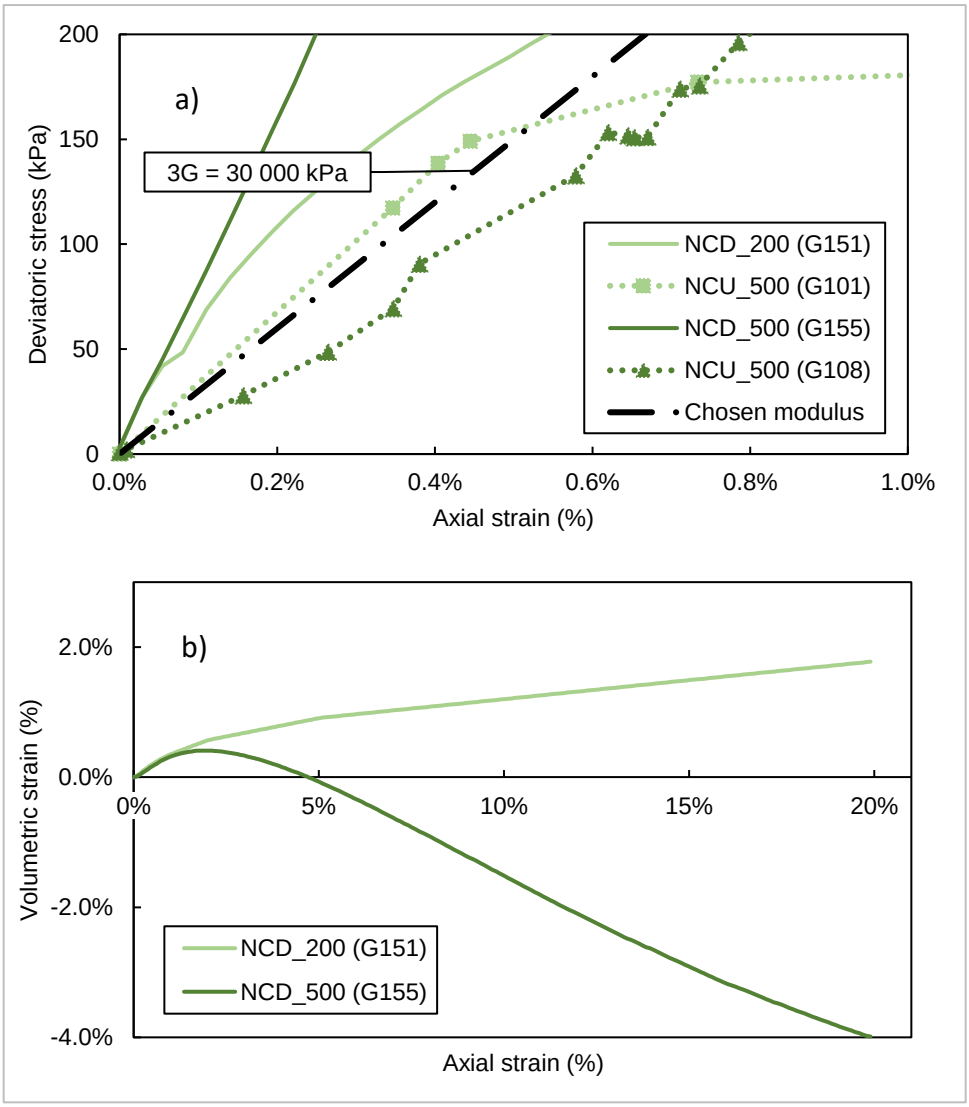

Figure 3.16: Determination of parameters for the Nerlerk sand: a) shear modulus and b) dilation angle

3.3.1.5 Summary

The shear phase of the triaxial tests results on the four materials were reviewed. Several graphs were plotted showing the behaviour of the tailings during shearing and ultimately these graphs were used to estimate several soil parameters. Unlike the theoretical curves which predict contractive behaviour for loose tailings, the undrained tests all showed a tendency for initial contraction and then strong dilation which is typical of reconstituted samples that have been prepared using the SD sample preparation method. This is discussed further in Section 2.4.1.2.

A summary of the interpreted soil parameters is shown in Table 3.2. Due to the discrepancy between the 75 kPa and 200 kPa results, it was decided that a dilation angle of zero would be set for all the tailings materials. The estimated initial tangent moduli appear to be on the upper bound of values expected for tailings materials.

Table 3.2: Summary of the soil parameters derived from the triaxial test results

	Mohr-Coulomb friction angle (φ')	Cohesion (c')	Initial tangent modulus (E_i)	Dilation angle (ψ)
Gold tailings	39°	0 kPa	26 000 kPa	0°
Iron tailings	35°	0 kPa	34 667 kPa	0°
Platinum tailings	38°	0 kPa	65 000 kPa	0°
Nerlerk sand	34.4°	0 kPa	26 000 kPa	0°

3.3.2 Normalisation of stress-strain curves

To implement the proposed method of determining a FoS using limit equilibrium methods where strain compatibility along the failure surface is maintained, it was necessary to normalise the stress-strain curves. This was required as triaxial tests were only performed at two discrete effective confining stress values, one of which was discarded due to ram friction effects, leaving only one stress level. The stress-strain curves were therefore normalised by the stress at failure to provide stress-strain curves that could be scaled based on the stress level in the slope.

In addition to normalising the data based on the mean effective stress at failure, two specific changes were made: the first was to re-define the end point for the CU tests that exhibited a dilative tendency as the first time the stress path started to show phase transfer behaviour from contractive to dilative behaviour as shown in Figure 3.17a. For samples that exhibited a contractive tendency only (the Nerlerk sand), this point was simply defined as the intersection with the yield strength envelope (e.g. Konrad, 1993). This was done so that the behaviour of potentially contractive material could be adequately assessed.

The second change was to limit the undrained shear strength mobilised to the maximum shear strength defined by the Yield Strength Ratio (YSR) as shown in Figure 3.17b. The YSR was defined as the ratio of the shear strength at the failure point to the initial confining stress as shown in Equation (38). This process was conducted as described below for the four materials considered.

Note that this normalisation was done by refining the stress paths in p'-q space and then carrying these changes across to the stress-strain graphs. To simplify the process, it was further decided that only the tests conducted on the tailings material at 200 kPa would be used as the tests at 75 kPa were likely influenced by the ram friction. The tests at 500 kPa were used for the Nerlerk sand.

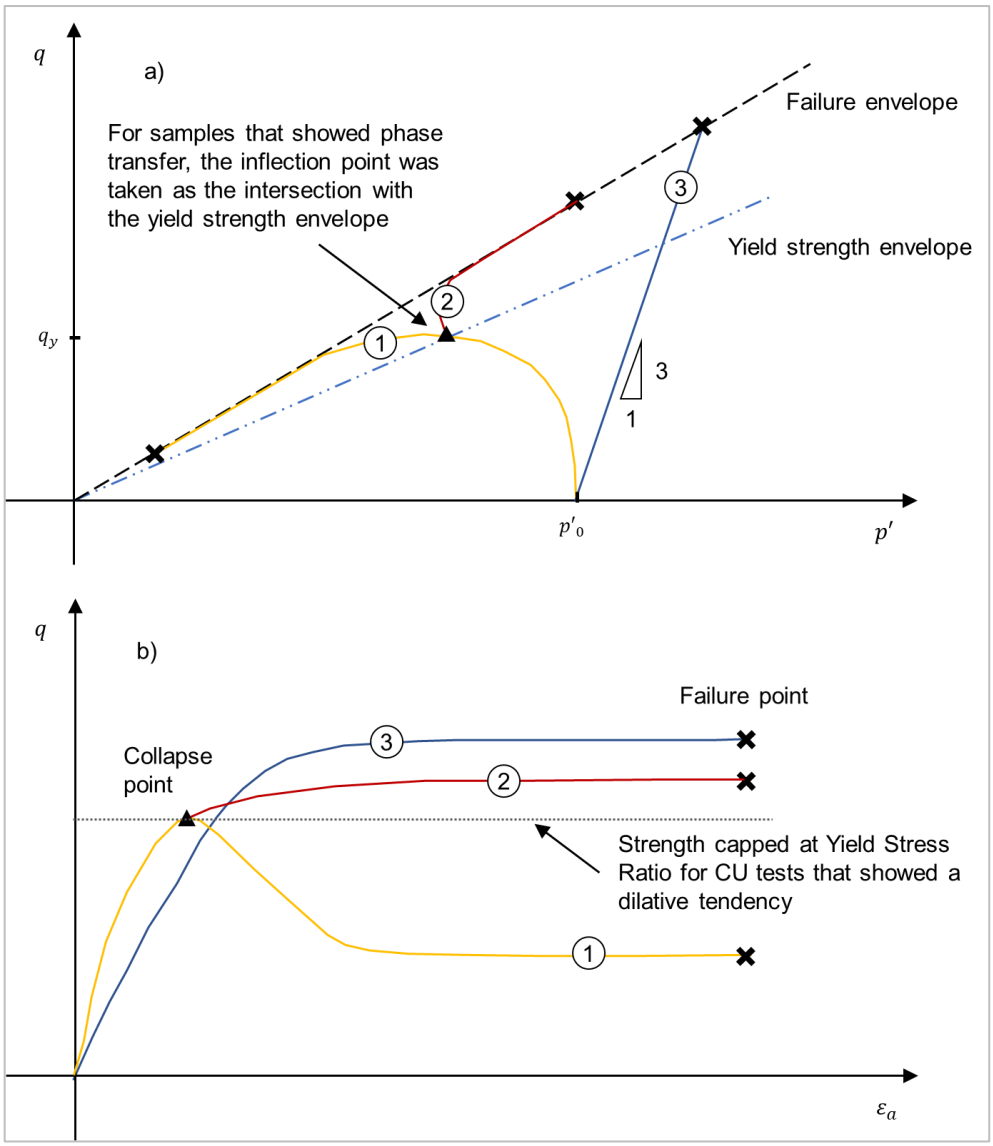

Figure 3.17: Normalisation process used for the proposed method: a) deviatoric stress vs. mean effective stress and b) deviatoric stress vs. axial strain

$$YSR = \frac{q_y}{p'_0} \tag{38}$$

Where:

YSR = Yield stress ratio

q_y = Yield deviator stress at collapse point (kPa)

p'_0 = Initial confining stress (kPa)

3.3.2.1 Gold tailings

The normalisation of the stress paths observed during the shear phase of the triaxial tests conducted for the gold tailings is shown in Figure 3.18. The measured data are indicated in a lighter

colour and denoted GCD and GCU for the CD and CU tests, respectively. The normalised curves are differentiated from the measured curves with an “N” as a prefix.

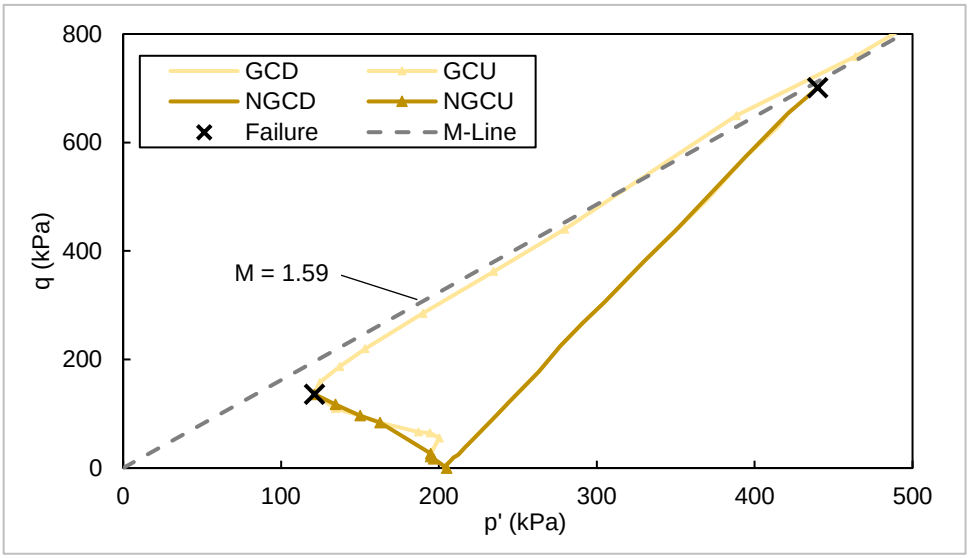

Figure 3.18: Normalisation of the stress paths of the gold tailings

The normalisation process as descried above results in the stress-strain curves shown in Figure 3.19. These normalised curves enable direct comparison with the FoS values obtained from the limit equilibrium analysis. It is clear that a lower strength is mobilised for the CU test when compared to the CD test. In addition, significantly less axial strain is mobilised for the CU test to reach failure (0.8%) when compared to the axial strain mobilised for the CD test to reach failure (11.8%). The dashed line represents the YSR limit imposed on the undrained shear strength.

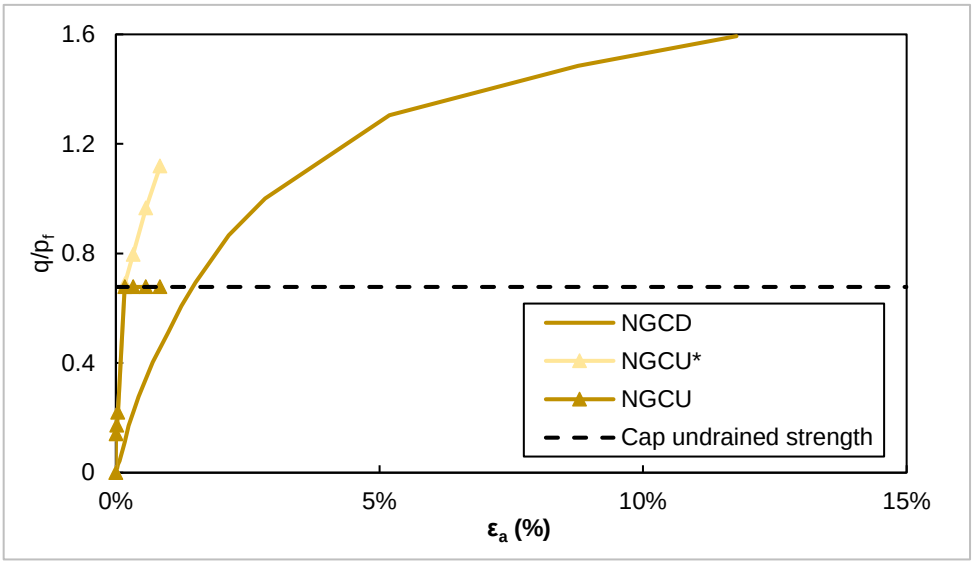

Figure 3.19: Normalised stress-strain curves for the gold tailing

3.3.2.2 Iron tailings

The normalisation of the stress paths observed during the shear phase of the triaxial tests conducted for the iron tailings is shown in Figure 3.20. The measured data are indicated in a lighter colour and denoted ICD and ICU for the CD and CU tests, respectively. The normalised curves are differentiated from the measured curves with an “N” as a prefix.

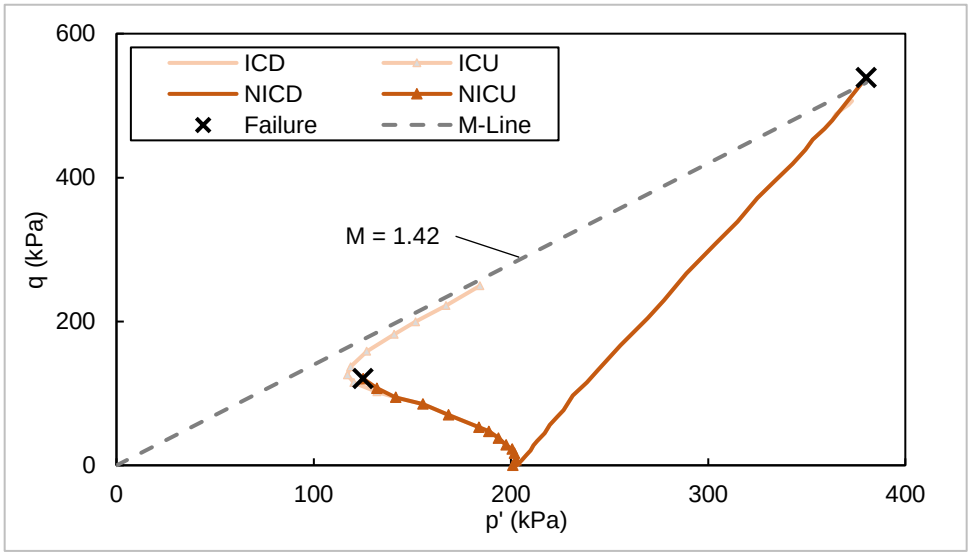

Figure 3.20: Normalisation of the stress paths for the iron tailings

Once the normalisation process was complete, the stress-strain curves shown in Figure 3.21 were developed. As was noted with the gold tailings, lower strengths are mobilised for the CU test and significantly less axial stain is mobilised for the CU test to reach failure (0.7%) when compared to the axial strain mobilised for the CD to reach failure (13.4%).

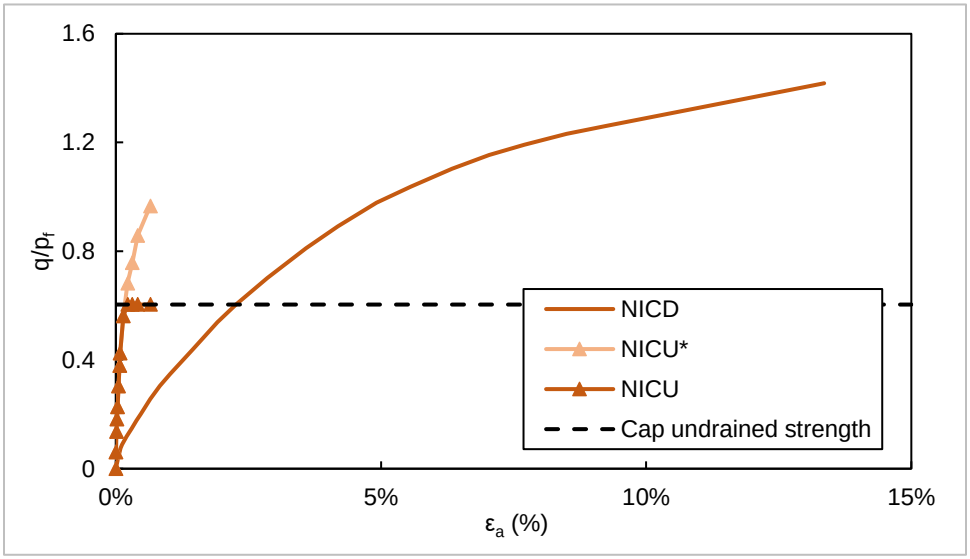

Figure 3.21: Normalised stress-strain curves for the iron tailings

3.3.2.3 Platinum tailings

The normalisation of the stress paths observed during the shear phase of the triaxial tests conducted for the platinum tailings is shown in Figure 3.22. The measured data are indicated in a lighter colour and denoted PCD and PCU for the CD and CU tests, respectively. The normalised curves are differentiated from the measured curves with an “N” as a prefix.

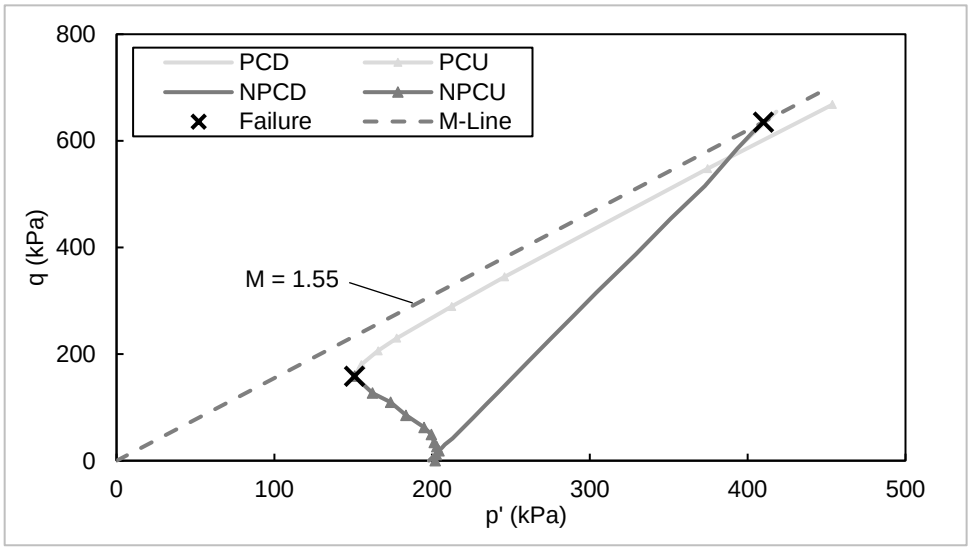

Figure 3.22: Normalisation of the stress paths for the platinum tailings

Once the normalisation process was complete, the stress-strain curves shown in Figure 3.23 were developed. The same trend as was seen in the gold and iron tailings is observed in the platinum tailings. Lower strengths are mobilised for the CU test and significantly less axial stain is mobilised for the CU test to reach failure (0.6%) when compared to the axial strain mobilised for the CD to reach failure (6.5%).

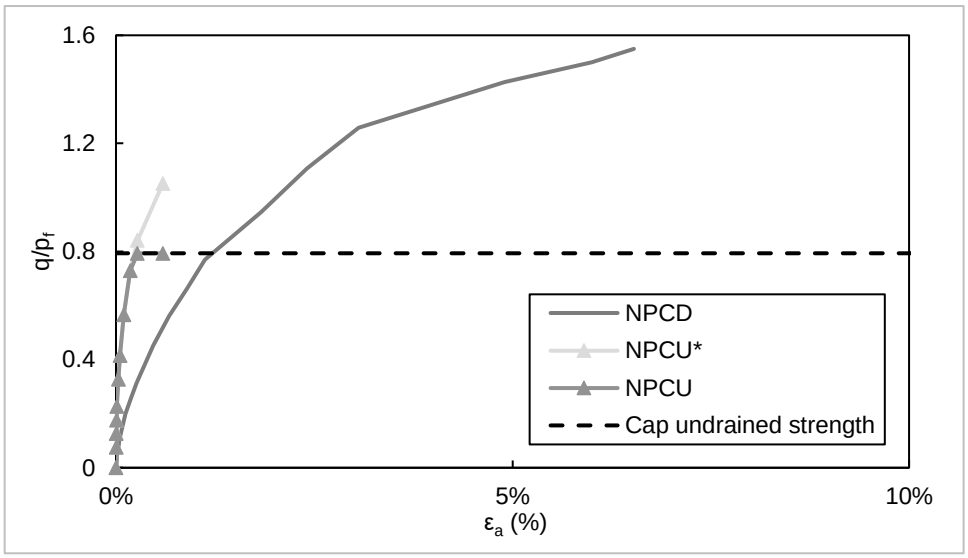

Figure 3.23: Normalised stress-strain curves for the platinum tailings

3.3.2.4 Nerlerk sand

The normalisation of the stress paths observed during the shear phase of the triaxial tests conducted for the Nerlerk sand is shown in Figure 3.24. The measured data is indicated in a lighter colour and denoted NCD and NCU for the CD and CU tests, respectively. The normalised curves are differentiated from the measured curves with an “N” as a prefix.

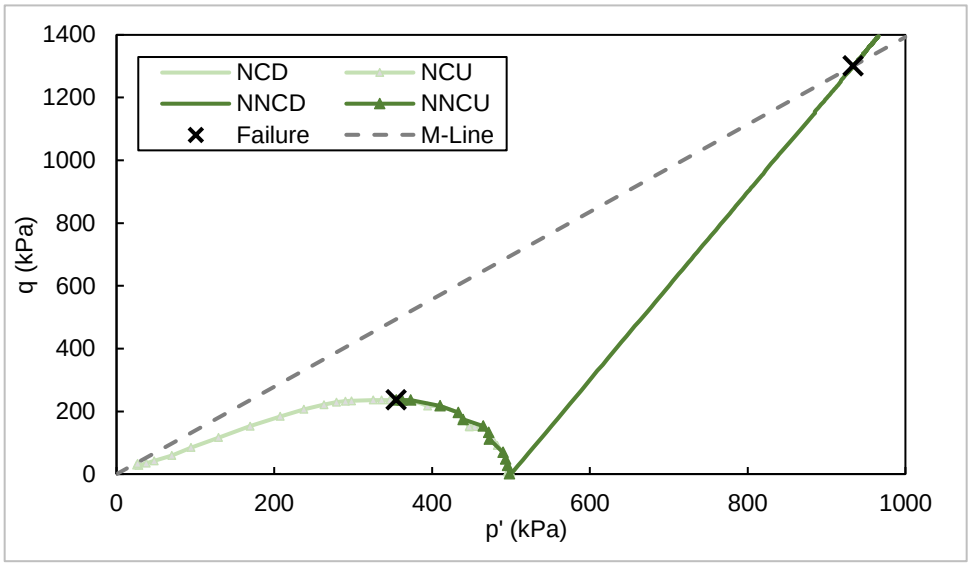

Figure 3.24: Normalisation of the stress paths for the Nerlerk sand

Once the normalisation process was complete, the stress-strain curves shown in Figure 3.25 were developed. The same trend as was seen in the tailings material is observed in the Nerlerk sand. Lower strengths are mobilised for the CU test and significantly less axial stain is mobilised for the

CU test to reach failure (1.0%) when compared to the axial strain mobilised for the CD to reach failure (19.9%).

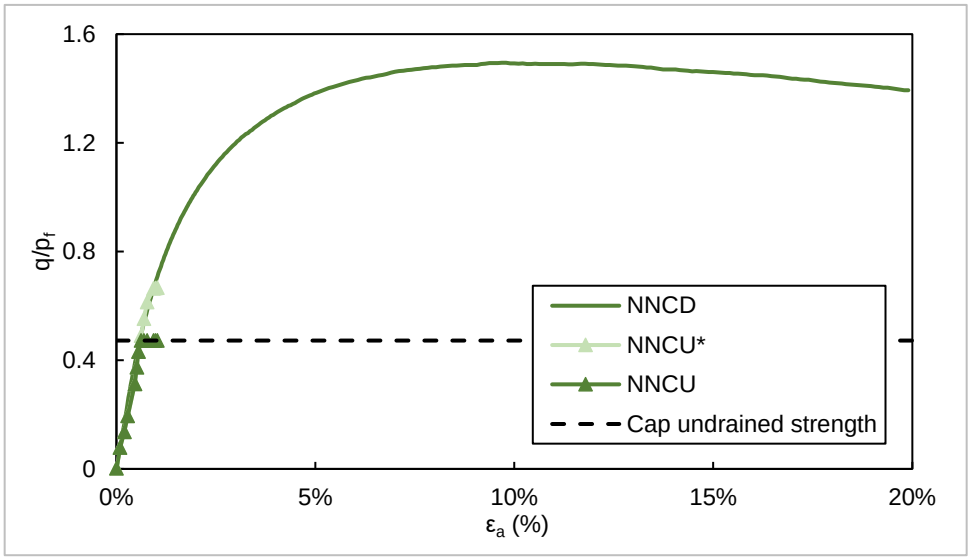

Figure 3.25: Normalised stress-strain curves for the Nerlerk sand

3.3.2.5 Summary

The measured data from the CU triaxial tests results were normalised such that the failure points were defined as the inflection point where a dilative tendency was noticed or the collapse point where a contractive tendency was noticed. Further, the peak CU strengths were limited based on the YSR. A summary of the interpreted YSR values is shown in Table 3.3. It should be noted that the YSRs determined for all four materials were greater than those that could be expected if alternative methods such as interpretation of undrained strengths using CPTu data were used (e.g. Olson & Stark, 2003b; Sadrekarimi, 2014). Undrained stress ratios determined using these methods are shown for reference.

Table 3.3: Summary of the soil parameters derived from the normalised triaxial test results

	Interpreted Yield Stress Ratio (YSR)*	Comparable value from literature	Literature reference
Gold tailings	0.34	0.24	Dillon & Wardlaw (2010)
Iron tailings	0.30	0.22	Morgenstern et al. (2016)
Platinum tailings	0.40	0.24	SRK (2017)
Nerlerk sand	0.24	0.21	Olson (2001)

* determined from triaxial test results

This normalisation was done so that the results obtained from the conventional limit equilibrium analyses could be directly compared to the results obtained using the proposed strain mobilisation method. In general, it was found that lower strengths were achieved during the CU test and that significantly less axial strain was mobilised in the case of the CU tests to reach failure when compared to the CD tests. A summary of all the normalised stress-strain curves is shown in Figure 3.26.

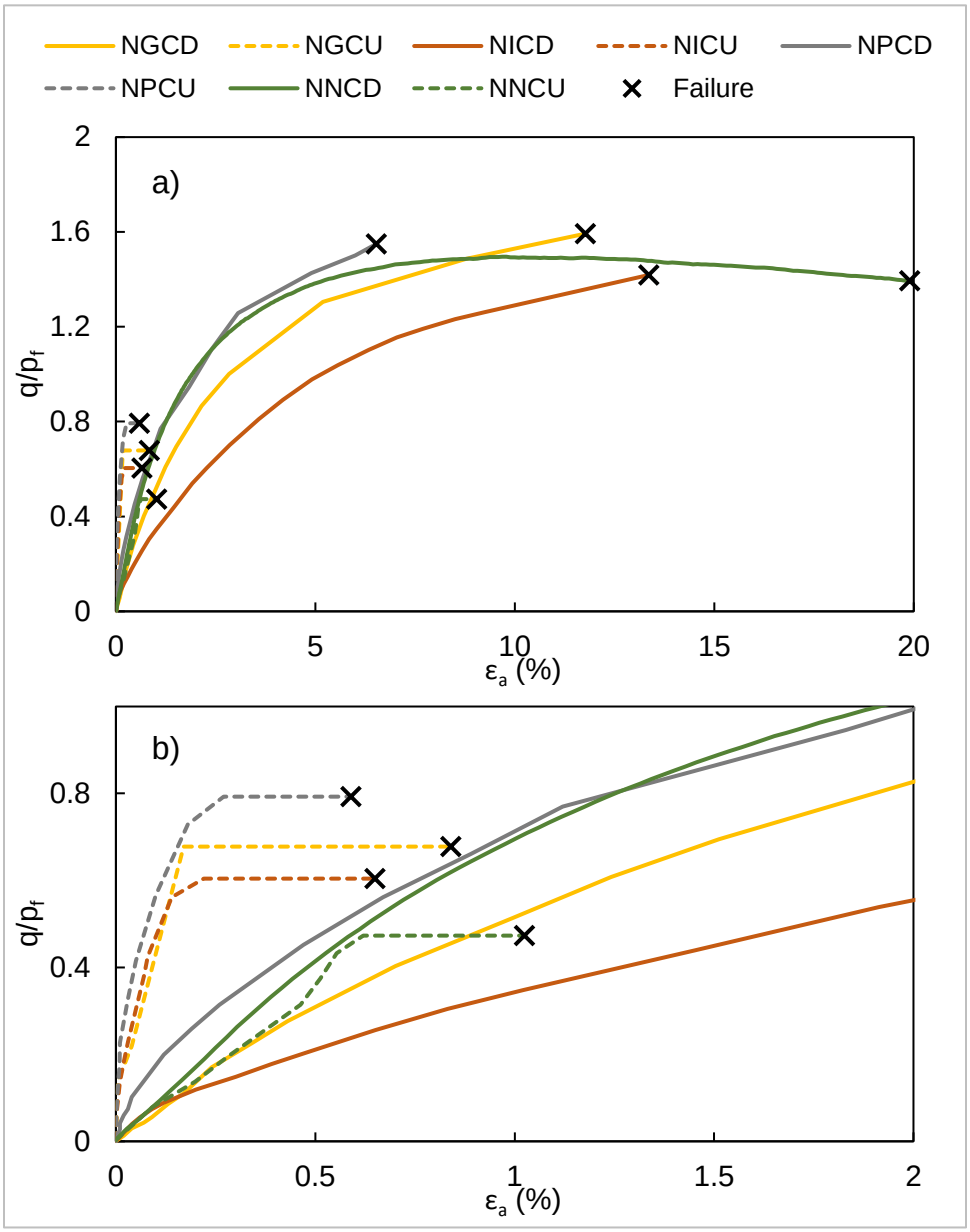

Figure 3.26: Summary of the normalised stress-strain curves for all four materials

3.4 MS EXCEL SPREADSHEET TO SOLVE LIMIT EQUILIBRIUM METHOD

Once the review and normalisation of the triaxial data was complete, the next step was to develop a spreadsheet capable of interpreting the geometric properties from a SLOPE/W output file and using limit equilibrium methods to calculate a FoS. The purpose, development and verification of this spreadsheet is explained in this section.

A Microsoft Excel spreadsheet was developed to calculate the FoS against failure of a defined slip surface based on Bishop's, Janbu's and Spencer's methods. The rational for developing the spreadsheet was for the FoS for the critical slip surface to be re-assessed based on different strength criteria requiring options not available in commercial packages. The slip surface geometry and material properties were all defined based on an output from a commercial software package and the FoS recalculated for various scenarios within the spreadsheet.

The spreadsheet was validated by verifying the results against hand calculations and results from commercial software packages. Figure 3.27 shows the FoS determined from the spreadsheet compared to the FoS determined from GeoStudio. With an R-squared value of 0.99, the spreadsheet was considered to be able to correctly interpret the geometric output from SLOPE/W and calculate the FoS according to Bishop's, Janbu's and Spencer's methods. Details of this verification process can be found in Appendix C.

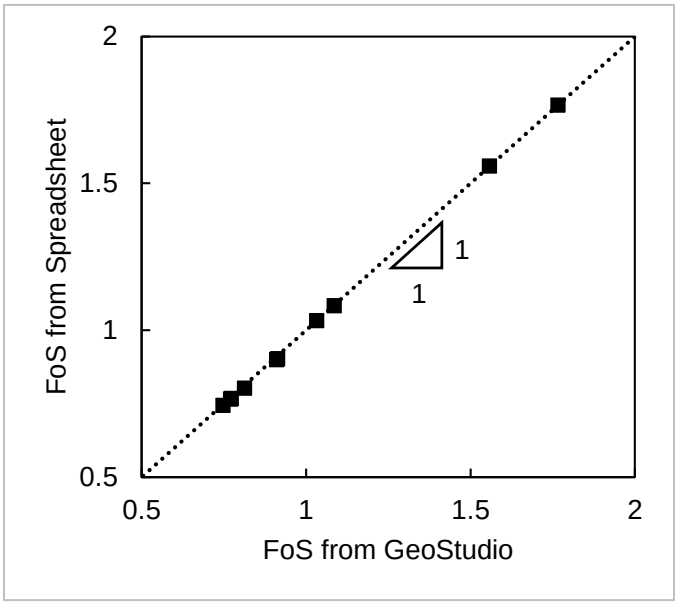

Figure 3.27: Correlation between FoS values obtained from GeoStudio and the spreadsheet

3.5 SLOPE STABILITY ANALYSIS

3.5.1 Cross sections assessed

Once the FoS formulation was derived, the triaxial data reviewed and normalised and the spreadsheet developed, the FoS formulation needed to be implemented. To achieve the objectives of the study, it was necessary to conduct slope stability analyses and calculate FoS values for comparison purposes. To ensure that a variety of geometries were assess, it was decided that three hypothetical slopes would be assessed. These slopes are represented as two-dimensional cross sections. For each cross section, up to three material zones were identified as indicated in Figure 3.28. The first cross section (Cross Section A) is a uniform 30 m high embankment at a slope of 1(v):3(h) and is shown in Figure 3.28a. Two material zones were identified: one above the phreatic surface and another below the phreatic surface.

The second cross section (Cross Section B) is of a hypothetical tailings dam as shown in Figure 3.28b. The tailings dam is 30 m high, there is a 5 m high compacted starter wall at the toe and there are two 9 m wide benches with 9 m high intermediate slopes at 1(v):1.5(h) resulting in an overall effective slope of 1(v):2.3(h). These are typical parameters observed on tailings dams in South Africa although the trend is to move towards flatter slopes approaching 1(v):3(h). Three material zones were identified: one for the foundation material, one for the zone below the phreatic surface and one for the starter wall and zone above the phreatic surface.

The third cross section (Cross Section C) is similar to Cross Section B except that the starter wall is assumed to be lined with a geosynthetic barrier. It was assumed that the geosynthetic barrier was designed in such a manner that the critical shear interface lies within the tailings material, thus eliminating slip surfaces through the starter wall. This cross section was selected as most new tailings dams will likely need to be lined to comply with the recent legislation where mine tailings is now considered a waste product and therefore this scenario is expected to be common in the future. Again, three material zones were identified: one for the foundation material and starter wall, one for the zone below the phreatic surface and one for the zone above the phreatic surface.

For each cross section, pore pressures were defined based on a piezometric line with hydrostatic conditions below the phreatic surface. No negative pore pressures were considered, the grid and radius slip surface definition was used, and the minimum slip depth considered was 5 m. No optimisation of the critical slip surface was considered. Although this is a hypothetical slope, the parameters were chosen as they represent conditions typically seen on upstream constructed tailings dams.

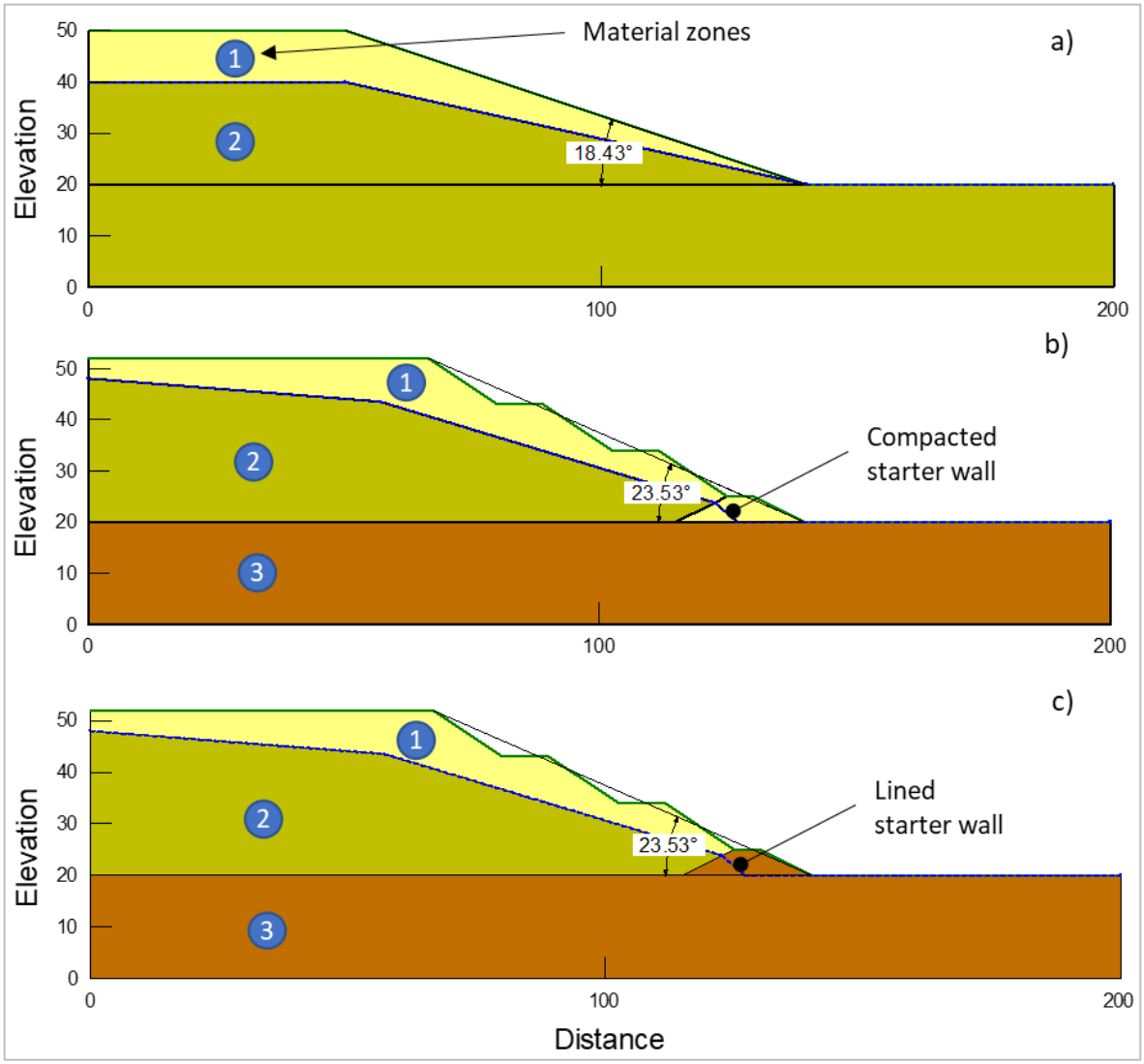

Figure 3.28: Cross sections assessed: a) uniform slope, b) typical tailings dam with a compacted starter wall, c) typical tailings dam with a lined starter wall

3.5.2 Scenarios assessed

To ensure that adequate comparisons could be drawn between the proposed method and current methods, six scenarios in terms of assumptions with regard to drained and undrained behaviour and the method of analysis used were assessed for each cross section described in Section 3.5.1. These scenarios are explained further in this section and the results of these analyses are shown and discussed in Chapter 4.

3.5.2.1 Scenario 1: Limit equilibrium analysis using Effective Strength Analysis strengths

For this scenario, a friction angle and a cohesion intercept were used to define the strength of the

material in all material zones and shown in Table 3.4. These strength parameters were obtained from the triaxial test data and a summary of these parameters is shown in Table 3.5. The analysis was conducted using the GeoStudio SLOPE/W software package and the output of this scenario was a single deterministically calculated FoS. The critical slip surface identified was subsequently exported for use in Scenarios 2, 4, 5 and 6.

Table 3.4: Material strength parameters used for Scenario 1

	Material Zone 1	Material Zone 2	Material Zone 3
Cross Section A	φ', c'	φ', c'	N/A
Cross Section B	φ', c'	φ', c'	Bedrock (impenetrable)
Cross Section C	φ', c'	φ', c'	Bedrock (impenetrable)

Table 3.5: Summary of soil parameters used for the limit equilibrium analyses

	Friction angle (φ')	Cohesion intercept (c')	Unit weight (γ)	Undrained strength ratio $\frac{s_u(yield)}{\sigma'_{v0}}$
Gold tailings	39°	0 kPa	20 kN/m^3	0.34
Iron tailings	35°	0 kPa	20 kN/m^3	0.30
Platinum tailings	38°	0 kPa	20 kN/m^3	0.40
Nerlerk sand	34.4	0 kPa	20 kN/m^3	0.24

3.5.2.2 Scenario 2: Limit equilibrium analysis using strengths from Undrained Strength Analysis

For this scenario, a combination of friction angles, cohesion intercepts and undrained yield strength ratios were used to define the strength of the material in the various material zones as shown in Table 3.6. The critical slip surface identified as part of Scenario 1 was used for the analysis. Material below the specified phreatic surface was assumed to be susceptible to undrained shearing and was therefore assigned an undrained yield strength ratio while material above the phreatic surface was assumed to not be susceptible to undrained shearing and was assigned a friction angle and cohesion intercept. This is in line with a first order approach when considering undrained shearing in tailings dams (Anglo American, 2018). The analysis was conducted using the GeoStudio SLOPE/W software package and the output of this scenario was a single deterministically calculated FoS.

Table 3.6: Material strength parameters used for Scenario 2

	Material Zone 1	Material Zone 2	Material Zone 3
Cross Section A	φ', c'	$\frac{S_{u(yield)}}{\sigma'_{v0}}$	N/A
Cross Section B	φ', c'	$\frac{S_{u(yield)}}{\sigma'_{v0}}$	Bedrock (impenetrable)
Cross Section C	φ', c'	$\frac{S_{u(yield)}}{\sigma'_{v0}}$	Bedrock (impenetrable)

3.5.2.3 Scenario 3: Finite element analysis using the strength reduction method

For this scenario, all material zones were assigned the same strength model as shown in Table 3.7. The analyses were conducted using the SIGMA/W package the GeoStudio 2020. An initial in situ analysis was specified where both the stress state and pore pressures in the soil were fully defined. Iterations were then performed where, for each iteration, the strength of the soil was reduced, and the stress state recalculated. Based on this new stress state, a simple analysis of the forces driving failure compared to the forces resisting failure was conducted and a FoS was calculated. This iterative process continued until a FoS of 1.0 was achieved. The ratio upon which the strength of the soil was required to be reduced by to achieve this FoS of 1.0 is defined as the Strength Reduction Factor which is presented as a Safety Factor (SF). An example of this analysis tree is shown in Figure 3.29

Table 3.7: Material strength parameters used for Scenario 3

	Material Zone 1	Material Zone 2	Material Zone 3
Cross Section A	φ', c', v, E_i	φ', c', v, E_i	N/A
Cross Section B	φ', c', v, E_i	φ', c', v, E_i	Bedrock (impenetrable)
Cross Section C	φ', c', v, E_i	φ', c', v, E_i	Bedrock (impenetrable)

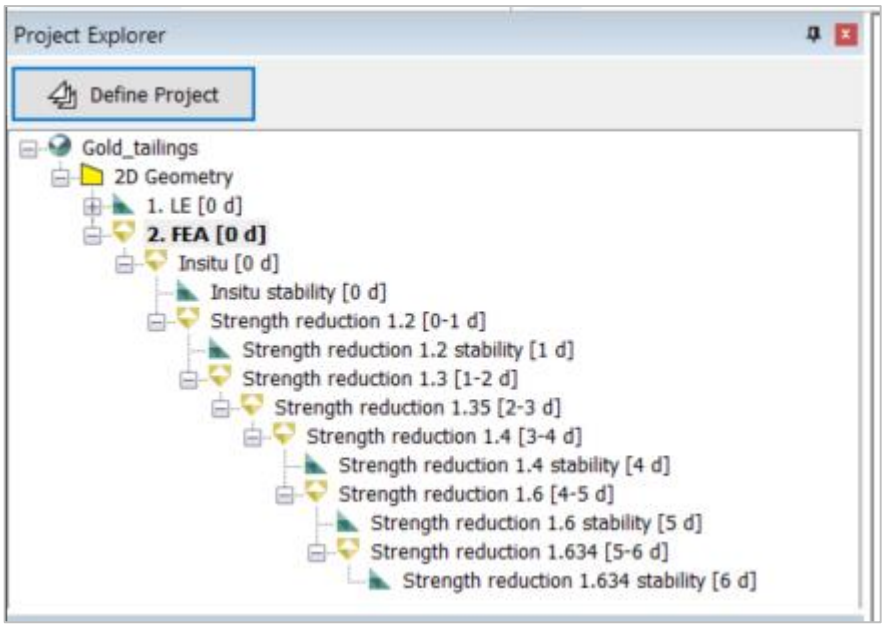

Figure 3.29: Example of a finite element analysis tree for the Strength Reduction Stability method

The output of this scenario was a single SF which is comparable to a calculated FoS obtained from a limit equilibrium analysis. A summary of the material properties used in the analyses is shown in Table 3.8. Details on the determination of these parameters can be found in Section 3.3.

Table 3.8: Summary of the strength parameters used for the finite element analysis

	Friction angle (φ')	Cohesion intercept (c')	Initial tangent modulus (E_i)	Poisson ratio (v)	Dilation angle (ψ)
Gold tailings	39°	0 kPa	26 000 kPa	0.3	0°
Iron tailings	35°	0 kPa	34 667 kPa	0.3	0°
Platinum tailings	38°	0 kPa	65 000 kPa	0.3	0°
Nerlerk sand	34.4°	0 kPa	26 000 kPa	0.3	0

3.5.2.4 Scenario 4: Spreadsheet-based strain mobilisation analysis using CD strengths only

The spreadsheet-based strain mobilisation method that considers strain compatibility within the limit equilibrium framework, described in Section 3.2, was used to calculate the FoS for Scenario 4. The critical slip surface identified as part of Scenario 1 was used and the strength parameters were based on the measured strengths obtained from the appropriate triaxial tests and are shown in Table 3.9. For Scenario 4, it was assumed that only the drained strengths were mobilised and therefore only the results from the CD triaxial tests were used. The output of this scenario was a calculated FoS evolution based on gradual strain mobilisation. Note that a uniform shear strain

distribution was assumed along the entire slip surface.

Table 3.9: Material strength parameters used for Scenario 4

	Material Zone 1*	Material Zone 2*	Material Zone 3
Cross Section A	$\frac{q_i}{p'_f}, based\ on\ CD\ results$	$\frac{q_i}{p'_f}, based\ on\ CD\ results$	N/A
Cross Section B	$\frac{q_i}{p'_f}, based\ on\ CD\ results$	$\frac{q_i}{p'_f}, based\ on\ CD\ results$	Bedrock (impenetrable)
Cross Section C	$\frac{q_i}{p'_f}, based\ on\ CD\ results$	$\frac{q_i}{p'_f}, based\ on\ CD\ results$	Bedrock (impenetrable)

*CD refers to results from the CD triaxial tests

3.5.2.5 Scenario 5: Spreadsheet-based strain mobilisation analysis using CU strengths only

For this scenario, the spreadsheet-based strain mobilisation method that considers strain compatibility within the limit equilibrium framework, described in Section 3.2, was used to calculate the FoS. The critical slip surface identified as part of Scenario 1 was used and the strength parameters were based on the measured strengths obtained from the appropriate triaxial tests and are shown in Table 3.10. For Scenario 5, it was assumed that only the undrained strengths were mobilised and therefore only the results from the CU triaxial tests were used. The output of this scenario was a calculated FoS evolution based on gradual strain mobilisation. It should be noted that the undrained shear strength was capped at the Yield Stress Ratio as discussed in Section 3.3.2.

Table 3.10: Material strength parameters used for Scenario 5

	Material Zone 1*	Material Zone 2*	Material Zone 3
Cross Section A	$\frac{q_i}{p'_f}, based\ on\ CU\ results$	$\frac{q_i}{p'_f}, based\ on\ CU\ results$	N/A
Cross Section B	$\frac{q_i}{p'_f}, based\ on\ CU\ results$	$\frac{q_i}{p'_f}, based\ on\ CU\ results$	Bedrock (impenetrable)
Cross Section C	$\frac{q_i}{p'_f}, based\ on\ CU\ results$	$\frac{q_i}{p'_f}, based\ on\ CU\ results$	Bedrock (impenetrable)

*CU results refers to the results from the CU triaxial tests

3.5.2.6 Scenario 6: Spreadsheet-based strain mobilisation analysis using combined CD and CU strengths

For this scenario, the spreadsheet-based strain mobilisation method that considers strain compatibility within the limit equilibrium framework, described in Section 3.2, was used to calculate

the FoS. The critical slip surface identified as part of Scenario 1 was used and the strength parameters were based on the measured strengths obtained from the appropriate triaxial tests and are shown in Table 3.11. For Scenario 6, it was assumed that drained strengths were mobilised above the phreatic surface and that undrained strengths were mobilised below the phreatic surface in line with the distinctions as defined for Scenario 2. Therefore, results from both the CD and CU triaxial tests were used. The output of this scenario was a FoS evolution based on gradual strain mobilisation.

Table 3.11: Material strength parameters used for Scenario 6

	Material Zone 1*	Material Zone 2*	Material Zone 3
Cross Section A	$\frac{q_i}{p'_f}, based\ on\ CD\ results$	$\frac{q_i}{p'_f}, based\ on\ CU\ results$	N/A
Cross Section B	$\frac{q_i}{p'_f}, based\ on\ CD\ results$	$\frac{q_i}{p'_f}, based\ on\ CU\ results$	Bedrock (impenetrable)
Cross Section C	$\frac{q_i}{p'_f}, based\ on\ CD\ results$	$\frac{q_i}{p'_f}, based\ on\ CU\ results$	Bedrock (impenetrable)

*CD results refers to results from the CD triaxial tests and CU results refers to the results from the CU triaxial tests

4 RESULTS

4.1 INTRODUCTION

The previous chapter discusses the derivation of the FoS formulation used to calculate a FoS value based on the limit equilibrium methods where strain compatibility along the failure surface is maintained. Details on how the strain mobilisation method would be implemented were also provided. As the method requires triaxial data for implementation, a review was conducted on a set of the triaxial data and normalised stress-strain curves were developed. The verification of the strain mobilisation method to interpret geometric properties from SLOPE/W and calculate FoS values according to limit equilibrium methods was also discussed. Finally, details on how the slope stability analysis would be conducted were presented. This chapter focuses on presenting and analysing the results from the stability analyses conducted.

A series of slope stability analyses were conducted for three hypothetical slopes. Four materials were considered, and, for each material, six scenarios were assessed in the manner described in Section 3.5.2. A description of these six scenarios is repeated for reference in Table 4.1. The material strengths assigned to the various material zones were varied for the different scenarios. Scenarios 1, 2 and 3 were assessed using SLOPE/W and a single calculated FoS value was obtained while Scenarios 4, 5 and 6 were assessed using the strain mobilisation method and an evolution of the calculated FoS with increasing strain was obtained. The results are presented per cross section analysed and a comparison of the findings is provided.

Table 4.1: Summary of the six scenarios assessed

Scenario	Description
1	Conventional limit equilibrium analysis considering drained strength parameters
2	Conventional limit equilibrium analysis considering both drained and undrained strength parameters
3	Finite element analysis using the Strength Reduction Stability method
4	New strain mobilisation method considering drained strength parameters
5	New strain mobilisation method considering undrained strength parameters
6	New strain mobilisation method considering both drained and undrained strength parameters

Although comparisons between the calculated FoS values for all six scenarios were drawn, two comparisons were of particular importance. The first was the comparison between Scenario 1 and

Scenario 4. This comparison would demonstrate if the proposed method is able to correctly interpret the geometric properties of the critical slip surface identified in SLOPE/W and calculate a comparable FoS to conventional limit equilibrium methods when considering drained strength parameters only. The second was the comparison between Scenario 2 and Scenario 6. This comparison would determine whether there is any difference in calculated FoS when current limit equilibrium methods to assess slope stability when undrained shearing is expected compared to a proposed method where strain compatibility is maintained.

Other comparisons that were drawn included a comparison between Scenario 1 and Scenario 2. This comparison would confirm that the calculated FoS when considering drained strengths is significantly greater than the calculated FoS when considering undrained strengths using conventional limit equilibrium methods. For all the materials assessed, for all three cross sections, it was found that the FoS calculated for Scenario 2 was significantly lower than the FoS calculated for Scenario 1. This is in line with findings by others (e.g. Olson, 2001).

A comparison between Scenario 4 and Scenario 5 would confirm that the same trend as observed using conventional limit equilibrium methods was found using the proposed method (i.e. that the calculated FoS when considering drained strengths is significantly greater than the calculated FoS when considering undrained strengths). For all the materials assessed, for all three cross sections, it was found that the FoS calculated for Scenario 5 was significantly lower than the FoS calculated for Scenario 4.

A comparison between Scenario 1 and Scenario 3 would show if limit equilibrium and finite element methods could provide similar calculated FoS results. This varied between the cross sections and is discussed under the applicable section in the report.

Finally, a comparison between Scenario 5 and Scenario 6 would demonstrate if there is a difference in calculated FoS when only undrained strengths are considered compared to the calculated FoS when a split between drained and undrained material zones were identified (i.e. determine the influence of the slices that exhibit to the calculated FoS). This also varied between the cross sections and is discussed under the applicable section in the report.

4.2 CROSS SECTION A: UNIFORM SLOPE

Cross Section A is the simplest cross section comprising a uniform 30 m high embankment at a slope of 1(v):3(h). The result from SLOPE/W showing the calculated FoS for Scenario 1 for the gold tailings for Cross Section A is shown in Figure 4.1. The solid lines depicting an arc are

indicative of zones of increased shear stress that developed during Scenario 3 where a finite element analysis was conducted using the Strength Reduction Stability method. Additional results from the GeoStudio analyses can be found in Appendix D.

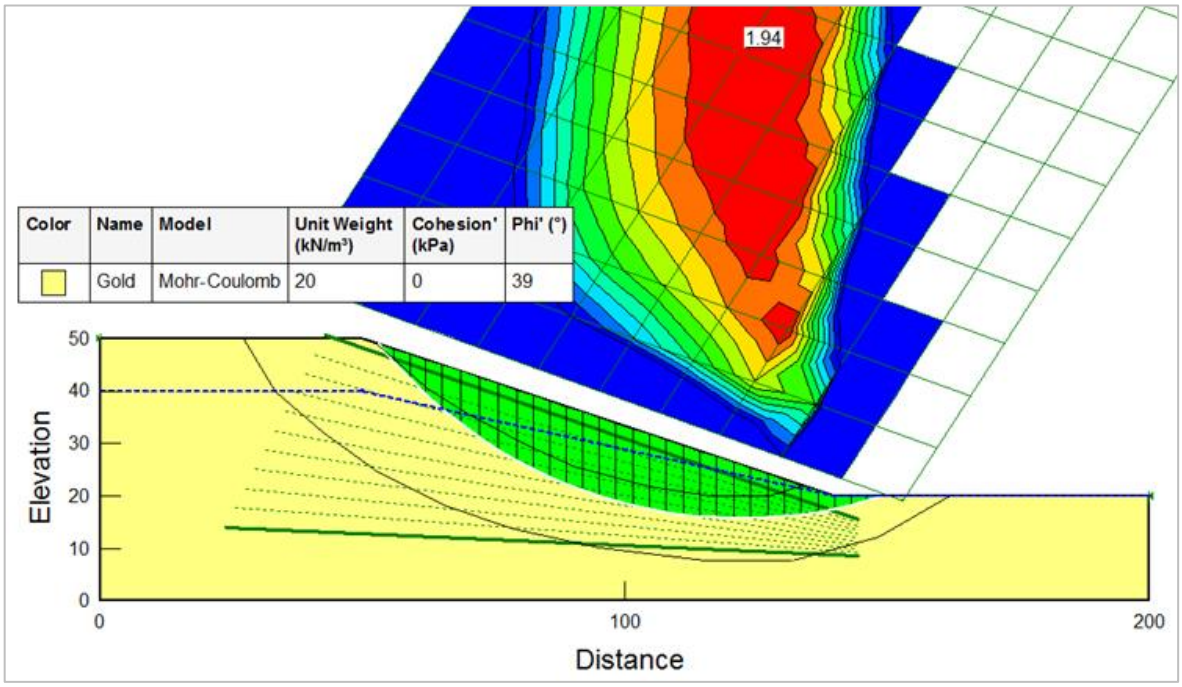

Figure 4.1: Results from the stability analysis on the platinum tailings for Cross Section A

A summary of the FoS results for the four materials for Cross Section A is shown in Table 4.2. Individual results for the four materials considered are shown in Figure 4.2, Figure 4.3, Figure 4.4 and Figure 4.5 respectively. These figures show how the calculated FoS evolves as shear strain is mobilized along the critical failure surface chosen from Scenario 1 for the scenarios based on the strain mobilisation method (i.e. Scenarios 4, 5 and 6).

4.2.1 Comparison between Scenario 1 and Scenario 4

From Table 4.2, it can be seen that the calculated FoS of 1.94 for Scenario 1, where conventional limit equilibrium effective stress analysis was conducted, is comparable to the peak calculated FoS of 1.91 for Scenario 4, where the strain mobilisation method was used considering CD strengths only. This observation can also be seen for analyses conducted on the iron tailings, the platinum tailings and the Nerlerk sand. It was found that the difference in calculated FoS varied between 0.01 and 0.13 which represents a difference of between 1% and 8%. It was also found that the difference was larger for the iron tailings and Nerlerk sand when compared to the gold and platinum tailings, with the FoS values calculated as part of Scenario 1 being lower than those calculated as

part of Scenario 4.

4.2.2 Comparison between Scenario 2 and Scenario 6

From Table 4.2, it can be seen that the calculated FoS of 0.97 for Scenario 2, where limit equilibrium undrained stress analysis was conducted, is comparable to the peak calculated FoS of 1.03 for Scenario 6, where the strain mobilisation method was used considering CD and CU strengths applied to the same material zones as those used for Scenario 2. This is the crux of the study and shows that there is little difference to the calculated FoS when using conventional limit equilibrium methods compared to the calculated FoS using a proposed limit equilibrium method where compatibility of strains in considered. This may be due to the fact that the slip surface assessed was dominated by material in the CU zone. However, it is likely that this will be the case in most scenarios where undrained shearing occurs. This observation can also be seen for analyses conducted on the iron tailings, the platinum tailings and the Nerlerk sand. It was found that the difference in calculated FoS varied between 0.04 and 0.06 which represents a difference of between 4% and 7%. It was also found that the difference in calculated FoS for Scenario 2 and Scenario 6 for the four materials was similar, with the FoS values calculated as part of Scenario 2 being lower than those calculated as part of Scenario 6.

4.2.3 Other comparisons

The calculated FoS of 1.94 for Scenario 1 (using the conventional limit equilibrium effective stress analysis method) for the gold tailings is comparable to the calculated SF of 1.80 for Scenario 3 (using the finite element Strength Reduction Stability method). This observation can also be seen for analyses conducted on the iron tailings, the platinum tailings and the Nerlerk sand. It was found that the difference in calculated FoS varied between 0.03 and 0.14 which represents a difference of between 2% and 8%. It was also found that the difference in calculated FoS for Scenario 1 and Scenario 3 for the four materials was similar with the FoS values calculated as part of Scenario 1 being greater than those calculated as part of Scenario 3.

The peak calculated FoS of 1.00 for Scenario 5 (using the strain mobilisation method, considering CU strengths only) is not very different to the peak calculated FoS of 1.03 for Scenario 6 (using the strain mobilisation method, considering both CD and CU strengths). This shows that the influence of the slices that were assumed to be in a state where drained strengths would be mobilised is low and that the stability is driven by the slices that were assumed to be in a state where undrained strengths would be mobilised.

This observation can also be seen for analyses conducted on the iron tailings, the platinum tailings and the Nerlerk sand. It was found that the difference in calculated FoS varied between 0.01 and 0.03 which represents a difference of between 1% and 4%. It was also found that the difference in calculated FoS for Scenario 5 and Scenario 6 for the four materials was similar, with the FoS values calculated as part of Scenario 5 being lower than those calculated as part of Scenario 6. Details of these comparisons can be found in Appendix E.

Table 4.2: Summary of FoS results obtained for the various scenarios for Cross Section A

	1. LE (ESA)	2. LE (USA)	3. FEA (SRS)	4. CD strengths	5. CU strengths	6. Combined CD, CU strengths
Gold tailings	1.94	0.97	1.80	1.91	1.00	1.03
Iron tailings	1.68	0.85	1.65	1.79	0.90	0.91
Platinum tailings	1.87	1.12	1.74	1.88	1.15	1.17
Nerlerk sand	1.64	0.70	1.51	1.77	0.71	0.74

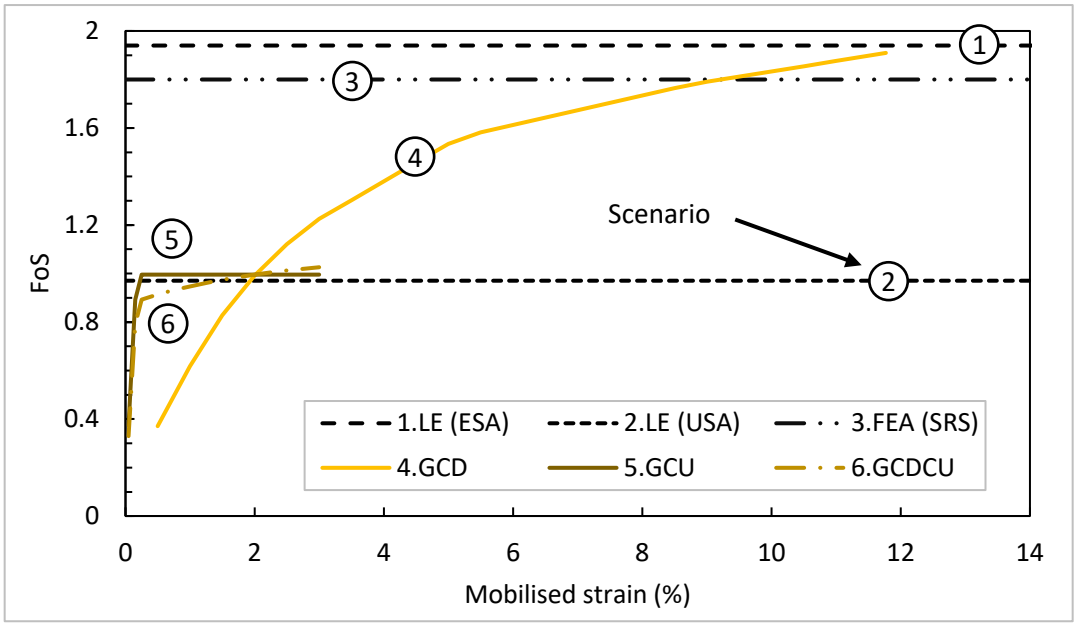

Figure 4.2: Results from the stability analyses on the gold tailings for Cross Section A

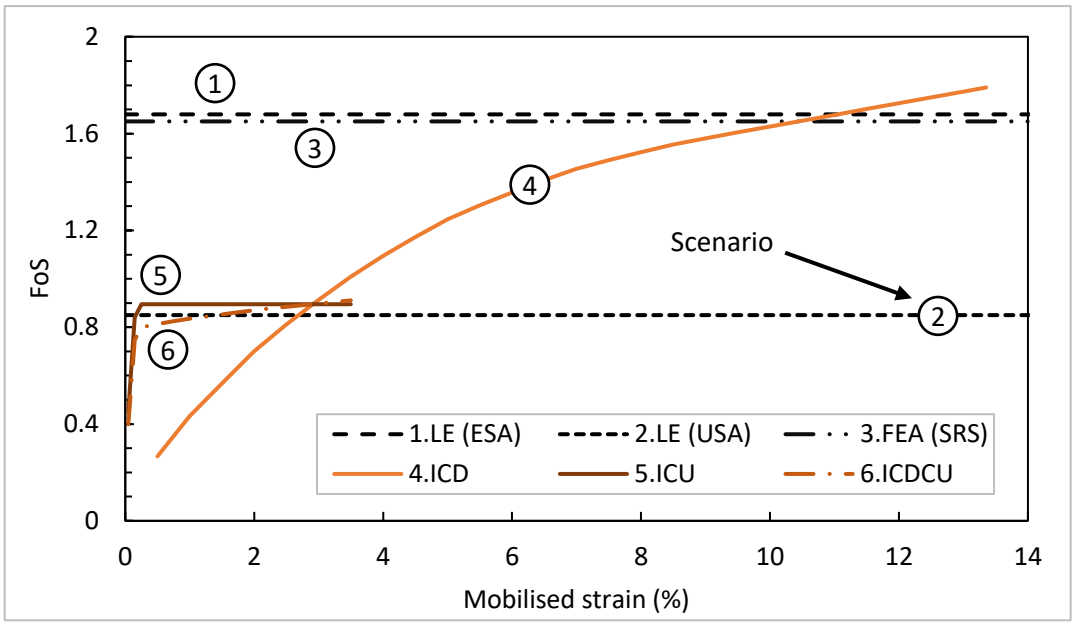

Figure 4.3: Results from the stability analyses on the iron tailings for Cross Section A

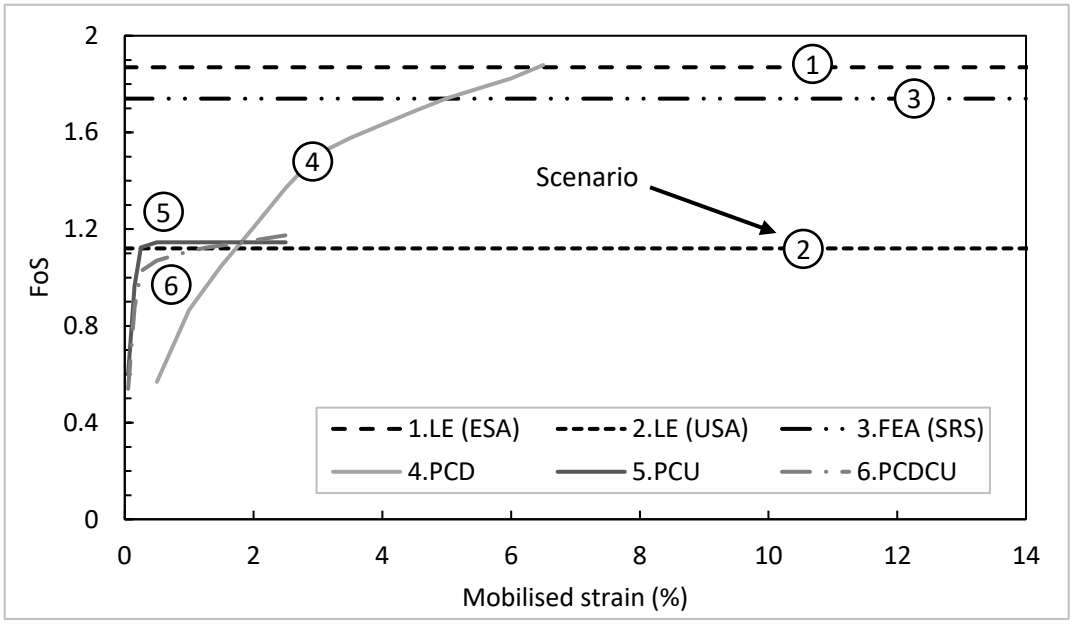

Figure 4.4: Results from the stability analyses on the platinum tailings for Cross Section A

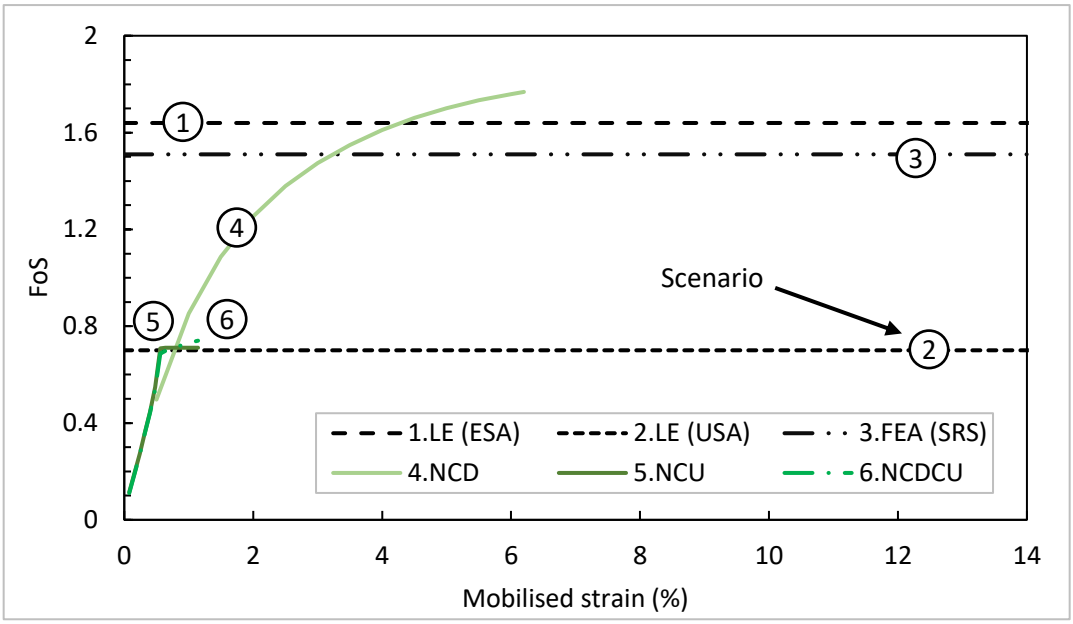

Figure 4.5: Results from the stability analyses on the Nerlerk sand for Cross Section A

4.3 CROSS SECTION B: TYPICAL UPSTREAM TAILINGS DAM WITH A COMPACTED STARTER WALL

Cross Section B is that of a hypothetical upstream tailings dam. The tailings dam is 30 m high, there is a 5 m high compacted starter wall at the toe and there are two 9 m wide benches with 9 m high intermediate slopes at 1(v):1.5(h) resulting in an overall effective slope of 1(v):2.3(h). The result from SLOPE/W showing the calculated FoS for the gold tailings for Scenario 1 for Cross Section B is shown in Figure 4.6. Additional results from the GeoStudio analyses can be found in Appendix D.

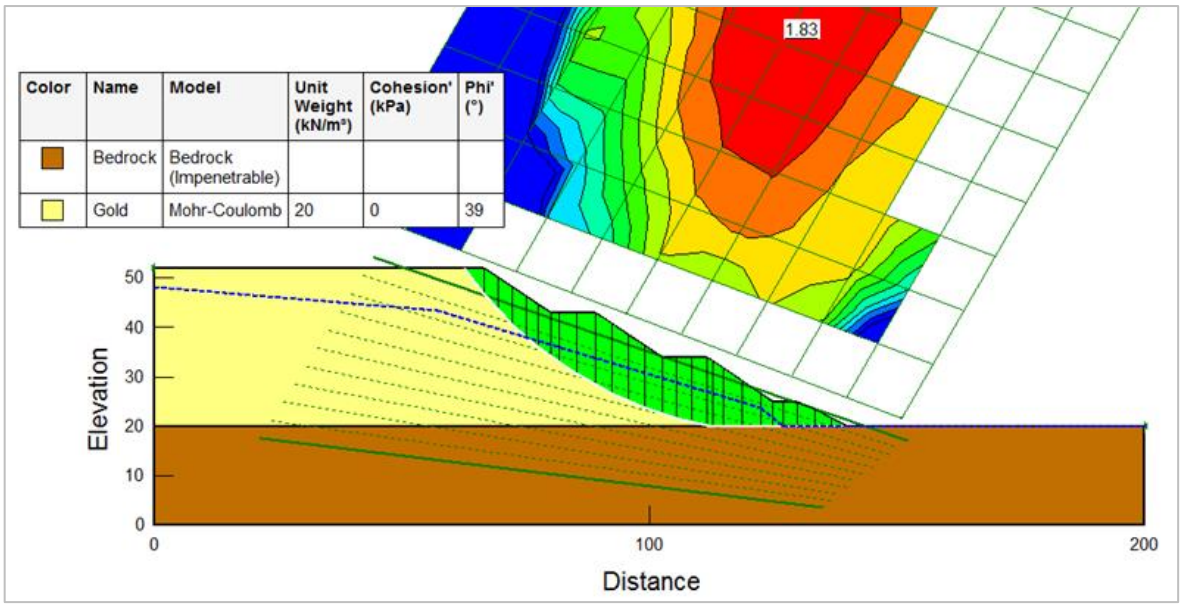

Figure 4.6: Output from SLOPE/W for Scenario 1 of the gold tailings for Cross Section A

A summary of the FoS results for the four materials for Cross Section B is shown in Table 4.3. Individual results for the four materials are shown in Figure 4.7, Figure 4.8, Figure 4.9 and Figure 4.10 respectively. These figures show how the calculated FoS evolves as shear strain is mobilized for the scenarios based on the strain mobilisation method (i.e. Scenarios 4, 5 and 6).

4.3.1 Comparison between Scenario 1 and Scenario 4

From Table 4.3, it can be seen that the calculated FoS of 1.83 for Scenario 1, where conventional limit equilibrium effective stress analysis was conducted, is comparable to the peak calculated FoS of 1.92 for Scenario 4, where the strain mobilisation method was used considering CD strengths only. This difference is larger than the difference noted for Cross Section A. This observation can also be seen for analyses conducted on the iron tailings, the platinum tailings and the Nerlerk sand. It was found that the difference in calculated FoS varied between 0.09 and 0.23 which represents a difference of between 5% and 15%. It was also found that the difference was larger for the iron tailings and Nerlerk sand when compared to the gold and platinum tailings, with the FoS values calculated as part of Scenario 1 being greater than those calculated as part of Scenario 4.

4.3.2 Comparison between Scenario 2 and Scenario 6

From Table 4.3, it can be seen that the calculated FoS of 1.27 for Scenario 2, where limit equilibrium undrained stress analysis was conducted, is comparable to the peak calculated FoS of 1.08 for Scenario 6, where the strain mobilisation method was used considering CD and CU

strengths applied to the same material zones as those used for Scenario 2. Again, this difference is larger than the difference noted for Cross Section A. Although the difference is large, it is believed that a contributing factor is that the calculated FoS values for Scenarios 1 and 4 are not as similar as was found for Cross Section A. It is believed that if this influence were to be removed, there would be little difference to the calculated FoS when using conventional limit equilibrium methods compared to the calculated FoS using a proposed limit equilibrium method where compatibility of strains in considered.

This observation can also be seen for analyses conducted on the iron tailings, the platinum tailings and the Nerlerk sand. It was found that the difference in calculated FoS varied between 0.12 and 0.20 which represents a difference of between 9% and 20%. This large difference in calculated FoS values indicates that the proposed strain mobilisation method may be less reliable when the slip surface passes through alternating drained and undrained material zones as is the case for Cross Section B where the undrained material zone is between the drained zone at the crest and the drained starter wall at the toe.

It was also found that the difference in calculated FoS for Scenario 2 and Scenario 6 for the four materials was similar with the FoS values calculated as part of Scenario 2 being greater than those calculated as part of Scenario 6. The strain mobilisation method therefore underestimates the FoS for Cross Section B. This may be due to the assumptions made regarding interslice forces. The assumptions made were similar to those made as part of the Fellenius method which is known to provide lower (more conservative) FoS values when compared to other methods (e.g. Fredlund & Krahn, 1977).

4.3.3 Other comparisons

The calculated FoS of 1.83 for Scenario 1 (using the conventional limit equilibrium effective stress analysis method) for the gold tailings is quite different to the calculated SF of 2.17 for Scenario 3 (using the finite element Strength Reduction Stability method). This observation can also be seen for analyses conducted on the iron tailings, the platinum tailings and the Nerlerk sand. It was found that the difference in calculated FoS varied between 0.34 and 0.47 which represents a difference of between 17% and 30%. It was also found that the difference in calculated FoS for Scenario 1 and Scenario 3 for the four materials was similar, with the FoS values calculated as part of Scenario 1 being lower than those calculated as part of Scenario 3.

The peak calculated FoS of 1.00 for Scenario 5 (using the strain mobilisation method, considering CU strengths only) is not very different to the peak calculated FoS of 1.08 for Scenario 6 (using

the strain mobilisation method, considering both CD and CU strengths). This shows that the influence of the slices that were assumed to be in a state where drained strengths would be mobilised is small and that the stability is driven by the slices that were assumed to be in a state where undrained strengths would be mobilised. This observation can also be seen for analyses conducted on the iron tailings, the platinum tailings and the Nerlerk sand. It was found that the difference in calculated FoS varied between 0.04 and 0.08 which represents a difference of between 4% and 11%. It was also found that the difference in calculated FoS for Scenario 5 and Scenario 6 for the four materials was similar, with the FoS values calculated as part of Scenario 5 being lower than those calculated as part of Scenario 6.

In general, it was found that there were significant differences between the various scenarios for Cross Section B. This may indicate the need to consider interslice forces when the geometry becomes more complex with the failure surface passing through more than one material type, illustrating a need to improve the method. Additional details of these comparisons can be found in Appendix E.

Table 4.3: Summary of FoS results obtained for the various scenarios for Cross Section B

	1. LE (ESA)	2. LE (USA)	3. FEA (SRS)	4. CD strengths	5. CU strengths	6. Combined CD, CU strengths
Gold tailings	1.83	1.27	2.17	1.92	1.00	1.08
Iron tailings	1.58	1.11	2.05	1.80	0.90	0.94
Platinum tailings	1.77	1.35	2.17	1.89	1.15	1.23
Nerlerk sand	1.55	0.99	1.82	1.78	0.71	0.79

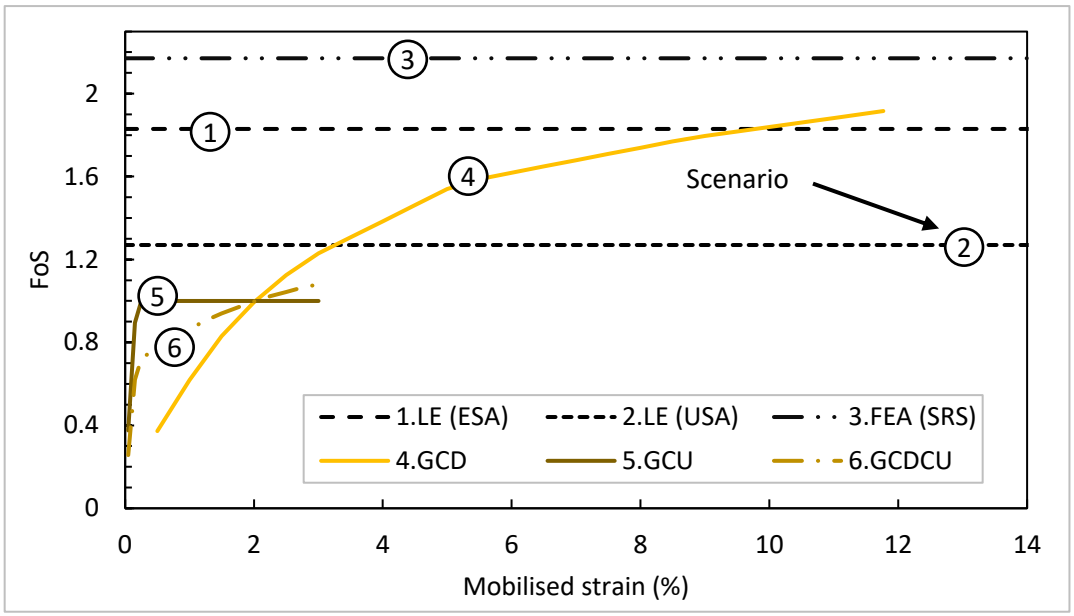

Figure 4.7: Results from the stability analyses on the gold tailings for Cross Section B

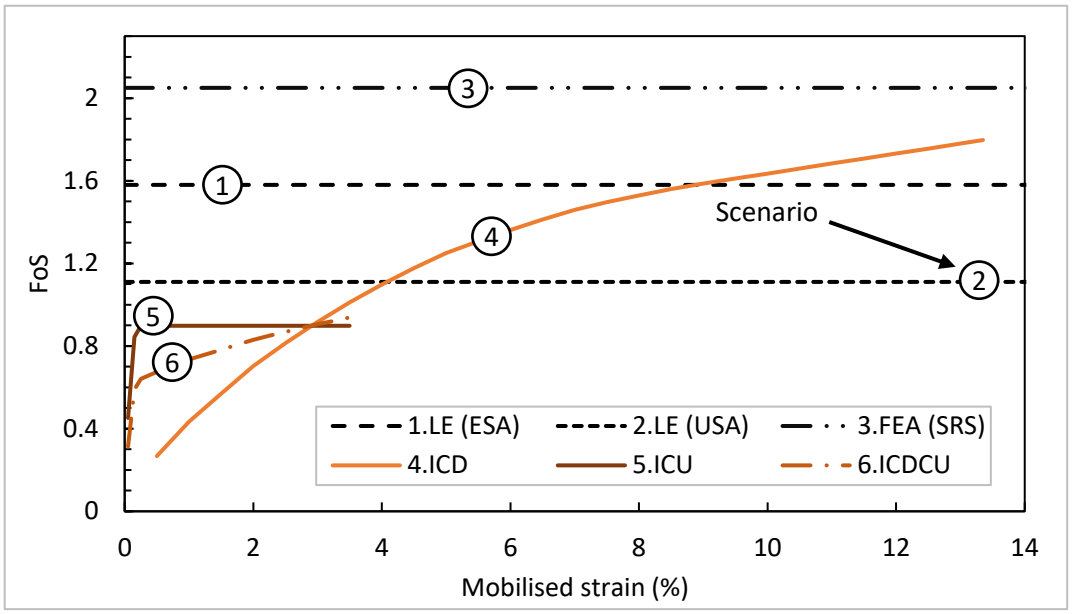

Figure 4.8: Results from the stability analyses on the iron tailings for Cross Section B

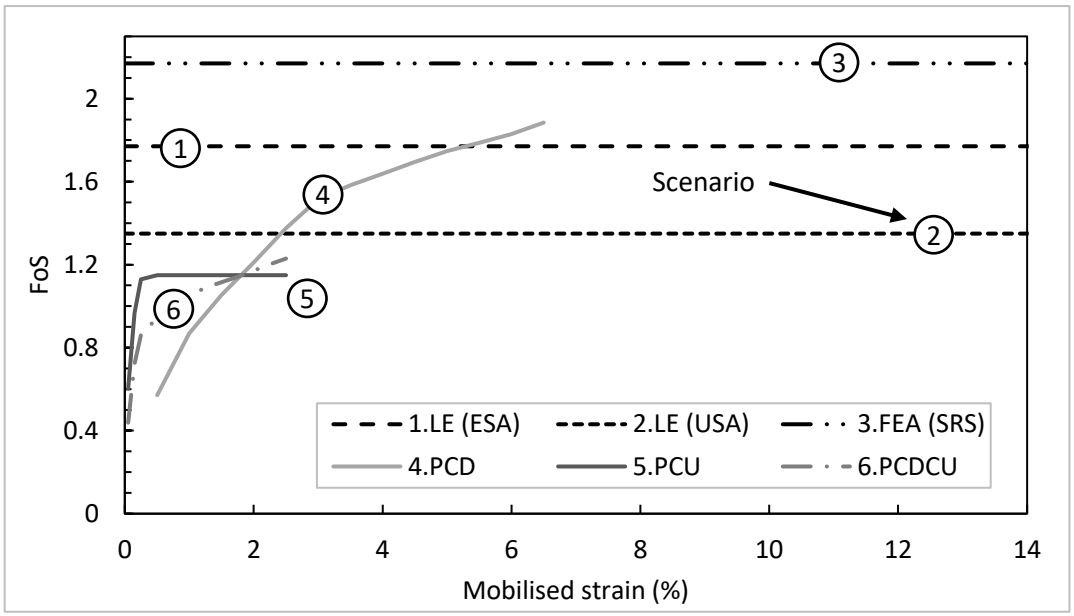

Figure 4.9: Results from the stability analyses on the platinum tailings for Cross Section B

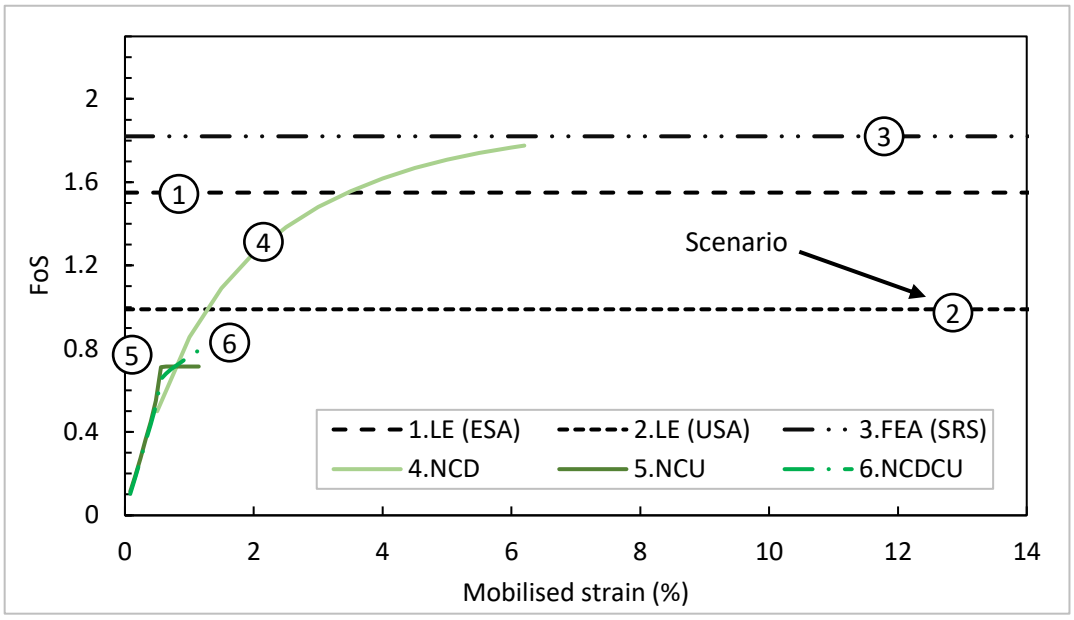

Figure 4.10: Results from the stability analyses on the Nerlerk sand for Cross Section B

4.4 CROSS SECTION C: TYPICAL UPSTREAM TAILINGS DAM WITH A LINED STARTER WALL

Cross Section C is similar to Cross Section B (i.e. an upstream tailings dam) except that the starter wall is assumed to be lined with a geosynthetic barrier. It was assumed that the geosynthetic barrier was designed in such a manner that the critical shear interface lies within the tailings material, thus eliminating slip surfaces through the starter wall. The results from SLOPE/W showing the calculated FoS for Scenario 1 for the gold tailings for Cross Section C is shown in Figure 4.11.

Additional results from the GeoStudio analyses can be found in Appendix D.

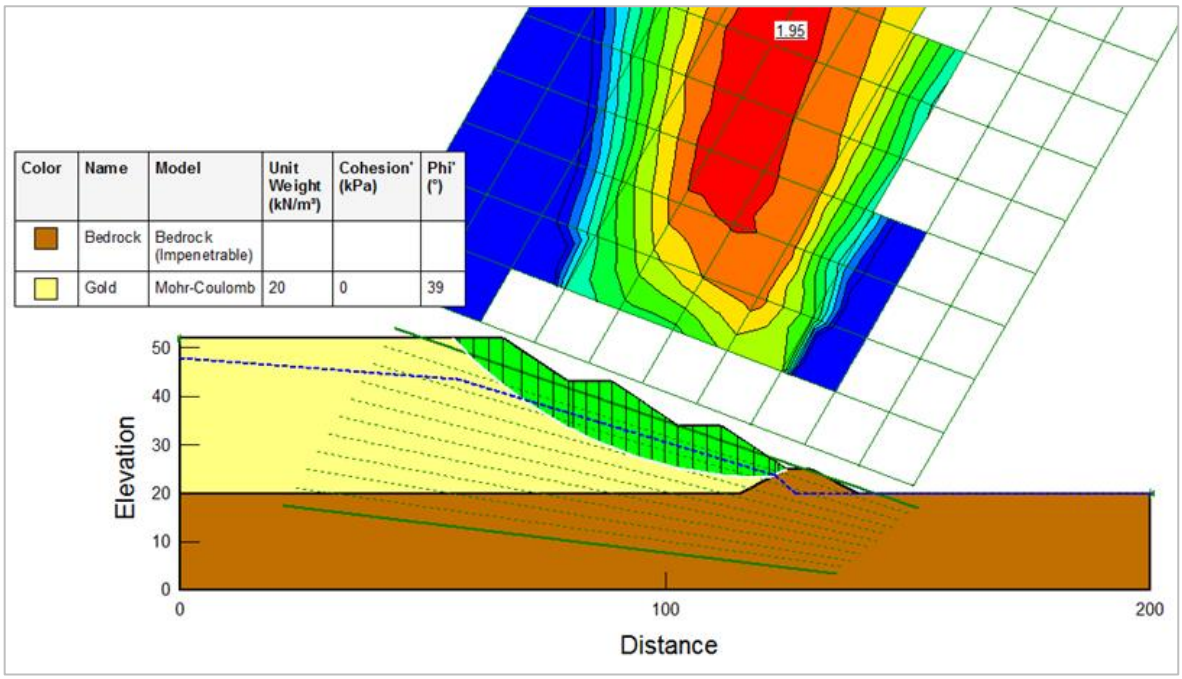

Figure 4.11: Output from SLOPE/W for Scenario 1 of the gold tailings for Cross Section C

A summary of the FoS results for the four materials for Cross Section A is shown in Table 4.4. Individual results for the four materials are shown in Figure 4.12, Figure 4.13, Figure 4.14, and Figure 4.15 respectively. These figures show how the calculated FoS changes as shear strain is mobilized for the scenarios based on the strain mobilisation method (i.e. Scenarios 4, 5 and 6).

4.4.1 Comparison between Scenario 1 and Scenario 4

From Table 4.4, it can be seen that the calculated FoS of 1.95 for Scenario 1, where conventional limit equilibrium effective stress analysis was conducted, is comparable to the peak calculated FoS of 1.92 for Scenario 4, where the strain mobilisation method was used considering CD strengths only. This trend can also be seen for analyses conducted on the iron tailings, the platinum tailings and the Nerlerk sand. It was found that the difference in calculated FoS varied between 0.0 and 0.13 which represents a difference of between 0% and 8%. It was also found that the difference was larger for the iron tailings and Nerlerk sand when compared to the gold and platinum tailings, with the FoS values calculated as part of Scenario 1 being lower than those calculated as part of Scenario 4.

4.4.2 Comparison between Scenario 2 and Scenario 6

From Table 4.4, it can be seen that the calculated FoS of 1.09 for Scenario 2, where limit equilibrium undrained stress analysis was conducted, is comparable to the peak calculated FoS of 1.05 for Scenario 6, where the strain mobilisation method was used considering CD and CU strengths applied to the same material zones as those used for Scenario 2. This shows that there is little difference to the calculated FoS when using conventional limit equilibrium methods compared to the calculated FoS using a proposed limit equilibrium method where compatibility of strains in considered. This observation can also be seen for analyses conducted on the iron tailings, the platinum tailings and the Nerlerk sand. It was found that the difference in calculated FoS varied between 0.01 and 0.05 which represents a difference of between 1% and 6%. It was also found that the difference in calculated FoS for Scenario 2 and Scenario 6 for the four materials was similar with the FoS values calculated as part of Scenario 2 being greater than those calculated as part of Scenario 6. The strain mobilisation method therefore also underestimates the FoS for Cross Section C.

4.4.3 Other comparisons

The calculated FoS of 1.95 for Scenario 1 (using the conventional limit equilibrium effective stress analysis method) for the gold tailings is quite different to the calculated SF of 1.80 for Scenario 3 (using the finite element Strength Reduction Stability method). This observation can also be seen for analyses conducted on the iron tailings, the platinum tailings and the Nerlerk sand. It was found that the difference in calculated FoS varied between 0.01 and 0.42 which represents a difference of between 1% and 25%. It was also found that the difference in calculated FoS for Scenario 1 and Scenario 3 was lowest for the Nerlerk sand but similar for the three tailings materials, with the FoS values calculated as part of Scenario 1 being lower than those calculated as part of Scenario 3.

The peak calculated FoS of 1.00 for Scenario 5 (using the strain mobilisation method, considering CU strengths only) is not very different to the peak calculated FoS of 1.05 for Scenario 6 (using the strain mobilisation method, considering both CD and CU strengths). This shows that the influence of the slices that were assumed to be in a state where drained strengths would be mobilised is small and that the stability is driven by the slices that were assumed to be in a state where undrained strengths would be mobilised.

This observation can also be seen for analyses conducted on the iron tailings, the platinum tailings and the Nerlerk sand. It was found that the difference in calculated FoS varied between 0.03 and 0.06 which represents a difference of between 3% and 8%. It was also found that the difference in

calculated FoS for Scenario 5 and Scenario 6 for the four materials was similar, with the FoS values calculated as part of Scenario 5 being lower than those calculated as part of Scenario 6. Details of these comparisons can be found in Appendix E.

Table 4.4: Summary of FoS results obtained for the various scenarios for Cross Section C

	1. LE (ESA)	2. LE (USA)	3. FEA (SRS)	4. CD strengths	5. CU strengths	6. Combined CD, CU strengths
Gold tailings	1.95	1.09	2.17	1.92	1.00	1.05
Iron tailings	1.69	0.95	2.11	1.80	0.90	0.93
Platinum tailings	1.89	1.21	2.24	1.89	1.15	1.20
Nerlerk sand	1.65	0.82	1.66	1.78	0.71	0.77

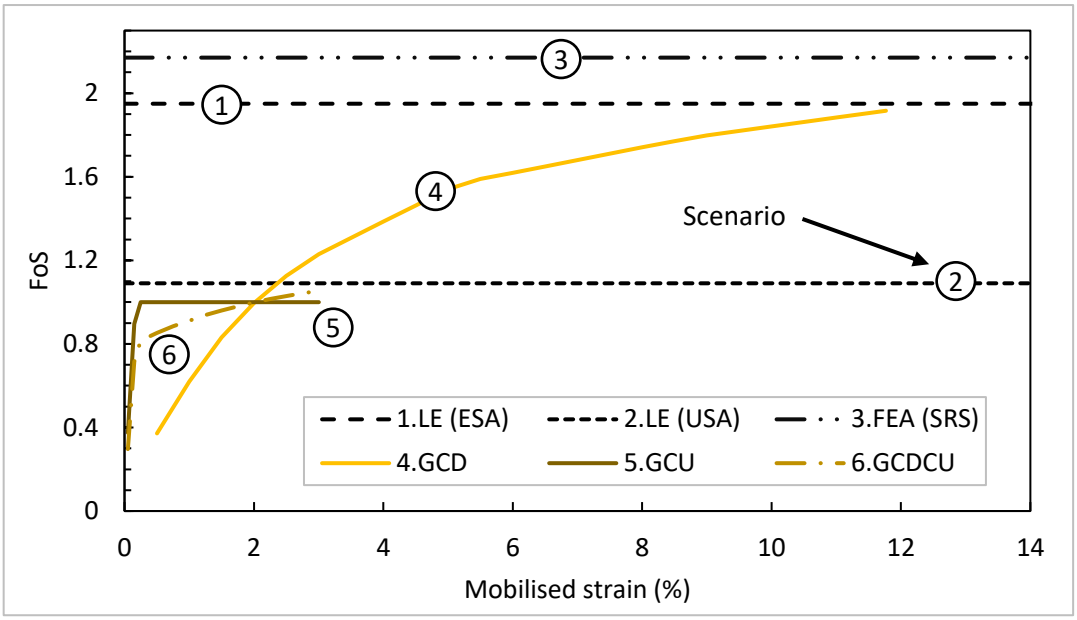

Figure 4.12: Results from the stability analyses on the gold tailings for Cross Section C

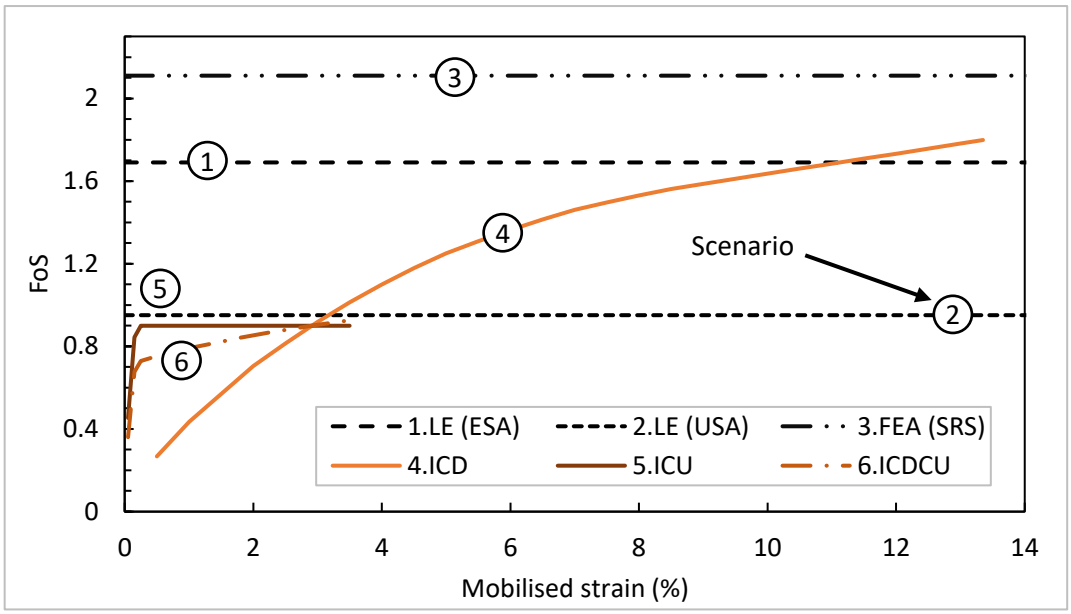

Figure 4.13: Results from the stability analyses on the iron tailings for Cross Section C

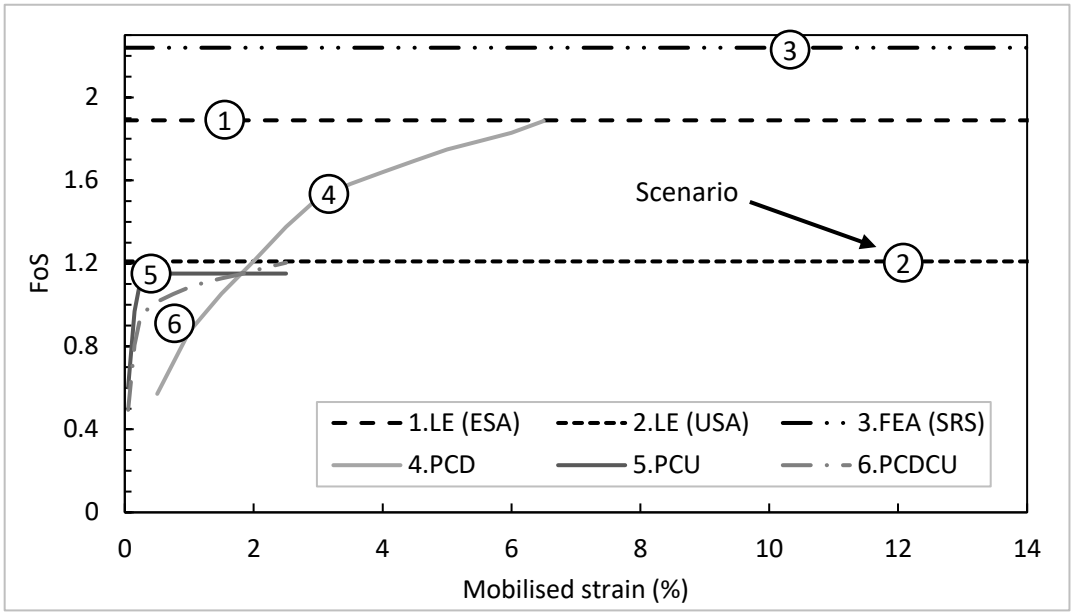

Figure 4.14: Results from the stability analyses on the platinum tailings for Cross Section C

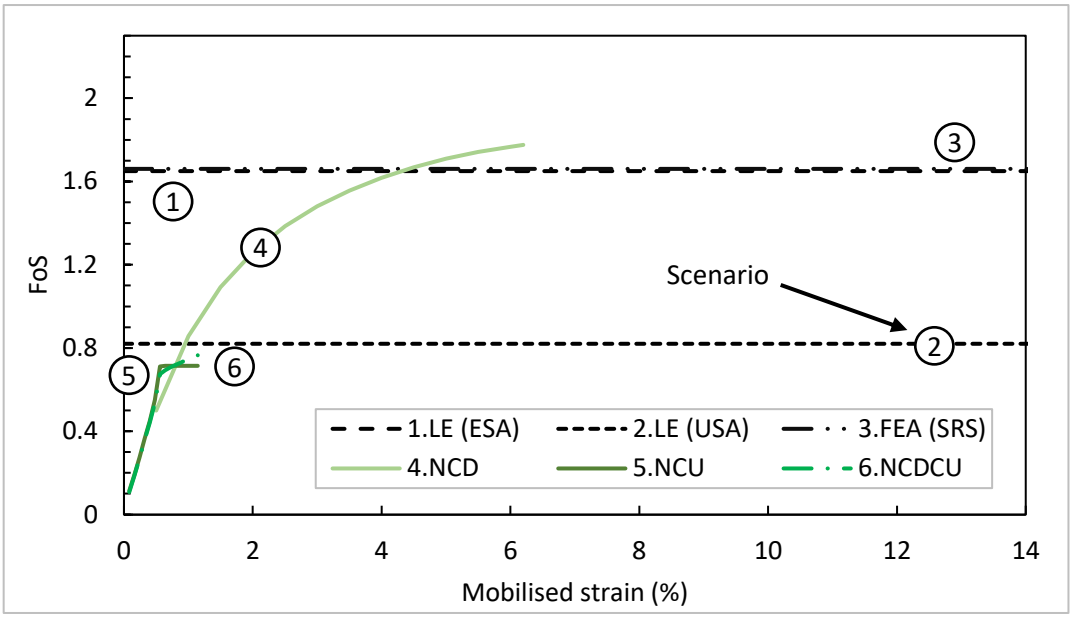

Figure 4.15: Results from the stability analyses on the Nerlerk sand for Cross Section C

4.5 FINITE ELEMENT ANALYSIS

4.5.1 Maximum deviatoric strain

One of the assumptions made when conducting limit equilibrium analyses is that there will be sufficient shear strain to mobilise the peak strength of the soil. For the proposed method where strain compatibility on the failure surface is maintained, a further assumption was made that the shear strains along the base of the slip surface would be uniform (i.e. the magnitude of shear strain at the beginning slice of the slip surface would be the same as the magnitude of the shear strain at the end slice of the slip surface. One of the key advantages of finite element analysis is that both strain compatibility and equilibrium can be satisfied and that no assumptions need to be made regarding shear strains. Rather, these are determined as part of the Strength Reduction Stability method.

As part of Scenario 3, finite element analyses were conducted. The results from theses analyses, where the strength reduction stability analysis was used are shown in Figure 4.16. The deviatoric strains for the four materials for Cross Section A are shown at failure (i.e. at the point when a FoS of 1.00 was achieved). It was found that in general the maximum deviatoric strains obtained were smallest at the crest and increased to be the greatest at the toe. This is in line with the findings of others (e.g. Fern et al., 2017). It is clear that the shear strains along the base of the slip surface are not uniform and that this should be considered in similar future limit equilibrium studies where attempts at maintaining strain compatibility are made.

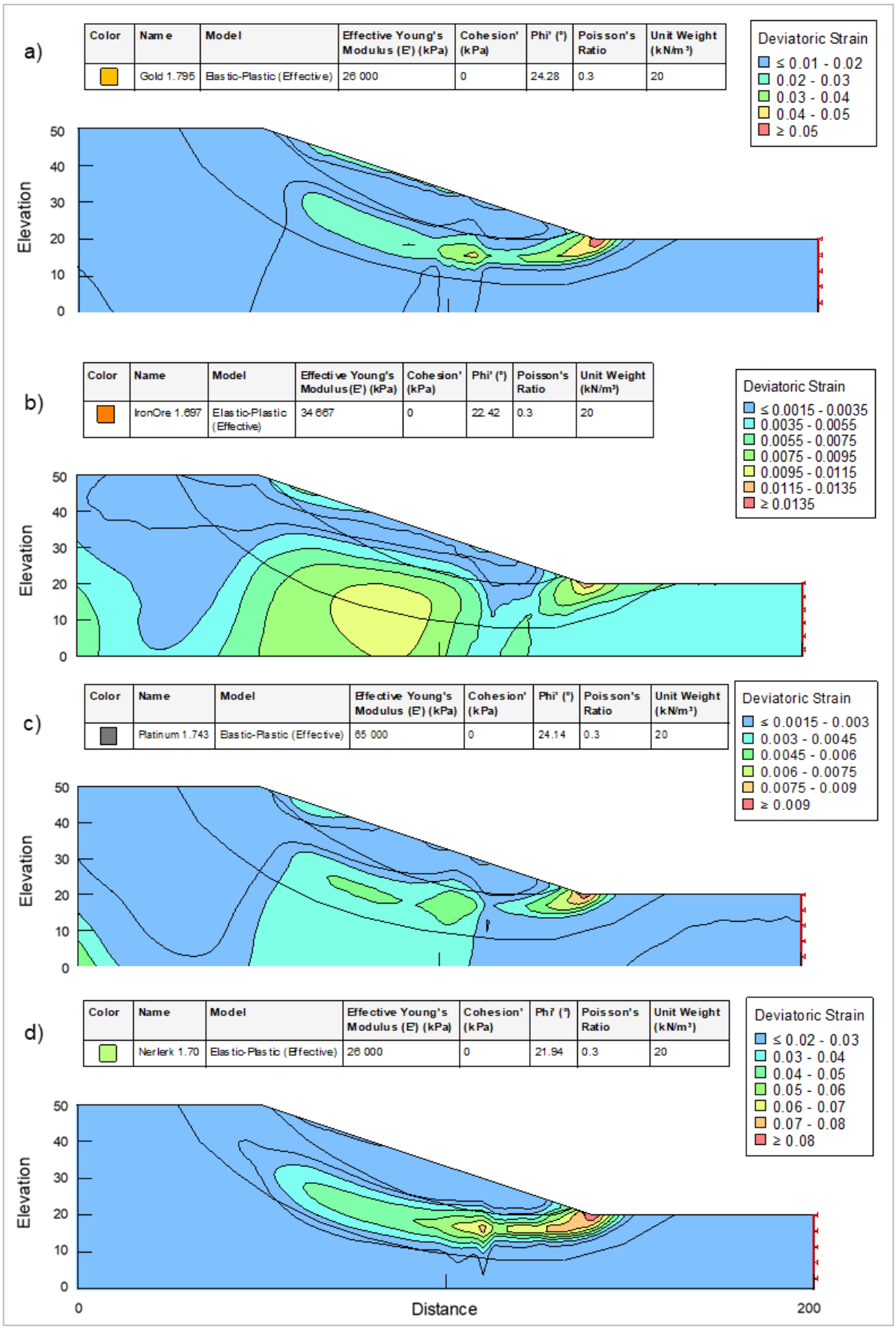

Figure 4.16: Maximum displacement contours from the finite element strength reduction analyses for Cross Section A for: a) gold tailings, b) iron tailings, c) platinum tailings and d) Nerlerk sand

4.5.2 Shear band propagation

As part of the Strength Reduction Stability method, the strength of the soil was steadily reduced until a FoS of 1.00 was achieved. Since a constitutive material model was used, it is possible to identify elements that have yielded at each iteration. This was done for the gold tailings for Cross Section A and is shown in Figure 4.17. It is clear that, as the strength of the soil was reduced, more and more elements started to yield. The Strength Reduction Factor (SRF) noted is the ratio by which the strength of the soil, represented in terms of $\tan \varphi'$ and c' was reduced. By displaying the yielded elements at each iteration, incremental yielding from the toe was noted, followed by yielding at the centre of the slope. These yielded elements eventually joined to form a zone of increased shear stress. In line with the general definition, failure (FoS of 1.00) was achieved when this zone was continuous from the crest to the toe.

Looking at Figure 4.17b, it may appear that there are boundary effects as the yielding starts from the foundation. However, the lower boundary of the model was extended and yielding still occurred at the same location. Therefore, it was concluded that the material yielding in this location was a result of the slope geometry and material strengths rather than a boundary effect.

No clear zone of increased shear stress development was noted for Cross Sections B and C in any of the three tailings materials. It is believed that this is due to the simple constitutive plastic soil model used and a more advanced model may be more appropriate. Nonetheless, the SFs obtained are still somewhat comparable and did allow conclusions to be drawn. It is recommended that more advanced soil models are used in further studies to ensure shear zones develop when finite element strength reduction analysis is conducted to assess the stability of a slope.

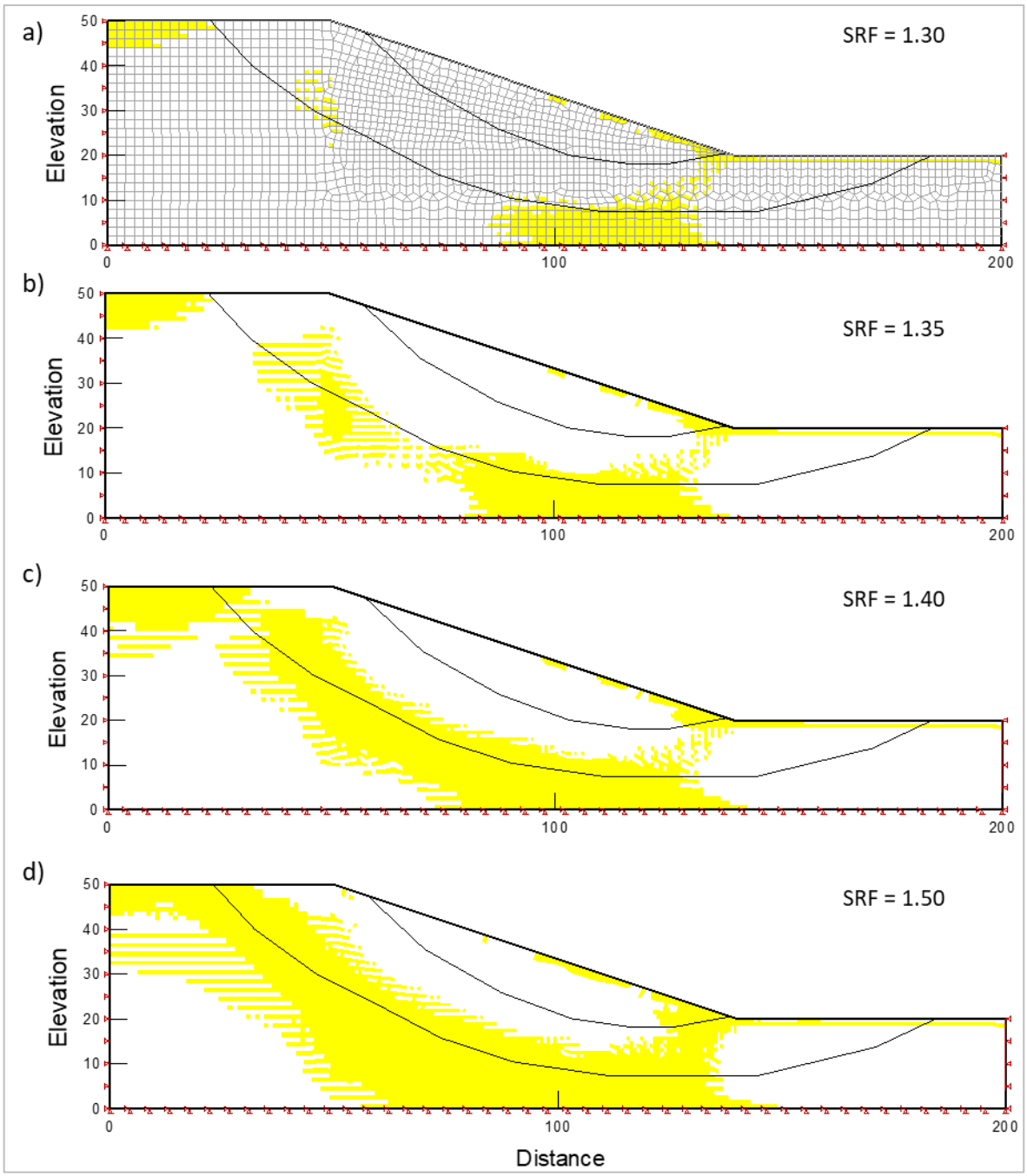

Figure 4.17: Results from the finite element strength reduction analysis showing elements that have yielded and the development of a continuous zone of increased shear stress for SRFs of a) 1.30, b) 1.35, c) 1.40 and d) 1.50

4.6 DISCUSSION

The aim of this study was to investigate whether attempting to maintain strain compatibility along the failure surface provides the same or different FoS to conventional slope stability analyses and whether this type of analysis should be considered in the future. To achieve this, a FoS formulation that considered strain compatibility was developed and was implemented for a series of slope

stability analyses. Conventional limit equilibrium and finite element analyses were also conducted and the calculated FoS results were compared. A discussion on the review of the triaxial data is provided, followed by a discussion on the implementation of the strain mobilisation method and the interpretation of the results.

4.6.1 Review of triaxial data

To implement the strain mobilisation method, results from CD and CU triaxial compression tests were required and a review was conducted on a series of tests conducted on three tailings materials and Nerlerk sand.

When considering the undrained behaviour of loose tailings at low confining stresses, the expectation is that strain softening (contractive) behaviour will occur. This is based on the observations by other researchers initially on clean sands but eventually also extended to silty tailings (e.g. Castro, 1969; Olson & Stark, 2003a; Sadrekarimi, 2014). This expectation has also been highlighted in the findings of the investigations into the recent tailings dam failures around the world (e.g. Morgenstern et al., 2015; Robertson et al., 2019),

However, upon closer inspection of these investigations it becomes apparent that these tests upon which these expectations were developed were predominantly conducted on reconstituted samples and that the Moist Tamping (MT) sample preparation method was used. As discussed in Section 2.4.1, it has been established that the sample preparation method does significantly influence the mechanical behaviour of the soil in Consolidated Undrained (CU) triaxial compression tests.

With this in mind, when reviewing the results from the CU triaxial tests conducted on the tailings material, it was found that the samples tested did not show the strain-softening behaviour expected from loose tailings material. Rather, the samples showed an initial contractive tendency followed by strong dilative tendency. This is typical for samples prepared using the Slurry Deposition (SD) method, which was done in this case for the tailings materials. This behaviour is in line with findings from other researchers (e.g. Chang et al., 2011; Corrêa & Filho, 2019). Due to this dilative tendency, no collapse surface or yield strength envelope developed. Therefore, the interpreted yield undrained shear strengths were greater than those suggested for use by Sadrekarimi (2014).

These relationships proposed by Sadrekarimi (2014), discussed in Section 2.5.1, were derived from a database of CPTu tests and CU triaxial test results on a variety of soils. Upon closer investigation of the soil database used to define these proposed relationships, it becomes evident

that the soils tested to develop the proposed relationships clearly exhibited strain-softening behaviour which was expressed in the form of an undrained brittleness index. This is discussed further in Section 2.5.1. The tailings material tested in this study (prepared using the SD method), exhibited a near zero undrained brittleness index and it can therefore be expected that the proposed equations do not compare well to the measured values.

Strain-softening behaviour was however, noted for the Nerlerk sand (prepared using the MT sample preparation method) and the derived Yield Stress Ratio (YSR) of 0.24 is comparable to those found by others (e.g. Olson, 2001) and those interpreted using other methods such as estimations based on CPTu data (e.g. Sadrekarimi, 2014). However, this may simply be a result of the MT sample preparation method used. It has been shown that samples prepared using the MT method always seem to show contractive behaviour. Therefore, this may not be representative of the true behaviour of the soil expected in the field.

4.6.2 Implementation of the strain mobilisation method

Slope stability analyses were conducted for three hypothetical slope cross sections for four materials. For each material, six scenarios were assessed by means of a commercial software package as well as a Microsoft Excel spreadsheet, developed to allow the gradual mobilisation of shear resistance, based on progressively increasing the mobilised shear strain to be implemented. Conventional limit equilibrium methods were considered, and the results were compared to the results obtained from the implementation of the proposed FoS formulation where strain compatibility is considered. The FoS formulation method is a spreadsheet-based strain mobilisation method and produced an evolution of the mobilised FoS values which were calculated dependant on the assumed amount of mobilised shear strain along the base of each slice along the slip surface.

When considering drained strengths, it is well established that rigorous limit equilibrium methods are capable of representing the stability of a slope (e.g. Vick, 1983; Blight, 2009). Therefore, if it is assumed that Scenario 1, where effective strength parameters were used and the FoS was calculated according to Spencer's method, is an accurate representation of the stability of a slope under drained conditions, then the proposed method when considering drained strengths only (i.e. Scenario 4) can be deemed accurate for Cross Sections A and C. In other words, the proposed FoS formulation is able to calculate a FoS against failure of a slope when drained strengths are considered to an absolute value difference of less than 8% compared to current methods. It is believed that the larger difference in calculated FoS for Cross Section B is due to the need to more rigorously consider the interslice forces when more complex geometries are assessed.

It is not so simple to agree on a method to accurately represent the stability of a slope under undrained conditions. The most logical approach is to back-analyse case histories where undrained failure did occur (e.g. Olson, 2001). These studies have resulted in several methods of conducting undrained stability analyses. A popular method is to use limit equilibrium methods where both drained and undrained strength parameters are used (e.g. Brown & Gillani, 2016; Anglo American, 2018). For this study, this method was implemented as Scenario 2. If it assumed that Scenario 6, where drained and undrained strength parameters were used and the FoS was calculated according to the limit equilibrium formulation presented, is an accurate representation of the stability of the slope under undrained conditions, then the current method considering drained and undrained shear strengths is deemed to be accurate.

In general, when considering stability analyses where both drained and undrained strengths are mobilised along the same failure surface, it was found that the calculated FoS using the proposed method converged to the calculated FoS using current methods. For Cross Section A, the proposed method produced higher FoS values while in Cross Sections B and C, the proposed method produced lower (probably over-conservative) values than the current methods. This is largely due to disregarding interslice forces which are favourable in terms of stability and considering these forces gives a higher FoS. For Cross Sections A and C, the difference between the FoS calculated using the currently accepted method (Scenario 2) and the FoS calculated using the proposed method (Scenario 6) varied between 0.01 and 0.06, indicating that the currently accepted method calculates FoS values accurately and that there is no need to consider limit equilibrium methods where strain compatibility is maintained.

It should be noted that this correlation is a function of the slip surface and cross section geometry and may not be applicable to all cross sections assessed. For example, Cross Section B did not show a good correlation between the two methods. The large difference in calculated FoS values indicates that the proposed strain mobilisation method may be less reliable when the slip surface passes through alternating drained and undrained material zones as is the case for Cross Section B where the undrained material zone is between the drained zone at the crest and the drained starter wall at the toe. A reason could be that complex geometries require interslice forces to be considered more realistically than what was done for this work

As part of the implementation of the proposed method, an assumption was made that uniform shear strains were mobilised along the entire slip surface. The finite element strength reduction analysis conducted showed that the shear strains along the base of the slip surface can generally be expected to be non-uniform. Rather the magnitude of shear strain varied along the slope surface

with the maximum deviatoric strain occurring at the toe of the slope. This varying shear strain was also seen by other researchers (e.g. Fern et al., 2017) and indicates that the assumption of uniform shear strain along the entire slip surface may not be a good assumption prior to failure. It is recommended that more realistic strain mobilisation distributions be considered further in future studies

5 CONCLUSIONS AND RECOMMENDATIONS

5.1 CONCLUSIONS

This chapter presents the conclusions reached after the analysis of the data presented and provides recommendations for future research. Each objective discussed in Section 1.2 of this report is addressed.

5.1.1 Effect of strain mobilisation on the calculated factor of safety against failure

Current limit equilibrium slope stability analyses do not consider strain compatibility. Rather, it is assumed that sufficient shear strain develops to mobilise the shear strength used in the limit equilibrium formulations. This is important when drained and undrained strengths are used in the same analysis as it is known that these strengths are mobilised at different rates with regard to strain development.

A new formulation was proposed to determine a FoS against failure using limit equilibrium methods where strain compatibility is maintained along the failure surface. The FoS formulation considers the shear stress on the failure envelope as a function of deviator stress, determined from a Mohr circle at failure and then uses triaxial test data to relate the mobilised shear stress on the failure surface for use in simplistic limit equilibrium formulations to shear strain. In summary, the mobilised strength at the base of each slice was specified, based on an assumed increment of mobilised shear strain. By progressively increasing the assumed mobilised strain, an evolution of the FoS was calculated. Similar to the method by Fellenius, interslice forces were disregarded so that the consideration of equilibrium in the proposed formulation is less rigorous that the more sophisticated limit equilibrium methods such as the methods by Spencer and Morgenstern-Price. A general consequence of this is that the FoS calculated using the proposed method are possibly more conservative.

Drained and undrained triaxial compression stress paths were determined for three tailings materials: gold, iron and platinum. As an additional check, data from triaxial compression tests on Nerlerk sand done by others were also assessed. After adjusting the curves as described in Section 3.3, slope stability analyses were conducted for three hypothetical slopes for the four above-mentioned materials and the three slope geometries. For each material, six scenarios were assessed by means of a commercial software package (GeoStudio 2020) as well as a Microsoft Excel spreadsheet developed to implement the proposed method.

In general, when considering stability analyses where drained and undrained strengths are used, it was found that the calculated FoS using the proposed method converged to the calculated FoS using current methods. For Cross Section A, the proposed method produced higher FoS values while in Cross Sections B and C, the proposed method produced lower values than the current methods. For Cross Sections A and C, the difference between the FoS calculated using the currently accepted method (Scenario 2) and the FoS calculated using the proposed method (Scenario 6) varied between 0.01 (1%) and 0.06 (7%), indicating that the proposed method provides FoS values comparable to those calculated using currently accepted methods where the failure surface passes predominantly through a single material type. For such a case, there does not appear to be a need to consider limit equilibrium methods where strain compatibility is maintained.

It should be noted that the good correlation may be somewhat specific to the slip surface and cross section geometry analysed and may not be applicable to all cross sections. For example, Cross Section B, where the failure surface passes through more than one material type, did not show a good correlation between the two methods, illustrating that interslice forces probably need more careful consideration than in the current implementation.

5.1.2 Effect of sample preparation method on the stress-strain behaviour noted during undrained shear in triaxial compression

Ideally, laboratory tests should be conducted on undisturbed soil samples so that the state of the soil tested is the same as the state of the soil in the field. The state of the soil comprises several aspects including stress history, density, current stress conditions and fabric. It is relatively simple to reproduce the density and stress conditions if undisturbed samples cannot be obtained and reconstituted samples are used as a substitute. However, it is not simple to recreate the stress history and fabric.

Several sample preparation methods are available, and each method has its own advantages and limitations. As per the discussion in Section 2.4.1, various researchers have shown that the sample preparation method used to create loose samples can have an effect on the material response during shearing. It has been shown that the Moist Tamping (MT) method produces samples that contract during shearing while Slurry Deposition (SD) method produces samples that initially have a contractive tendency but then show a dilative tendency to steady state (e.g. Zlatovic & Ishihara, 1997; Chang et al., 2011; Corrêa & Oliveira Filho, 2019). Although neither of these methods are

able to capture the fabric of the soil in situ (Chang et al., 2011), the SD is seen as the preferred method for loose tailings sample preparation as it is believed to more closely represent the slurry deposition methods used on many tailings dams (Corrêa & Filho, 2019).

5.1.3 Comparison of the theoretical and triaxial compression behaviour under undrained conditions in loose tailings

When considering the undrained behaviour of loose tailings at low confining stresses, the expectation is that strain softening (contractive) behaviour will occur. This is based on the observations by other researchers initially on clean sands but eventually also extended to silty tailings (e.g. Castro, 1969; Olson & Stark, 2003a; Sadrekarimi, 2014). However, upon closer inspection of these investigations it becomes apparent that these tests were predominantly conducted on reconstituted samples and that the Moist Tamping sample preparation method was used. As discussed in Section 2.4.1, it has been established that the sample preparation method does significantly influence the mechanical behaviour of the soil in Consolidated Undrained (CU) triaxial compression tests.

With this in mind, when reviewing the results from the CU triaxial tests conducted, it was found that the samples tested did not show the strain-softening behaviour expected from loose tailings material. Rather, the samples showed an initial contractive tendency followed by strong dilative tendency. This is typical for samples prepared using the Slurry Deposition (SD) method. This is in line with findings from other researchers (e.g. Chang et al., 2011; Corrêa & Filho, 2019). The result is that no collapse surface or yield strength envelope developed.

5.1.4 Comparison of the measured undrained shear strength mobilised during CU triaxial compression tests to the empirical strength proposed by Sadrekarimi (2014)

Based on the findings of the investigations into the recent tailings dam failures around the world (e.g. Morgenstern et al., 2015; Robertson et al., 2019), it is a concern that saturated, loose, silty material such as tailings would exhibit strain-softening behaviour when subjected to undrained shearing at relatively low effective confining stress values. However, strain-softening or contractive behaviour was not seen during the CU tests on the three tailings materials (prepared using the SD method). Rather, it was found that the material initially contracted but then strongly dilated to failure. Therefore, the interpreted yield undrained shear strengths were greater than those suggested for use by (Sadrekarimi, 2014).

Strain-softening behaviour was however, noted for the Nerlerk sand (prepared using the MT sample preparation method) and the derived Yield Stress Ratio (YSR) of 0.24 is comparable to those found by others (e.g. Olson, 2001) and those interpreted using other methods such as estimations based on CPTu data (e.g. Sadrekarimi, 2014). However, this may simply be a result of the MT sample preparation method used. It has been shown that samples prepared using the MT method always seem to show contractive behaviour. Therefore, this may not be representative of the true behaviour of the soil expected in the field.

5.2 RECOMMENDATIONS

Based on the findings of this study, several recommendations for future work have been developed. This section discusses these recommendations.

5.2.1 Review of additional materials

As only three tailings materials were assessed, it is recommended that the use of the proposed method where limit equilibrium methods considering strain compatibility be extended to additional tailings materials such as kimberlite and copper to confirm that the findings of this study is applicable to those material types as well. Natural soils can also be considered.

5.2.2 Review of assumptions regarding interslice forces

In the proposed strain mobilisation method presented, it was assumed that the resultant of the interslice forces is zero, similar to what was assumed as part of the Fellenius method. However, a larger difference in calculated FoS value between the conventional methods and the proposed method was noted for Cross Section B which may indicate that the proposed method is less reliable when slip surfaces pass through alternating drained and undrained material zones. A way to improve this may be a more rigorous consideration of the interslice forces. It is therefore recommended that a strain mobilisation technique is developed which more rigorously considers the interslice forces.

5.2.3 Review of shear strain mobilisation assumptions

As part of the analysis, an assumption was made that uniform shear strains were mobilised along the entire length of the slip surface. While this may be an approximately true when the actual slip

failure takes place, it is not the case as failure develops. Results from the finite element analysis conducted and observations by other (e.g. Fern et al., 2017) show that the shear strains at failure along the base of the slip surface are not uniform in the development of failure. It was found that the shear strains vary along the slip surface and are greatest at the toe and smallest at the crest. Therefore, the assumption that the shear strains are uniform along the base of the slip surface may not be appropriate. It is recommended that this aspect be considered further in future studies.

5.2.4 Review of interpreted shear strains from the triaxial test results

During the shear phase of a triaxial compression test, the axial strain is measured. However, it is convenient to interpret soil parameters using shear strain. Therefore, a relationship between the measured axial strain and interpreted shear strain is required. For CU tests, where there is no volumetric strain, this relationship is simple to derive (i.e. the shear strain is equal to the axial strain). However, for CD tests, there is volumetric strain and if radial strains are not measured, some assumptions need to be made to allow shear strains to be calculated. Details of the assumptions made for this study can be found in Appendix B. To avoid the need of these assumptions, the radial strain should be measured during the shear phase.

5.2.5 Investigation into sample preparation methods for triaxial testing

Results from the shear phase of the consolidated undrained triaxial tests conducted on reconstituted samples were assessed. It is clear from the results that the theoretical strain softening response expected from loose tailings was not observed. In fact, two of the samples (the gold and platinum tailings) dilated after initial contraction and, as a result no Yield Strength Envelope developed. This meant that the interpreted peak undrained shear strength when normalised to the mean effective stress at failure was similar to the peak drained strength when normalised to the mean effective stress at failure. This is very different to the undrained shear strengths used in practice, which are generally in the range of 0.20 to 0.30 times the vertical effective stress and opposed to drained strengths which are generally in the range of 0.45 to 0.70 times the normal effective stress, for a 25° and 35° friction angle respectively (Olson & Stark, 2003b). Although the ratios are based on two different stresses, vertical effective stress and normal effective stress, there is typically a negligible difference between these stresses in geotechnical problems (Olson, 2001).

To gain a better understanding of why there is generally not such large difference in measured drained and undrained strengths from triaxial tests based on SD prepared samples compared to

those based on MT samples which tend to contract to steady state, it is recommended that a site investigation be conducted with associated laboratory testing.

As part of the investigation, field testing should incorporate CPTu testing to identify zones that exhibit potentially contractive and potentially dilative behaviour. These materials should then be sampled as carefully as possible and then taken to a laboratory for testing, typically in a CU triaxial compression test. Although CU triaxial tests have been performed on undisturbed samples, the focus has been on the effect of sampling and method if preparation to best reproduce the in situ fabric (Chang et al., 2011). The tests that do show this strain softening behaviour have all been conducted using the MT preparation method which creates very loose samples (Castro, 1969; Been et al., 1991; Shuttle & Cunning, 2007; Morgenstern et al., 2016). In fact, using this preparation method, it is sometimes possible to prepare samples with even greater void ratios that the e_{max} values calculated based on standard test methods (Corrêa & Filho, 2019), which seems to suggest that these states are unlikely to exist in situ.

In summary, the industry is currently struggling on determining sample preparation methods such that the samples are prepared as close to the in situ state as possible in order to verify if the theoretical strain softening behaviour can be observed. It is believed that a study similar to the one outlined above would help to answer this question.

6 REFERENCES

Anglo American. 2018. *Managing static liquefaction risk in upstream tailings dams, supporting guideline to AA TS 602*. Anglo American Plc. Guideline document GDL-001. South Africa.

ASTM. 2012. Standard test method for performing electronic friction cone and piezocone penetration testing of soils. *ASTM D-5778*. American Society for Testing and Materials. United States of America.

Atkinson, J. H. and Bransby, P. L. 1978. *The mechanics of soils: an introduction to critical state soil mechanics*. 1st ed. McGraw-Hill, London.

Baziar, M. H. and Dobry, R. 1991. Liquefaction ground deformation predicted from laboratory tests. *2nd International Conference on Recent Advances in Geotechnical Earthquake Engineering and Soil Dynamics*. March, Missouri, paper no. 32.

Been, K. 2016. Characterizing mine tailings for geotechnical design. *Australian Geomechanics Journal*, Vol 50, No 4, December, pp 59–78.

Been, K. Jefferies M. G. and Hachey, J. 1991. The critical state of sands. *Géotechnique*, Vol 41, No 3, September, pp 365–381.

Bishop, A. W. 1955. The use of the slip circle in the stability analysis of slopes. *Géotechnique*, Vol 5, No 1, March, pp 7–17.

Bishop, A. W. and Henkel, D. J. 1962. *The measurement of soil properties in the triaxial test*. 2nd ed. Edward Arnold, London.

Bjerrum, L. and Landva, A. 1966. Direct simple-shear tests on a Norwegian quick clay. *Géotechnique*, Vol 16, No 1, March, pp 1–20.

Blight, G. 2009. *Geotechnical engineering for mine waste storage facilities*. 1st ed. CRC Press, London.

Bosman, D. E. Basson, J. R. Tente, T. and Basson, G. R. 2011. *South African Committee on Large Dams (SANCOLD)-Volume II-Guidelines on freeboard for dams*. SANCOLD. Report No: 1759/2/11 Pretoria.

Brown, B. and Gillani, I. 2016. Common errors in the slope stability analyses of tailings dams. *1st Asia Pacific Slope Stability in Mining Conference*. September, Perth, pp 545–556.

Budhu, M. and Britto, A. 1987. Numerical analysis of soils in simple shear devices. *Soils and Foundations*, Vol 27, No 2, June, pp 31–41.

Castro, G. 1969. *Liquefaction of sands*. PhD Thesis. Harvard University, Massachusetts.

Chang, N. Heymann, G. and Clayton, C. 2011. The effect of fabric on the behaviour of gold tailings. *Géotechnique*, Vol 61, No 3, March, pp 187–197.

Chen, W. F. 1975. *Limit analysis and soil plasticity*. 1st ed. Elsevier Science Publishers, Amsterdam.

Corrêa, M. M. and Oliveira Filho, W. L. 2019. Impact of methods used to reconstitute tailings specimens on the liquefaction potential assessment of tailings dams. *REM-International Engineering Journal*, Vol 72, No 3, September, pp 507–513.

Coulomb, C. A. 1773. Essay on the rules of maximis and minimis applied to some problems of equilibrium related to architecture. *Academy of Royal Science Memorial Physics*, Vol *7*, pp 343–382.

Dabeet, A. 2014. *Discrete element modeling of direct simple shear response of granular soils and model validation using laboratory tests*. PhD Thesis. University of British Columbia, Vancouver.

Dillon, M. J. and Wardlaw, H. J. 2010. Strength and liquefaction assessment of tailings. *1st International Seminar on the Reduction of Risk in the Management of Tailings and Mine Waste*, September, pp 347–360.

do Carmo, F. F. Kamino, L. H. Y. Junior, R. T. de Campos, I. C. do Carmo, F F S, G., Mauro, M. and L. 2017. Fundão tailings dam failures: the environment tragedy of the largest technological disaster of Brazilian mining in global context. *Perspectives in Ecology and Conservation*, Vol 15, No 3, July, pp 145–151.

Drucker, D. C. Prager, W. and Greenberg, H. J. 1952. Extended limit design theorems for continuous media. *Quarterly of Applied Mathematics*, Vol 9, No 4, January, pp 381–389.

Duncan, J. M. Wright, S. G. and Brandon, T. L. 2014. *Soil strength and slope stability*. 1st ed. John Wiley & Sons, New Jersey.

Eckersley, D. 1990. Instrumented laboratory flowslides. *Géotechnique*, Vol 40, No 3, September, pp 489–502.

Fern, E. J. de Lange, D. A. Zwanenburg, C. Teunissen, J. A. M. Rohe, A. and Soga, K. 2017. Experimental and numerical investigations of dyke failures involving soft materials. *Engineering Geology*, Vol 219, March, pp 130–139.

Fourie, A. B. Blight, G. E. and Papageorgiou, G. 2001. Static liquefaction as a possible explanation for the Merriespruit tailings dam failure. *Canadian Geotechnical Journal*, Vol 38, No 4, August, pp 707–719.

Franks, D. M. Stringer, M. Torres-Cruz, L. A. Baker, E. Valenta, R. Thygesen, K. Matthews, A. Howchin, J. Barrie, S. 2021. Tailings facility disclosures reveal stability risks. *Scientific Reports*, , Vol 11, No 1, March, pp 1–7

Fredlund, D. G. and Krahn, J. 1977. Comparison of slope stability methods of analysis. *Canadian Geotechnical Journal*, Vol 14, No 3, August, pp 429–439.

Fredlund, D. G. Krahn, J. and Pufahl, D. E. 1981. The relationship between limit equilibrium slope stability methods. *International Conference on Soil Mechanics and Foundation Engineering*, Vol *3*, June, Stockholm, pp 409–416.

Griffiths, D. V. and Lane, P. A. 1999. Slope stability analysis by finite elements. *Géotechnique*, Vol 49, No 3, June, pp 387–403.

Gylland, A. Thakur, V. and Emdal, A. 2016. Extended interpretation basis for the vane shear test. *17th Nordic Geotechnical Meeting*, May, Reyjavik.

Høeg, K. Dyvik, R. and Sandbækken, G. 2000. Strength of undisturbed versus reconstituted silt and silty sand specimens. *Journal of Geotechnical and Geoenvironmental Engineering*, Vol 126, No 7, July, pp 606–617.

Jamiolkowski, M. Ladd, C. C. Germaine, J. T. and Lancellotta, R. 1985. New developments in field and laboratory testing of soils. *11th International Conference on Soil Mechanics and Foundation Engineering*, Vol 1, August, San Fransicso, pp 57–153.

Jamiolkowski, M. and Masella, A. 2015. Geotechnical characterization of copper tailings at Zelazny Most Site. *3rd International Conference on the Flat Dilatometer*, Rome, pp 25–42.

Janbu, N. 1954. Application of composite slide circles for stability analysis. *Proceedings of the European Conference of Earth Slopes*, Vol 3, Stockholm, pp 43–49.

Jefferies, M. and Been, K. 2015. *Soil liquefaction: a critical state approach*. 2nd ed. CRC press, London.

Jefferies, M. G. 1993. Nor-Sand: a simple critical state model for sand. *Géotechnique*, Vol 43, No 1, March, pp 91–103.

Kim, K Prezzi, M. Salgado, R. and Lee, W. 2010. Penetration rate effects on cone resistance measured in a calibration chamber. *2nd International Symposium on Cone Penetration Testing*, Vol 2, May, California, pp 200-208.

Kim, K. Prezzi, M. Salgado, R. and Lee, W. 2008. Effect of penetration rate on cone penetration resistance in saturated clayey soils. *Journal of Geotechnical and Geoenvironmental Engineering*, Vol 134, No 8, August, pp 1142–1153.

Klohn Crippen Berger (KCB) 2017. Study of tailings management technologies. *MEND Report 2.50.1*.

Knappett, J. and Craig, R. F. 2012. *Craig's soil mechanics*. 8th ed. Spon Press, London.

Konrad, J. M. 1993. Undrained response of loosely compacted sands during monotonic and cyclic compression tests. *Géotechnique*, Vol 43, No 1, March, pp 69–89.

Koutsoftas, D. C. and Ladd, C. C. 1985. Design strengths for an offshore clay. *Journal of Geotechnical Engineering*, Vol 111, No 3, March, pp 337–355.

Krahn, J. 2003. The 2001 RM Hardy Lecture: The limits of limit equilibrium analyses. *Canadian Geotechnical Journal*, Vol 40, No 3, June, pp 643–660.

Krahn, J. 2018. *Stability modeling with geostudio*. GEO-SLOPE International. Canada.

Kulhawy, F. H. and Mayne, P. W. 1990. *Manual on estimating soil properties for foundation design*. Electric Power Research Institution. United States of America.

Ladd, C. C. 1991. Stability evaluation during staged construction. *Journal of Geotechnical Engineering*, Vol 117, No 4, April, pp 540–615.

Ladd, R. S. (1978). Preparing test specimens using undercompaction. *Geotechnical Testing*

Journal, Vol 1, No 1, March, pp 16–23.

Lade, P. V. 2016. *Triaxial testing of soils*. 1st ed. John Wiley & Sons, West Sussex.

Li, W. and Coop, M. R. 2019. Mechanical behaviour of Panzhihua iron tailings. *Canadian Geotechnical Journal*, Vol 56, No 3, March, pp 420–435.

Malkawi, A. I. H. Hassan, W. F. and Sarma, S. K. 2001. Global search method for locating general slip surface using Monte Carlo techniques. *Journal of Geotechnical and Geoenvironmental Engineering*, Vol 127, No 8, August, pp 688–698.

Martin, T. E. and McRoberts, E. C. 1999. Some considerations in the stability analysis of upstream tailings dams. 6*th International Conference on Tailings and Mine Waste*, Vol 99, January, Rotterdam, pp 287–302.

Meigh, A. C. 1987. Cone penetration testing - methods and interpretation. *Ground Engineering Report: In-situ Testing*. Construction Industry Research and Information Association (CIRIA), London.

Morgenstern, N. R. 2018. Geotechnical risk, regulation, and public policy. *Soils and Rocks*, Vol 41, No 2, May, pp 107-129.

Morgenstern, N. R. and Price, V. E. 1965. The Analysis of the stability of general slip surfaces. *Géotechnique*, Vol 18, No 3, March, pp 393–394.

Morgenstern, N. R. Vick, S. G. and Van Zyl, D. 2015. *Report on Mount Polley tailings storage facility breach*. Report of Independent Expert Engineering Investigation and Review Panel. Prepared on Behalf of the Government of British Columbia and the Williams Lake and Soda Creek Indian Bands.

Morgenstern, N. R. Vick, S. G. Viotti, C. B. and Watts, B. D. 2016. *Fundão tailings dam review panel report on the immediate causes of the failure of the Fundão Dam*. SAMARCO.

Narainsamy, Y. Geldenhuys, L. and Hörtkorn, F. 2019. Use of mode of shear for undrained slope stability analysis. *17th African Regional Conference on Soil Mechanics and Geotechnical Engineering*, Cape Town, October.

Olson, S. M. 2001. *Liquefaction analysis of level and sloping ground using field case histories and penetration resistance*. PhD Thesis. University of Illinois, Illinois.

Olson, S. M. and Mattson, B. B. 2008. Mode of shear effects on yield and liquefied strength ratios. *Canadian Geotechnical Journal*, Vol 45, No 4, April, pp 574–587.

Olson, S. M. and Stark, T. D. 2003a. Use of laboratory data to confirm yield and liquefied strength ratio concepts. *Canadian Geotechnical Journal*, Vol 40, No 6, December, pp 1164–1184.

Olson, S. M. and Stark, T. D. 2003b. Yield strength ratio and liquefaction analysis of slopes and embankments. *Journal of Geotechnical and Geoenvironmental Engineering*, Vol 129, No 8, August, pp 727–737.

Parry, R. H. G. 2004. *Mohr circles, stress paths and geotechnics*. 2nd ed. CRC Press, London.

Randolph, M. F. and Hope, S. 2004. Effect of cone velocity on cone resistance and excess pore

pressures. *International Symposium on Engineering Practice and Performance of Soft Deposits*, June, Osaka, pp 147–152.

Reid, D. and Fanni, R. 2020. A comparison of intact and reconstituted samples of a silt tailings. *Géotechnique*, Vol 70, No 12, December, pp 1–47.

Robertson, P K. 2009. Interpretation of cone penetration tests—a unified approach. *Canadian Geotechnical Journal*, Vol 46, No 11, November, pp 1337–1355.

Robertson, P K. 2012. Interpretation of in-situ tests--some insights. *4th International Conference on Geotechnical and Geophysical Site Characterisation*, Pernambuco, September, pp 1–22.

Robertson, P. K. de Melo, L. Williams, D. J. and Wilson, G. W. 2019. *Report on the expert panel on the technical causes of the failure of the Feijão dam 1*. Vale.

Robertson, P. K. 2010. Estimating in-situ soil permeability from CPT & CPTu. *2nd International Symposium on Cone Penetration Testing*, May, California.

Robertson, P. K. and Campanella, R. G. 1983. Interpretation of cone penetration tests. Part I: Sand. *Canadian Geotechnical Journal*, Vol 20, No 4, November, pp 718–733.

Roscoe, K. H. 1953. An apparatus for the application of simple shear to soil samples. *3rd International Conference on Soil Mechanics and Foundation Engineering*, August, Zurich, pp 186-191.

Sadrekarimi, A. 2014. Effect of the mode of shear on static liquefaction analysis. *Journal of Geotechnical and Geoenvironmental Engineering*, Vol 140, No 12, December, pp 1-12.

Sarma, S. K. 1973. Stability analysis of embankments and slopes. *Géotechnique*, Vol 23, No 3, September, pp 423–433.

Sasitharan, S. Robertson, P. K. Sego, D. and Morgenstern, N. R. 1993. Collapse behavior of sand. *Canadian Geotechnical Journal*, Vol 30, No 4, August, pp 569–577.

Shuttle, D. A. and Cunning, J. 2007. Liquefaction potential of silts from CPTu. *Canadian Geotechnical Journal*, Vol 44, No 1, January, pp 1–19.

Sladen, J. A. D'hollander, R. D. and Krahn, J. 1985. The liquefaction of sands, a collapse surface approach. *Canadian Geotechnical Journal*, Vol 22, No 4, November, pp 564–578.

Sloan, S. W. 2013. Geotechnical stability analysis. *Géotechnique*, Vol 63, No 7, June, pp 531-571.

SLOPE/W. 2001. *A software package for slope stability analysis*. GEO-SLOPE International. Canada.

South Africa Bureau of Standards. 1998. *SABS 10286: Code of practice for mine residue*. SABS. South Africa.

Soydemir, C. 1972. Anisotropy in undrained strength observed through special simple shear tests. *Norwegian Geotechnical Institute internal report 50320-8*. NGI, Norway.

Spencer, E. 1967. A method of analysis of the stability of embankments assuming parallel inter-slice forces. *Géotechnique*, Vol 17, No 1, March, pp 11–26.

SRK Consulting. 2017. *Mototolo platinum mine - 2017 piezocone testing, stability and mitigation*

design at Helena TSF - level 1 design report. SRK Consulting. South Africa.

Stark, T. D. 1987. *Mechanisms of strength loss in stiff clay*. PhD Thesis. Virginia Polytechnic Institute and State University, Virgina.

Terzaghi, K. Peck, R. B. and Mesri, G. 1996. *Soil mechanics in engineering practice*. 3rd ed. John Wiley & Sons, New York.

Torres Cruz, L. A. 2016. *Use of the cone penetration test to assess the liquefaction potential of tailings storage facilities*. PhD Thesis. University of the Witwatersrand, Johannesburg.

Tumay, M. T. Hatipkarasulu, Y. and Yilmaz, R. 2017. Evaluation of undrained shear strength of soft soils using CPT and VST technologies. *19th International Conference on Soil Mechanics and Geotechnical Engineering*. September, Seoul, pp 665-668.

TÜV-SÜD. 2018. *Auditoria Técnica de Segurança 2° Ciclo 2018*. TÜV-SÜD. RC-SP-102/18. Brazil.

Vardanega, P. J. Lau, B. H. Lam, S. Y. Haigh, S. K. Madabhushi, S. P. G. and Bolton, M. D. 2012. Laboratory measurement of strength mobilisation in kaolin: link to stress history. *Géotechnique Letters*, Vol 2, No 1, Mar, pp 9–15.

Vermeulen, N. J. (2001). *The composition and state of gold tailings*. PhD Thesis. University of Pretoria, Pretoria.

Vick, S. G. 1983. *Planning, design, and analysis of tailings dams*. 1st ed. Wiley, New York.

Wagener, F. 1997. The Merriespruit slimes dam failure: overview and lessons learnt. *Joernaal van Die Suid-Afrikaanse Instituut van Siviele Ingenieurswese*, Vol 39, No 3, January, pp 11–15.

Wijewickreme, D. Sriskandakumar, S. and Byrne, P. 2005. Cyclic loading response of loose air-pluviated Fraser River sand for validation of numerical models simulating centrifuge tests. *Canadian Geotechnical Journal*, Vol 42, No 2, April, pp 550–561.

Wroth, C. P. 1965. The prediction of shear strains in triaxial tests on normally consolidated clays. *6th International Conference of Soil Mechanics and Foundation Engineering*, Vol 1, September, Montreal, pp 417–420.

Yu, H. S. Salgado, R. Sloan, S. W. and Kim, J. M. 1998. Limit analysis versus limit equilibrium for slope stability. *Journal of Geotechnical and Geoenvironmental Engineering*, Vol 124, No 1, January, pp 1–11.

Zheng, H. Liu, D. F. and Li, C. G. 2008. On the assessment of failure in slope stability analysis by the finite element method. *Rock Mechanics and Rock Engineering*, Vol 41, No 4, August, pp 629-639.

Zhu, D. Y. Lee, C. F. and Jiang, H. D. 2003. Generalised framework of limit equilibrium methods for slope stability analysis. *Géotechnique,* Vol 53, No 4, May, pp 377-395.

Zienkiewicz, O. C. 1971. *The finite element method in engineering science*. 2nd ed. McGraw-Hill, London.

Zlatovic, S. and Ishihara, K. 1997. Normalized behavior of very loose non-plastic soils: effects of fabric. *Soils and Foundations*, Vol 37, No 4, December, pp 47–56.

7 APPENDIX A – DETAILED TRIAXIAL TEST RESULTS

7.1 INTRODUCTION

A series of triaxial compressions tests were conducted at the University of Pretoria on three tailings materials: gold, iron and platinum. Results from triaxial tests conducted by others on the Nerlerk sand (Jefferies & Been, 2015) are also presented for reference. A sieve analysis of the material tested was conducted and the results are shown in Figure 7.1. It can be seen that the gold and platinum tailings classify as a silty sand, the iron tailings as a silt and the Nerlerk sand as a sand. A summary of the key parameters of the tests is shown in Table 7.1.

Table 7.1: Key parameters of the triaxial tests assessed

Test ID	Material	Triaxial test type	Sample preparation method	Initial confining effective stress (p_0)
GCU_75*	Gold tailings	CU	Slurry Deposition	75 kPa
GCU_200*	Gold tailings	CU	Slurry Deposition	200 kPa
GCD_75*	Gold tailings	CD	Slurry Deposition	75 kPa
GCD_200*	Gold tailings	CD	Slurry Deposition	200 kPa
ICU_75*	Iron tailings	CU	Slurry Deposition	75 kPa
ICU_200*	Iron tailings	CU	Slurry Deposition	200 kPa
ICD_75*	Iron tailings	CD	Slurry Deposition	75 kPa
ICD_200*	Iron tailings	CD	Slurry Deposition	200 kPa
PCU_75*	Platinum tailings	CU	Slurry Deposition	75 kPa
PCU_200*	Platinum tailings	CU	Slurry Deposition	200 kPa
PCD_75*	Platinum tailings	CD	Slurry Deposition	75 kPa
PCD_200*	Platinum tailings	CD	Slurry Deposition	200 kPa
NCU_G101**	Nerlerk sand	CU	Moist Tamped	500 kPa
NCU_G108**	Nerlerk sand	CU	Moist Tamped	500 kPa
NCD_G151**	Nerlerk sand	CD	Moist Tamped	200 kPa
NCD_G155**	Nerlerk sand	CD	Moist Tamped	500 kPa

* tested at the University of Pretoria

** data from Jefferies & Been (2015)

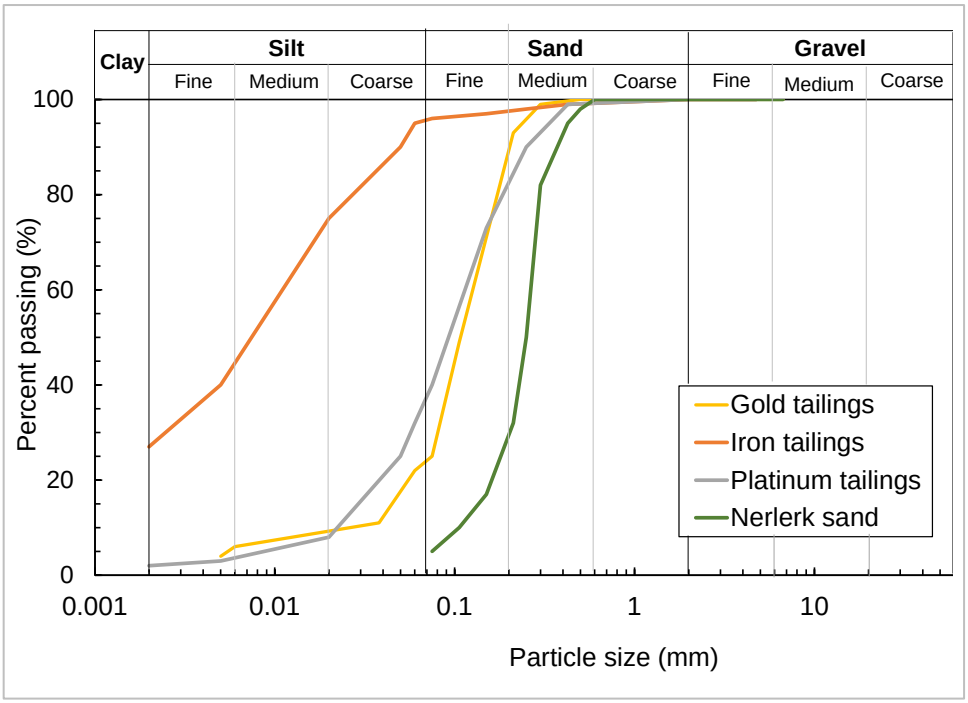

Figure 7.1: Particle size distributions of the materials tested

7.2 GOLD TAILINGS

The stress paths observed during the shear phase of the gold tailings, plotted in p'-q space, are shown in Figure 7.2. It is clear that after initial contraction, the undrained tests dilated to failure. A failure envelope with an M-value of 1.59 is also shown for reference. This M-value represents a friction angle of 39°.

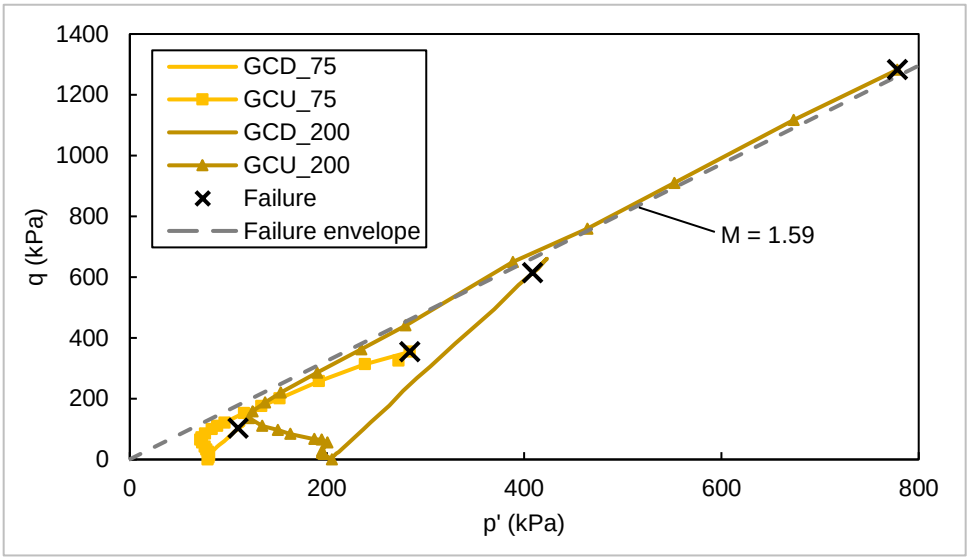

Figure 7.2: Stress paths of the gold tailings

The stress paths observed were also plotted in deviatoric stress versus axial strain space as shown in Figure 7.3a. The failure points are shown with black crosses. For both the CU tests, it appears that there is still a rate of change of excess pore pressure at the end of the test indicating that steady state may not have been reached (see Figure 7.3b). A similar observation can be made regarding the rate of change of volumetric strain at the end of the test for the CD test at 200 kPa (see Figure 7.3c). However, there is an indication that the CD test at 75 kPa may have reached steady state.

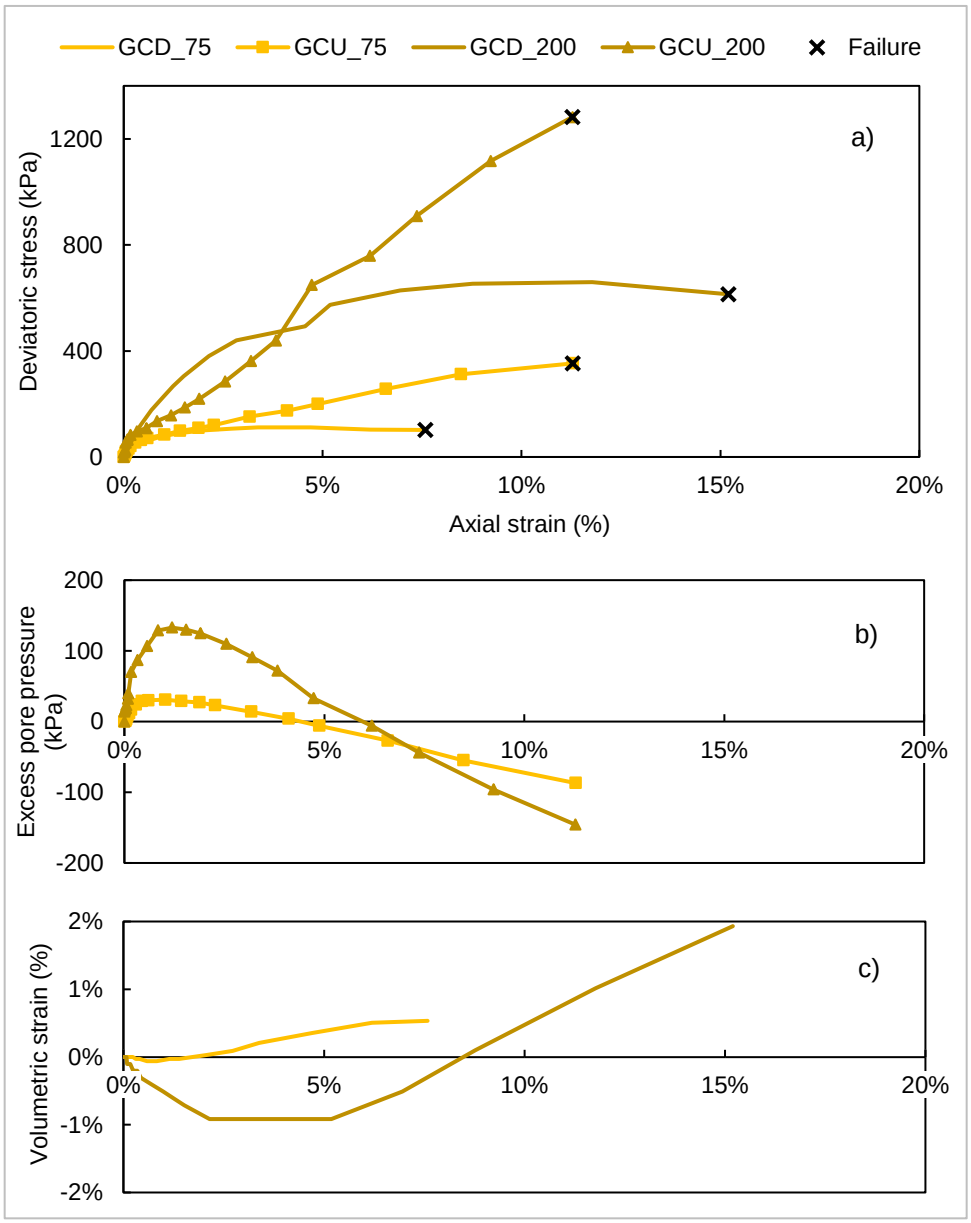

Figure 7.3 Shear phase of the gold tailings showing: a) deviatoric stress, b) excess pore pressure and c) volumetric strain against axial strain

Additional soil parameters were also derived from the triaxial test data. Figure 7.4a shows a plot of

deviatoric stress versus axial strain. The initial tangent modulus was determined as a best fit for the stress-strain curves and a chosen modulus value of 30 000 kPa. It is clear that the modulus value differs depending on drainage condition and stress level. It appears that the modulus increases with stress level and is greater for drained shearing conditions when compared to undrained shearing conditions. Although there is no consistent linear slope in the curves, a value of 30 000 kPa was chosen as a representative value for the gold tailings. The GCD_200 test follows this slope through to 0.3% axial strain and the GCU_75 through to 0.1% axial strain. The GCU_200 is steeper than the chosen value while the GCD_75 is flatter

Figure 7.4b shows a plot of volumetric strain versus axial strain. A dilation angle of 16° could be assigned to the material. Although two different dilations angles could be derived, it was decided that a dilation angle of 0° should be used for the gold tailings as it is believed that it would be more representative of a loose gold tailings sample prone to liquefaction.

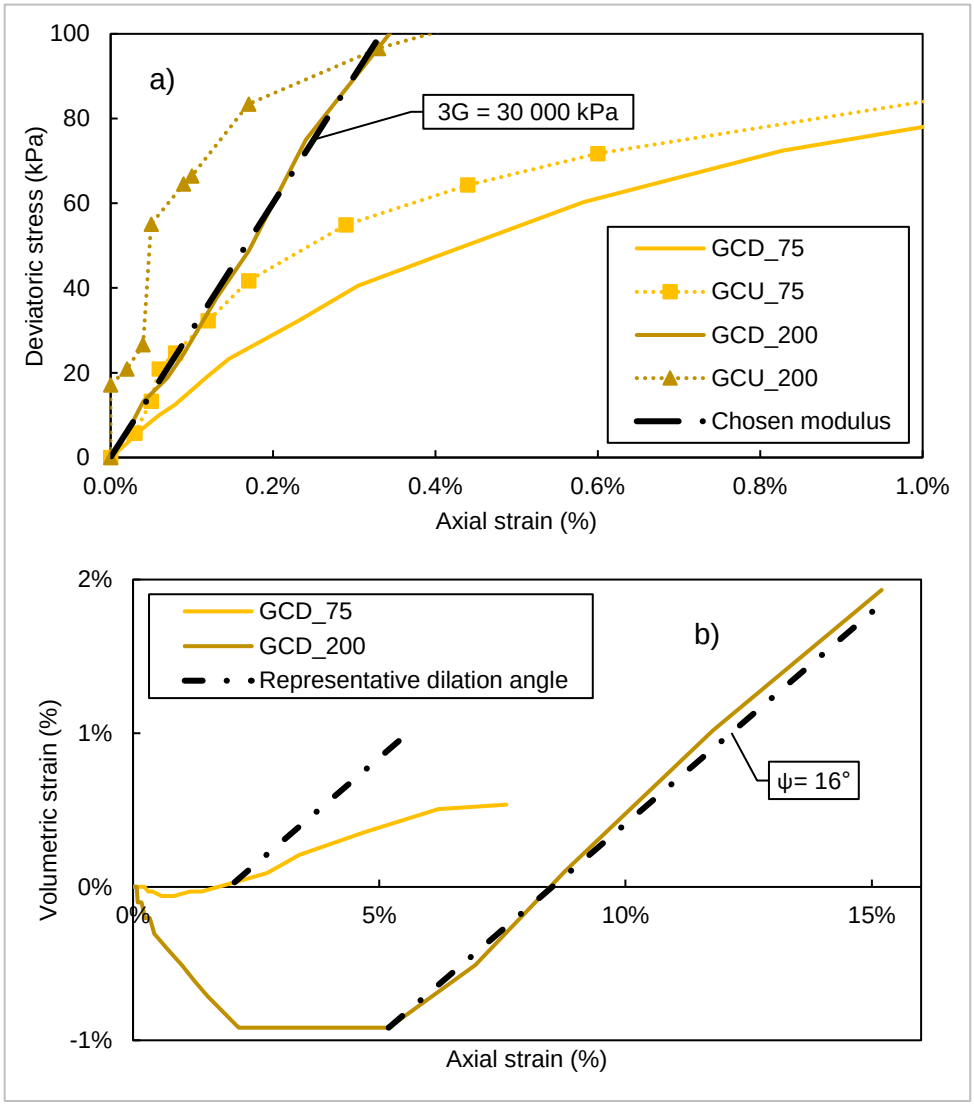

Figure 7.4: Interpreted soil parameters for the gold tailings: a) stiffness modulus and b) dilation angle

7.3 IRON TAILINGS

The stress paths observed during the shear phase of the iron tailings, plotted in p'-q space, are shown in Figure 7.5. It is clear that after initial contraction, the undrained tests dilated to failure. A failure envelope with an M-value of 1.42 is also shown for reference. This M-value represents a friction angle of 35°.

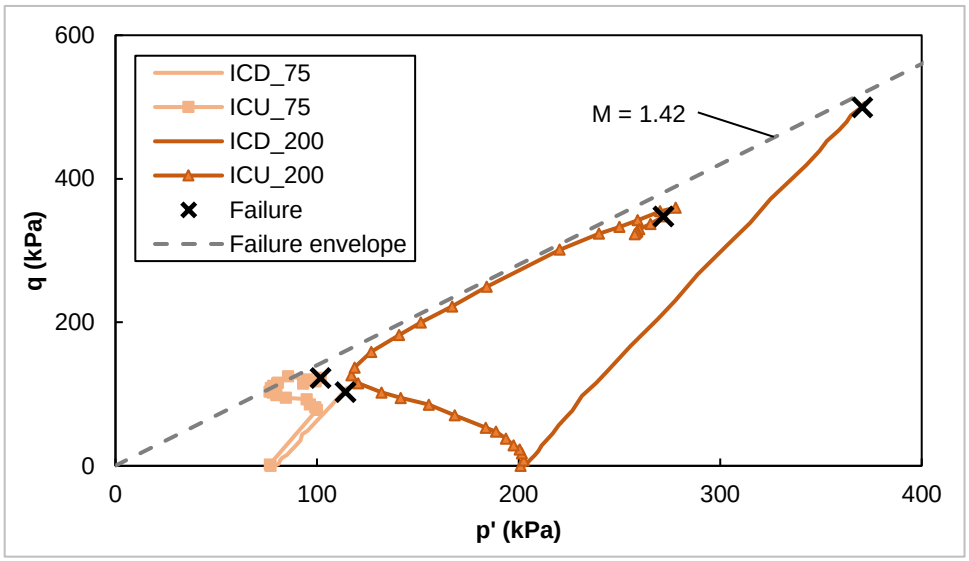

Figure 7.5: Stress paths of the iron tailings

The stress paths observed were also plotted in deviatoric stress versus axial strain space as shown in Figure 7.6a. The failure points are shown with black crosses. For both the CU tests, it appears that there is still a rate of change of excess pore pressure at the end of the test indicating that steady state may not have been reached (see Figure 7.6b). A similar observation can be made regarding the rate of change of volumetric strain at the end of the test for the CD test at 200 kPa (see Figure 7.6c). However, there is an indication that the CD test at 75 kPa may have reached steady state. Note that due to the poor data obtained for the CD test 200 kPa, these results were not plotted.

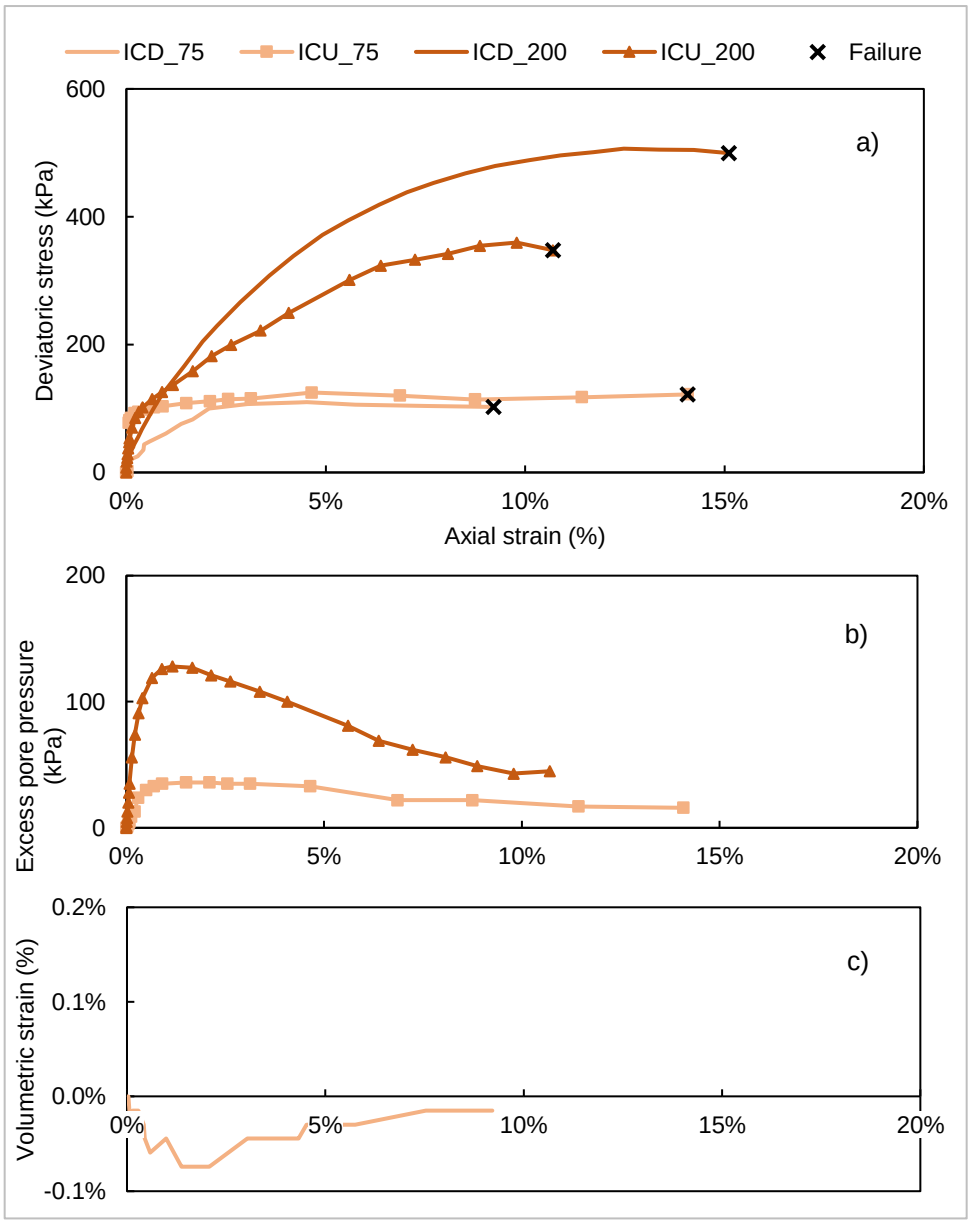

Figure 7.6: Shear phase of the iron tailings showing: a) deviatoric stress, b) excess pore pressure and c) volumetric strain against axial strain

Additional soil parameters were also derived from the triaxial test data. Figure 7.7a shows a plot of deviatoric stress versus axial strain and a chosen modulus value of 40 000 kPa. It is clear that the modulus value differs depending on drainage condition and stress level. It appears that the modulus increases with stress level and is greater for drained shearing conditions when compared to undrained shearing conditions. Figure 7.7b shows a plot of volumetric strain versus axial strain. A dilation angle of 0.4° could be assigned to the material. However, it was decided that a dilation angle of 0° should be used as a conservative approach.

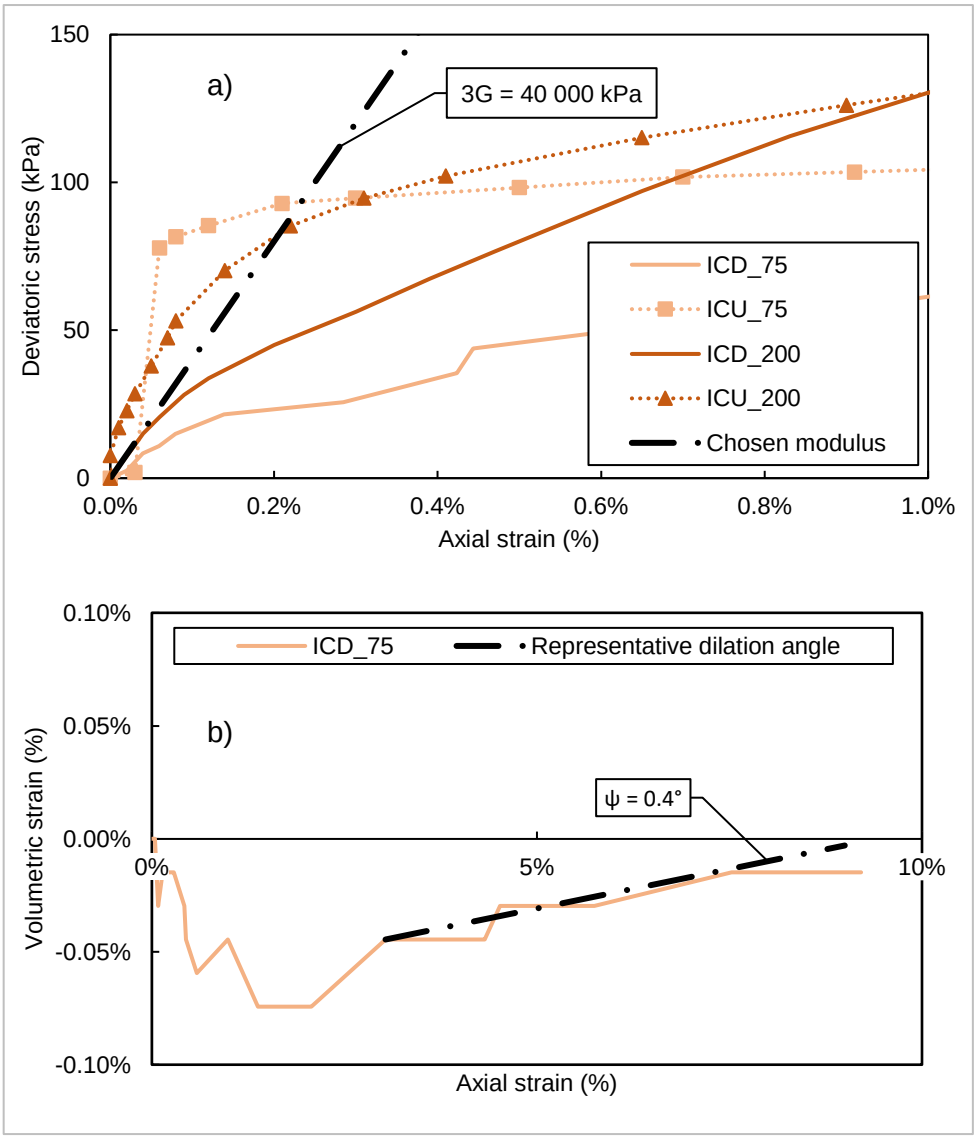

Figure 7.7: Interpreted soil parameters for the iron tailings: a) stiffness modulus and b) dilation angle

7.4 PLATINUM TAILINGS

The stress paths observed during the shear phase of the platinum tailings, plotted in p'-q space, are shown in Figure 7.8. It is clear that after initial contraction, the undrained tests dilated to failure. A failure envelope with an M-value of 1.55 is also shown for reference. This M-value represents a friction angle of 38°.

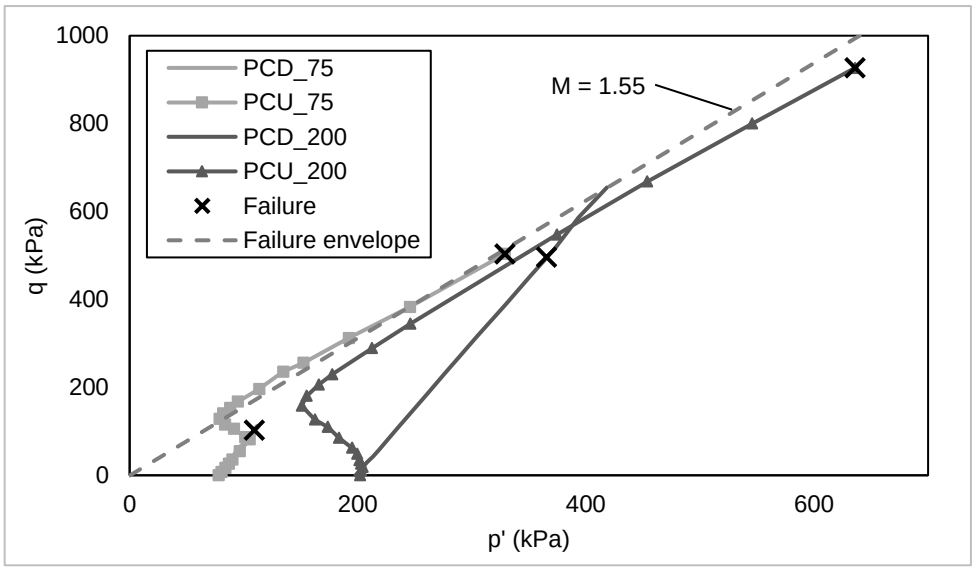

Figure 7.8: Stress paths of the platinum tailings

The stress paths observed were also plotted in deviatoric stress versus axial strain space as shown in Figure 7.9a. The failure points are shown with black crosses. For both the CU tests, it does appear that there is still a rate of change of excess pore pressure at the end of the test indicating that steady state may not have been reached (see Figure 7.9b). A similar observation can be made regarding the rate of change of volumetric strain at the end of the test for the CD test at 200 kPa (see Figure 7.9c). However, there is an indication that the CD test at 75 kPa may have reached steady state.

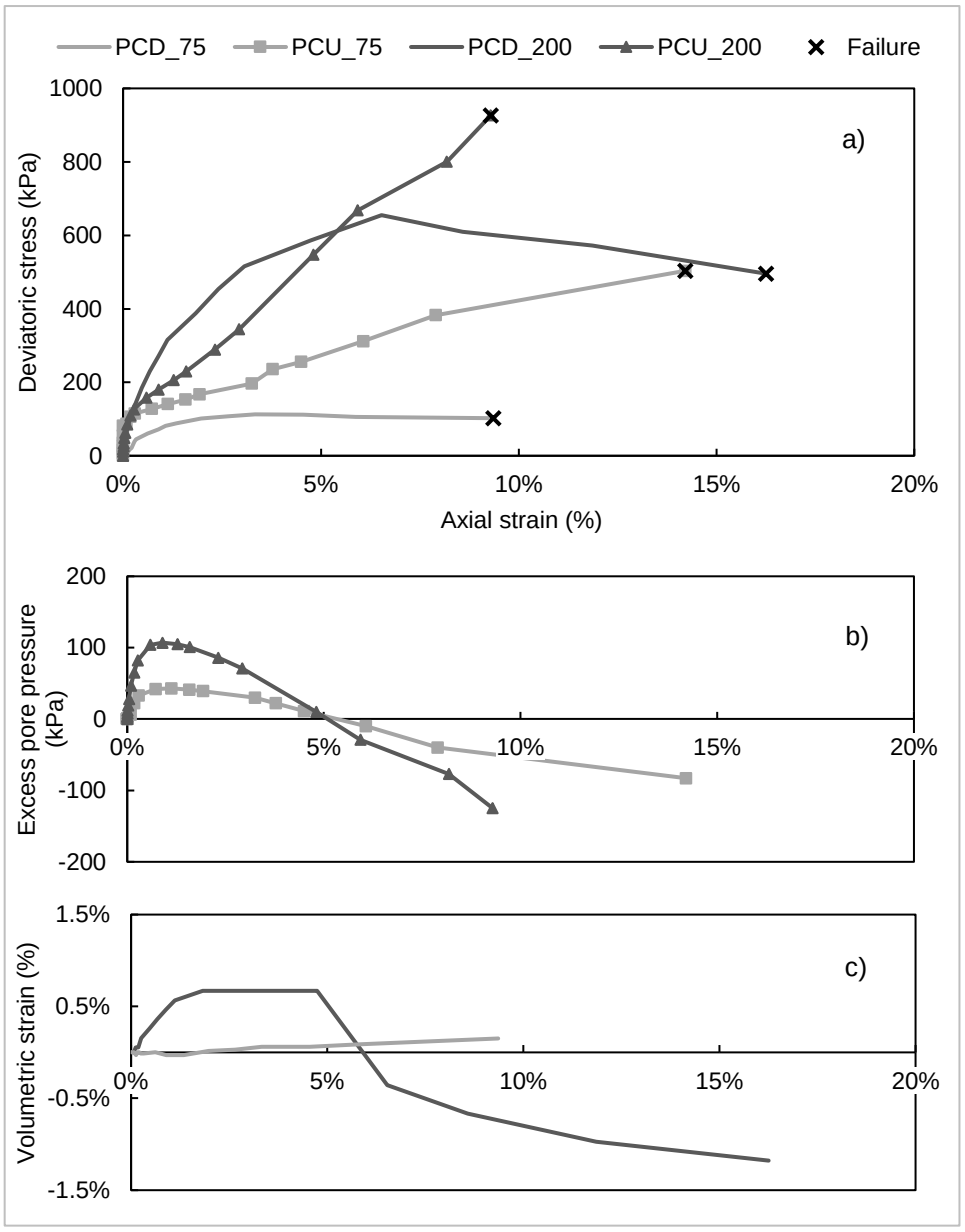

Figure 7.9: Shear phase of the platinum tailings showing: a) deviatoric stress, b) excess pore pressure and c) volumetric strain against axial strain

Additional soil parameters were also derived from the triaxial test data. Figure 7.10a shows a plot of deviatoric stress versus axial strain and a chosen modulus value of 75 000 kPa. It is clear that the modulus value differs depending on drainage condition and stress level. It appears that the modulus increases with stress level and is greater for drained shearing conditions when compared to undrained shearing conditions. Figure 7.10b shows a plot of volumetric strain versus axial strain. A dilation angle of 1.0° could be assigned to the material. However, it was decided that a dilation angle of 0° should be used as a conservative approach.

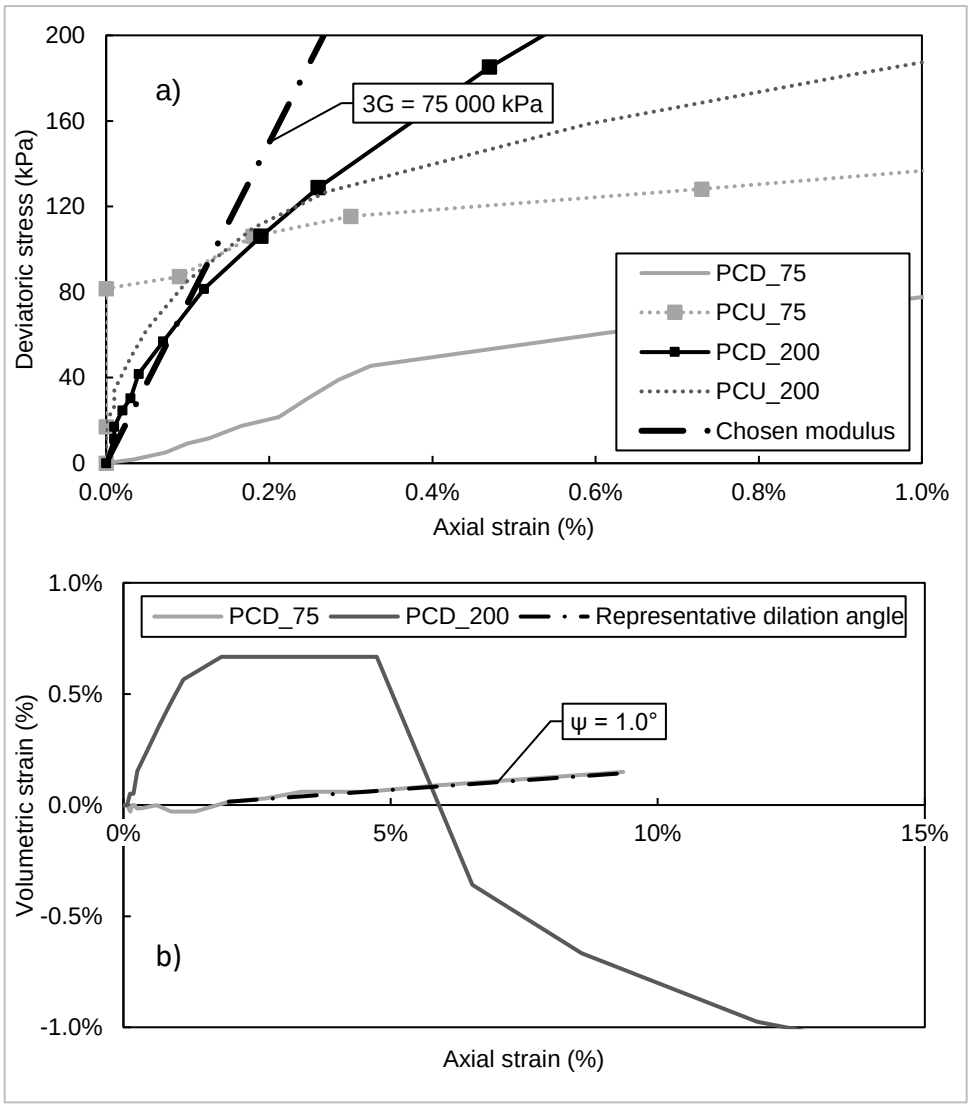

Figure 7.10 Interpreted soil parameters for the platinum tailings: a) stiffness modulus and b) dilation angle

7.5 NERLERK SAND

The stress paths observed during the shear phase of the iron tailings, plotted in p'-q space, are shown in Figure 7.11. It is clear that after initial contraction, the undrained tests dilated to failure. A failure envelope with an M-value of 1.39 is also shown for reference. This M-value represents a friction angle of 34.4°.

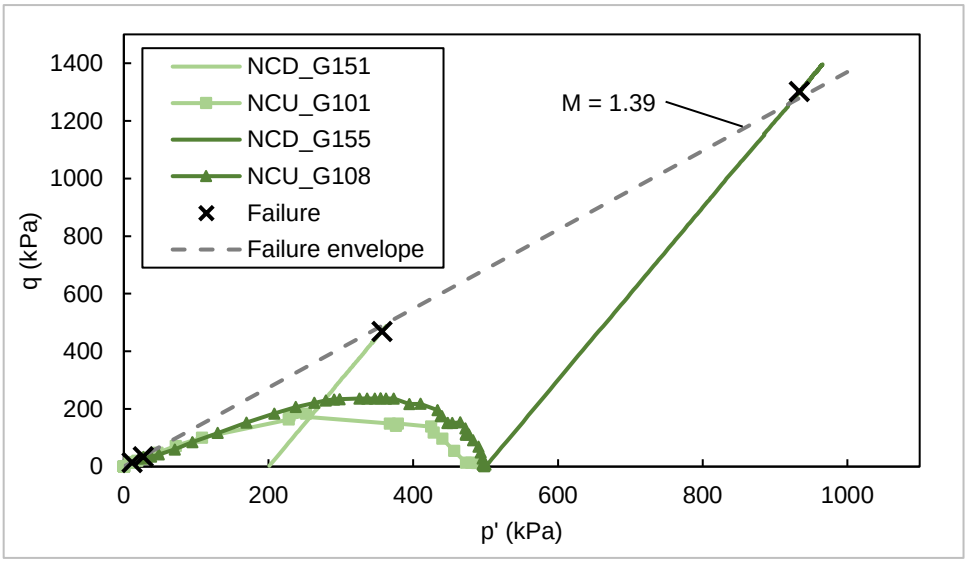

Figure 7.11: Stress paths of the Nerlerk sand

The stress paths observed were also plotted in deviatoric stress versus axial strain space as shown in Figure 7.12a. The failure points are shown with black crosses. For both the CU tests, it appears that there is no rate of change of excess pore pressure at the end of the test indicating that steady state may have been reached (see Figure 7.12b). A similar observation can be made regarding the rate of change of volumetric strain at the end of the test for the NCD_G154 test (see Figure 7.12c). However, there is an indication that the NCD_G155 test may not have reached steady state.

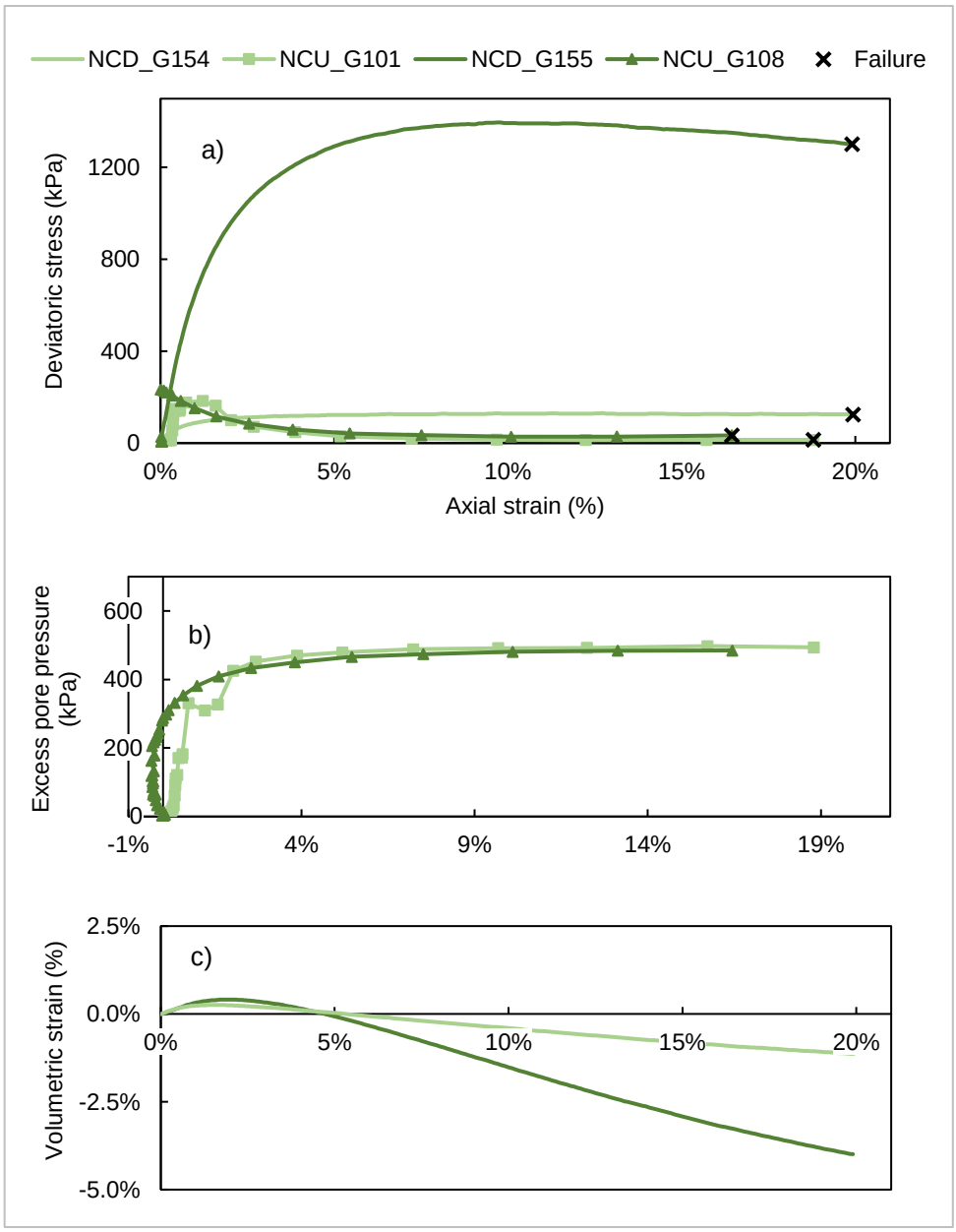

Figure 7.12: Shear phase of the Nerlerk sand showing: a) deviatoric stress, b) excess pore pressure and c) volumetric strain against axial strain

Additional soil parameters were also derived from the triaxial test data. Figure 7.13a shows a plot of deviatoric stress versus axial strain and a chosen modulus value of 30 000 kPa. It is clear that the modulus value differs depending on drainage condition and stress level. It appears that the modulus increases with stress level and is greater for drained shearing conditions when compared to undrained shearing conditions. Figure 7.13b shows a plot of volumetric strain versus axial strain. As the samples did not dilate during drained shearing, no dilation angle could be assigned.

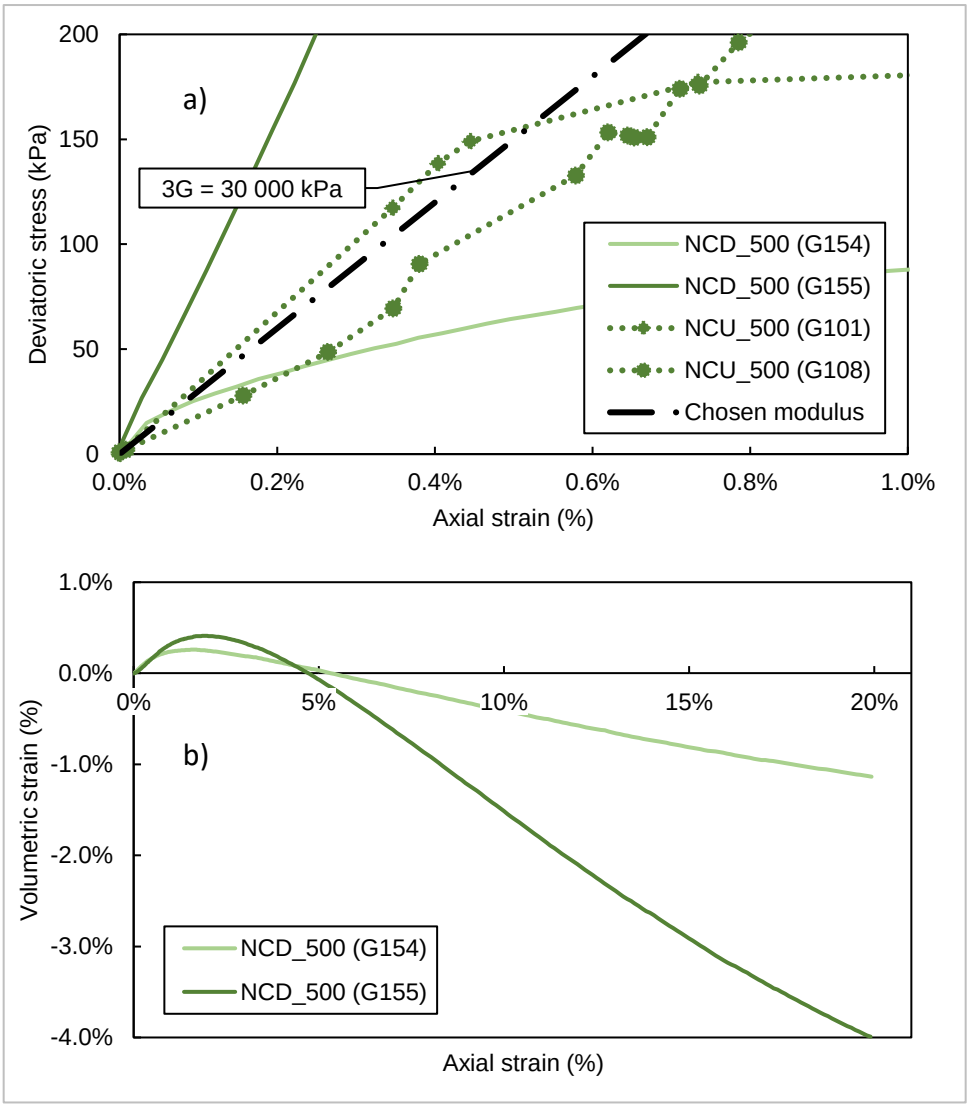

Figure 7.13: Interpreted soil parameters for the Nerlerk sand: a) stiffness modulus and b) dilation angle

7.6 SUMMARY

Results from a series of triaxial compression tests conducted on four materials were presented. Three materials (the gold, iron and platinum tailings) were tested at the University of Pretoria and the fourth material was obtained from others (Jefferies & Been, 2015). Stress paths were plotted and the soil parameters shown in Table 7.2 were interpreted for use in the study.

Table 7.2: Key interpreted soil parameters

	φ' (°)	c' (kPa)	E' (MPa)	Ψ (°)	Yield strain (CU)	Failure strain (CD)
Gold tailings	39	0	26 000	0	1.19%	11.8%
Iron tailings	35	0	34 667	0	0.90%	13.4%
Platinum tailings	38	0	65 000	0	0.90%	6.53%
Nerlerk sand	34.4	0	26 000	0	1.03%	19.9%

8 APPENDIX B – INTERPRETING AXIAL AND SHEAR STRAINS FROM THE TRIAXIAL TEST DATA

8.1 INTRODUCTION

During the study, several assumptions were made regarding axial strains measured in the triaxial test and interpreted shear strains. The intent of this Appendix is to provide some background to these assumptions and motivate why they were made in the study.

8.2 AXIAL AND SHEAR STRAINS

Axial strains were measured during the shearing phase of the triaxial tests conducted. However, shear strains were required for the analysis. Therefore, a relationship between axial strains and shear strains was required. This was done by considering the amount of work required to shear a triaxial specimen. The relationship can be written in the form of Equation (8.1) (Lade, 2016).

$$dW = \sigma_1 . d\varepsilon_1 + \sigma_2 . d\varepsilon_2 + \sigma_3 . d\varepsilon_3 \quad (8.1)$$

Under axis-symmetrical conditions, such as those in a triaxial, cell $\sigma_2 = \sigma_3$ and $d\varepsilon_2 = d\varepsilon_3$. Therefore, Equation (8.1) can be simplified to Equation (8.2).

$$\varepsilon_s = \frac{2}{3}(\varepsilon_1 - \varepsilon_3) \quad (8.2)$$

Volumetric strain is the sum of the axial strain in three dimensions as shown in Equation (8.3).

$$\varepsilon_v = \varepsilon_1 + \varepsilon_2 + \varepsilon_3 \quad (8.3)$$

Since $\varepsilon_2 = \varepsilon_3$ in a triaxial cell, Equation (8.3) reduces to Equation (8.4).

$$\varepsilon_v = \varepsilon_1 + 2 * \varepsilon_3 \quad (8.4)$$

8.2.1 Consolidated undrained triaxial compression tests

In undrained shearing, $\varepsilon_v = 0$ and in a triaxial cell $\varepsilon_1 = \varepsilon_a$. By substituting Equation (8.2) into Equation (8.4), Equation (8.5) can be derived. This implies that in an undrained triaxial compression test the axial strains measured are numerically equivalent to the shear strains mobilised in the sample.

$$\varepsilon_s = \varepsilon_{\mathrm{a}} \tag{8.5}$$

8.2.2 Consolidated drained triaxial compression tests

In drained shearing, $\varepsilon_v \neq 0$. However, ε_1 can still be linked to ε_3 using Poisson's ratio (v) as shown in Equation (8.6).

$$\varepsilon_3 = v.\varepsilon_1 \tag{8.6}$$

Substituting Equation (8.6) into Equation (8.2) results in Equation (8.7). This implies that in a drained triaxial compression test the axial strains measured are not necessarily numerically equivalent to the shear strains mobilised in the sample.

$$\varepsilon_s = \frac{2}{3}.\varepsilon_a(1+v) \tag{8.7}$$

For a Poisson's ratio of 0.3, the shear strains in a consolidated drained triaxial test are numerically equivalent to 0.87 times the axial strains as shown by Equation (8.8). This changes to 0.99 times the axial strains for a Poisson's ratio of 0.49 as shown in Equation (8.9). Therefore, by assuming that the shear strains are equal to the axial strain in a consolidated drain triaxial test, there is a liner error of approximately 13% for a Poisson's ratio of 0.3.

$$\varepsilon_s = 0.87.\varepsilon_{\mathrm{a}} \qquad Assuming\ v = 0.3 \tag{8.8}$$

$$\varepsilon_s = 0.99.\varepsilon_{\mathrm{a}} \qquad Assuming\ v = 0.49 \tag{8.9}$$

8.3 SUMMARY

By using elastic theory and comparing the relationships between volumetric strain and shear strain, it has been shown that the axial strains measured during the shear phase of a consolidated undrained triaxial test are numerically equal to the shear strains. It was also shown that the axial strains measured during the shear phase of a consolidated drained triaxial test are not equal to the shear strains. Rather, the shear strains are related to the axial strains through the Poisson's ratio of the material. For a Poisson's ratio of 0.3, the shear strains in a consolidated drained triaxial test are numerically equivalent to 0.87 times the axial strains. Therefore, by assuming that the shear strains are equal to the axial strain in a consolidated drain triaxial test, there is a liner error of approximately 13% for a Poisson's ratio of 0.3.

9 APPENDIX C –SPREADSHEET TO CALCULATE FOS FOR A DEFINED SLIP SURFACE

9.1 INTRODUCTION

A Microsoft Excel spreadsheet was developed to calculate the FoS against failure of a defined slip surface based on Bishop's, Janbu's and Spencer's methods. The spreadsheet was validated by verifying the output calculated FoS values against the results from a commercial software package.

9.2 VERIFICATION OF SPREADSHEET

Before the spreadsheet could be used for analysis, it needed to be verified. It was decided that the FoS values determined from the spreadsheet would be compared to the FoS values determined from the SLOPE/W module of the commercial software package GeoStudio 2020. To ensure the spreadsheet was sufficiently robust, a variety of material strength models, pore pressure conditions, material zone and FoS limit equilibrium methods were used. A hypothetical 20 m high embankment with a 1(v):3(h) slope was created in SLOPE/W with several material zones and phreatic surface locations (see Figure 9.1).

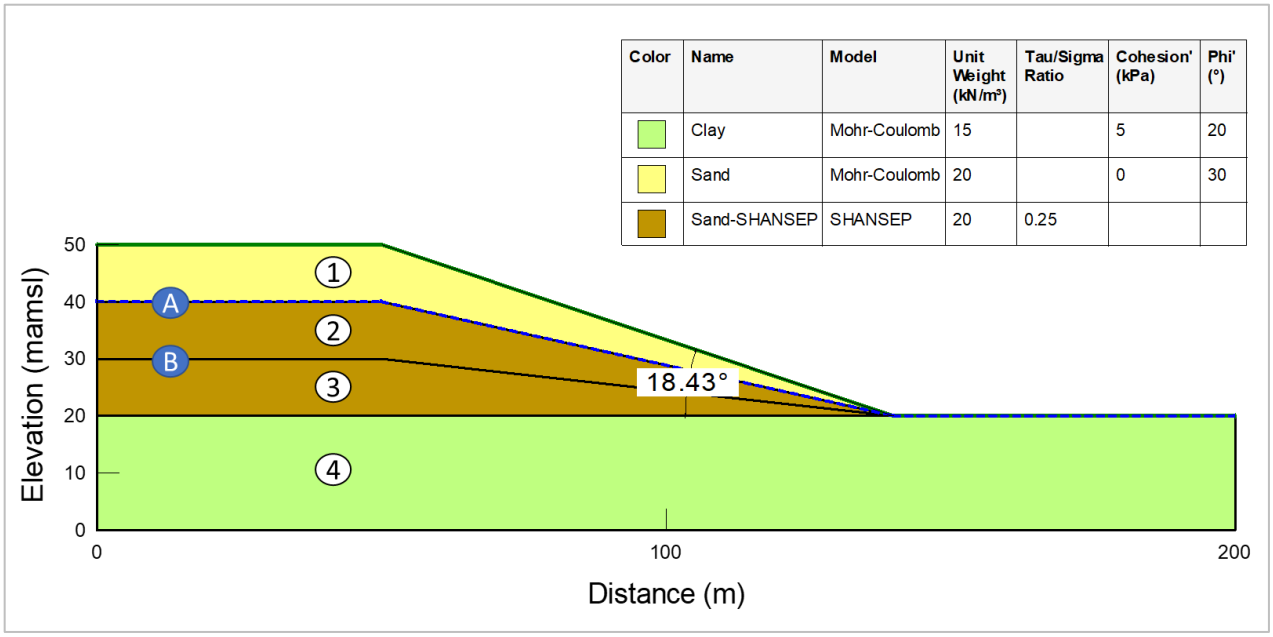

Figure 9.1: Model used for spreadsheet verification

A summary of the scenarios assessed is shown in Table 9.1

Table 9.1: Scenarios assessed as part of the spreadsheet verification

Scenario		Material zone				Phreatic surface	FoS Method
ID	Ref	1	2	3	4	None, A or B	
1	2a	Sand	Sand	Sand	Clay	None	Spencer
2	2b	Sand	Sand	Sand	Clay	B	Spencer
3	2c	Sand	Sand	Sand	Clay	A	Spencer
4	2ci	Sand	Sand	Sand	Clay	A	Bishop
5	2cii	Sand	Sand	Sand	Clay	A	Janbu
6	3a	Sand	Sand	Sand	Sand	None	Spencer
7	3b	Sand	Sand	Sand*	Clay	B	Spencer
8	3c	Sand	Sand*	Sand*	Clay	A	Spencer
9	3ci	Sand	Sand*	Sand*	Clay	A	Bishop
10	3cii	Sand	Sand*	Sand*	Clay	A	Janbu

* SHANSEP strength model used.

Figure 9.2 shows the FoS determined from GeoStudio compared to the FoS determined from the spreadsheet. With an R-squared value of 0.99, the spreadsheet was considered to be able to correctly interpret the geometric output from SLOPE/W and calculate the FoS according to Bishop's, Janbu's and Spencer's methods.

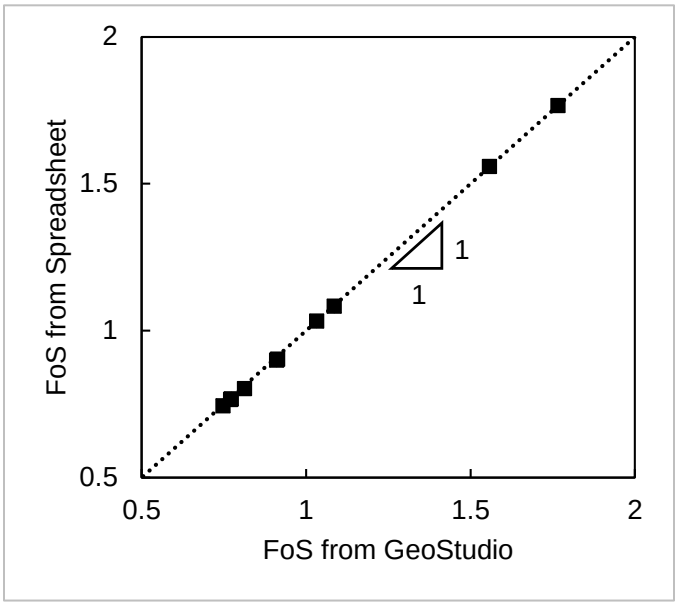

Figure 9.2: Correlation between FoS values obtained from GeoStudio and the spreadsheet

9.3 SUMMARY

As part of the study, a method was required to interpret the geometric properties of a critical slip surface provided by a commercial software package (SLOPE/W) and re-assess a calculated FoS for various strength inputs. A spreadsheet was developed and was verified against results from SLOPE/W. It was shown that the spreadsheet was able to calculate FoS values comparable to the calculated FoS values from SLOPE/W with an R-squared value of 0.99. The spreadsheet was therefore deemed able to correctly interpret the geometric output from SLOPE/W.

10 APPENDIX D – DETAILED RESULTS FROM GEOSTUDIO

10.1 INTRODUCTION

Analyses were conducted using the SLOPE/W and SIGMA/W modules of the GeoStudio 2020 software package. Three types of analyses were conducted: Effective Stress Analysis (ESA) using limit equilibrium methods; Undrained Strength Analysis (USA) using limit equilibrium methods, and Finite Element Analysis (FEA) using the Strength Reduction Method. The analyses were conducted for three cross sections and for each cross section four materials were assessed. The results were obtained as a Factor of Safety (FoS) for the ESA and USA analyses and a (SF) for the FEA analysis. Both these values represent the ratio of the forces resisting failure to the forces causing failure.

10.2 CROSS SECTION A

Cross Section A is a uniform 30 m high embankment at a slope of 1(v):3(h) and is shown in Figure 10.1. Two material zones were identified: one above the phreatic surface and another below the phreatic surface.

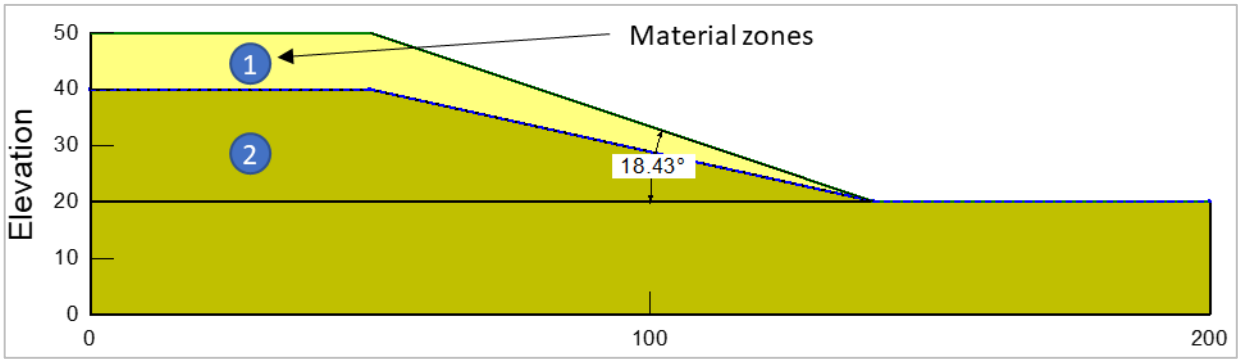

Figure 10.1: Material zones for Cross Section A

Results of the analyses conducted for Cross Section A are shown in Figure 10.2, Figure 10.3, Figure 10.4, and Figure 10.5 for the gold tailings, iron tailings, platinum tailings and Nerlerk sand respectively. As a plastic soil model was used, it is possible to display the elements that have yielded and reached a plastic state within the modelling software. If these elements were continuous from the crest of the slope to the toe of the slope when a FoS of 1.00 was calculated, it was determined that a shear band had developed. For Cross Section A, a clearly defined shear band did develop and the two solid arcs in the figures represent the bounds within which the shear band developed. A summary of the results is shown in Table 10.1.

Table 10.1: Summary of results for Cross Section A

	FoS (ESA)	FoS (USA)	SF (FEA)
Gold tailings	1.94	0.97	1.80
Iron tailings	1.68	0.85	1.65
Platinum tailings	1.87	1.12	1.74
Nerlerk sand	1.64	0.70	1.51

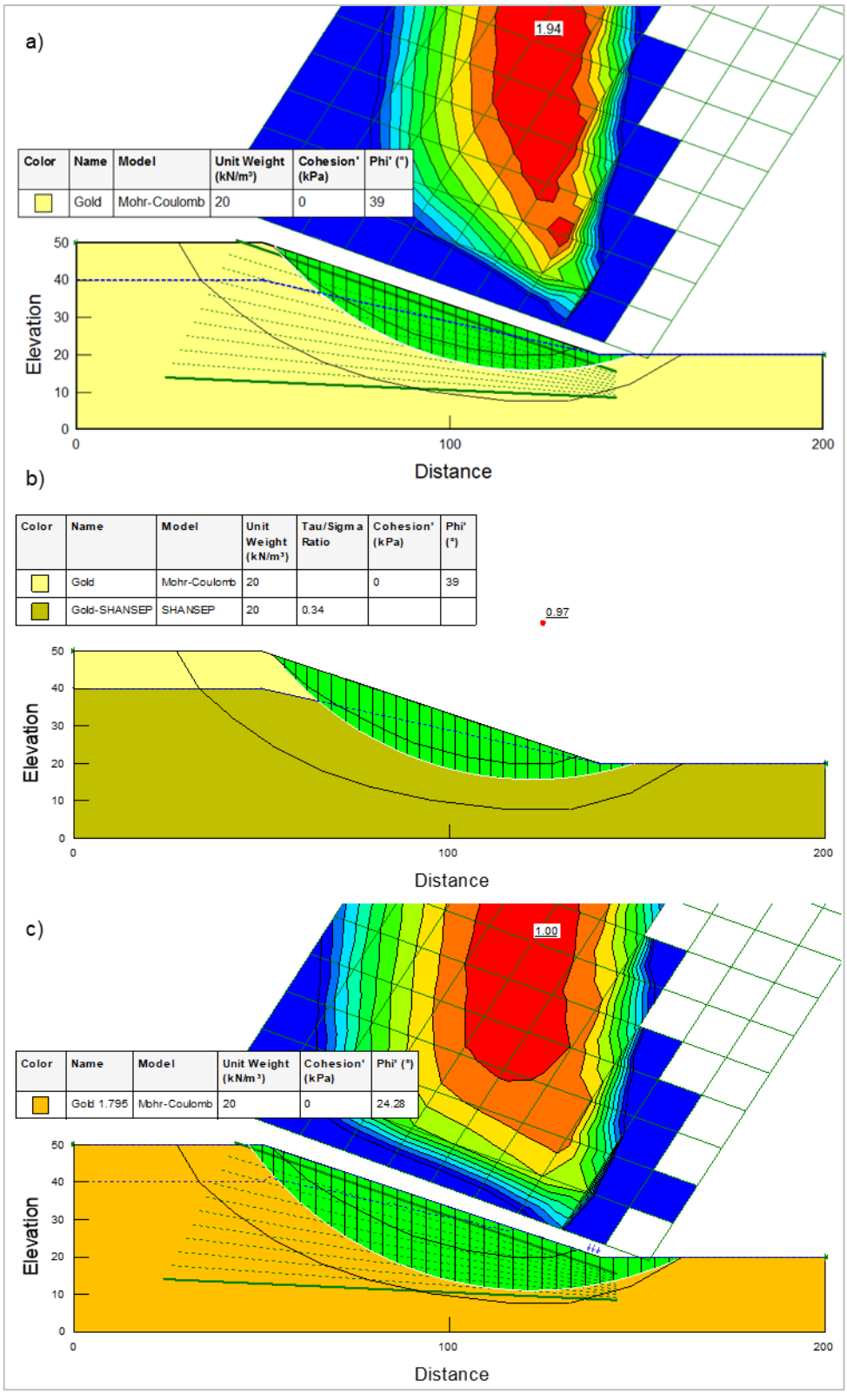

Figure 10.2:Results for the gold tailings for Cross Section A: a) ESA, b) USA, c) FEA

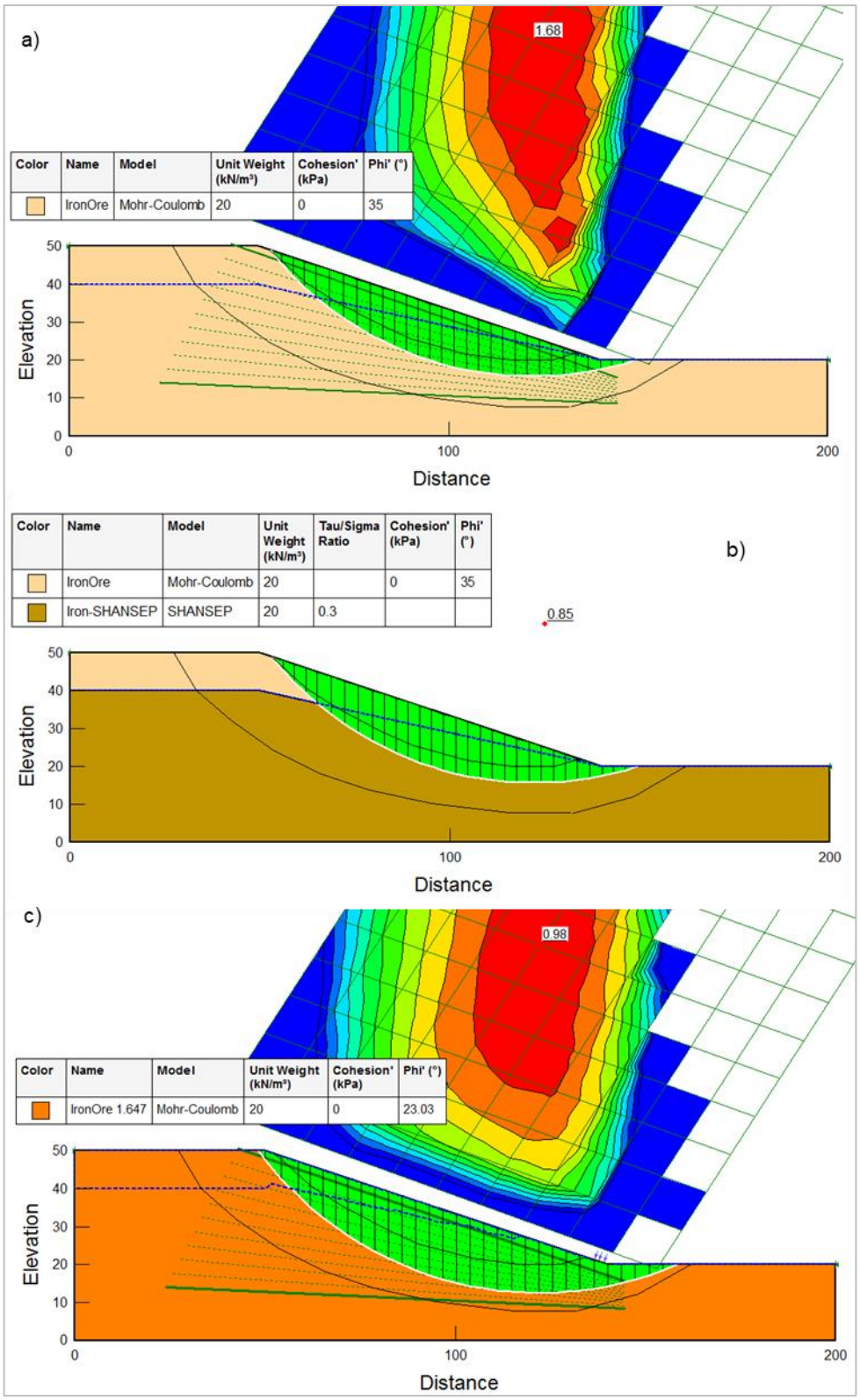

Figure 10.3: Results for the iron tailings for Cross Section A: a) ESA, b) USA, c) FEA

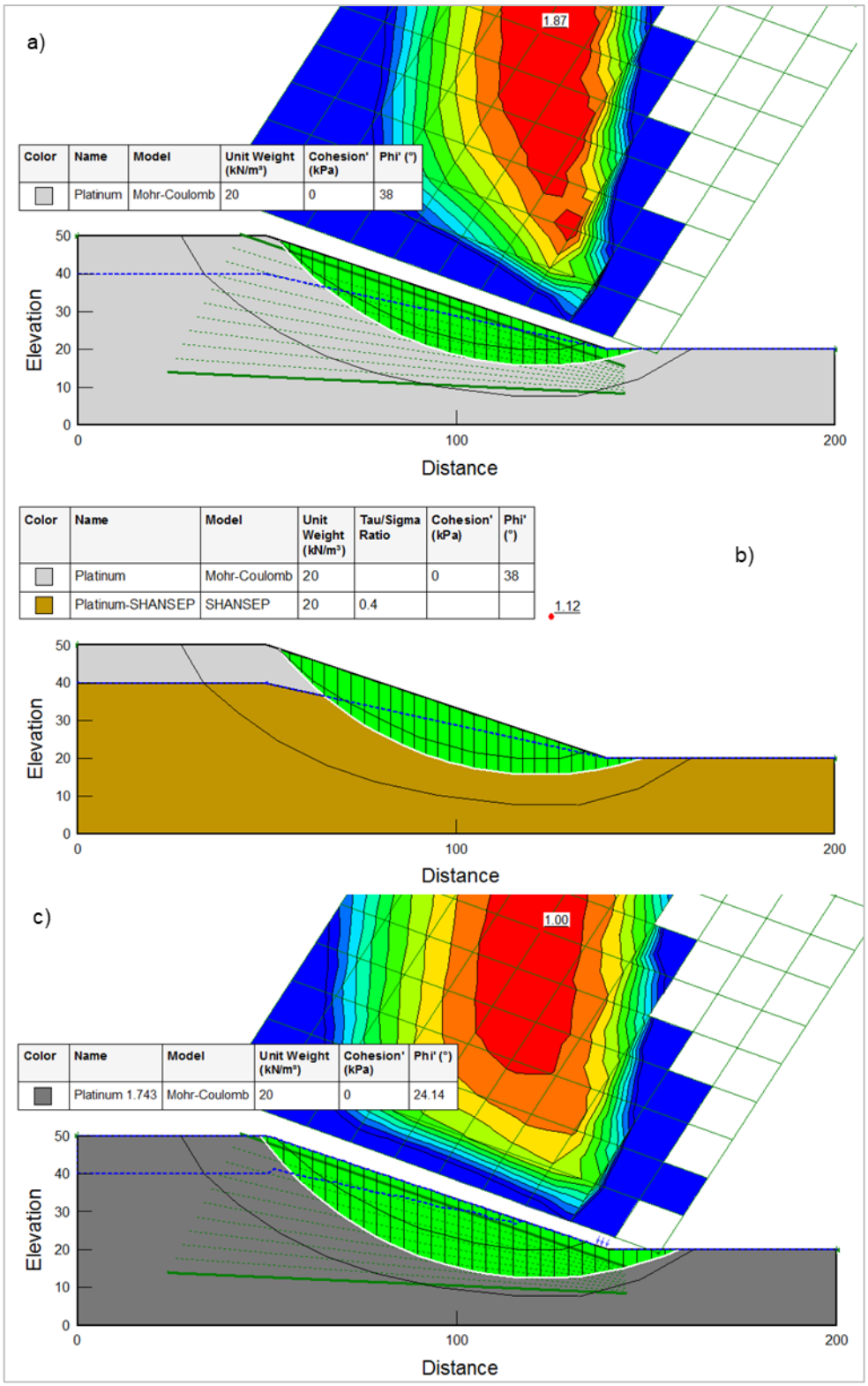

Figure 10.4: Results for the platinum tailings for Cross Section A: a) ESA, b) USA, c) FEA

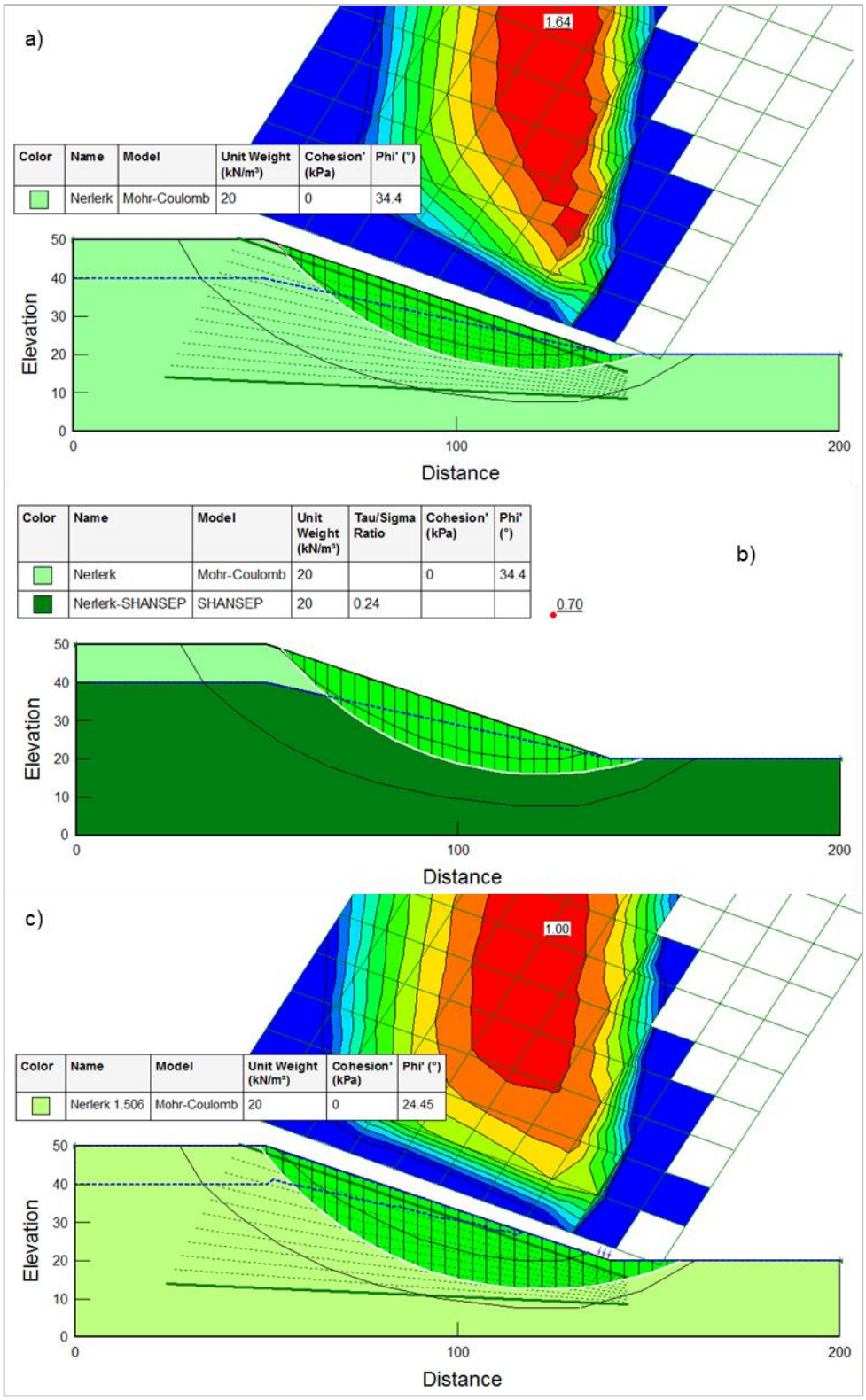

Figure 10.5: Results for the Nerlerk sand for Cross Section A: a) ESA, b) USA, c) FEA

10.3 CROSS SECTION B

The second cross section (Cross Section B) is of a hypothetical tailings dam as shown in Figure 10.6. The tailings dam is 30 m high, there is a 5 m high compacted starter wall at the toe and there are two 9 m wide benches with 9 m high intermediate slopes at 1(v):1.5(h) resulting in an overall effective slope of 1(v):2.3(h). These are typical parameters observed on tailings dams in South Africa although the trend is to move towards flatter slopes approaching 1(v):3(h). Three material zones were identified: one for the foundation material, one for the zone below the phreatic surface and one for the starter wall and zone above the phreatic surface.

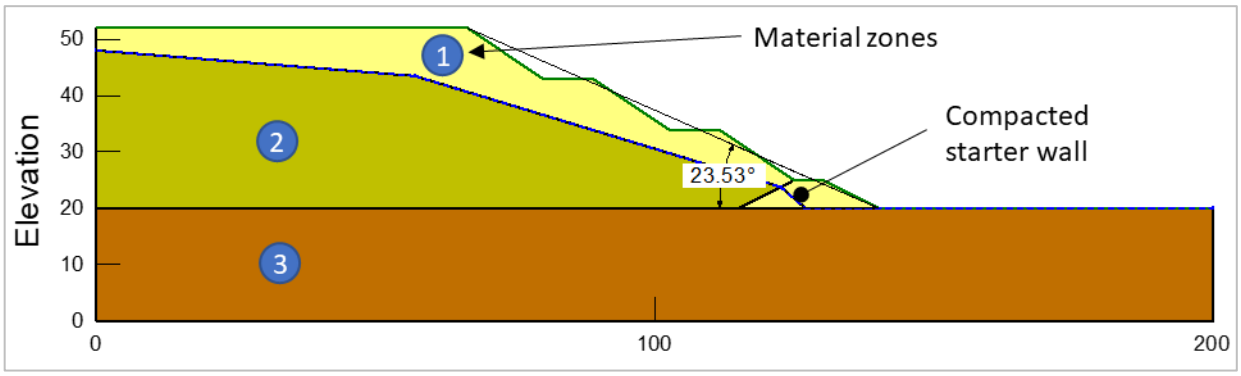

Figure 10.6: Material zones for Cross Section B

Results of the analyses conducted for Cross Section B are shown in Figure 10.7, Figure 10.8, Figure 10.9, and Figure 10.10 for the gold tailings, iron tailings, platinum tailings and Nerlerk sand respectively. A summary of the results is shown in Table 10.2.

Table 10.2: Summary of results for Cross Section B

	FoS (ESA)	FoS (USA)	SF (FEA)
Gold tailings	1.83	1.27	2.17
Iron tailings	1.58	1.11	2.05
Platinum tailings	1.77	1.35	2.17
Nerlerk sand	1.55	0.99	1.82

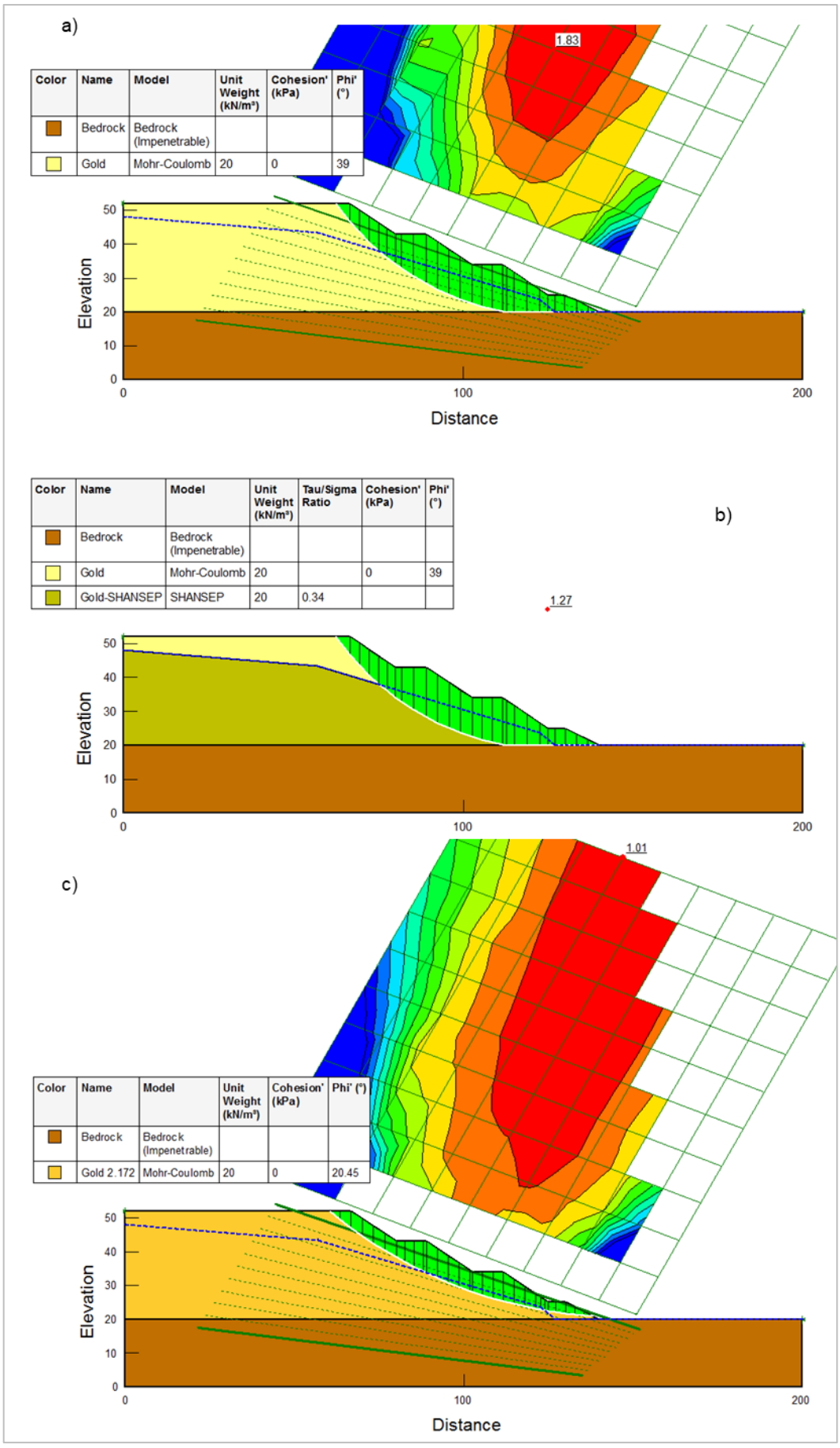

Figure 10.7: Results for the gold tailings on Cross Section B: a) ESA, b) USA, c) FEA

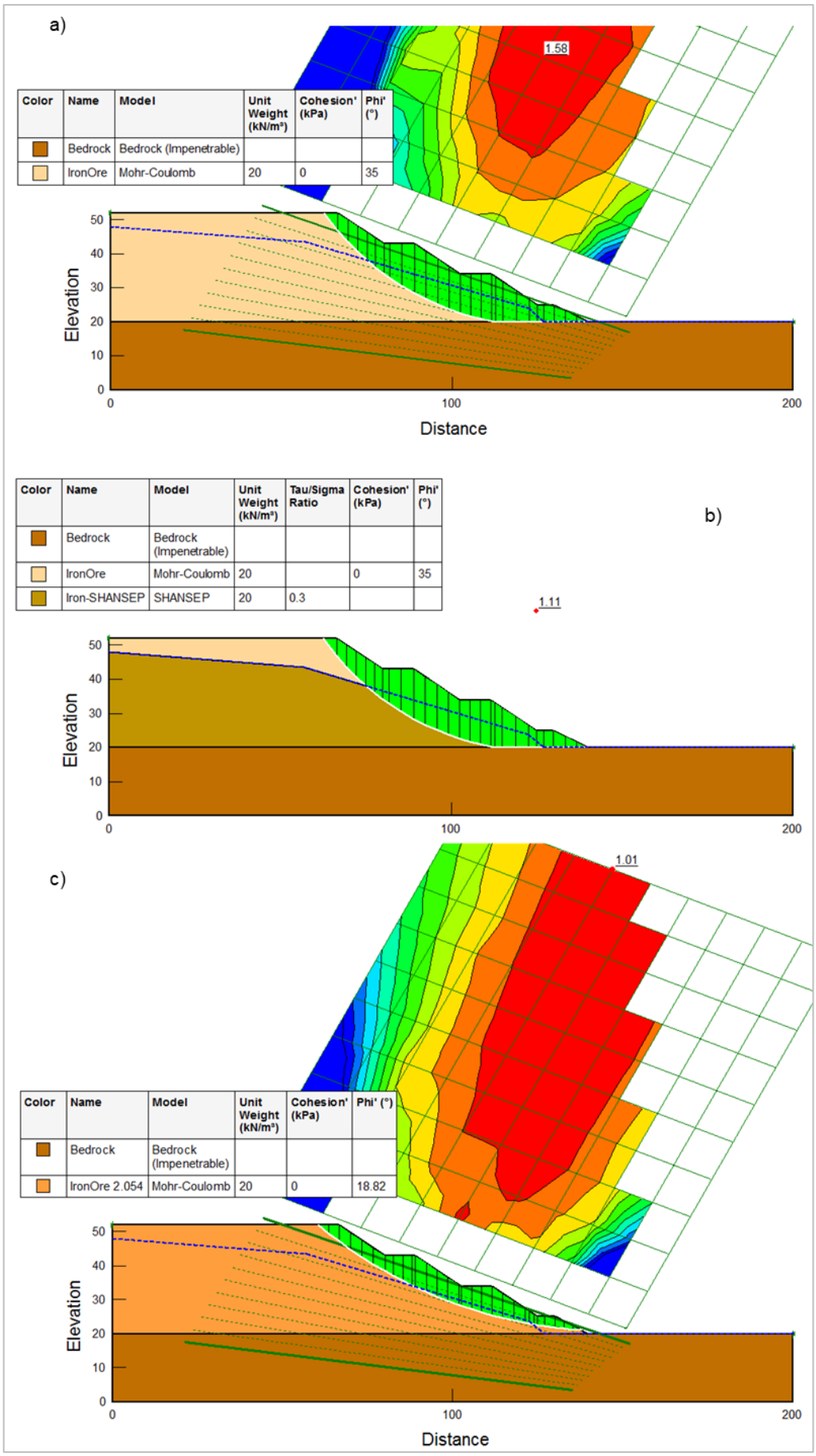

Figure 10.8: Results for the iron tailings on Cross Section B: a) ESA, b) USA, c) FEA

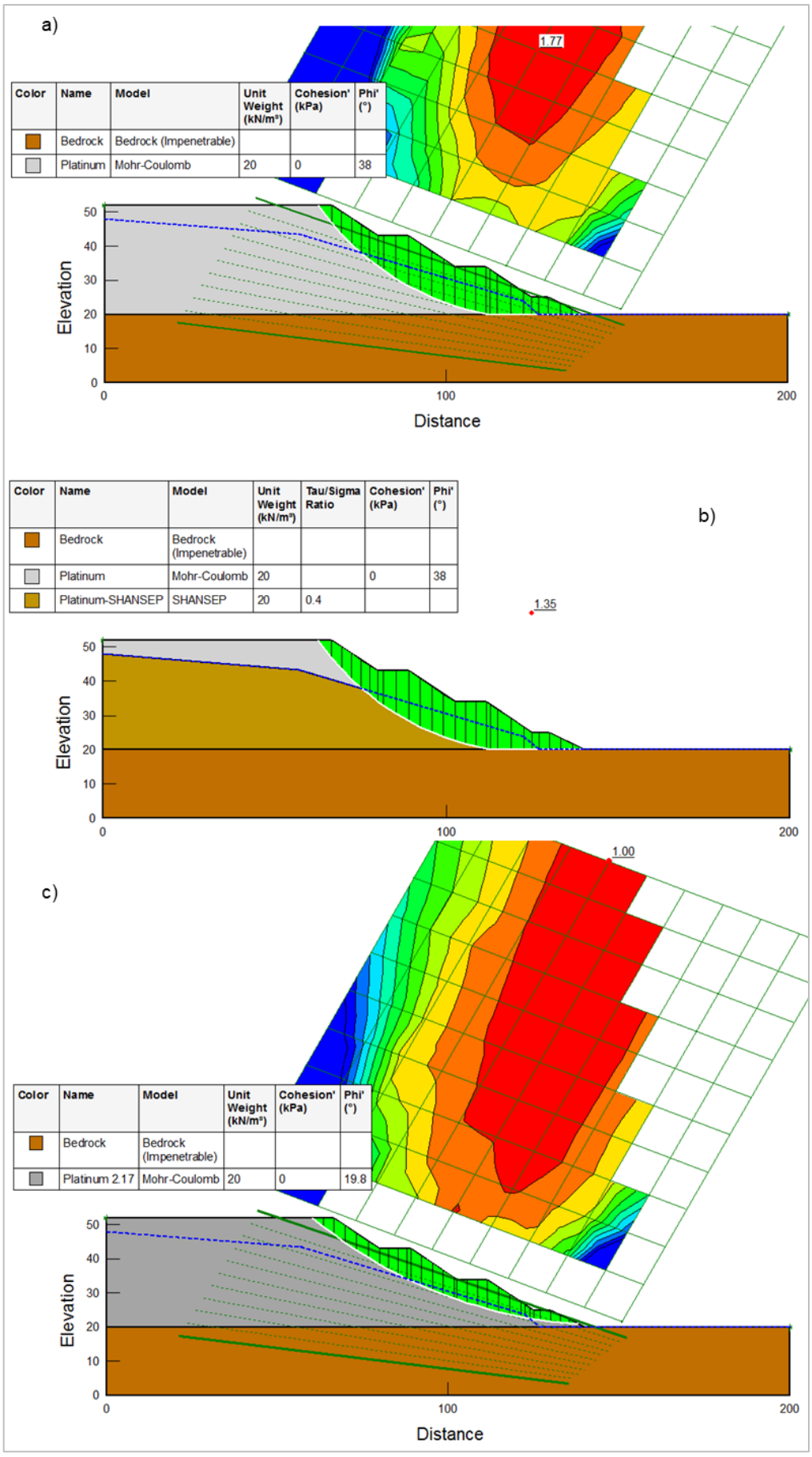

Figure 10.9: Results for the platinum tailings on Cross Section B: a) ESA, b) USA, c) FEA

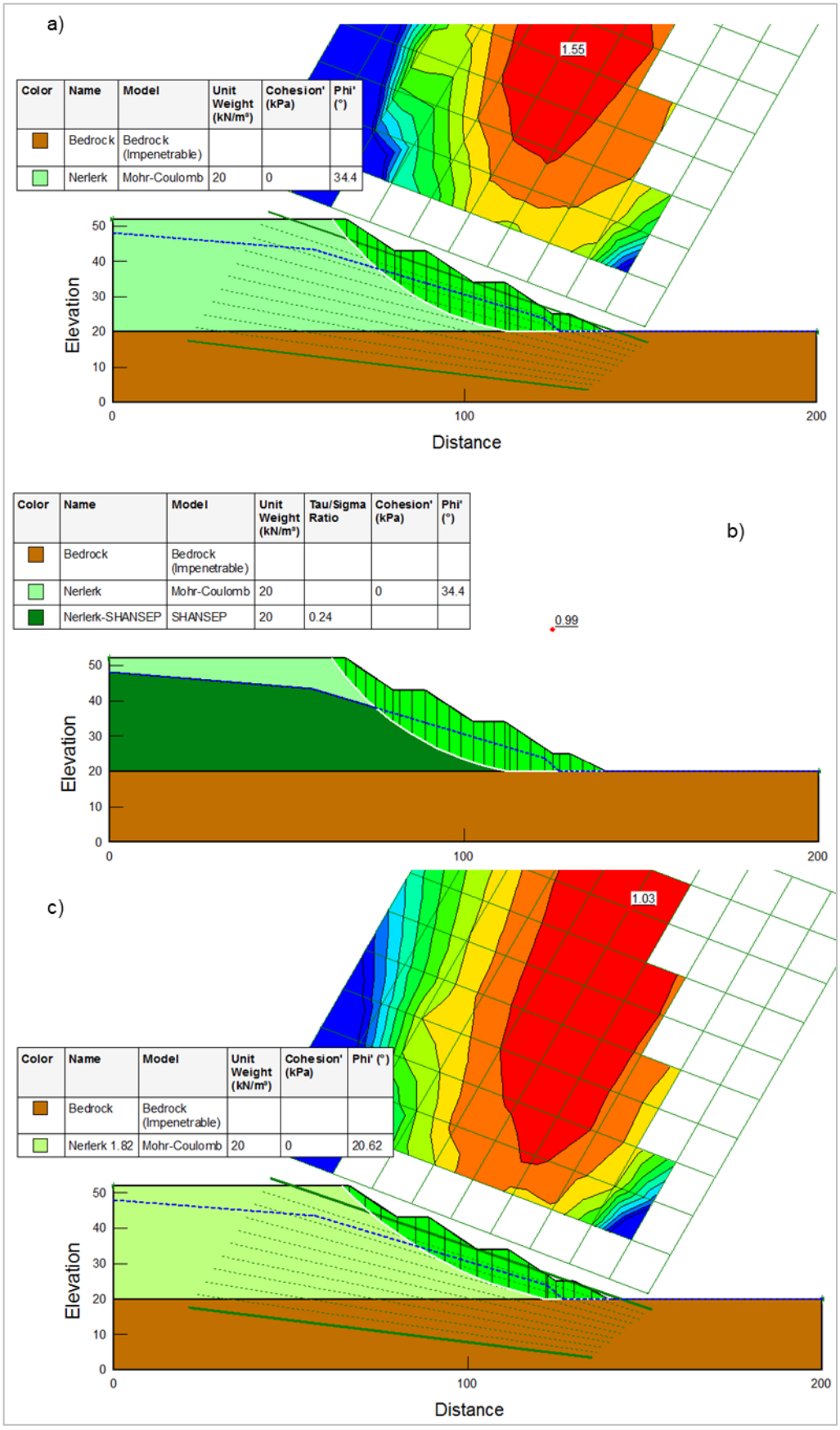

Figure 10.10: Results for the Nerlerk sand on Cross Section B: a) ESA, b) USA, c) FEA

10.4 CROSS SECTION C

The third cross section (Cross Section C) is the same cross section as Cross Section B with the exception that the starter wall is assumed to be lined with a geosynthetic barriers including a geomembrane and geogrid thus eliminating slip surfaces through the starter wall. It was assumed that the geosynthetic barrier was designed in such a manner that the critical shear interface still lies within the tailings material. This cross section (shown in Figure 10.11) was selected as most new tailings dams will likely need to be lined to comply with the recent legislation where mine tailings is now considered a waste product and therefore this scenario is expected to be common in the future. Again, three material zones were identified: one for the foundation material and starter wall, one for the zone below the phreatic surface and one for the zone above the phreatic surface.

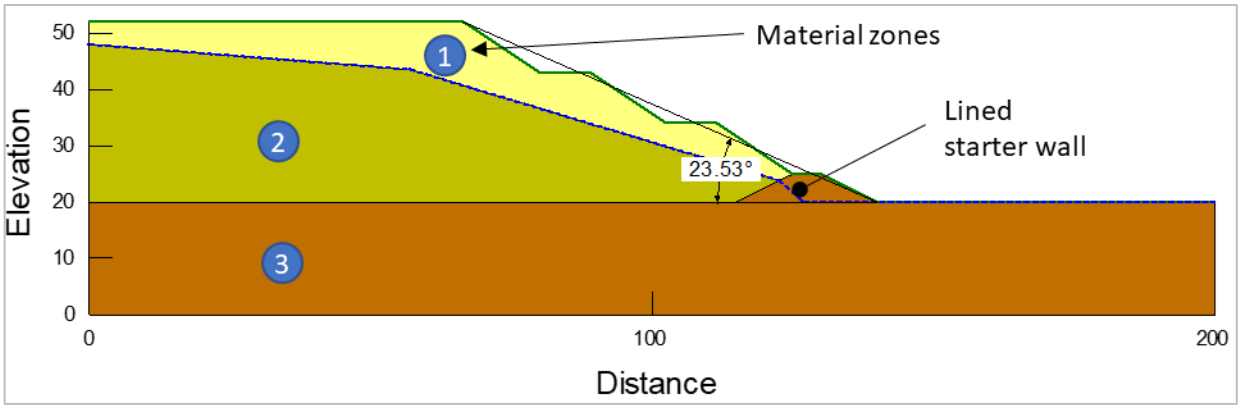

Figure 10.11: Material zones for Cross Section C

Results of the analyses conducted for Cross Section C are shown in Figure 10.12, Figure 10.13, Figure 10.14 and Figure 10.15 for the gold tailings, iron tailings, platinum tailings and Nerlerk sand respectively. A summary of the results is shown in Table 10.3.

Table 10.3: Summary of results for Cross Section C

	FoS (ESA)	FoS (USA)	SF (FEA)
Gold tailings	1.95	1.09	2.17
Iron tailings	1.69	0.95	2.11
Platinum tailings	1.89	1.21	2.24
Nerlerk sand	1.65	0.82	1.66

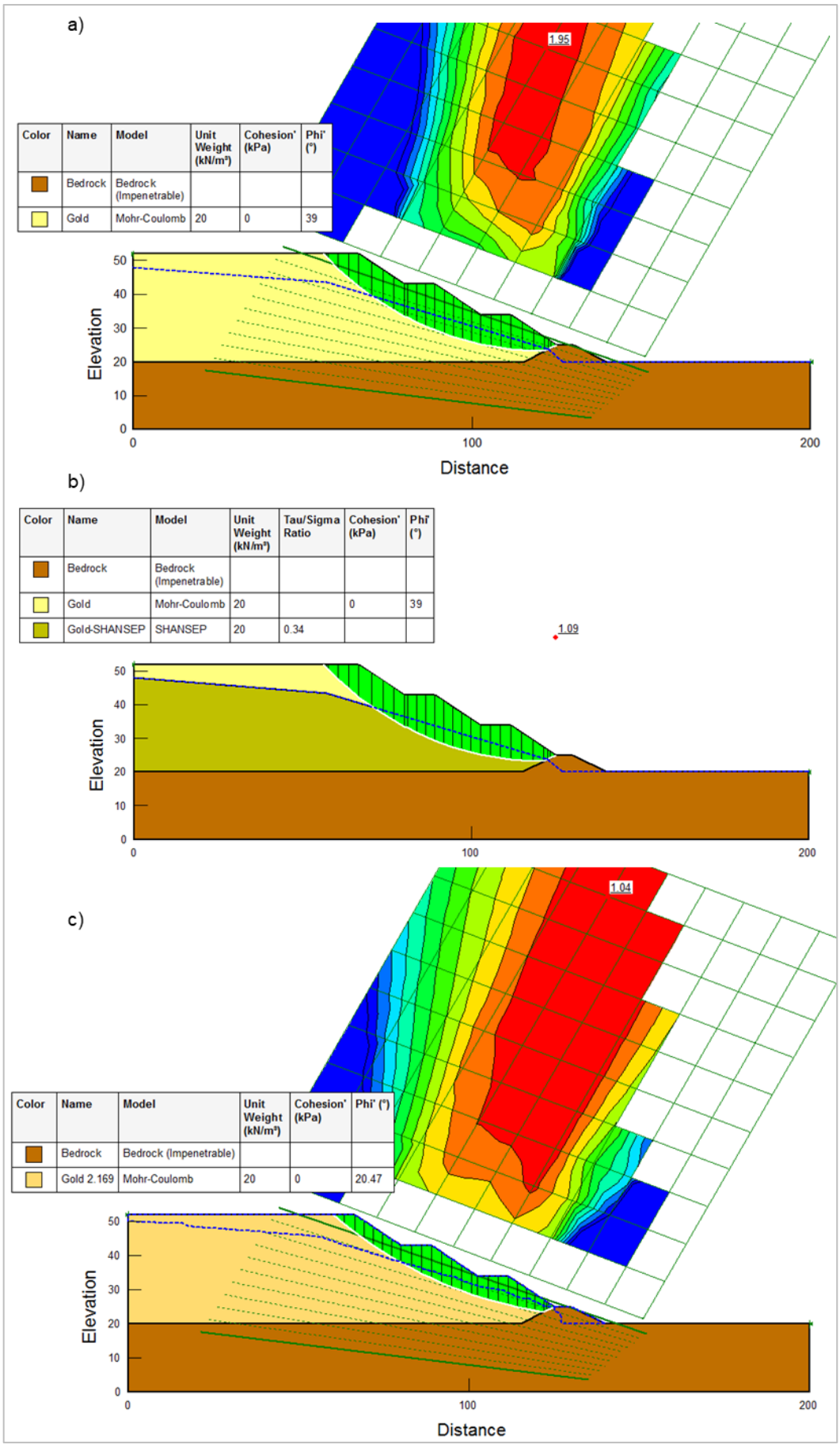

Figure 10.12: Results for the gold tailings on Cross Section C: a) ESA, b) USA, c) FEA

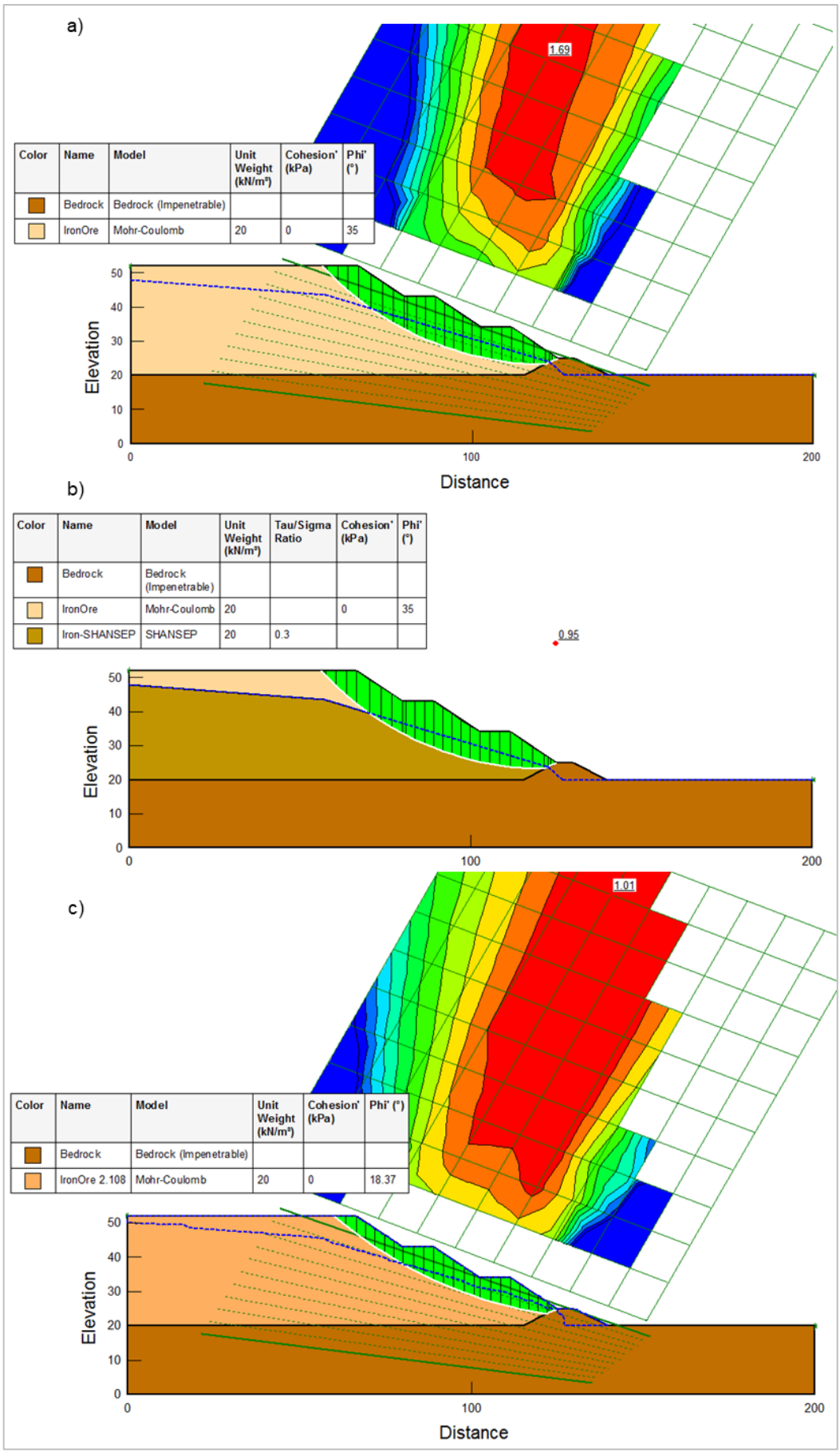

Figure 10.13: Results for the iron tailings on Cross Section C: a) ESA, b) USA, c) FEA

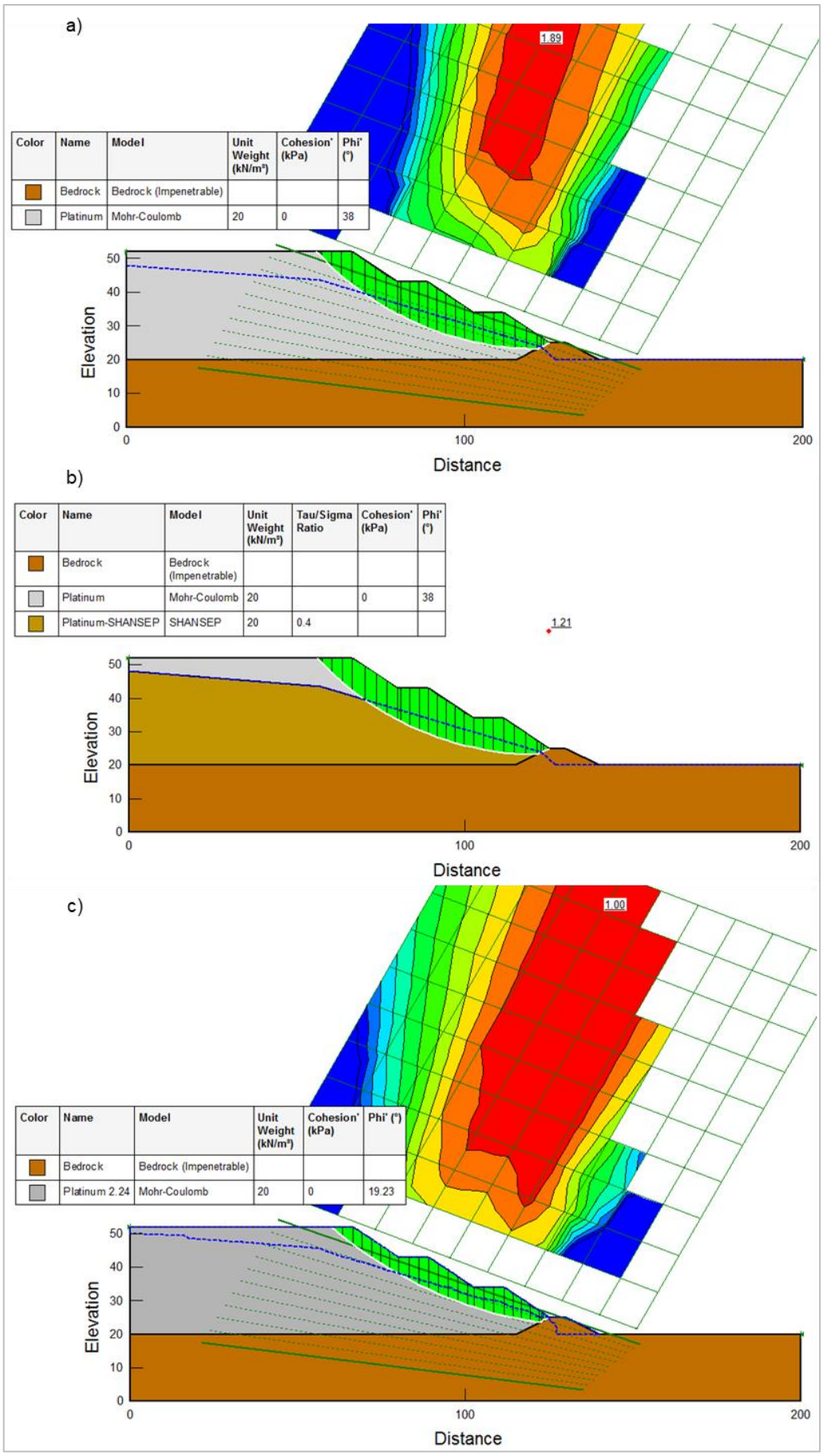

Figure 10.14: Results for the platinum tailings on Cross Section C: a) ESA, b) USA, c) FEA

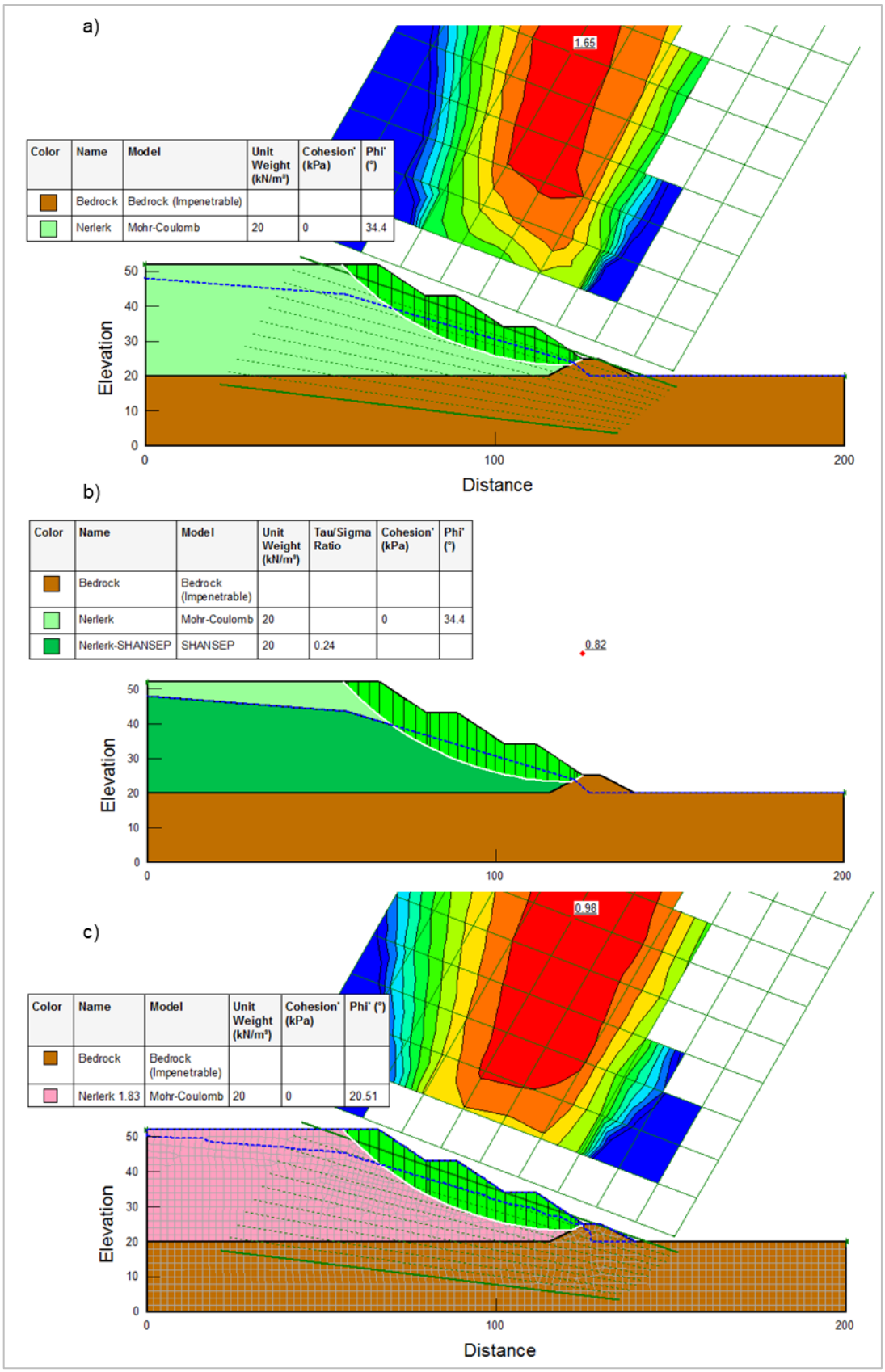

Figure 10.15: Results for the Nerlerk sand on Cross Section C: a) ESA, b) USA, c) FEA

10.5 SUMMARY

Analyses were conducted using the SLOPE/W and SIGMA/W modules of the GeoStudio 2020 software package. Three cross sections were assessed and for each cross section, four materials were considered. The results from these analyses were presented and were used to evaluate the proposed method to determine a FoS based on strain compatibility.

11 APPENDIX E – DETAILED FOS RESULTS AND COMPARISONS

11.1 INTRODUCTION

A series of scenarios were assessed to calculate a FoS against failure for three specific cross sections considering four materials. This Appendix provides the detailed results from these analyses.

11.2 CROSS SECTION A

A summary of the calculated FoS values for the six scenarios assessed for Cross Section A is shown in Table 11.1.

Table 11.1: Summary of calculated FoS values for the six scenarios for Cross Section A

	1. LE (ESA)	2. LE (USA)	3. FEA (SRS)	4. CD strengths	5. CU strengths	6. Combined CD, CU strengths
Gold tailings	1.94	0.97	1.80	1.91	1.00	1.03
Iron tailings	1.68	0.85	1.65	1.79	0.90	0.91
Platinum tailings	1.87	1.12	1.74	1.88	1.15	1.17
Nerlerk sand	1.64	0.70	1.51	1.77	0.71	0.74

Several comparisons were drawn between the various scenarios and these are shown in Table 11.2 and Table 11.3.

Table 11.2: Results for Cross Section A

	Scenario 1	Scenario 4	Difference	Difference		Scenario 2	Scenario 6	Difference	Difference
Gold tailings	1.94	1.91	0.03	2%		0.97	1.03	0.06	6%
Iron tailings	1.68	1.79	0.11	7%		0.85	0.91	0.06	7%
Platinum tailings	1.87	1.88	0.01	1%		1.12	1.17	0.05	4%
Nerlerk sand	1.64	1.77	0.13	8%		0.70	0.74	0.04	6%

Table 11.3: Results for Cross Section A (cont.)

	Scenario 1	Scenario 3	Difference	Difference		Scenario 5	Scenario 6	Difference	Difference
Gold tailings	1.94	1.80	0.14	7%		1.00	1.03	0.03	3%
Iron tailings	1.68	1.65	0.03	2%		0.90	0.91	0.01	1%
Platinum tailings	1.87	1.74	0.13	7%		1.15	1.17	0.02	2%
Nerlerk sand	1.64	1.51	0.13	8%		0.71	0.74	0.03	4%

11.3 CROSS SECTION B

A summary of the calculated FoS values for the six scenarios assessed for Cross Section A is shown in Table 11.4.

Table 11.4: Summary of calculated FoS values for the six scenarios for Cross Section B

	1. LE (ESA)	2. LE (USA)	3. FEA (SRS)	4. CD strengths	5. CU strengths	6. Combined CD, CU strengths
Gold tailings	1.83	1.27	2.17	1.92	1.00	1.08
Iron tailings	1.58	1.11	2.05	1.80	0.90	0.94
Platinum tailings	1.77	1.35	2.17	1.89	1.15	1.23
Nerlerk sand	1.55	0.99	1.82	1.78	0.71	0.79

Several comparisons were drawn between the various scenarios and these are shown in Table 11.5 and Table 11.6.

Table 11.5: Results for Cross Section B

	Scenario 1	Scenario 4	Difference	Difference		Scenario 2	Scenario 6	Difference	Difference
Gold tailings	1.94	1.91	0.03	2%		0.97	1.03	0.06	6%
Iron tailings	1.68	1.79	0.11	7%		0.85	0.91	0.06	7%
Platinum tailings	1.87	1.88	0.01	1%		1.12	1.17	0.05	4%
Nerlerk sand	1.64	1.77	0.13	8%		0.70	0.74	0.04	6%

Table 11.6: Results for Cross Section B (cont.)

	Scenario 1	Scenario 3	Difference	Difference		Scenario 5	Scenario 6	Difference	Difference
Gold tailings	1.94	1.80	0.14	7%		1.00	1.03	0.03	3%
Iron tailings	1.68	1.65	0.03	2%		0.90	0.91	0.01	1%
Platinum tailings	1.87	1.74	0.13	7%		1.15	1.17	0.02	2%
Nerlerk sand	1.64	1.51	0.13	8%		0.71	0.74	0.03	4%

11.4 CROSS SECTION C

A summary of the calculated FoS values for the six scenarios assessed for Cross Section A is shown in Table 11.7.

Table 11.7: Summary of calculated FoS values for the six scenarios for Cross Section C

	1. LE (ESA)	2. LE (USA)	3. FEA (SRS)	4. CD strengths	5. CU strengths	6. Combined CD, CU strengths
Gold tailings	1.95	1.09	2.17	1.92	1.00	1.05
Iron tailings	1.69	0.95	2.11	1.80	0.90	0.93
Platinum tailings	1.89	1.21	2.24	1.89	1.15	1.20
Nerlerk sand	1.65	0.82	1.66	1.78	0.71	0.77

Several comparisons were drawn between the various scenarios and these are shown in Table 11.8 and Table 11.9.

Table 11.8: Results for Cross Section C

	Scenario 1	Scenario 4	Difference	Difference		Scenario 2	Scenario 6	Difference	Difference
Gold tailings	1.94	1.91	0.03	2%		0.97	1.03	0.06	6%
Iron tailings	1.68	1.79	0.11	7%		0.85	0.91	0.06	7%
Platinum tailings	1.87	1.88	0.01	1%		1.12	1.17	0.05	4%
Nerlerk sand	1.64	1.77	0.13	8%		0.70	0.74	0.04	6%

Table 11.9: Results for Cross Section C (cont.)

	Scenario 1	Scenario 3	Difference	Difference		Scenario 5	Scenario 6	Difference	Difference
Gold tailings	1.94	1.80	0.14	7%		1.00	1.03	0.03	3%
Iron tailings	1.68	1.65	0.03	2%		0.90	0.91	0.01	1%
Platinum tailings	1.87	1.74	0.13	7%		1.15	1.17	0.02	2%
Nerlerk sand	1.64	1.51	0.13	8%		0.71	0.74	0.03	4%

11.5 SUMMARY

A series of scenarios were assessed to calculate a FoS against failure for three specific cross sections considering four materials. Detailed results were presented and were used to achieve the objectives of the study.